Absorption Heat Recovery

John S. Currie,

Doctor of Philosophy,

University of Edinburgh.

August 1994.

Declaration.

The work described in this thesis is the original work of the author and was carried out without the assistance of others, except where explicit credit is given in the text. It has not been submitted, in whole or in part, for any other degree at any University.

John Swan Currie

Acknowledgements.

The completion of this thesis would not have been possible without the help of many, many people. First of all, I would like to thank my wife, Seona, for continually pushing me to get finished and for also taking time to proof read my work, even though her handwriting was impossible to read. Special mentions go out to Kevin Wright, a fellow conspirator, and Colm Fitzgerald for putting up with both Kevin's and my own antics in the office- doing a PhD, does make you behave oddly sometimes.

Within the Department of Chemical Engineering, there are a whole host of people who need to be thanked for their help throughout the project, none more so than the workshop- Kenny Fee, Bobby Hogg, Rab Kilgour and Tommy Murray. Thanks to Matthew Rea, an electronic wizard and also to Neil Skilling, another wizard (computer wizard), who answered my stupid questions and more importantly recovered lost files when ever they were accidentally scrubbed. Lastly, I'd like to thank my supervisor, Colin Pritchard, for keeping me on the right track and also Cui for some interesting and useful ideas.

During my placement at ICI(FCMO), Grangemouth there were several people who helped me find my way around. In particular, my industrial supervisor, Kumar Abhinava, and his predecessor, Mike Muskett. As well as Hamish M^{c}Arthur and several others on the site, including Glen M^{ac}Creath and Stuart Ramsay.

Lastly, my mum and dad for sending me to the B.B.C (Big Bad City) and Uni. in the first place; its been a long haul but well worth it. Any acknowledgements would not be complete without thanking Mr B, Paul Bonini, who for his many sins is a good friend and an even better cook.

Abstract.

Industrial drying operations are highly energy intensive, usually utilising a primary energy source to provide the necessary heat for the production of a wide range of materials. The use of hot air as the heat and mass transfer medium leads to a resultant loss of energy through the venting of humid exhaust streams.

An absorption heat transformer pilot plant was designed and constructed to investigate the potential of recovering this waste heat. Using a two stage cycle, simulated dryer exhaust streams were successfully dehumidified and reheated.

The first stage of the transformer employed a direct contact process which used a concentrated absorbent solution, in this case aqueous lithium bromide solution, to reduce the humidity of the gas stream. This stage was followed by an indirect contact process using a novel absorption column to reheat the 'dry' gas. It was found that, based on initial water vapour partial pressures of around 0.2 bar, exit partial pressures as low as 0.04 bar were achievable. Temperature lifts of 50 - 70 degC were possible in the reheat column, while the maximum exit gas temperature achieved was 160 °C.

In conjunction with the experimental studies, a computer simulation program was also written. Results of the model show that the absorption process was extremely rapid, occurring within the first 5 cm (6%) of the absorption column. A good comparison between the experimental and computer results was achieved. A preliminary design of an industrial heat transformer was also proposed following an industrial case study of a spray drying operation.

One man's "magic" is another man's engineering. "Supernatural" is a null word.

Excerpts from the Notebooks of Lazarus Long;
taken from "Time enough for love" by Robert Heinlein

The reason atoms become chemistry professors has got to be that something in nature does not like laws of chemical equilibrium or the law of gravity or the laws of thermodynamics or any other law that restricts the molecules' freedom. They only go along with laws of any kind because they have to, preferring an existence that does not follow any laws whatsoever.

"LILA: An inquiry into morals" by Robert M. Pirsig

Contents

List of Figures

List of Tables

0.1 Nomenclature

Symbol	Description
α, β	Coefficients to calculate the interfacial temperature and pressure (Chapter 5, Equations 5.2, 5.3 and 5.4 see also Brunk [24]) [-]
α, β, γ, θ	Coefficients used to calculate voidage (Chapter 5, Equations 5.15, 5.16 and 5.17). [-]
γ	Liquid phase activity (Chapters 2 and 7). [-]
δz	Slice thickness, used in simulation models. [m/ ft]
ϵ	Voidage. [-]
ε	Heat exchanger effectiveness. [-]
ζ	Exergetic efficiency of a heat pump cycle. [-]
λ	Enthalpy of the steam in the reheat column. [Jg^{-1}]
Λ	Wilson activation energy (Chapter 7). [-]
μ	Viscosity [g $m^{-1}s^{-1}$/ lb $hr^{-1}ft^{-1}$]
ρ	Density [kg m^{-3}]
ΔG^E_{max}	Excess Gibbs free energy (Chapter 2) [$kJkg^{-1}$]
Δh^E	Excess heat of mixing (Chapter 2) [$kJkg^{-1}$]
Δh	Change in enthalpy. [Jg^{-1}]
ΔS	Change in entropy. [$Jg^{-1}K^{-1}$]
ΔT	Temperature difference. [degC]
Σv	Atomic diffusion volume (Chapter 5, Equation 5.13) [-]
A, B, C	Antoine constants (Chapter 7, Equation 7.1) [-]
A_O	Available heat transfer area [m^2]
A_{ann}	Cross sectional annular area in reheat column. [m^2]
C	Stream heat capacity = ($\dot{m}$. c_P). [JK^{-1}]
COP	Coefficient of performance. [-]
COP_e	Enthalpic coefficient of performance. [-]
D	Diffusivity. [cm^2s^{-1}/ ft^2hr^{-1}]
E'_{ij}, E''_{ij}	Constants used to find the Wilson Energy of a binary mixture with components 'i' and 'j' (Chapter 7, Equation 7.4). [J $kmol^{-1}K^{-1}$]
F_G, F_L	Mass transfer coefficients for the gas and liquid phases. [(lb.mol) $hr^{-1}ft^{-2}$]
F_r	Circulation ratio = LiBr mass flow/ Steam mass flow. [-]
G	Total gas mass flow. [(lb mol) $hr^{-1}ft^{-2}$]
G'	Gas mass velocity. [lb $hr^{-1}ft^{-2}$]

Symbol	Description
H	Gas humidity. [g- $_{H_2O}$ (g- $_{dry\ air}$)$^{-1}$]
L, L'	Liquid flowrate. [lb hr^{-1}ft^{-1}]
M	Molecular weight. [lb (lb.mol)$^{-1}$]
M_O	Mass transfer rate (Chapter 4, Tables 4.8 and 4.9) [gs^{-1}m^{-3}]
Nu	Nusselt number. [-]
Q	Heat. [W or Wm^{-2}]
Q_O	Heat transfer rate (Chapter 4, Tables 4.8 and 4.9) [kWm^{-3}]
P_T	System pressure (Chapter 7) [bar/ psi]
Pr	Prandtl number. [-]
R	Gas constant (Chapter 7, Equation 7.4)) [J kmol^{-1} K^{-1}]
%RH	Percentage water vapour relative humidity in gas stream. [-]
Re	Reynolds number. [-]
Sc	Schmidt number. [-]
T	Temperature. [°C/ K]
U_O	Overall outside heat transfer coefficient $(HTC)_O$. [Wm^{-2}K^{-1}]
$(U.A)_O$	External HTC x External surface area. [WK^{-1}]
V	Molar volume of refrigerant component (See Chapter 7). [cc g.mol^{-1}]
W	Work. [W]
a_{inter}	Specific interfacial area [m^{-1}]
a_{ij}, b_{ij}	Concentration dependent constants used to calculate the interfacial temperature (Chapter 5, Equations 5.2 and 5.3) [-]
c_P	Specific heat capacity. [Jg^{-1}K^{-1}]
d	Diameter [m]
d_H	Hydraulic mean diameter [m]
d_S	Equivalent spherical diameter of packing. [m]
h	Enthalpy of the LiBr solution. [Jg^{-1}] or Stream heat transfer coefficients [Wm^{-2}K^{-1}]
h_t	Liquid holdup, used in calculating voidage (Chapter 5, Equations 5.14 and 5.16) [-]
k, k'	Empirical coefficient used in simulation model (Chapter 5, Equations 5.17 and 5.18) [-]
k_1, k_2, k_3	Constants used to find the interfacial temperature or pressure (Chapter 5, Equation 5.1) [-]
k	Thermal conductivity [Wm^{-1}K^{-1}]
$\dot{m}$	Mass flowrate. [gs^{-1}]
p	Partial or vapour pressure of a component. [bar]
w	LiBr concentration. [%w/w]
x	Liquid mole fraction. [-]
y	Vapour mole fraction. [-]

Subscripts

CW	Cooling water.
G	Gas stream.
HP	Heat transformer.
HT	Heat pump.
H_2O	Water vapour.
I	Inner absorption tube of the reheat column.
LM	Log mean, for either temperature difference or area difference.
LiBr	Aqueous lithium bromide solution.
O	Outer annular space of the reheat column.
RS	Steam in reheat column.
absn	w.r.t. the estimated maximum absorption temperature.
amb	w.r.t. ambient conditions
av	Average value.
bot	Reference to the bottom of the reheat column.
high	Refers to the quality of heat- $\sim$ 150- 160 °C.
i	'i'th slice down through reheat column (Chapter 5).
i+1	'i+1'th slice, used in simulation model.
in	Inlet value.
inter	Reference to the interface between the vapour and liquid phase.
losses	Heat losses from pipework to surroundings.
low	Refers to the quality of heat- usually ambient.
medium	Refers to the quality of heat- $\sim$ 100 °C.
out	Outlet value.
top	Reference to the top of the reheat column.

Subscripts

*	Equilibrium conditions.
o	Bulk conditions.

Chapter 1

Introduction.

1.1 The Efficient Use of Energy.

Process integration and energy efficiency were not commonplace within the chemical industry until the 1970s because energy was cheap and fuel resources were thought to be inexhaustible. The oil crises of 1973/74 and 1979 caused oil prices to escalate, forcing companies to look at ways of conserving energy. Pinch technology and process heat integration methods were developed as a result and are now common design features of modern chemical plants.

The current oil price has dropped considerably since 1979 and immediate fuel shortages are no longer a problem. However, new problems are being faced by the chemical industry, in particular the environmental impact of burning fossil fuels.

The majority of the electricity generated in Britain, in 1990, came from the burning of fossil fuels- oil, gas or coal. About a quarter of the electricity consumed came from nuclear fuels whilst only 2 % came from renewable energy sources [218]. An approximate breakdown of the primary energy consumption within the European Community, in 1984, is shown in Figure 1.1 [25]. Despite the fact that the bar chart dates from 1984 the relative percentages of each category will have remained approximately constant and are indicative of the whole Community as well as individual countries.

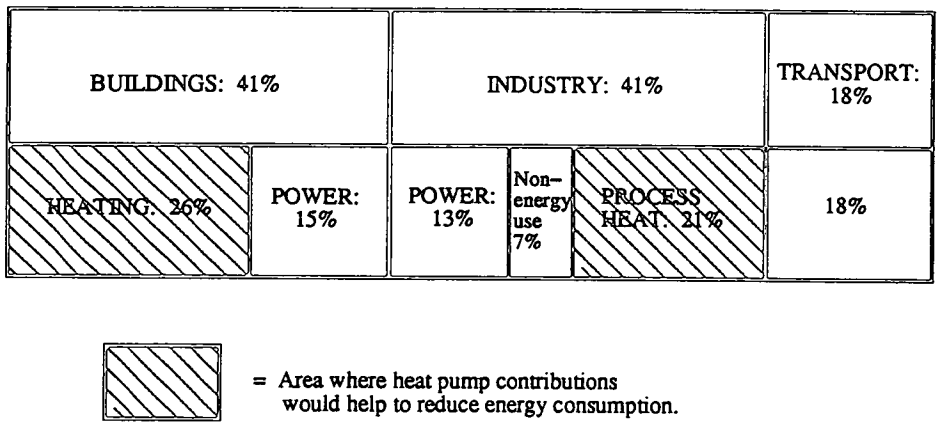

Figure 1.1: Fuel consumption in the EC for 1984.

Figure 1.1 highlights two main areas where savings could be achieved. Zegers [25], indicated that the potential savings within the building sector were between 8- 13 % and those within the industrial sector about 10 %. Heat pump cycles were proposed as the means to achieve these savings, see Section 1.2. For example, the heating of a building requires temperatures in the range 70- 90 °C, which can easily be obtained by heat pump cycles. The cycles are more efficient than conventional boilers and thus reduce the amount of oil burnt in providing

heat. In the industrial sector, further savings could be achieved if the maximum temperature possible within a cycle could be increased above 120 °C, thereby extending the applicability and attraction of such a system. Several innovative research projects have been established with the aim of reducing primary energy consumption and recovering waste heat.

Carbon dioxide causes the 'greenhouse effect', which helps to sustain an environment suitable for life on earth. However, the average temperature of the earth had increased by just over 0.5 °C over a period of 100 years up to 1988 and it is expected that it will continue to rise in the future. The reason for this is the increase in the amount of carbon dioxide in the atmosphere, caused by man's activities- burning fossil fuels, burning rain forests and intensified farming techniques. The amount of carbon dioxide in the atmosphere increased by 11 % over the period 1954- 1988 [132].

In Germany there are strict regulations relating to carbon dioxide emissions requiring companies to reduce emissions by making processes more efficient. Encompassed in these regulations is the requirement that each company reduces its overall energy consumption rather than shifting the burden to the power stations, which must burn more fuel to meet increased power demands. Indeed a carbon tax may be introduced, in Europe, in an attempt to reduce carbon dioxide emissions.

Nuclear power does not produce carbon dioxide, however, it is unlikely that there will be a major switch to nuclear power in Britain. In order to establish an extensive nuclear network the short term result would be an increase in the consumption of fossil fuels, while the nuclear infrastructure is established. Hence, any gains achieved by switching to nuclear power could only be realised in the long term.

Another alternative is the use of renewable energy sources such as wind, water, solar power and even biomass heat sources. Biomass and geothermal projects are not as widespread as the other renewable energy sources, which have gained more recognition. Several large scale projects are currently operating using solar power. Indeed there are examples of absorption heat cycles which provide heating and air conditioning for buildings by utilising solar energy as the heat source ([162], [55]).

Windmills and watermills were commonly used for the grinding of corn prior to the introduction of electricity. Coupled with today's technology these methods are capable of generating several megawatts of electricity. In California there are huge wind farms with approximately 14 thousand wind turbines providing a combined power output of 1210MW of electricity. There are also several wind turbines projects in Canada, Denmark, the Netherlands and also in Britain. A prototype wave power generation scheme was also built on the Island of Islay in 1991.

These projects are environmentally sound but the visual impact of these projects is large. Any major switch to renewable energy sources must be investigated thoroughly before implementation and it is unlikely that the energy policy in Britain will change in the near future. Therefore the environmental pollution caused by burning fossil fuels should be minimised by making processes more efficient, reducing the primary fuel consumption, and also by recovering waste heat.

The EC currently provides financial assistance for innovative projects which try to address some of the environmental problems faced today, one such scheme is THERMIE. Other funding can be obtained from the British government for energy saving projects, providing that the project has financial support from at

least one industrial company, for whom the project would directly benefit. The type of projects receiving assistance focus upon increasing the efficiency of processes and the reduction of atmospheric pollutants such as carbon dioxide, sulphur dioxide and nitrous oxides [26].

1.2 Heat Pump Technology.

The potential for energy recovery within the chemical industry is huge. Current environmental concerns, as well as economic issues, are helping to establish energy recovery systems within the industry.

The simplest way to recover waste energy is the exchange of heat between a waste heat stream and an incoming stream. However, the majority of this waste heat is available at low temperatures, 40- 80 °C, where it is uneconomical to recover, requiring the upgrading of the heat to a level suitable for use. Heat pump cycles are capable of extracting heat from a low temperature stream, and upgrading it to a higher, more useful level (see Section 1.2.1), at the expense of using a small amount of high grade energy. They are extremely versatile and are used for a wide variety of heating and cooling duties.

The most commonly used heat pumps are vapour compression cycles, which utilise the evaporation and condensation of a refrigerant fluid at different pressure levels to extract and deliver the heat at the desired temperatures. A compressor provides the driving force to move the fluid around the circuit.

Another type of cycle is the absorption heat pump, which again operates at two pressure levels. The refrigerant is vaporised in a low temperature, low pressure evaporator, extracting heat from the surroundings. It is then absorbed into a liquid absorbent, releasing medium grade heat. The absorbent solution, containing the refrigerant, is pumped to a high pressure, where the absorbent is regenerated by evaporating the refrigerant using a high grade heat source. Pure refrigerant vapour is then transferred to a condenser, which again releases medium grade heat. The liquid refrigerant is then returned to the low pressure evaporator, while the liquid absorbent is returned to the absorber. In this cycle there is no need for a compressor as the working fluid is transferred between pressure levels using pumps. However, their use is not as extensive as vapour compression cycles. Comprehensive descriptions of these systems are provided in Section 1.2.2.

Heat pumps have also been used to minimise the effect of 'pinch' points which occur within heat integrated systems. In a chemical process it is common to have a set of streams which must be cooled and a set which must be heated. Rather than using cold and hot utilities, respectfully, for each stream, it is common to devise a system to minimise the use of these utilities by integrating the heat transferred between hot and cold streams.

All the streams to be cooled are grouped together, as are the streams which must be heated. The results can be shown graphically on a composite curve graph, Figure 1.2a), where the streams being cooled are above those being heated. A 'pinch' point occurs in a process when the difference in the temperature between the two composite curves is less that required for exchanging heat across the streams. Conventionally, it was necessary to remove the 'pinch' point by adding heat to the 'hot side' of the process. However, this adds to the excess heat present below the 'pinch', which must be removed by using a cold utility stream, for example cooling water, Figure 1.2a).

Alternatively, some of the excess heat below the pinch point can be used as the heat source for a heat pump cycle. The cycle upgrades the heat to a level suitable for delivery at a temperature above the 'pinch' point, Figure 1.2b). The resultant effect is a reduction in the amount of hot and cold utilities required by the process [71].

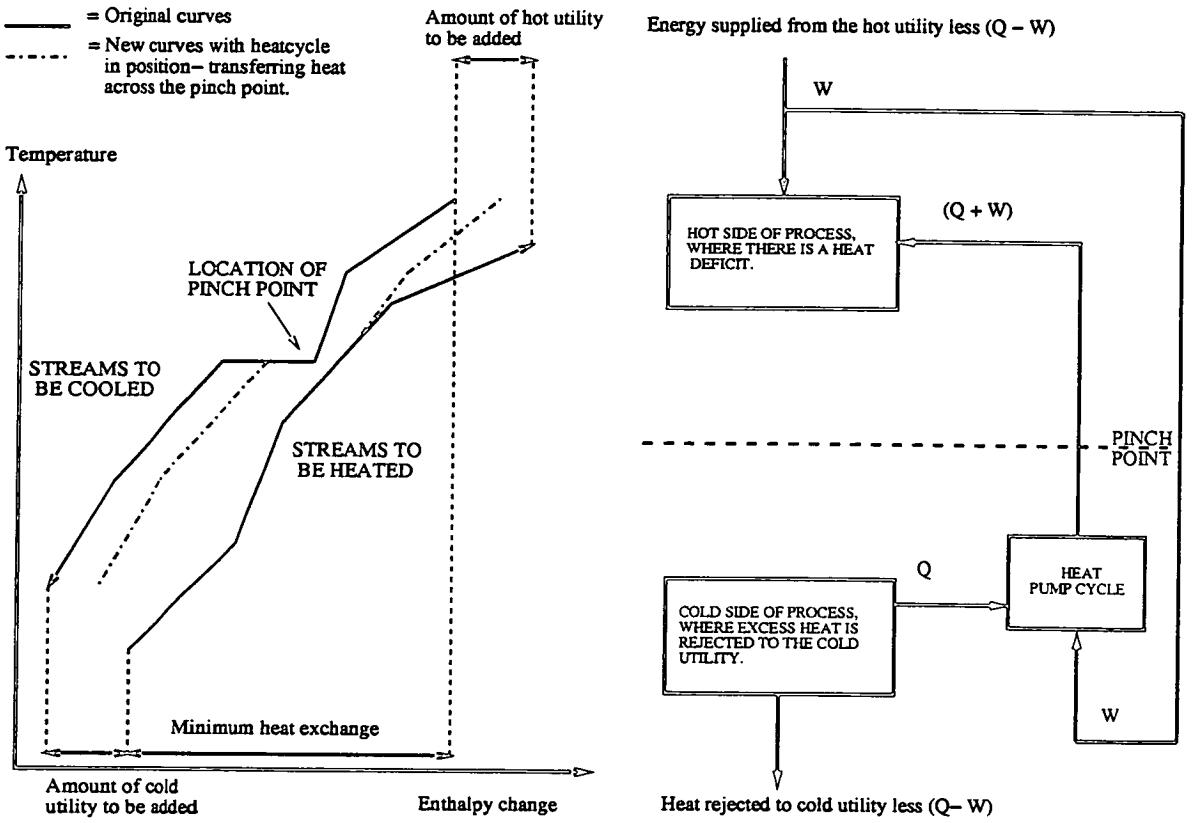

Figure 1.2: Utilisation of a heat pump cycle to overcome a 'pinch' point within a process. a) Composite Curves. b) Schematic of process with heat pump.

1.2.1 Vapour Compression Cycles.

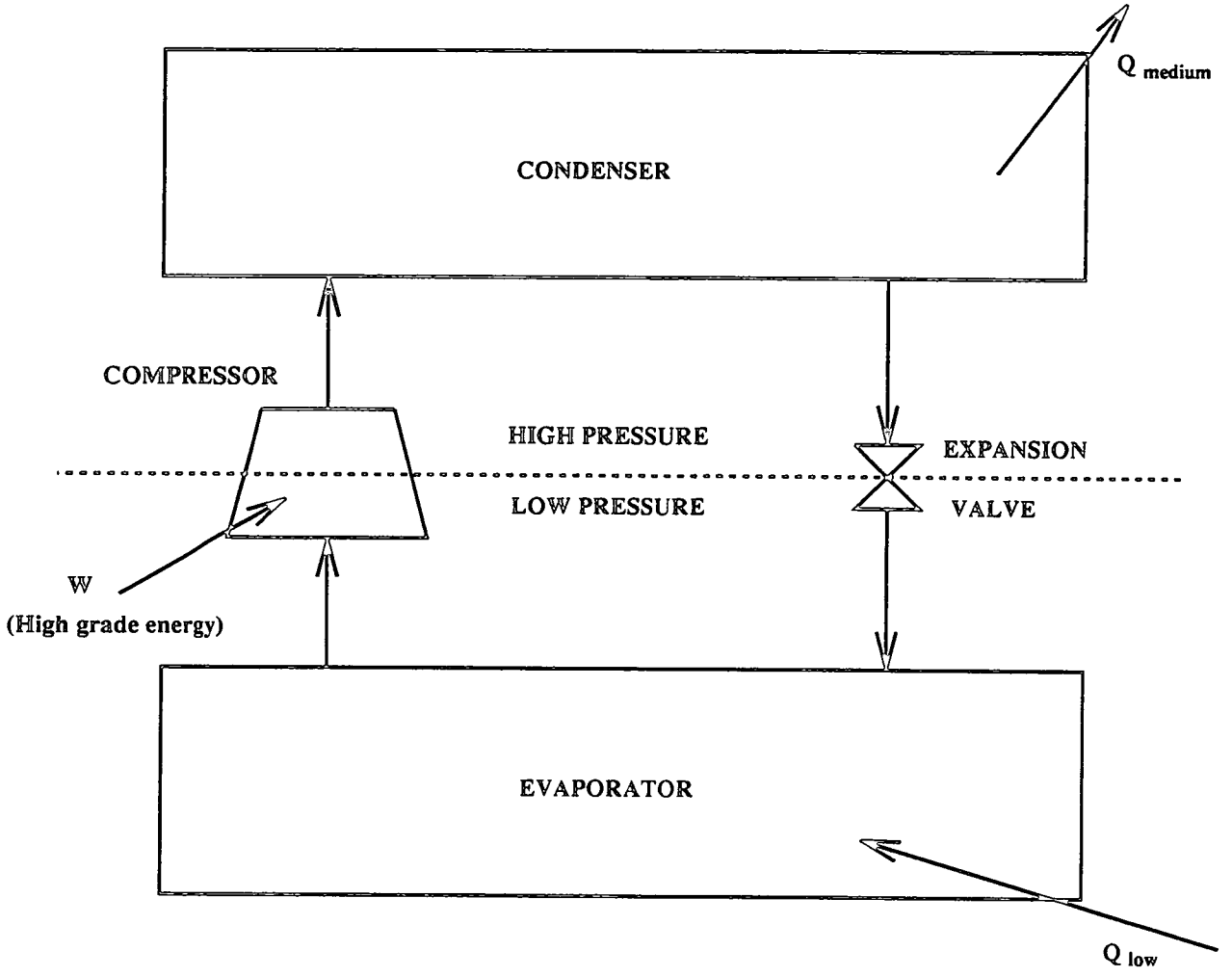

Figure 1.3: Vapour compression heat pump.

A vapour compression cycle consists of a condenser, an evaporator, a compressor and an expansion valve, Figure 1.3. The principal aim is to transfer heat from one temperature level to another, using a working fluid, commonly called a refrigerant. It is necessary to use a high grade energy source (electricity, steam, gas engine) to drive the compressor, however the amount used is less than the amount of heat delivered (or removed) by the cycle.

$$Q_{low} + W = Q_{medium} \tag{1.1}$$

The liquid refrigerant in the low pressure evaporator is vaporised using heat from a low grade temperature heat source, usually at or below ambient temperature depending on the duty. The refrigerant vapour is then compressed and flows into the high pressure condenser, where it condenses releasing its heat of condensation to the surrounding heat sink. The release of heat occurs at a higher temperature than the original heat source, Equation 1.1. The cycle is completed by throttling the liquid back to the low pressure evaporator via an expansion valve.

The cycle can operate in two ways, as a heat pump upgrading heat from one temperature level to another, or more commonly as a refrigerator, whose uses range from domestic appliances to industrial chillers. The efficiency of the cycle is based upon the amount of heat removed in the evaporator, which provides the cooling. In Japan and the United States vapour compression cycles are extensively used for air conditioning in cars and buildings.

Refrigerants.

The majority of vapour compression cycle machines use CFCs (chlorofluorocarbons) as the working fluid. The main refrigerants currently used are R11 and R12, which are used in a wide range of sectors (domestic, commercial, industry, transport and air conditioning) [184]. R12 has a low boiling point, -29.8 °C and is therefore widely used in domestic and retail freezers, where it is necessary to chill food to 3- 4 °C and also for freezing down to temperatures around -20 °C. The main use of R11 is as the working fluid for air conditioning units, which operate at higher temperatures, the normal boiling point for R11 is 23.8 °C. Other working fluids which have been used in compression cycles are ammonia, R22 (chlorodifluoromethane), propane and

butane. CFCs were thought to be the ideal working fluid as they are nontoxic, nonflammable, compatible with common lubricants, exhibit good thermodynamic properties and they are extremely stable. However, they are now seen to be causing the destruction of the ozone layer [132]. In 1974 it was proposed that CFCs were causing the breakdown of ozone, which subsequently led to the creation of an ozone hole over the South Pole. The resultant effect is that more of the sun's harmful UV- rays reach the Earth's surface, Figure 1.4a).

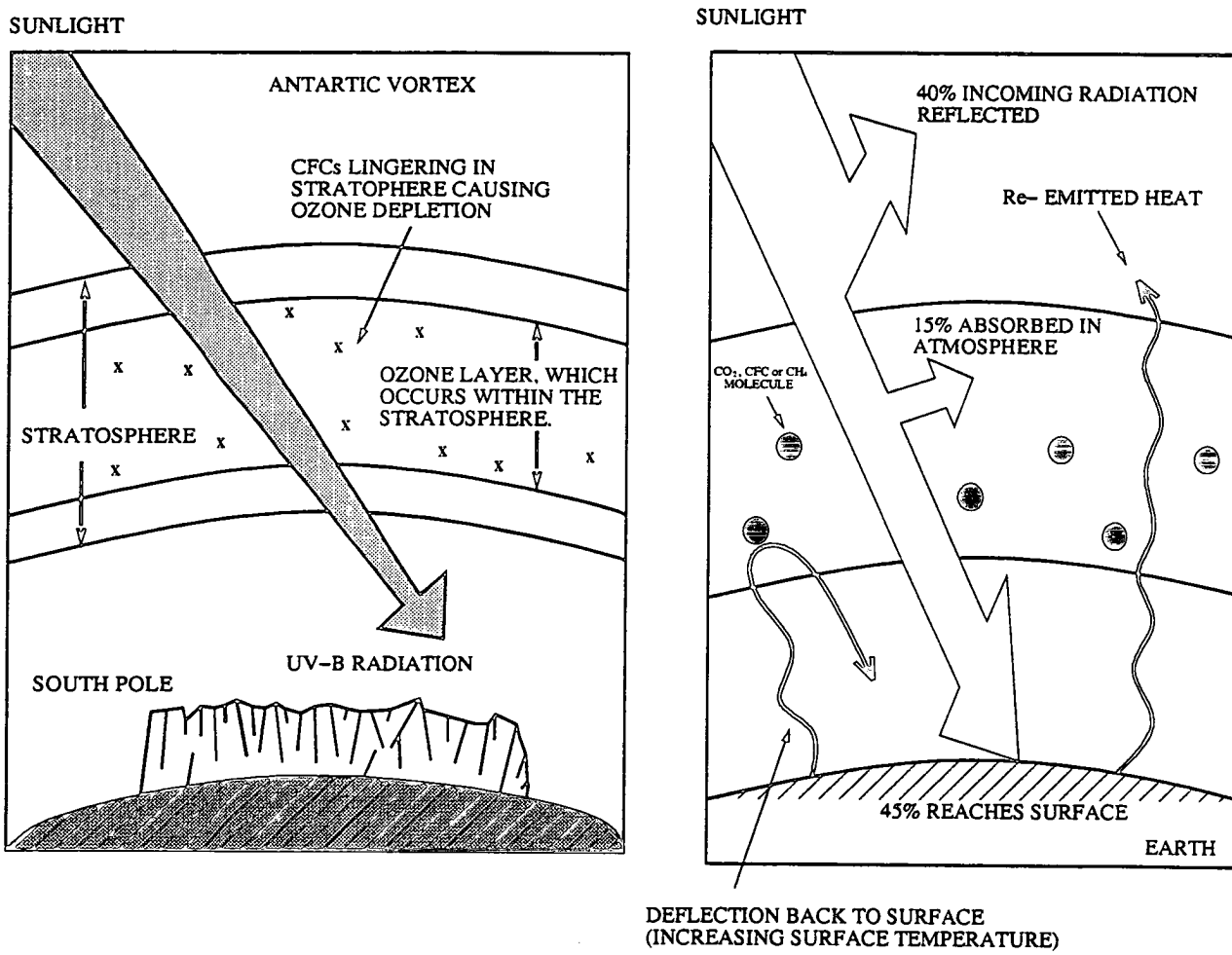

Figure 1.4: a) Ozone hole above South Pole. b) Distribution of the sun's energy.

The problem stems from the fact that CFCs are highly stable. When refrigerants leak from equipment, they do not break down but accumulate within the stratosphere, where the majority of ozone exists. Once in the stratosphere they break down with the aid of UV- radiation resulting in the formation of reactive chlorine radicals ($Cl^{\cdot}$) which then break down ozone into its constituent oxygen molecules in a chain reaction.

CFCs have also been associated with the increase in global warming, commonly referred to as the 'greenhouse effect'. The main atmospheric pollutants are carbon dioxide, methane and CFCs, which create a screen around the globe and reflect heat radiated from the surface back to the ground causing a rise in temperature, Figure 1.4b) ([132]). Therefore their use is being phased out under the terms of the Montreal Protocol which favours refrigerants with a low ODP (ozone deletion potential) and low GWP (global warming potential), see Figure 1.5.

Possible replacement refrigerants for CFCs are HFCs (hydrofluorocarbons), which include R134a (tetrafluoroethane) and R32 (difluoromethane) as substitutes for R11 and R12 (which are the most commonly used refrigerants). The use of R22 (HCFC- hydrochlorofluorocarbon) is also expected to increase; however, it may still be phased out in the future as it which still contains chlorine.

Further to this, it is felt that the straight replacement of CFCs, like R11 (trichlorofluoromethane) and R12 (dichlorodifluoromethane), with a pure charge of new refrigerant will not be possible because of the differences in the physical properties of the new refrigerants (boiling points, heat capacity, density). The use of refrigerant mixtures has been suggested instead. The composition of the mixture is such that it closely matches the performance of the cycle using

CFCs. However, this could lead to the preferential leakage from the apparatus of the most volatile component, thereby altering the respective concentrations of the refrigerants and possibly the cycle performance. Care must be taken to prevent refrigerant leakage otherwise, the cycle would require periodic 'topping up' so as to restore the blend to its original composition. Indeed another important change which manufacturers face is that the new refrigerants may not be compatible with lubricating oils presently used in heat pump equipment, making it necessary to develop a range of new oils.

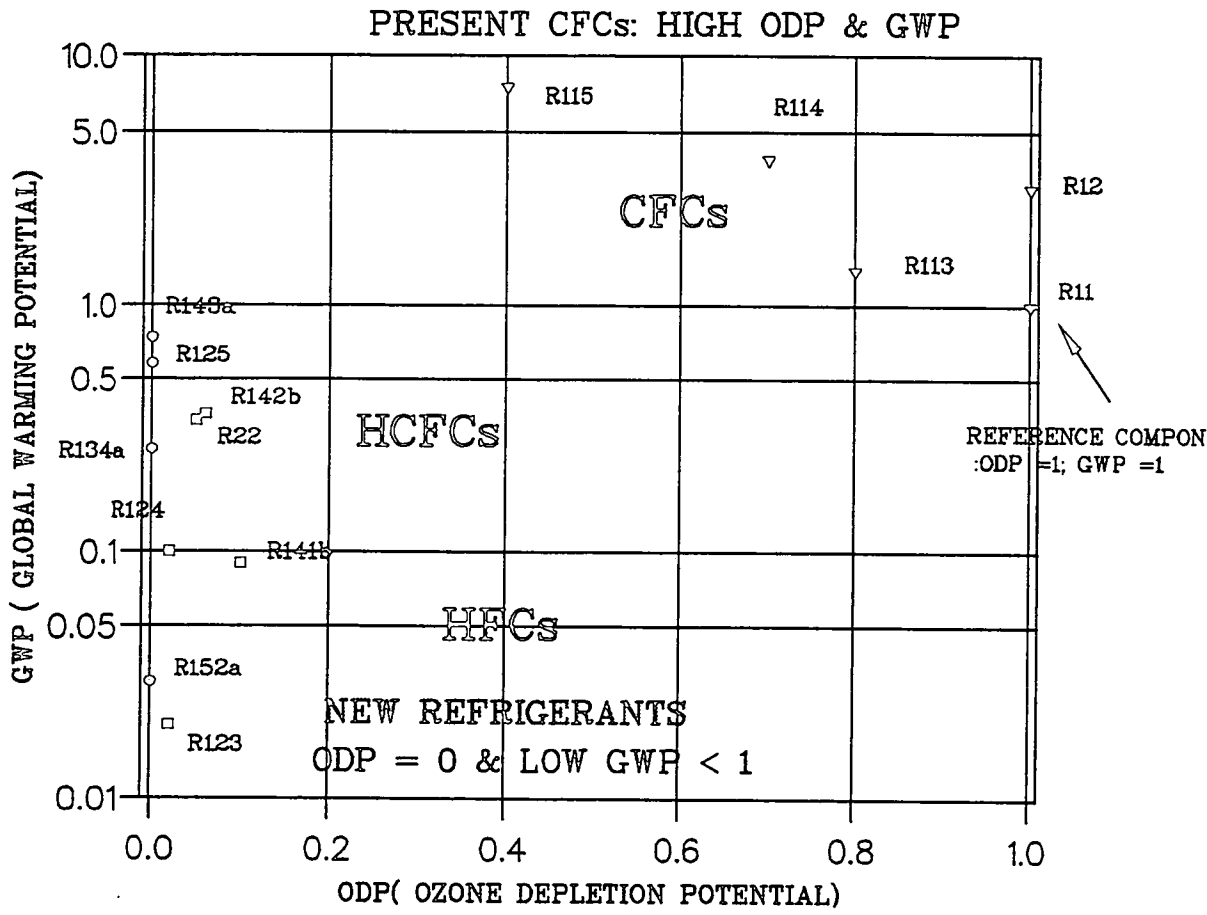

Figure 1.5: Environmental impact of refrigerants.

1.2.2 Absorption Cycles.

Absorption cycles utilise the exothermic heat liberated upon the mixing of the refrigerant vapour and absorbent streams used in the cycle, to generate useful heat. An absorption cycle operates at two pressure levels and consists of four main components:

- Evaporator- Liquid refrigerant is vaporised by taking heat from the supplied heat source.
- Condenser- Heat is removed from the refrigerant vapour causing it to condense and release heat to a heat sink.
- Absorber- The liquid absorbent, weak in refrigerant, is mixed with pure refrigerant vapour. The refrigerant is absorbed into the solution releasing the heat of mixing and condensation, which is removed by an external heat sink.
- Generator- After absorbing the refrigerant vapour, the absorbent solution is restored to its original concentration by evaporating the refrigerant, using an external heat source.

Single stage cycles operate at two pressure levels, in a heat pump the evaporator- absorber pair operate at low pressure, whilst the condenser-generator pair operate on the high pressure side of the cycle. The opposite is true for a heat transformer. Both types of absorption cycle usually operate at three temperature levels, which are classified as 'low', 'medium' and 'high'. Absorption heat pumps, like vapour compression heat pumps, take heat at a low energy level and upgrade it to a useful level by using a small amount of high grade energy, Figure 1.6. Whereas a heat transformer takes an

energy stream, usually a waste heat stream, and generates a stream at a high temperature level, at the expense of downgrading the remainder to a low temperature level, which is usually ambient. Typical temperatures, which can be achieved in the absorber, range from 100- 170 °C, while waste heat streams are usually in the range 60-90 °C.

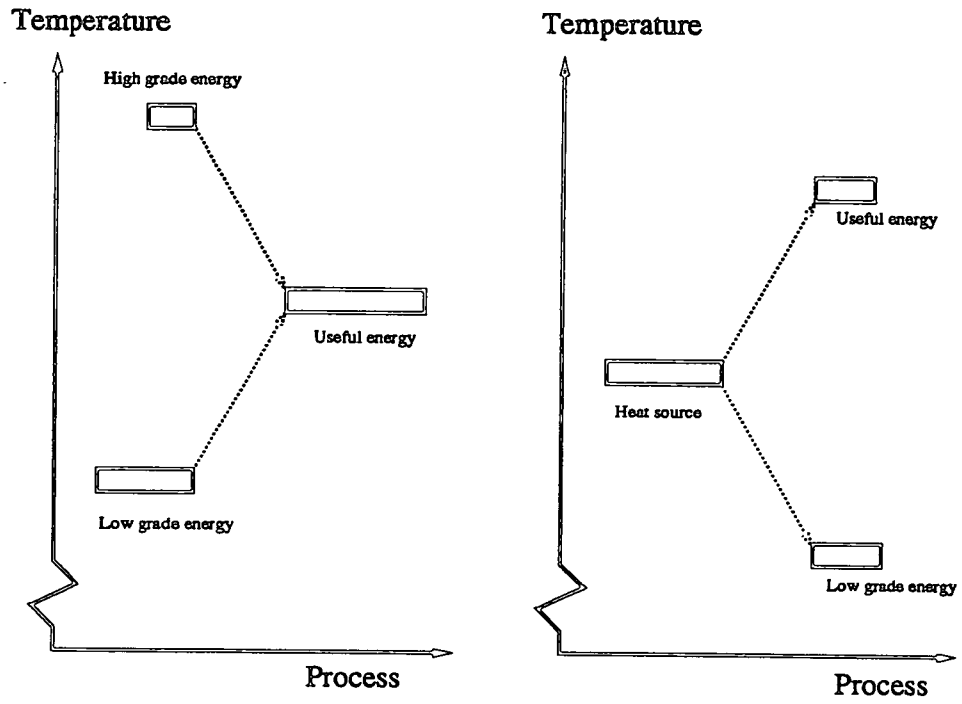

Figure 1.6: a)Heat pump b)Heat transformer.

Absorption cycles each include two pumps and an expansion valve to allow the transfer of streams between vessels, see Figures 1.7, 1.8 and 1.9. The main vessels of a single stage cycle are essentially heat exchangers, which are easy to manufacture and are mechanically simple. In some cases turbulence promoters are inserted to improve mass and heat transfer within a vessel. There is no need for specialised or complex equipment, therefore the system requires less maintenance and hence costs less to operate than a vapour compression heat pump.

Essential to the operation of an absorption cycle is the choice of working fluid pair. The majority of cycles used currently use either ammonia/ water or water/lithium bromide as the working medium. Both these fluid pairs have operating limitations and research is being carried out to find new fluid pairs. The main problems associated with using ammonia/ water are that there is a small difference between the boiling points of ammonia and water. The consequence of this means that a rectification stage is required to ensure complete separation of the refrigerant from the absorbent after the generator. Ammonia/ water is not suited for high temperature operation as the system would need to be operated at a very high pressure in order to achieve the high exit temperature from the absorber.

The water/ lithium bromide fluid pair is prone to crystallisation at high concentrations and low temperatures. It is not recommended that this fluid pair be used for chilling duties where the evaporator temperature drops below about 5 °C, as this could lead to problems with the water freezing. Chapter 2, 'Absorption working fluids', discusses the selection and evaluation of fluid working pairs in more detail as well as providing examples of systems utilising different working fluids.

Heat Pumps.

In heat pump cycles the generator uses high grade energy to regenerate the strong absorbent solution from the absorbent- refrigerant mixture delivered from the absorber. Useful heat is extracted in the absorber and condenser stages at a moderate temperature level, whilst low grade heat is used to vaporise the refrigerant in the evaporator. Refrigeration cycles are primarily concerned with the amount of heat removed in the low temperature evaporator.

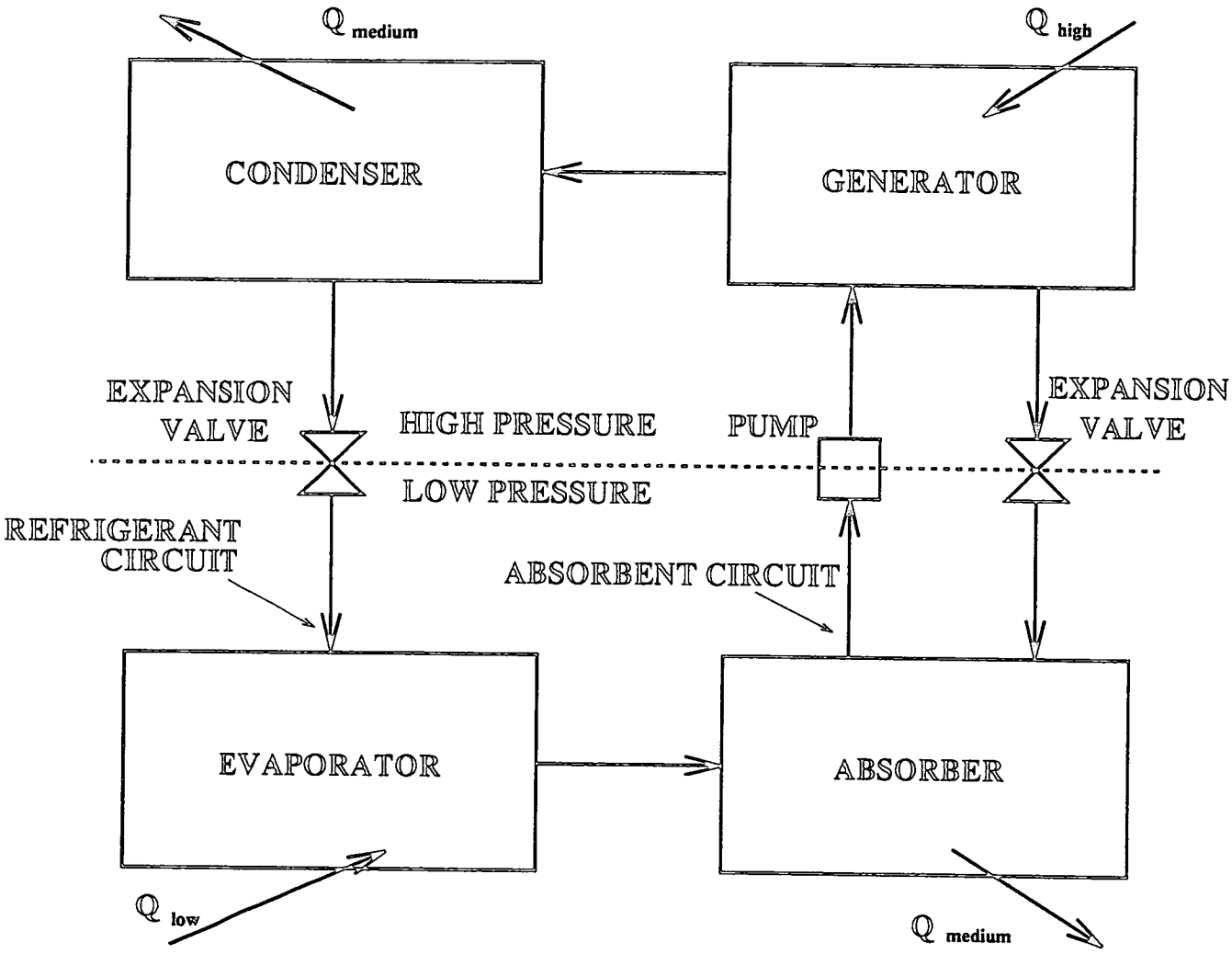

Figure 1.7: Absorption heat pump.

Absorption cycles are commonly used as chillers and air conditioners in Japan and the USA, using gas as the high grade heat source in the generator ([39], [158], [160]). Other absorption cycles utilise solar power as the heat source for the generator, these are generally for domestic heating and air conditioning duties ([205],[55]).

Heat pump cycles are often used to provide hot water and heating for domestic buildings with several examples of large scale heat pumps found in Japan and Sweden ([93], [151], [113]). Typical working fluid pairs are ammonia/ water and water/ lithium bromide. One project in Japan used a heat pump to recover waste heat from a water stream and used it to preheat a boiler feed stream[151]. Due to special tariffs, natural gas is the most commonly used energy source used in the generators of absorption heat pump cycles in Japan, thereby promoting the use of absorption heat recovery, chilling and air conditioning units.

Heat Transformers.

Heat transformers (sometimes called 'Reverse heat pumps' or 'Type II heat pumps') are used to upgrade and recover waste heat, which can then be used elsewhere. The transformer cycles have an economic advantage over conventional heat pump cycles as they do not require high grade energy to operate. Several industrial absorption heat transformers use waste heat as the energy source, greatly reducing running costs as these heat sources are usually free and in some cases may have a negative cost. Therefore, if the waste heat was not utilised by the cycle there would be a subsequent cost associated in disposing of the heat (eg. rejection of heat to a cooling tower). Indeed the only primary energy required for a heat transformer is that used to operate the solution pumps present in the cycle.

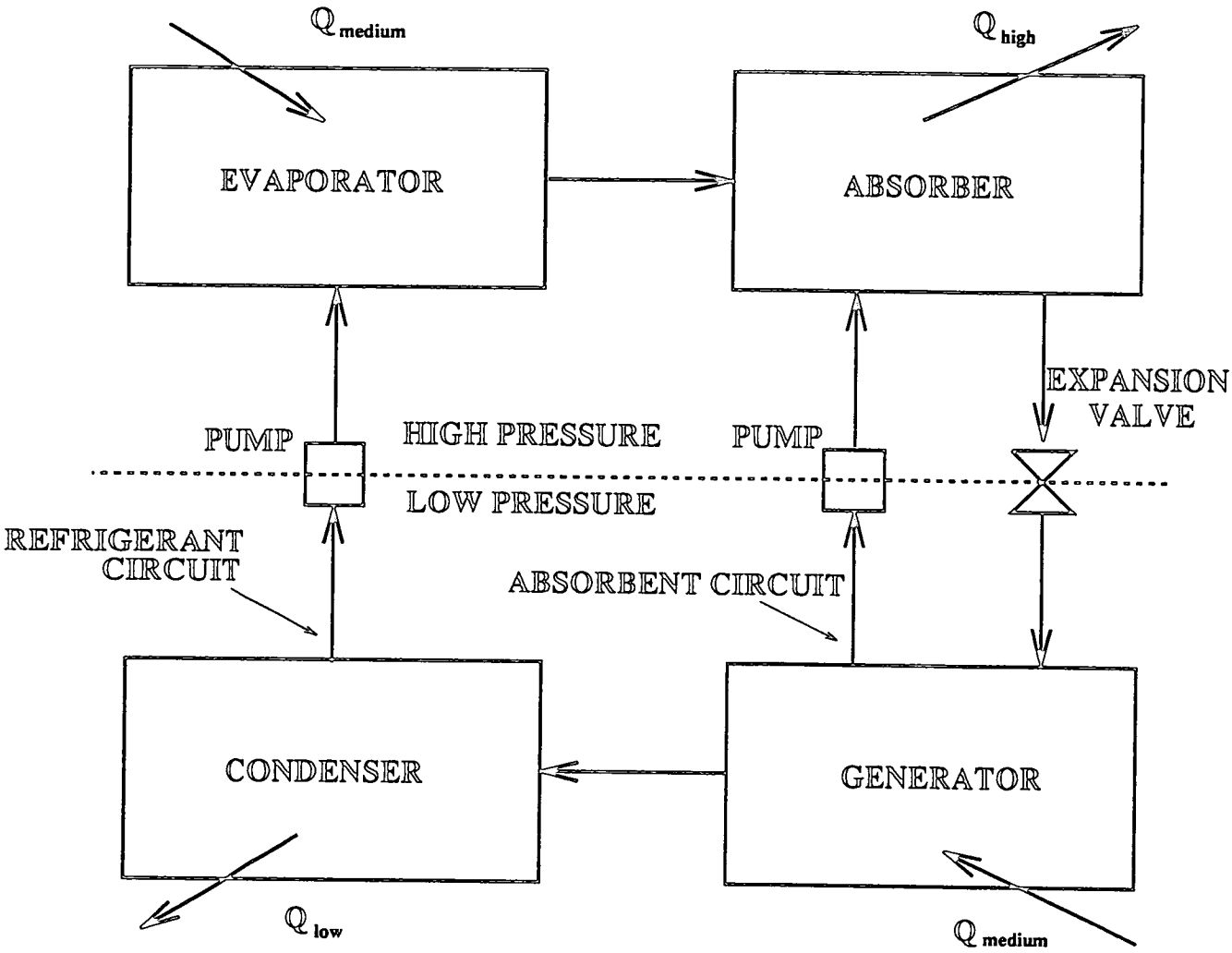

Figure 1.8: Absorption heat transformer.

In order to maximise the temperature generated in the absorber it is common practice to preheat the strong absorbent solution stream entering to the absorber with the hot, weak absorbent solution leaving the column. Figure 1.9 illustrates this feature of an absorption heat transformer (A.H.T) cycle.

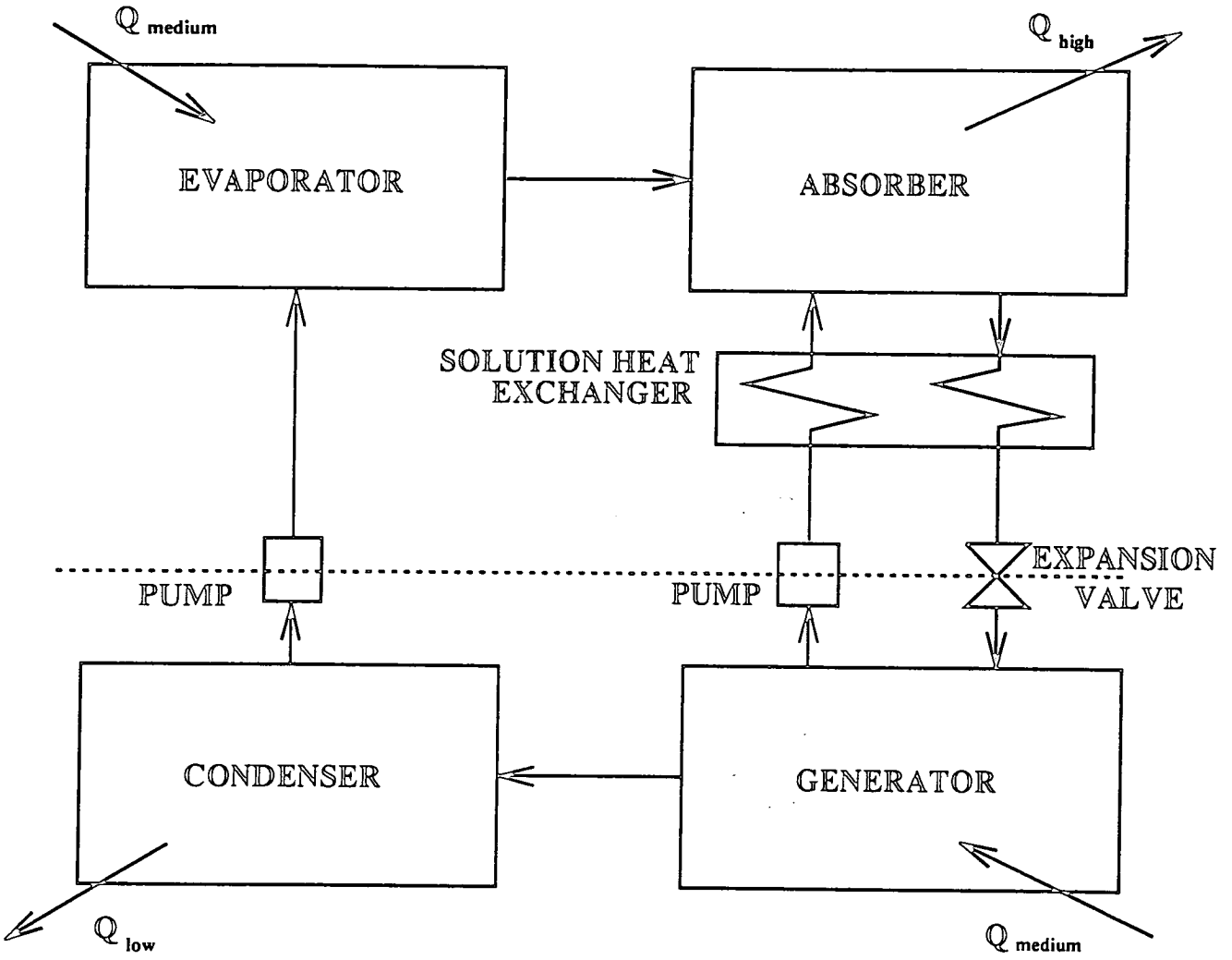

Figure 1.9: Absorption heat transformer with solution heat exchanger.

A heat transformer upgrades a proportion of the incoming energy at the expense of downgrading the remainder of the heat to a low temperature level, therefore the quantity of heat produced is less than the original amount, although it is of higher quality, Figure 1.6. The opposite is true for a heat pump cycle: a low grade energy stream is upgraded to a moderate level using a small amount of high grade energy. As such the quantity produced in the cycle is

greater than the high grade energy used, but it is of a lower quality. The efficiency of heat pump cycles will be discussed in more detail in the following Section 1.3, 'Performance Criteria'.

The relative temperature and pressure levels for each of the components in the cycle can be shown using either a Van't Hoff or a P-T-x diagram, Figure 1.10, which also shows the relative concentration of the absorbent solution at each point. The P-T-x diagram is useful for design purposes as it allows the engineer to specify the expected pressure and temperature levels within the cycle and hence the required absorbent concentrations. The diagram shown is for the water/ lithium bromide working pair. It can be seen from the diagram that the pressure levels for a heat transformer cycle, using water/ lithium bromide are 0.05 bar and 1 bar. The corresponding temperatures are 35 °C in the condenser, which is a reasonable temperature for a cooling water stream, and 100 °C in both the evaporator and generator, with an exit absorber temperature of around 160 °C. Care must be taken to ensure that the cycle does not operate to near the crystallisation line as this would inevitably cause operating difficulties. The maximum recommended lithium bromide concentration is 66- 68 %w/w, see Chapter 4, 'Experimental Studies'.

Hybrid Cycles.

In an attempt to make absorption cycles more efficient several researchers have been working on the development of advanced absorption cycles. Some examples of advanced cycles can be found in papers by S. Arh and B. Gašperšič [8] and W. Hölbling et al [140]. An example of an advanced cycle is proposed in Figure 1.12. The system couples two single stage cycles together, thereby enabling the use of different working fluid pairs in each cycle. An example of

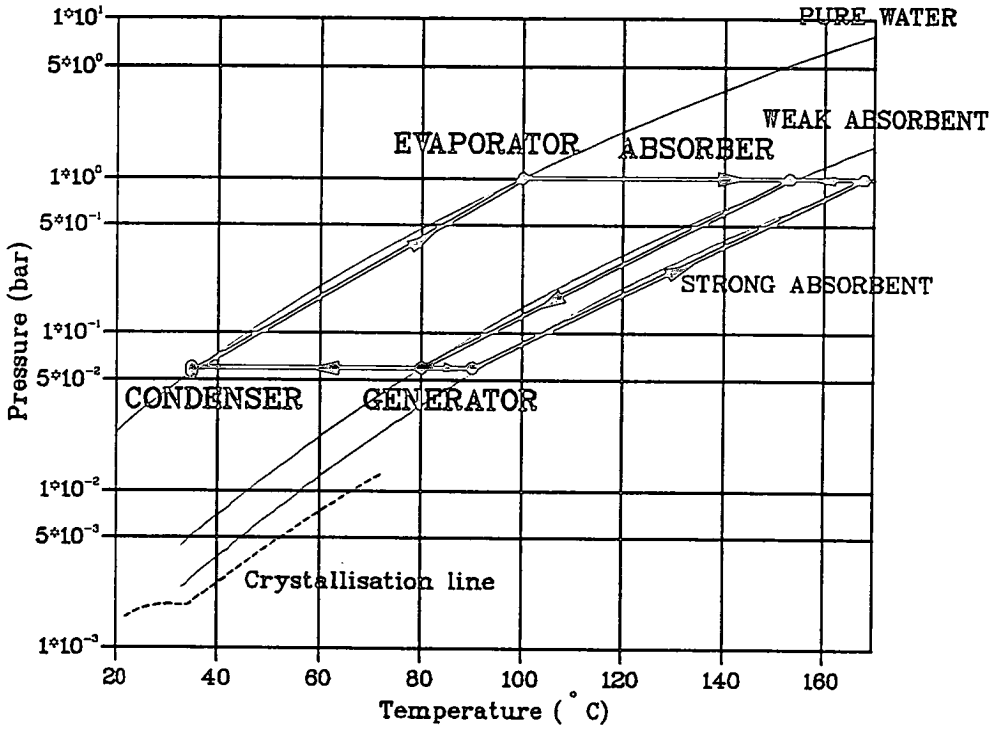

Figure 1.10: Representation of a heat transformer cycle on a P-T-x diagram, for H_2O/ LiBr.

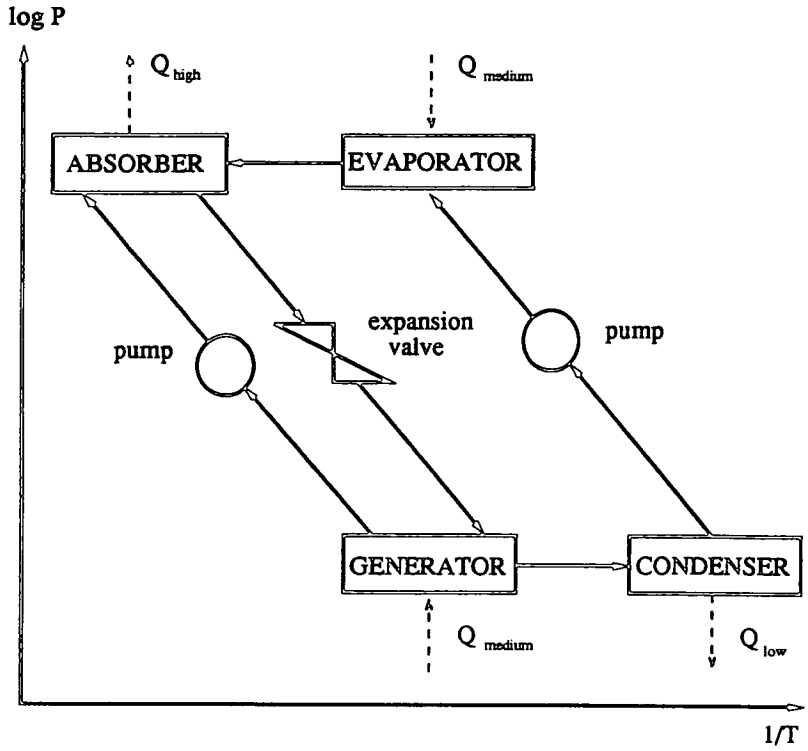

Figure 1.11: Representation of an A.H.T on a Van't Hoff plot.

this would be to have ammonia/ water operating in the low temperature cycle, with the evaporator operating at temperatures below zero, without difficulty; while the high temperature cycle could be operated with water/ lithium bromide without the need for an excessively high pressure on the absorber side, which would be necessary if ammonia/ water was used.

Another example of an advanced cycle is shown in Figure 1.13, which is commonly called a double effect cycle because of the double evaporator-absorber pair, although there is only one generator- condenser pair [140]. The cycle is designed to achieve a higher exit temperature from the second absorber, than would be possible with a single stage system. However, in order to achieve a higher temperature lift the efficiency of the cycle is reduced because a greater heat load is required in the generator, which has a larger absorbent solution inventory. A variation of this system uses a double generator- condenser pair

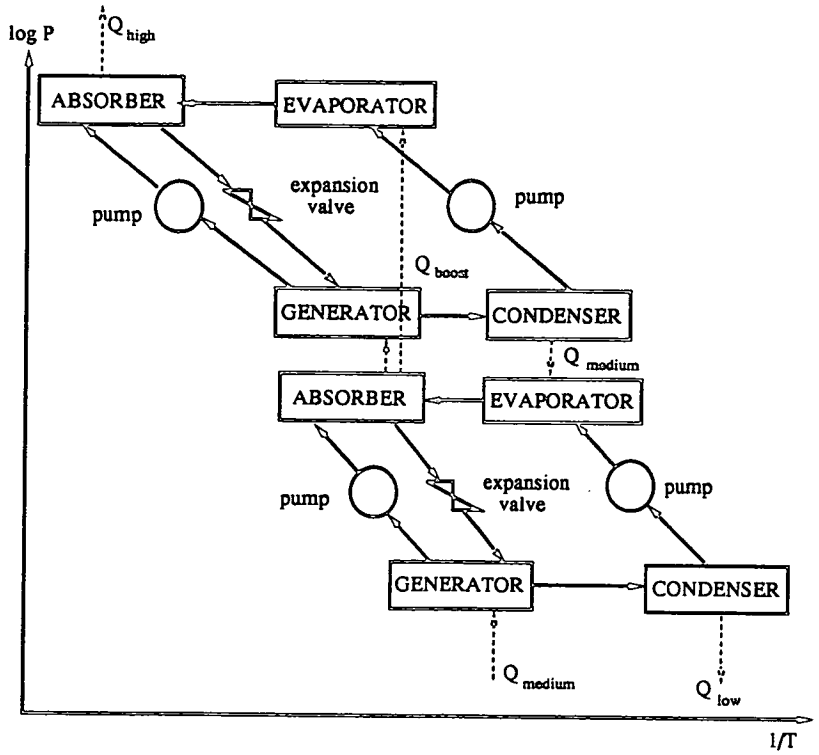

Figure 1.12: Example of a two stage absorption heat transformer.

and a single absorber- evaporator pair. Various other combinations of heat pump and transformer cycles are discussed in a paper by Alefeld [25].

Chemical Heat Pumps.

Solid chemical absorbents have also been used in heat pump cycles, where a refrigerant is absorbed into a solid absorbent, releasing the heat of reaction which is transferred to the heat sink. Once the absorbent is saturated with refrigerant it is then necessary to regenerate the absorbent bed by supplying heat to evaporate the refrigerant, which means that the cycle operates periodically. An example of a periodic cycle uses methanol as the refrigerant and calcium chloride as the solid absorbent, Figure 1.14 [25]. A continuous cycle could be designed which would have two units in parallel, with the process

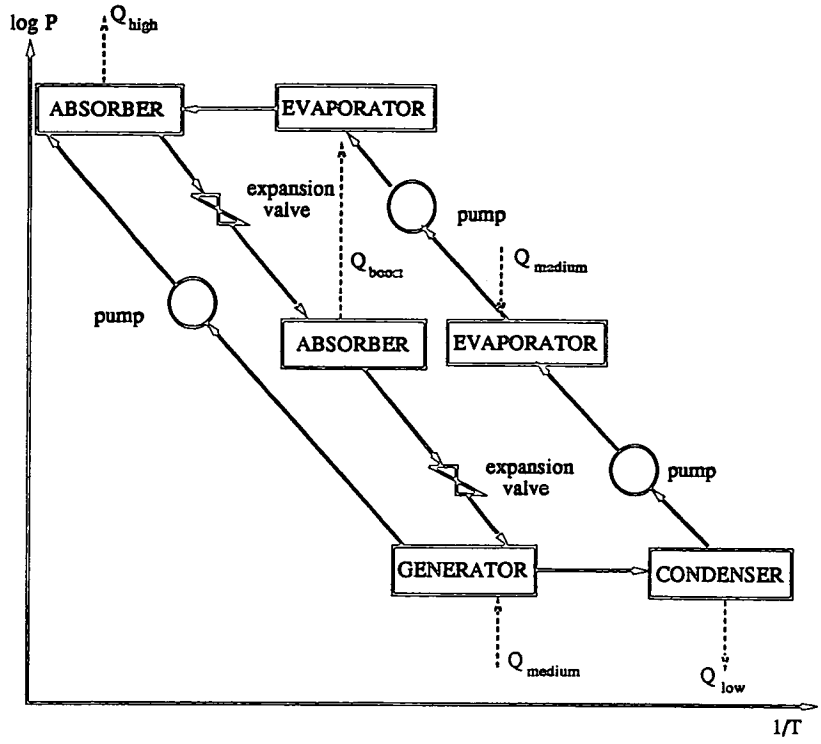

Figure 1.13: Representation of a double effect heat transformer.

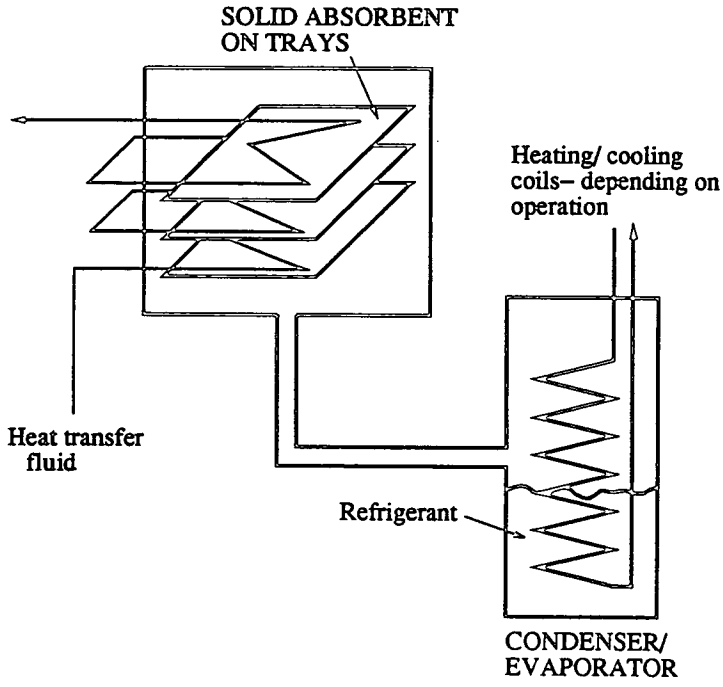

Figure 1.14: Example of a chemical heat pump- periodic operation.

switching beds when one cycle needs to be regenerated. Again, the use of solar energy as a heat source has been suggested. In order to make these cycles more efficient, studies have been carried out in order to enhance the heat and mass transfer characteristics of the absorbent bed .

1.3 Performance Criteria.

The most commonly used performance criterion for heat pump cycles is the coefficient of performance (COP). It is a measure of the amount of useful energy produced in a cycle divided by the amount of energy consumed. The COP of a cycle depends on its mode of operation- i.e whether it operates as a heat transformer (HT), heat pump (HP) or cooler respectively (Equations 1.2, 1.3 and 1.4).

$$COP_{HT} = \frac{Heat\ produced\ in\ absorber}{Heat\ consumed\ in\ the\ evaporator\ and\ generator} \tag{1.2}$$

$$COP_{HP} = \frac{Heat\ produced\ in\ the\ condenser\ and\ absorber}{Heat\ consumed\ by\ the\ generator} \tag{1.3}$$

$$COP_{Cooler} = \frac{Heat\ extracted\ in\ evaporator}{Heat\ consumed\ in\ generator} \tag{1.4}$$

The COP only gives a measure of the amount of heat produced it does not take into account the quality of the heat produced. A heat transformer must have a COP less than one, due to the fact that a proportion of the incoming energy has been upgraded to a higher quality, at the expense of downgrading the remainder to a lower level. Whereas, in a heat pump, a high grade energy stream is used to generate a larger quantity of lower quality heat. A better measure of the quantity of the heat produced is the enthalpic coefficient of performance, Equation 1.5. Another criterion which was proposed by Rivero and Le Goff [195] was the exergetic effectiveness of the cycle, defined as ζ, equation 1.6. The exergy terms are determined from a knowledge of the stream enthalpies and entropies ($\Delta H - T_o \Delta S$, where T_o is taken as ambient temperature).

$$COP_{Enth} = \frac{Net\ enthalpic\ increase\ in\ the\ absorber}{Net\ decrease\ in\ the\ evaporator\ and\ generator} \tag{1.5}$$

$$\zeta = \frac{Net\ exergy\ gain}{Net\ exergy\ supplied} \tag{1.6}$$

The temperature lift achieved by the cycle is another criterion which is used to measure the effectiveness of a cycle, it is a measure of the increase in temperature of the process stream being heated. Another definition, which is useful when considering a heat transformer cycle, is the difference between the exit temperature from the absorber and the temperature of the heat source. The heat source is usually a waste heat stream which is used in the evaporator and generator. The temperature lift therefore gives a measure of the effective temperature upgrading achieved by the heat transformer.

An important design parameter, which has been used by many workers, is the circulation ratio (F_r). It is the ratio of the absorbent solution mass flowrate to the mass flowrate of the refrigerant vapour. The ratio defines the flowrates of the streams around the cycle and hence the sizes of the individual components, which is turn can be used to give a rough costing of the system.

1.4 Scope of Project.

1.4.1 Energy Use in Drying.

Drying is a highly energy intensive operation and most industrial dryers operate on a single pass. Around 90 % of dryers employ hot gas as the heat transfer medium, discharging a hot, humid exhaust stream directly to atmosphere. It is a commonly used unit operation and each drying operation is product specific with some products being heat sensitive and others requiring drying to a specific moisture content. In wood drying it is important to ensure that the rate of drying does not cause the wood to warp. Table 1.1 [186] lists some of the dryer types currently used as well a brief description of their operation.

Approximately £110m year^{-1} is spent in the UK chemical industry [228] on providing energy for the drying of a wide range of products, examples of which are listed in Table 1.2 with further examples given in Masters' book 'Spray drying' (pp471- 475) [170].

Dryer	Brief description
Flash	Feed is exposed to a very hot gas stream for a few seconds- very high heat transfer rates.
Tray	Material is supported on trays and gas passed over/ through.
Conveyors	Material flows along a belt with gas passed over/ through.
Rotary	Product conveyed and showered into a rotating cylinder with hot gases passing over.
Spray	Feed sprayed into drying chamber- dried by direct contact with hot gas (co-/ counter- current flow).
Fluidised bed	Material to be dried is fluidised in a bed. Drying is achieved by fluidising with hot gases; may also have indirect contact heating coils within bed to aid the drying process.

Table 1.1: Brief description of a variety of drying operations.

Industry	Product	
Agriculture	Wood	Fertilisers
Biochemical	Pharmaceuticals	Yeast products
Chemical	Ceramics	Detergents
	Dyestuffs	Plastics
Food	Baby food	Egg- white, yolk, whole
	Fish	Milk- dried/ condensed
	Fruit	Vegetables
Manufacturing	Brick	China clay
	Gypsum	Paper/ board
	Plaster	Plaster board
	Textiles	Tiles

Table 1.2: Range of products dried industrially.

Spray Drying.

The product being dried usually enters the top of the drying chamber as a slurry. Nozzles or atomisers ensure that the feed stream gets evenly distributed within the chamber, which improves the mass and heat transfer between the hot gas stream and the solid particles. The inlet droplet size and the flow distribution within the drying chamber greatly affect the drying properties of the material being dried. A group at the AEA laboratory, SPS (Separation Process Services), have carried out extensive research into the modelling of the spray drying chamber, in an attempt to gain a better understanding of the drying mechanisms within the drying chamber [183]. It is essential that careful temperature control of the drying process is maintained to ensure that the dried solid meets the desired product specifications and that the final dried product does not become too dry otherwise it may decompose.

In most drying operations the exhaust gas stream has to be cleaned prior to discharge, as it usually contains fine particles of the dried product. There are different ways in which the gas can be cleaned before discharge including venturi scrubbers, cyclones, bag filters and electrostatic precipitators. These can be used individually or in conjunction with each other in order to improve the removal of particles from the exhaust gas stream. However, the stream is then usually vented to atmosphere without any heat recovery. The temperature of dryer exhaust streams is typically between 60- 80 °C, which is too low a temperature to justify heat recovery on economic grounds. In addition conventional methods of heat recovery could not be used because the process streams are humid gases.

The exhaust gas from the stack often causes an unsightly, visible plume that may still contain some fines material which could be deposited over the surrounding area. As most dryers use direct fired burners to generate the high temperatures required for drying, the exhaust gas stream contains carbon dioxide which is also released into the atmosphere. Therefore, economical and environmental reasons are forcing companies to look at ways to recover and recycle heat.

1.4.2 Heat Recovery From Dryers.

In the UK, the 'Energy Technology Support Unit' (ETSU) set up a program to increase the energy efficiency of dryers [119]. They found that potential savings of around 20 % could be achieved with little or no expenditure. The following were identified as areas where improvements could be achieved through better care of the dryers:

- Prevention of gas leaks into/ out of the chamber.
- Making sure the drying unit is kept clean.
- Better temperature control.
- Optimisation of the dryer conditions and flows.

The heat recovery from exhaust gas streams would also help to reduce the energy consumption of the dryer and therefore improve the dryer efficiency, however, this requires a greater investment by the company. Several booklets and guides have been produced by ETSU to increase energy efficiency awareness

and to encourage others to adopt heat recovery methods [121]. The scheme was set up in 1978 and by December 1985 250 demonstration projects had been established. It was estimated that savings of around 1.5 Mtce year^{-1} [1], valued at £30M had been achieved [119].

In an industrial spray drying operation, typical inlet gas temperatures are 500 °C, whilst saturated exhaust gas is vented at temperatures between 60- 80 °C (absolute humidity 0.16- 0.56 g- $_{H_2O}$ (g-$_{dry\ air}$)$^{-1}$). The scope for energy recovery is immense, particularly if the latent heat associated with the water content of the gas stream can be recovered. Some operations do attempt to recover the sensible heat associated with the exhaust gas stream, Figure 1.15 [31]. Another option for the recovery of heat is to use a conventional heat pump. However, in order to recover the latent heat the water vapour must be condensed, which in turn saturates the exhaust gas and leads to a visible plume from the stack.

1.4.3 Project Aims.

In order to recover and recycle the heat currently vented to atmosphere from a spray drying operation it was necessary to develop a system which simultaneously dehumidified and reheated the exhaust gas stream. The stream would then be suitable for recycle to the drying chamber, thereby reducing the overall energy consumption of the drying operation. For the process to be economically viable the temperature of the exit gas stream had to be boosted from around 80 °C to between 150- 200 °C. As well as reheating the gas stream it was also necessary to dehumidify the gas prior to recycling to the dryer inlet, otherwise the mass transfer driving force within the drying chamber would be

[1] Mtce year^{-1} = Million tonne coal equivalent per year

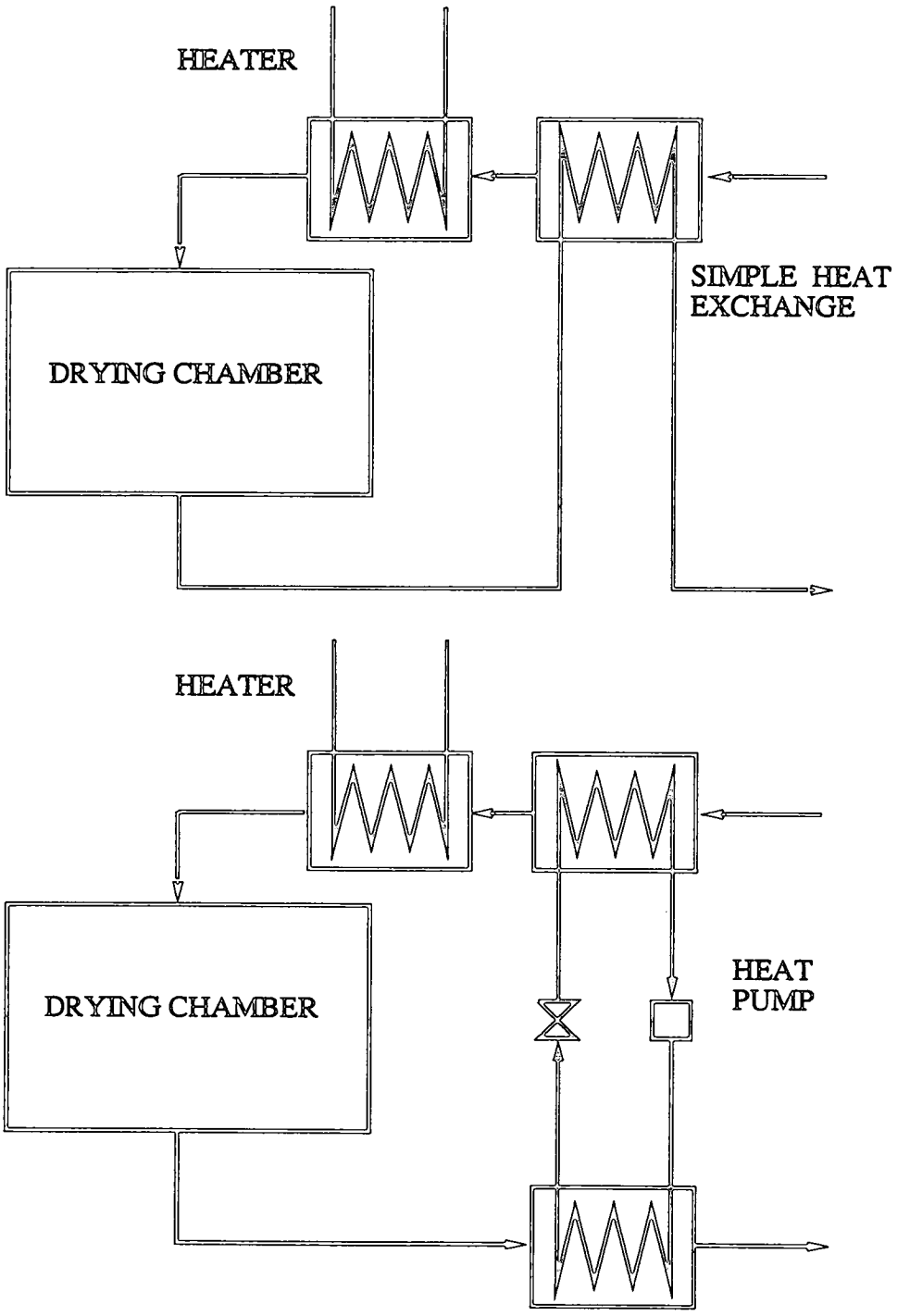

Figure 1.15: Examples of simple heat recovery from dryers.

reduced because of the increase in the partial pressure of water, thereby decreasing the efficiency of the drying process.

An absorption heat transformer was chosen as a means of dehumidifying and reheating the gas stream by direct contact with an absorbent stream. The water in the gas stream acts as the refrigerant, which was absorbed into the absorbent solution causing the temperature to increase. Figure 1.16 shows a simplified diagram of an open loop heat transformer. Lithium bromide was chosen as the absorbent solution for this study as it is highly hygroscopic and has favourable heat transfer properties.

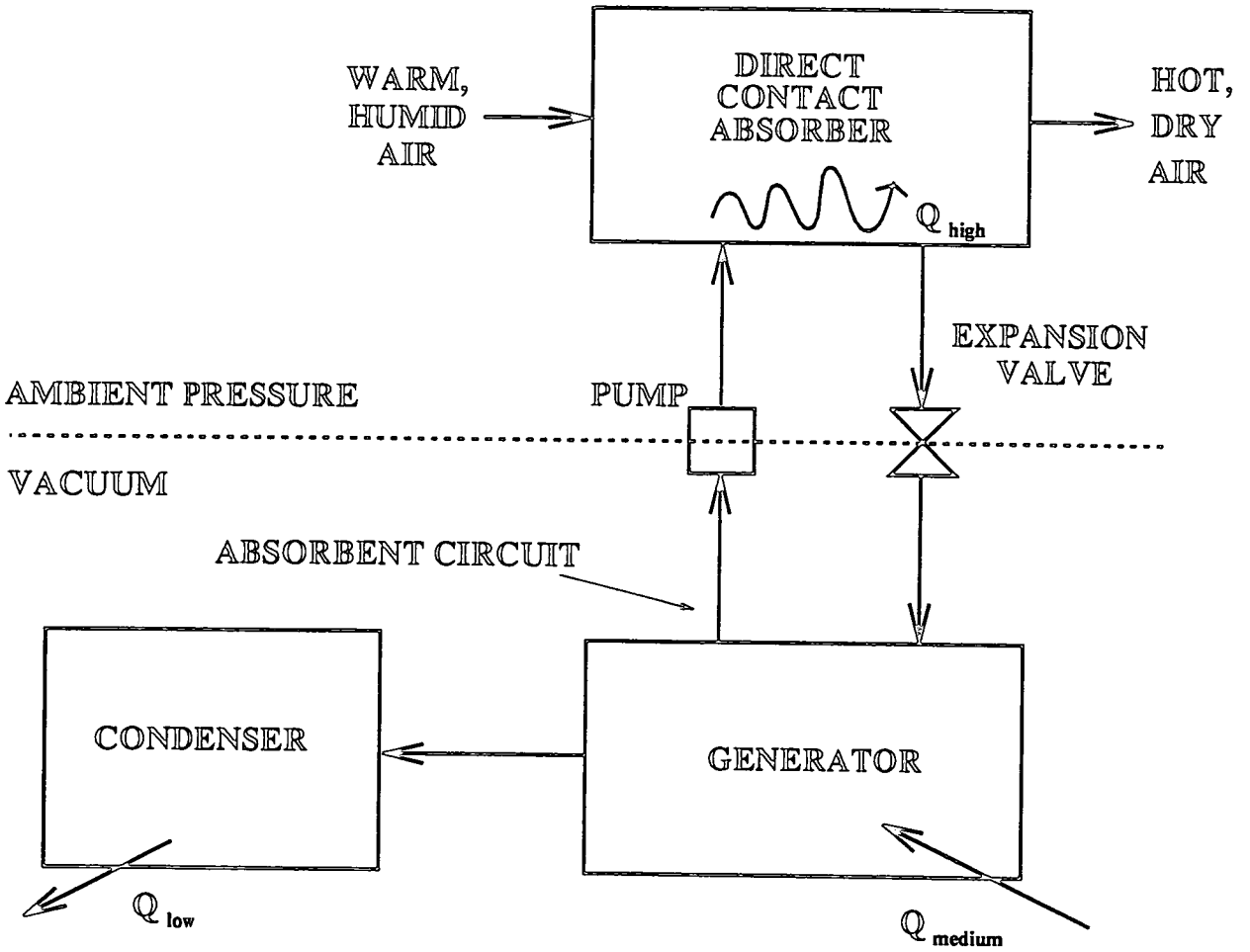

Figure 1.16: Single stage open loop absorption heat transformer.

An experimental pilot plant was constructed to investigate the performance of this type of heat transformer, Chapter 3 'Design and Construction'. Initial expectations were to achieve an exit temperature from the absorber of between 150- 200 °C, whilst also dehumidifying the gas stream from an initial absolute humidity of 0.20 g- $_{H_2O}$ $(g\text{-}_{dry\ air})^{-1}$ to between 0.03- 0.05 g- $_{H_2O}$ $(g\text{-}_{dry\ air})^{-1}$. Experimental results are presented and discussed in Chapter 4 'Experimental Studies'. Coupled with the experimental studies a computer model was written to simulate the absorption process, see Chapter 5, 'Computer Simulation Studies'. A study of the spray drying process was also undertaken, details and results of this study are provided in Chapter 6, 'Industrial Case Study'.

Chapter 2

Absorption Working Fluids.

2.1 Overview.

At present the application of absorption heat cycles (pumps and transformers) is restricted. Absorption cycles are mainly used for air conditioning and chilling duties. There are also a few examples of solar assisted absorption cycles which provide cooling and air-conditioning in buildings. The most common working fluid pair used in absorption cycles is water/ lithium bromide (LiBr). However, the use of water/ lithium bromide has its limitations because of crystallisation problems.

It has therefore become necessary to find alternative working fluids for absorption cycles for use in both industrial and domestic applications. Extensive work has already been carried out into finding new working fluids, as well as the development of new absorption cycles thereby ensuring the continued advancement of absorption technology.

A further area of research involves the use of heat transformers as heat recovery systems with the ability to achieve exit temperatures of around 200 °C from the absorbers. However, this would require working fluids which were capable of operating at high temperatures without decomposing.

The use of vapour compression cycles as refrigerators and heat pumps is more widespread. However, as a result of the Montreal Protocol it has become necessary to replace the CFC working fluids commonly used in these cycles. Therefore there is a potential market for reliable and efficient absorption cycles which would replace vapour compression units.

The following sections in this chapter deal with the applications of absorption cycles and the working fluids currently used in these systems. The potential for operating absorption cycles with new working fluids is also discussed.

2.1.1 History.

The principles of absorption heat generation date from the beginning of the 19^{th} Century when Leslie devised the first absorption cycle. Two vessels, one containing sulphuric acid the other water, were connected via a tube. A hand pump was used to establish a vacuum within the system thereby increasing the

rate of absorption of water into the sulphuric acid. As water vapour was absorbed into the acid, the temperature in the water vessel decreased because heat was being used to evaporate the water, which was being transferred to the acid vessel. Eventually the water temperature dropped to 0 °C, causing the remaining liquid to freeze. This process operated intermittently and once the mixture had reached a state of equilibrium it was then necessary to regenerate the sulphuric acid [15].

In the 1850 E. Carré developed the idea further and constructed a sulphuric acid/ water engine for the purpose of producing ice. F. Carré then patented a design for an absorption chiller which used ammonia and water as the working pair in 1862 ([141] and [209]). Vapour compression cycles were also under development around the same time and they became the preferred system for refrigeration because they were more efficient than the absorption cycles.

The manufacture of absorption machines experienced a renaissance following World War I as energy costs rose and the potential for utilising waste energy became important. In 1918 Altenkirch outlined the principles for the absorption heat transformer (described in Chapter 1, 'Introduction'). Nesselmann (a colleague of Altenkirch for some years) provided more comprehensive details of the absorption heat transformer in 1933 [210].

In the United States in the late 1950s, heat pump cycles, using ammonia/ water as the fluid pair, were developed for air conditioning duties. Indeed this type of absorption heat pump cornered the market until the mid 1970s, when reliability problems forced many manufacturers to stop making these units [39].

2.2 Desirable Fluid Properties.

As the drive to conserve energy becomes more important, the potential applications for absorption heat pumps and heat transformers increases making it necessary to develop systems to cope with this. Ammonia/ water and water/ lithium bromide systems are limited in their uses making it necessary to find new working fluids. The selection of an optimal working fluid pair for a particular application is an important parameter as it directly affects the cycle design and operation.

In order to evaluate new working fluids, criteria must be established to screen potential candidates. A range of the most important criteria used to evaluate potential refrigerant and absorbent mixtures have been proposed, a summary of which is provided in Table 2.1 ([3], [19], [145], [168], [194]).

The ideal working fluid pair should contain a refrigerant with a high latent heat of vaporisation. A large latent heat minimises the flow of refrigerant around the cycle, per kW of heat delivered. As a result the capital and operating costs of the cycle are reduced. From that point of view water is a particularly good refrigerant because its heat of vaporisation is 2257 $kJkg^{-1}$. Other potential refrigerants are trifluoroethanol (TFE), 2210 $kJkg^{-1}$, and hexafluoroisopropanol (HFIP), 3604 $kJkg^{-1}$ [152].

The difference between the pressure levels of the cycle should be kept as small as possible in order to minimise pumping requirements. The low pressure side of the heat transformer should be greater than 1 bar, so as to avoid using vacuum equipment. The high pressure side should not exceed a maximum pressure of 25 bar, thereby removing the need for expensive, high pressure equipment. In addition, it is not recommended to operate the cycle at pressures less than 0.01

Property	Reason
Large heat of vaporisation (refrigerant)	Reducing the fluid flow in the refrigerant circuit.
Low pressure differential between pressure levels	Reduces the required pumping energy.
Large difference in the boiling points of the refrigerant and absorbent	No rectification
Low solution viscosity	Reduces the pumping energy
High solution density	Reduces the pumping energy
Low solution heat capacity	Lower heat flux- smaller, cheaper exchangers
High thermal and chemical stability of both fluids	Do not want decomposition during normal operation
Feasible pressure range	Do not want to operate at high pressures. Easier to construct- less weight; cheaper.
Feasible temperature range	Solution must be able to meet design requirements
Nontoxic	
Nonflammable	
Noncorrosive	
Cheap	
Low environmental impact	
Readily available	

Table 2.1: Desirable mixture properties.

bar or greater than 50 bar as this adds considerably to the equipment cost.

The minimum difference in boiling points between the components should be greater than 150 degC so as to avoid the need for a rectification stage. The solution viscosity should be less than 10 cp (100 Nsm^{-2}) and the specific gravity at least 1.5, which means that the solution pumping requirements are kept low. The heat capacity of the solution should also be as small as possible, thereby reducing the heat flux in the solution heat exchanger and hence reducing its size and cost.

In addition to meeting the above thermodynamic and transport property requirements, it is necessary to ensure that the fluid pair has a low toxicity, is nonflammable and that its ecological impact is low. In Britain the COSHH[1] regulations control the use of hazardous chemicals. These regulations should be consulted to ensure that the correct safety precautions are adhered to during normal operation of the absorption cycle[122]. Low cost and high availability are also important features which must be investigated when choosing a fluid pair. Finally, the corrosive nature of the fluids affects the choice of construction materials and hence the capital cost of the equipment. Therefore, it is desirable to use a non- corrosive mixture so as to avoid the use of expensive and exotic construction materials. All of these factors must be considered when evaluating fluid pairs for a particular application.

[1]Control of Substances Hazardous to Health

2.3 Absorption Cycle Applications.

Table 2.2 illustrates some of the applications of industrial absorption units. Other examples of industrial applications have been reported by Plöcker [115] and also by CADDET [2][71]. CADDET also provides some examples of operating experiences with absorption heat transformers.

2.3.1 Industrial Applications.

The literature reviewed only contained a few examples of industrial absorption cycles. As such, operating experience with these systems was limited. The following section provides more background on the operating conditions and the performance of each of the examples as summarised in Table 2.2. Details of operational problems experienced with these examples are also discussed.

Domestic solar absorption chiller, Colorado, USA. Evacuated tubular solar collectors, using ethylene glycol/ water as the fluid in the collectors, were used to provide heat for an absorption unit. The generating temperature ranges between 70- 88 °C. Water/ lithium bromide was used as the working fluid pair in a state of the art chiller. As a comparison the operating temperature in the generator would need to be 90- 180 °C if ammonia/ water was used as the working fluid pair, depending on the type of heat rejection equipment. The duty of the chiller was 10.6 kW. [55]

[2]CADDET= Center for Analysis and Dissemination of Demonstrated Energy Technologies

Operation	Working fluid	Duty	Installed	Use	Ref.
Absorption cooler	H_2O/ LiBr	11 kW	1977	Space cooling	[55]
Heat pump	H_2O/ LiBr	1 MW	Oct. 1980	Water heating using waste heat	[151]
Heat pump	H_2O/ LiBr	7 MW	Nov. 1984	Heat to district heating using excess steam	[93]
Heat transformer	H_2O/ LiBr	6.7 MW	Oct. 1985	Produces steam from waste heat	[23], [149]
Heat transformer	H_2O/ NaOH	200 kW	1993	Inc. energy efficiency in a pulp mill	[58]
Absorption machines	H_2O/ LiBr	n/a	n/a	Chilling. Heating.	[158], [159] [160]

Table 2.2: Industrial examples of absorption cycles.

Heat pump. Dyeing plant, Osaka, Japan. This particular absorption cycle recovered heat from a waste water stream which was available at a temperature between 20- 50 °C. The heat source used in the generator was city gas, which was readily available and relatively cheap. The government promoted the use of non- petroleum fuel sources and a special tariff was available for use in energy saving applications. Hot water obtained from the unit is delivered at a temperature of about 80 °C.

A vapour compression heat pump was also considered instead of the absorption cycle. However, the efficiency of compression cycles drops drastically as the operating temperature increases, whereas the performance of absorption cycles remains approximately constant. Therefore the absorption cycle was the preferred option due to its greater flexibility of operation. The waste water stream was alkaline, a consequence of the dyeing process. Therefore the material of construction of the unit was stainless steel (type 316), which was also compatible with concentrated lithium bromide solutions. [151]

Heat pump. District heating, Trollhättan, Sweden. Two waste energy streams from a chemical plant were available at 150 °C and 60 °C (excess 10 bar steam and cooling water). They were used as the heat sources for an absorption heat pump. The heat pump had a duty of 7 MW, which was used to provide hot water to the district heating system at a temperature between 57- 75 °C. The working fluid pair used was water/ lithium bromide. Corrosion inhibitors were added to the solution to prevent corrosion. The cycle had been 100 % reliable and worked well even under part load. [93]

Heat transformer. Ethylene amine plant, Delfzijl, Netherlands. A heat transformer with a maximum capacity of 6.7 MW was commissioned in Delfzijl in October 1985. The unit was capable of producing 11 tonnes $hour^{-1}$ of steam at 145°C and 4.6 bar. Water/ lithium bromide was chosen as the working fluid. The materials of construction were titanium and stainless steel. After six months of trouble free operation at maximum capacity the transformer began to leak due to corrosion. The unit continued to operate at 30% of its maximum capacity without difficulty.

A study was set up to find ways to reduce the corrosion occurring in the transformer. Extensive studies were carried out using different compounds to try and find the best inhibitor and the optimum concentration required. At the time of construction of the unit there were only about 15 industrial heat transformers being used worldwide and operating experience was limited. The company felt that a data base should be set up cataloguing operating experience and problems, in an attempt to prevent the same problems being made by someone else. [149]

Heat transformer. Evaporation plant, Lund, Sweden. Following the successful testing of a 10 kW pilot plant, a full scale heat transformer was constructed at a pulp and paper mill in Lund, Sweden. The unit had a capacity of 200 kW and was designed to reduce the live steam consumption of the evaporation plant by 18.5 %. The heat transformer was incorporated into the last evaporator effect of the process and boosts the temperature of the unit from 70-101 °C. The working fluid pair in the unit was water/ sodium hydroxide, which was chosen because the operators were already familiar with its use. An extensive experimental study is under way to test the unit and find the optimal operating conditions.

Tokyo Gas Company Ltd. Absorption machines. In Japan absorption air conditioning equipment is readily used ([158], [159], [160]). There are three types of absorption machine manufactured by Tokyo Gas Company Limited, these are summarised in Table 2.3.

Type	Absorption refrigerating machine	Absorption water chiller- heater	Absorption heat pump
Function	Chilled water (4- 15 °C)	Chilled water (4- 15 °C) Hot water (40- 80 °C)	Hot water (50- 80 °C) Steam (140 °C or higher)
Input to generator	Steam, hot water ..	City gas, exhaust gas	City gas, waste hot water, waste steam
Application	Air- conditioning, cooling for process	Air- conditioning and heating	Hot water, heating

Table 2.3: Types of absorption machine used in Japan.

Absorption machines gained widespread acceptance in Japan following technical improvements back in the early 1970s, which made them more efficient, smaller and more reliable. These machines have played a major role in providing heating and air-conditioning for both individual buildings and district plants.

85 % of the machines used were of the chiller- heater type, which were developed in 1968. In 1983 a double effect type machine was introduced onto the commercial market. Since then, technological advancements have resulted in improvements to the double effect cycle. The areas where the heat pump was developed included increasing the efficiency of the solution heat exchangers, and also reducing the amount of absorbent fluid circulating in the system. Gas was used as the heat source for the generator because it was available at a special tariff. The machines had an expected lifetime of 15 years.

The most common working fluid pair used for absorption chillers was water/ lithium bromide because water has a high latent heat of vaporisation and also because lithium bromide is relatively harmless and chemically stable. Ammonia/ water was not used because of its toxic and flammable nature.

Research in Japan is currently under way to develop a machine which uses air as the low temperature heat source, instead of water which is currently used. However, during the winter months, when the unit is required for heating, the outside air temperature is around 0 °C. At such a low temperature it is difficult to use water as the refrigerant. Therefore, a double effect absorption unit has been developed which uses R22/ TEGDME (tetra ethylene glycol dimethylether) on the low pressure, low temperature side and water/ lithium bromide on the high pressure, high temperature side. Another alternative which had been suggested was the replacement of water with methanol, thus permitting a source temperature less than 0 °C because the freezing point of methanol is -97.7 °C.

2.3.2 Research Applications.

A summary of recent research activities relating to all aspects of absorption cycles and working fluids is provided in Table 2.4. These examples will be discussed in the following section.

University of Salford, UK. Theoretical and experimental studies. Several papers on the topic of heat pumps and transformers were published by the group at Salford between 1986- 1988. The papers comprised both experimental and theoretical work. The experimental setup consisted of a small glass heat pump from which the performance could be assessed depending on the operating conditions and the working fluid.

The fluids used for the experimental studies were aqueous solutions of lithium bromide, lithium chloride, calcium chloride and a (1:1 %w/w) mixture of lithium chloride- calcium chloride. Lithium bromide was studied as a possible absorbent because of its high solubility in water, favourable heat transport properties (high density, low heat capacity) and negligible vapour pressure in solution. However, its use was limited due to the risk of crystallisation at high concentrations and also its corrosive nature. Lithium chloride and calcium chloride were chosen as alternative working fluids because they were not as corrosive and were also cheaper than lithium bromide. Unfortunately their thermodynamic properties are not as good as those of lithium bromide. Analysis of the experimental results for the heat pump showed that aqueous lithium chloride cycle achieved higher temperature lifts than a unit using aqueous calcium chloride, however, the COP was lower.

Institute	Working fluid	Mode	Research	Reference
Uni. of Salford, UK	H_2O/ CaCl +LiCl H_2O/ LiCl, H_2O/ CaCl, H_2O/ LiBr, NH_3/ H_2O	HT/ HP	Theor^l & Expt^l	[107], [83], [84], [111], [61], [62]
Uni. of Salford, UK	H_2O- ethylene glycol/ LiBr	HP cooler	Expt^l	[85]
Uni. di Napoli, Italy	H_2O/ H_2SO_4	HT	Expt^l	[27]
Ecole Nat. Sup. d' Ing^r, Toulouse, France	Glycerol/ water	HP	Theor^l	[94]
Lab. de Energia Solar (UNAM), Temixco, México	NH_3/ $LiNO_3$	HT/ HP	Theor^l	[108], [109]
Uni. of Tech., Delft Netherlands	Trifluoroethanol/ Pyrrolidone	HT	Theor^l Expt^l	[224], [232]
Lab. des Sciences, Nancy, France	Water/ ethylene glycol	HT	Theor^l & Expt^l	[100], [103]
NRC, Ottawa, Canada	H_2O/ NaOH	HP	Theor^l	[207]
NCL, Pune, India.	H_2O/ LiI	HT/ HP	Theor^l	[76], [77], [78]
E.N.S.I.G.C. Toulouse, France.	H_2O/ $CaCl_2$- LiCl	HP	Theor^l	[47]
C.N.R Institute, S. Lucia, Italy.	NH_3- H_2O/ KOH	HP	Theor^l	[59]
Uni. of Padua, Italy	H_2O/ LiCl	HT	Theor^l: drying	[199], [200], [201]
Uni. of Lund, Sweden	H_2O/ NaOH, H_2O/ LiBr	HT/ HP	Expt^l & Theor^l (see also Table 2.2)	[1], [42], [43], [45], [58], [70], [128], [129], [130], [131]

Table 2.4: Absorption heat pump and heat transformer research activities.

HT- Absorption heat transformer; HP- Absorption heat pump

The theoretical studies investigated the performance of both absorption heat pumps and heat transformers. The following working fluid pairs were used- water/ calcium chloride, water/ lithium chloride (heat pump) and water/ lithium bromide, water/ lithium chloride and ammonia/ water (heat transformer) [107]. The results for the heat transformer showed that the COP for aqueous calcium chloride was best at low temperatures; while lithium chloride solutions were better at high temperatures.

All the papers reviewed indicated that as the flow ratio (absorbent/ refrigerant mass flow) was increased there was a corresponding drop in the COP. This was due to the fact that as the ratio was increased, more fluid was circulated around the system leading to greater heat losses, an increase in the pumping duty and also the heat load of the solution heat exchanger.

Another project conducted at the University of Salford was a feasibility study of an absorption cooler using water/ lithium bromide [68]. Experimental results showed that temperatures of around 10 °C could readily be obtained in the evaporator without crystallisation problems being encountered. A later study used a ternary mixture of water- ethylene glycol/ lithium bromide in an attempt to achieve lower operating temperatures in the evaporator. Ethylene glycol was used because it has a low freezing point, -11.5 °C, and a high miscibility in water. However, adding ethylene glycol to the solution increased its viscosity and so a mole ratio of 1 part ethylene glycol: 15 parts water was used. Results show that a temperature of 8 °C was possible in the evaporator. The heat loads and the COP of the ternary working fluid were higher than of the binary mixture.

Universita' di Napoli, Italy. Theoretical modelling. A simplified model of a heat transformer was developed to investigate the optimum operating conditions for the cycle. The performance criteria studied were the COP, the enthalpic efficiency and enthalpic value of the heat. The working fluid pair chosen was water/ sulphuric acid. This mixture was chosen in preference to water/ lithium bromide because it did not suffer from crystallisation problems at high absorbent concentrations. Ammonia/ water was discarded as a viable option because of its toxicity, flammability and the need for a high operating pressure. The results of the study indicate that the temperature lift was limited, suggesting that a two stage process would be preferable.

Ecole Nationale Supérieure d' Ingénieurs, Toulouse, France. Theoretical modelling. A simulation model investigating the performance of an absorption heat pump cycle utilising water/ glycerol as the working pair was studied by this group. Glycerol was chosen as the absorbent fluid instead of the commonly used lithium bromide because it is non-corrosive and does not pose any crystallisation problems. However, the separation of the water from the solution mixture was incomplete, which affected the performance of the cycle. In addition, the maximum operating temperature of the system could not exceed 200 °C because of glycerol decomposition. This restricted the applications which would be suitable for operation with this particular fluid pair.

The cycle was simulated in two different modes: partial evaporation with complete condensation of the vapour and partial evaporation with partial condensation followed by total condensation, Figure 2.1. The performance of the two stage condensation (rectification) cycle was greater than that of the single stage, total condensation cycle. In addition, it was also possible to achieve 99 %w/w pure water vapour from the evaporator using the two stage process.

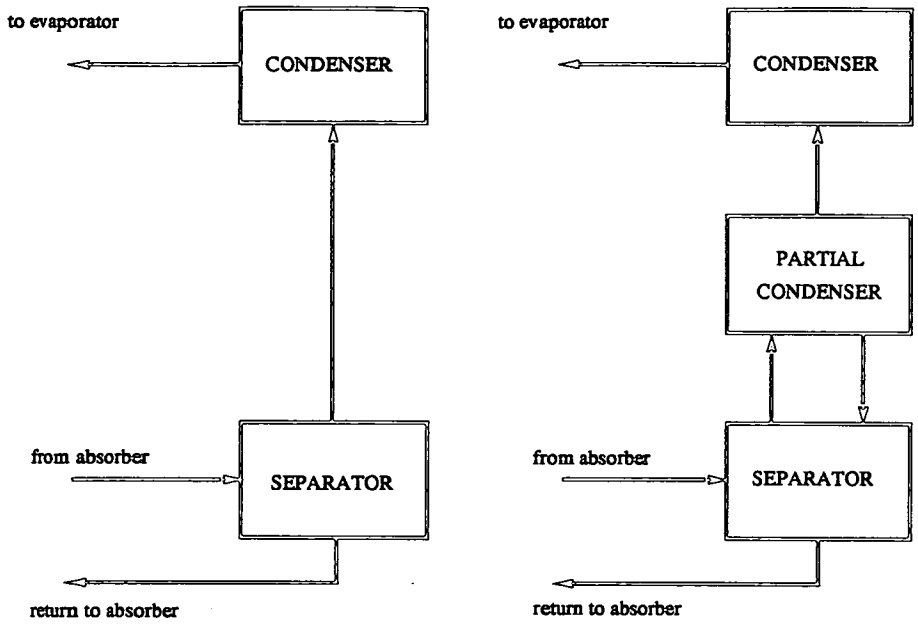

Figure 2.1: Partial evaporation with a) total condensation b)two stage condensation.

Laboratorio de Energia Solar de la UNAM, Temixco, Mexico. Heat pump simulation studies. The simulation of an absorption heat pump cycle operating at an evaporator temperature of -10 °C was carried out using ammonia/ lithium nitrate. The generator operated at a temperature of around 90 °C, which was of particular interest when using solar energy as the heat source for the cycle because it was generally available at this temperature. Ammonia/ water was not a feasible alternative because a generator temperature of 115 °C would be required in order to produce an evaporator temperature of -10 °C. The thermodynamic data used in this research was taken from a paper by Ferreira [125]. The results obtained from the simulation study indicated that the circulation ratio was as an important design parameter. The Carnot COP and the enthalpic COP were also presented for a range of operating temperatures.

Delft University of Technology, Delft, Netherlands. Absorption heat transformer test plant. The Refrigeration Laboratory at Delft University have carried out a wide range of research on absorption systems. Their investigations include a domestic absorption heat pump, using a ternary mixture of methanol/ lithium bromide- zinc bromide as the working fluid. Other work involved a solar driven refrigeration machine, using ammonia/ water as the working mixture and also fundamental research into heat and mass transfer phenomenon in falling film absorbers. The latest project concerned the design and construction of a 20 kW heat transformer.

After an extensive literature survey the group selected trifluoroethanol (TFE)/ pyrrolidinone (Pyr) as the most promising working pair despite the relative toxicity and cost of TFE. Advantages of this pair included a difference in boiling points between the components of 171 °C, avoiding the need for rectification; high solubility of the refrigerant in the absorbent; no crystallisation of the solution; and moderate refrigerant vapour pressures at high temperatures, thereby, reducing equipment costs. The solution also has a low viscosity and is thermally stable up to 200 °C.

A computer simulation model of the heat transformer was also developed in conjunction with the test rig to validate results [232]. The work of Zhuo investigated the influence of varying the operating conditions of the transformer so as to find its optimum performance. The two parameters which were of primary interest were the exit temperature and the amount of useful heat delivered.

Laboratiore des Sciences, Nancy, France. 'Reverse-rectification' heat pump. There is a demand for heat pumps to deliver heat at temperatures greater than 150 °C. However, it is difficult to construct a heat pump to achieve this. Common working fluids are unsuitable for such high temperatures: aqueous lithium bromide is highly corrosive, ammonia would require very high operating pressures and fluorocarbons are thermally unstable. A novel heat pump was constructed based on a multi-stage absorption column. Pure liquid absorbent enters at the top of the column where it is mixed with the refrigerant vapour causing the temperature of both streams to increase, the heat of absorption is then extracted. A test rig using a pentane/ octane mixture as the working pair obtained an exit temperature of 115 °C. The system was also successfully tested with a water/ ethylene glycol mixture achieving an exit temperature of 185 °C.

National Research Council, Canada. Theoretical absorption heat pump for wood drying. An open cycle absorption heat pump has been designed with a view to recovering waste heat from a wood drying operation. The cycle was designed using sodium hydroxide which is less corrosive and cheaper than lithium bromide. The purpose of the plant was to reheat and dehumidify an air stream from inlet conditions of 77 °C and 0.15 g- $_{H_2O}$ (g-$_{dry\ air}$)$^{-1}$ to 106 °C and 0.11 g- $_{H_2O}$ (g-$_{dry\ air}$)$^{-1}$, using a 60 %w/w sodium hydroxide solution. The next stage of this study was to be the construction of a laboratory scale rig to test these design conditions. However no other papers by this research group were found and so it was not known how well the cycle performed.

National Chemical Laboratory, Pune, India. Performances of a heat pump and a transformer. Design data were provided for various absorption cycles using a water/ lithium iodide mixture as the working medium. The cycles investigated were an absorption heat pump for cooling and heating and a heat transformer ([76], [77], [78]). The group also determined experimental thermodynamic data for the binary mixture, presenting it in a form suitable for use in computer programs. Thermodynamic data was also produced for a variety of other working fluid pairs ([75], [79]).

E.N.S.I.G.C., Toulouse, France. Theoretical studies and data measurements. The ternary mixture, water/ calcium chloride- lithium chloride (1: 1 %w/w), was proposed as an alternative working fluid mixture for use in absorption heat pump cycles. The preliminary experimental program established a set of reliable thermodynamic equations for this ternary fluid. Simulation studies investigating the performance of a heat pump cycle found that the COP of the cycle, operating with the ternary mixture, was inferior to a cycle employing water/ lithium bromide. It was concluded that the combination of cycle performance and fluid cost made the ternary mixture a viable alternative for use in absorption cycles ([47]).

C.N.R Institute, S. Lucia, Italy. Theoretical study of an absorption heat pump. A novel absorption heat pump cycle was proposed, which used two refrigerant- absorbent mixtures. The proposed working fluids were ammonia/ water and water/ potassium hydroxide. Conventional absorption cycles utilising ammonia/ water as the working mixture require rectification to ensure complete separation of the ammonia and water in the evaporator. This particular cycle replaced the normal evaporator used with a desorber, Figure 2.2. The water/ ammonia mixture leaving the absorber entered the desorber,

where rich potassium hydroxide solution absorbed the water. The ammonia was then evaporated and returned to the absorber. In the generator water was vaporised, before then being fed to the condenser. The liquid water was then mixed with the ammonia vapour in the absorber. Early analysis of the performance of the heat pump was encouraging, however, a more detailed study and optimisation was being conducted.

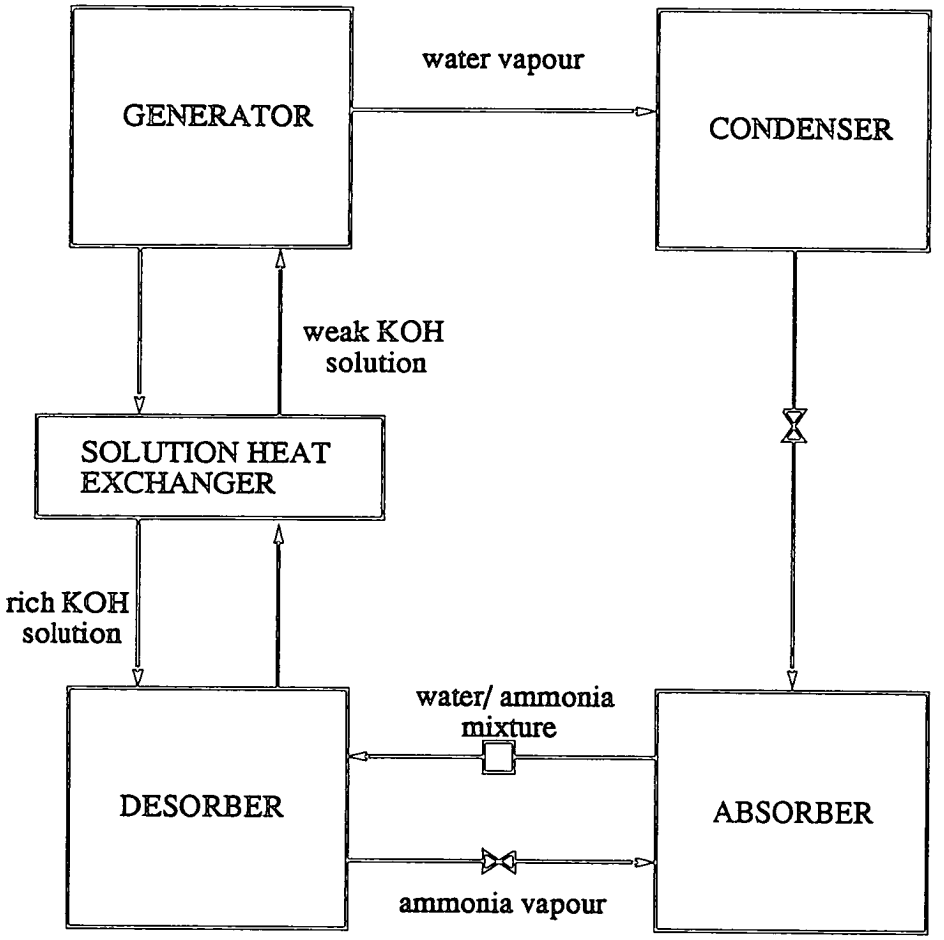

Figure 2.2: Absorption cycle operating with NH_3/ H_2O and H_2O/ KOH.

University of Padua, Italy. Theoretical studies with reference to air dehumidification. Scalabrin developed an absorption system for the dehumidification of dryer exhaust streams. A schematic of the drying operation with the absorption cycle is shown in Figure 2.3. The absorption system proposed uses a direct contact process to dehumidify the dryer exhaust stream

with aqueous lithium chloride. The absorbent solution is then regenerated by using an external air source to strip the absorbed water from the liquid stream. The materials being dried are heat sensitive, therefore the temperature of the dryer was low, ranging between 20- 48 °C.

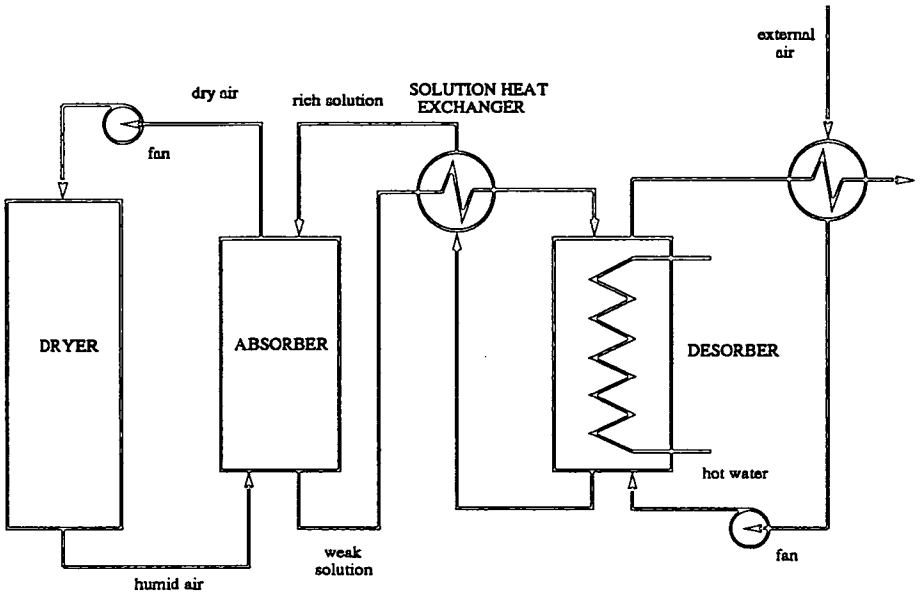

Figure 2.3: Open cycle low temperature dryer- dehumidifier.

The purpose of the research was to verify the validity of using an absorption system to dehumidify dryer exhaust streams. A simulation model of the absorption and desorption processes was developed, which was used to predict the efficiency of the system operating over a range of conditions.

University of Lund, Sweden. Theoretical and Experimental Studies. A wide range of activities have been undertaken by the Chemical Engineering Department (I) in Lund. The research covers both theoretical and experimental studies. Some of the work was concerned with developing a heat recovery system for the pulp and paper industry. In fact, a large scale (200 kW) heat transformer, using aqueous sodium hydroxide as the working fluid, was commissioned in 1993 at a local pulp and paper mill (Section 2.3.1).

Other research includes theoretical studies investigating the efficiency of both absorption heat pumps and transformers; the development of two computer simulation packages; experimental property prediction of lithium bromide. The simulation packages allow process flowsheets of different absorption systems to be designed. The program is highly flexible and estimates operating conditions and heat output for any system input [58]. The working fluid used in these computer packages is aqueous sodium hydroxide.

Summary. The research applications mentioned above cover a broad range of topics. These include heat pumps for air-conditioning, cooling and heating; and heat transformers. Several of the workers (University of Salford, United Kingdom; National Chemical Laboratory, India) provided details of the operating conditions and theoretical performance for heat pump and transformer cycles. These are of particular use in the design of absorption cycles. The working fluids are becoming more specialised for each application, in an attempt to increase the performance of the cycle. For example, ethylene glycol was proposed as a third component in the mixture water- lithium bromide in an attempt to lower the evaporator temperature in a chilling application without causing freezing. Other workers have investigated the potential of utilising absorption cycles in novel applications.

2.4 Existing Working Fluids.

Early absorption machines used ammonia/ water as the working fluid pair for applications such as refrigeration and chilling. The main reasons for the use of ammonia were its ready availability, low cost and high heat of vaporisation (1261 $kJkg^{-1}$) Other favourable properties of the mixture are its negative heat of absorption and thermal and chemical stability.

However, ammonia is toxic and flammable. In Japan it is difficult to commercialise equipment which uses ammonia because of strict legislations [118]. It is also necessary to provide a rectification section to ensure the complete separation of the ammonia and water, making the cycle more complex. The use of ammonia/ water for high temperature applications is also restricted because ammonia exhibits high vapour pressures at high temperatures.

In the 1950s lithium bromide became the preferred working fluid in absorption cycles. It exhibited the same favourable properties as ammonia/ water but was nontoxic. In addition there was no need for a rectification section as lithium bromide has a negligible vapour pressure. The flow of refrigerant around the system was reduced as the heat of vaporisation of water, the refrigerant, was about twice that of ammonia (2260 $kJkg^{-1}$).

An absorption cycle using water/ lithium bromide does not need to operate at high pressures. It can be seen from the Figure 2.4 that a pressure of a few bar enables operation at a high temperature. In most cases the high pressure side of the cycle would be atmospheric, while the low pressure side operates at an easily achieved vacuum.

However, lithium bromide does have limitations. Lithium bromide mixtures are

prone to crystallisation at high concentrations and low temperatures. The solubility line for aqueous lithium bromide is shown on the P-T-x diagram, Figure 2.4. Normally heat pump applications use lithium bromide at concentrations up to about 65 %w/w. These cycles can be operated without much difficulty providing the temperature of the concentrated absorbent was maintained above 45 °C (crystallisation temperature of a 65 %w/w solution). In such systems, during shut down of the plant, it would be necessary to dilute the absorbent concentration to less than 60 %w/w so as to prevent crystallisation. (The crystallisation temperature of a 60 %w/w solution is about 10 °C.) Another disadvantage of aqueous lithium bromide as a working fluid was that hot, concentrated solutions of lithium bromide are highly corrosive. Therefore, it is necessary to use either an expensive construction material, such as stainless steel (type 316), or corrosion inhibitors to reduce the corrosiveness of the solution.

2.5 Potential Working Fluids.

An extensive literature search was carried out by Robert Macriss [168] for the American Institute of Gas Technology, revealing over 300 publications concerning absorption working fluids. About half the papers contained primary sources of thermodynamic data on absorption working fluids. However, gaps in the data were identified, thereby hindering the development of new absorption systems. A lot of thermodynamic data remains 'in- house' because of its commercial relevance. Macriss' survey identified 20 different possible refrigerants and 59 absorbents, including binary, ternary and multicomponent systems. The key fluid systems are listed in Table 2.5.

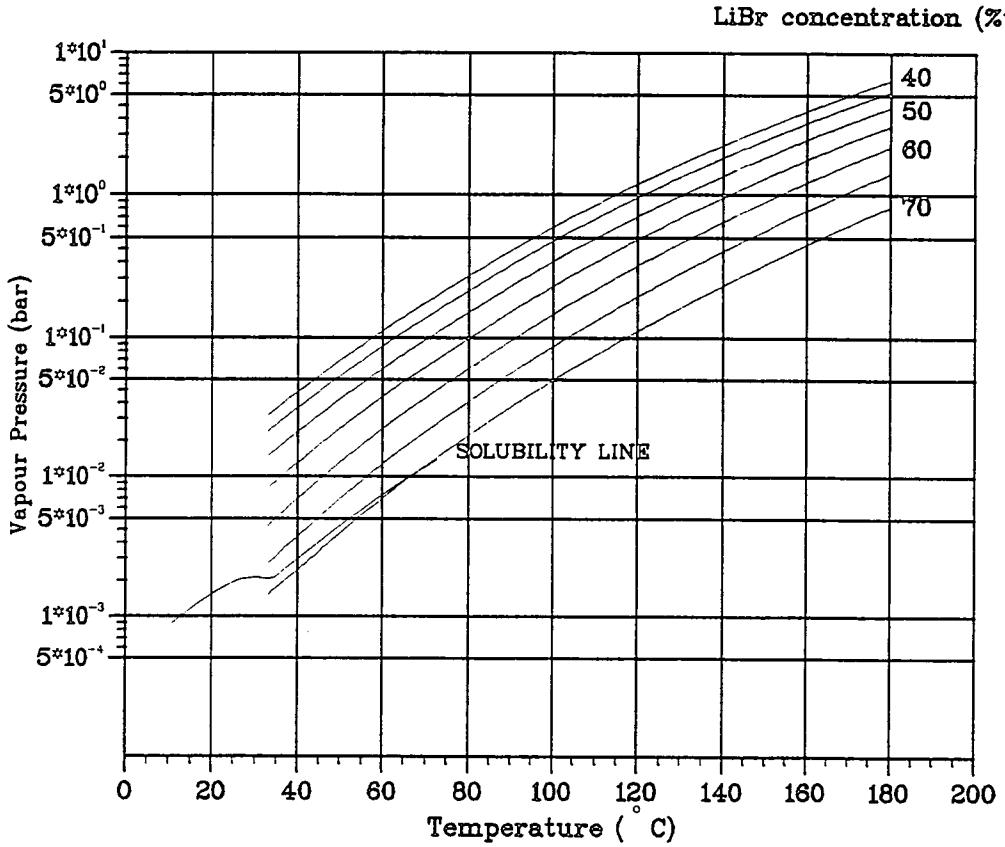

Figure 2.4: Vapour liquid equilibrium data for H_2O/ LiBr.

NH_3/ H_2O *	CH_3OH/ LiBr- $ZnBr_2$	R22/ DMETEG *
NH_3- H_2O/ LiBr	CH_3OH/ $ZnBr_2$ *	R124/ EFTE
NH_3- H_2O/ $LiNO_3$	CH_3NH_2- H_2O/ LiBr	R133a/ NMP
H_2O/ LiBr *	R21/ DMETEG	R133a/ DMETEG
H_2O/ LiBr- LiCl	R22/ DMF	TFE/ DMEDEG
H_2O/ LiBr- $ZnCl_2$	R22/ DMEDEG	TFE/ NMP
CH_3OH/ LiBr *		

Table 2.5: Key absorption fluid systems identified by Macriss.

*- multiple sources quoted

See Tables 2.11 and 2.12 for further details on these working fluids.

Instead of using water as a refrigerant, methanol has been suggested for use in chilling applications where the evaporator temperature is below 0 °C. Three component systems (NH_3- H_2O/ LiBr; NH_3- H_2O/ $LiNO_3$; H_2O/ LiBr- $ZnCl_2$, CH_3OH/ LiBr- $ZnBr_2$) have also been proposed. For example, lithium bromide can be added to the ammonia/ water system to reduce the water partial pressure and thus avoid the need for rectification. Another reason for adding a third component to a mixture is to reduce costs of the working fluid, without drastically affecting the cycle efficiency. This is the case with zinc chloride which has been added to binary mixtures of lithium bromide solutions.

The search for new absorption fluid pairs can be split into two categories: organic and inorganic systems. The University of Graz, Austria and the University of Essen, Germany, have carried out extensive searches for new organic absorption fluid mixtures. In addition some Japanese scientists have examined the thermophysical properties of electrolytic salt solutions. For example, Kashiwagi investigated the influence of additives on the performance of an absorption cycle when combined with commonly used absorption fluid pairs [152]. The work of each of these research groups is discussed in the following sections.

Commercial studies have also been carried out in order to establish new compression and absorption cycle working fluids. Access to this information was restricted and therefore not available for review. However, it was felt that, with respect to absorption working fluids, similar selection procedures and indeed final proposed mixtures to those presented here were obtained.

2.5.1 Organic Fluid Systems.

Both of the research groups discussed below, although using different selection criteria, adopt an initial screening process to find the most promising fluid pairs. Further tests were then carried out to evaluate the best mixtures. The initial screening processes used in theses studies focused upon using predictive methods to establish potential fluid mixtures.

University of Graz, Austria.

Extensive work was carried out at the University of Graz, Austria by Moser, Narodoslawsky and Otter ([88], [89], [60]) into the thermodynamic properties of new working fluids.

The experimental determination of thermodynamic properties is time consuming and costly especially when screening a large number of compounds to investigate their potential as absorption working fluids. Therefore, Narodoslawsky ([87], [88], [89]) established fundamental criteria based upon pure component and mixture properties that were used to screen potential refrigerant- absorbent mixtures. A summary of the pure component properties are listed in Table 2.6 and the desirable mixture properties outlined in Table 2.7 (Reproduced from [89]).

The mixing properties of the fluid system were based upon finding the maximum excess Gibbs free energy of the mixture, ΔG^E_{max} and its location, x_{max}. The Gibbs free energy is temperature dependent and related to the heat of mixing, Δh^E, by Equation 2.1. However, the equation was difficult to solve and a simpler one parameter equation was proposed by Narodoslawsky,

Equation 2.2, where 'd' was the coefficient of temperature dependence.

In addition, the excess Gibbs free energy can be related to the components' activity coefficients, γ, using Equation 2.3. Therefore, if ΔG^E_{max} was known for a particular mixture, it would then be possible to determine the activity coefficients of the components. Hence, for a given mixture composition and temperature it would be possible to determine the vapour pressure of the mixture. Consequently, the operating conditions of an entire absorption cycle can be simulated and studied from a knowledge of the mixture properties.

		Critical pressure	Critical temperature	Reduced boiling point	Latent heat of vaporisation
AHP	Refrigerant	High	Low	High	High
	Absorbent	Low	High	Low	High
AHT	Refrigerant	Low	High	Low	High
	Absorbent	Low	High	High	High

Table 2.6: Desirable critical parameters for working fluids mixtures.

	ΔG^E_{max}	x_{max}	Δh^E	d
AHP	-1000 to -2000 $Jmol^{-1}$	High	Moderately exothermic to slightly endothermic	Greater than 1
AHT	Slightly positive to highly negative	Medium to high	Exothermic	Less than 1

Table 2.7: Mixture criteria for optimum working pairs.

$$\frac{\partial(\Delta G^E/T)}{\partial(1/T)} = \Delta h^E \tag{2.1}$$

$$\Delta G^E = d.\Delta h^E \tag{2.2}$$

$$\frac{\Delta G^E}{(R.T)} = \sum(x_i \ln \gamma_i) \tag{2.3}$$

Narodoslawsky [87] also investigated the effect of varying the parameters ΔG^E, x and d on the performance of both absorption heat pump and heat transformer cycles. The loci of the optimal mixture properties for both of these systems are

illustrated on a Gmehling[3] diagram, Figure 2.5. The results obtained indicated that the most interesting fluid combinations for both absorption heat pump and heat transformer applications appeared in quadrants III and IV, Figure 2.5. For absorption heat pump applications it was desirable to have a fluid pair which exhibited a moderately exothermic to slightly endothermic heat of mixing, while the Gibbs free energy was negative and weakly dependent on the temperature.

Fluid mixtures for heat transformer applications had to have a heat of mixing which was highly exothermic and a negative Gibbs free energy, although a slightly positive Gibbs free energy was tolerated. In boths cases a strong negative deviation from Raoult's Law was required indicating that the refrigerant and absorbent have a strong affinity for each other.

A computer program was written by the Graz researchers [60] to evaluate the mixing properties of different fluids and to assess their potential as absorption working fluids. The UNIFAC[4]. computer package was used to calculate the physical properties of the pure components and hence the mixing properties. The UNIFAC model is used for a wide range of chemical engineering purposes. It is a renowned as a reliable computer package.(see Section 2.6).

The results from the screening process highlighted 12 possible refrigerants, which are listed in Table 2.8, and 36 possible absorbents. The refrigerants suggested were all hydrocarbons- alcohols and amines. Details of the performance of different types of refrigerants with a variety of different absorbent molecules is provided in the following paragraphs. A short list of the most promising fluid combinations is provided in Table 2.9.

[3]Gmehling, J and Kolbe, B: "Fluid phase equilibria". Volume 13 (1983); pp227- 242.
[4]UNIversal Quasi Chemical Functional Groups Activity Coefficients

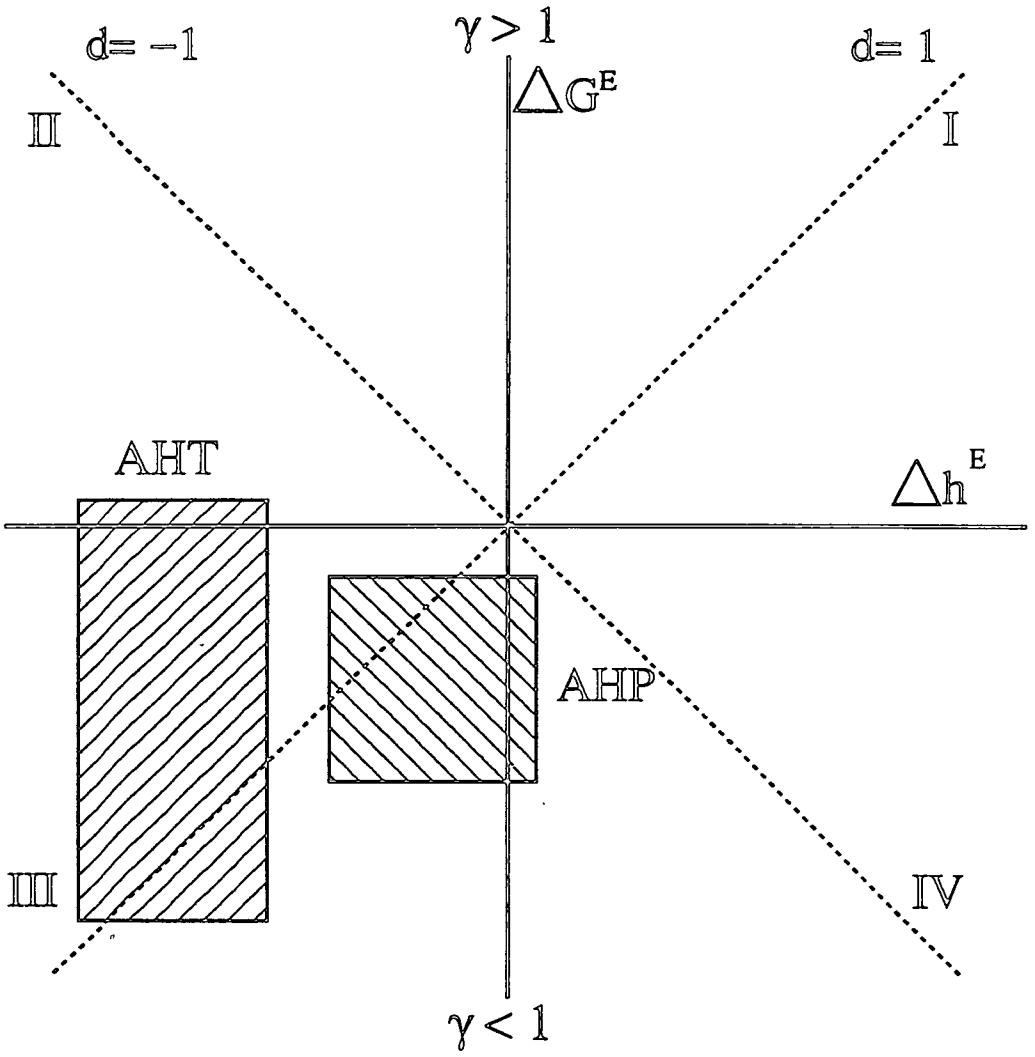

Figure 2.5: ΔG^E_{max} versus Δh^E showing areas of optimal working pairs.

Refrigerant	Chemical formula	Boiling point (°C)	Heat of vaporisation ($Jmol^{-1}$)
Carbon tetrachloride	CCl_4	76.6	30010
Chloroform	$CHCl_3$	61.1	29720
N- hexane	C_6H_{14}	68.7	28870
N- propanol	C_3H_7OH	97.2	41780
Ethanol	C_2H_5OH	78.4	38760
Methanol	CH_3OH	64.6	35270
N- propylamine	$C_3H_7NH_2$	48.7	29720
Ethylamine	$C_2H_5NH_2$	16.5	28050
Methylamine	CH_3NH_2	-6.2	24570
Dimethylamine	$(CH_3)_2NH$	6.8	26500
Trimethylamine	$(CH_3)_3N$	2.9	24110
Diaminoethane	$(CH_2NH_2)_2$	117.3	41860

Table 2.8: Proposed refrigerants by the University of Graz.

Discussion of refrigerants with various absorbents:

Hydrocarbons. Partially halogenated hydrocarbons were more promising refrigerants than fully halogenated hydrocarbons. Unfortunately only carbon tetrachloride and chloroform were tested using the UNIFAC model, as no other halogenated molecules were available. Therefore, chloroform was the preferred refrigerant. The most suitable absorbents for use with chloroform were ethers, esters and ketones. Table 2.9 lists the best combinations of absorbents with chloroform these include two ketones- acetophenone (APN), N- methyl pyrrolidinone (NMP) and one ester- diethylmalonate (DEM). However, the use of chloroform was discouraged because of its toxicity.

Alcohols. Alcohols also showed particular promise as refrigerants. However, two of the most important criteria for the selection of a working pair are the difference in the boiling points of the two components and also the heat of vaporisation of the refrigerant. If an alcohol were used as a refrigerant there

would need to be a trade- off between the two because as the refrigerant's molecular weight increased, the boiling point and heat of vaporisation also increased. Therefore, the best refrigerants were felt to be methanol and ethanol, which both had reasonably high heats of vaporisation and moderate boiling points. The use of methanol was restricted to low temperature as it decomposed at temperatures above 120 °C.

Long chain alcohols have also been used as absorbents in combination with alcoholic refrigerants. The results indicate that, the higher the degree of substitution on the long chain alcohol, the more suitable it is for use as an absorbent working fluid. The addition of an amino group to the absorbent helps to increases the ΔG^E_{max} and x_{max} of the mixture and hence its performance . The use of an aromatic alcohol, with a rising number of hydroxylic groups, as an absorbent is also highly promising. Two possible absorbents are dihydroxybenzene (DHB) and trihydroxybenzene (THB). However, care must be taken when the benzene derivatives (DHB, THB) because of their carcinogenic nature.

It is also possible to use ethers as absorbents; however, ΔG^E_{max} falls as the number of ether groups and the chain length of the ether increases. Lower molecular weight alcohols shift the location of ΔG^E_{max} to higher refrigerant concentrations, x_{max}. Therefore, the most interesting combination of alcohol-ether would be methanol and dimethyl ether tetra ethylene glycol (DMETEG).

Ketones are of particular interest as absorbents, especially heterocyclic molecules such as NMP. The mixing properties improve as the molecular weight of the refrigerant decreases. The best combination is methanol- NMP.

Amines. Amines can be used as refrigerants with long chain alcohols as the absorbent. The longer the alcohol chain and the more hydroxyl groups on the absorbent, the more interesting the combination. The best combinations are diaminoethane with either 1,4 butanediol or glycerol.

Refrigerant	Absorbent	ΔB.Pt (degC)	Refrigerant	Absorbent	ΔB.Pt (degC)
$CHCl_3$	APN	142.9	C_2H_5OH	THB	230.6
$CHCl_3$	DEM	137.9	C_3H_7OH	DHB	187.8
$CHCl_3$	NMP	139.9	C_3H_7OH	THB	211.8
CH_3OH	NMP	136.4	$(CH_2NH_2)_2$	1,4- BD	117.7
C_2H_5OH	DHB	206.6	$(CH_2NH_2)_2$	GLY	171.7

Table 2.9: Proposed working fluids pairs by the University of Graz.

University of Essen, Germany.

An extensive experimental program was carried out at the Institut für Angewandte Thermodynamik und Klimatechnik, University of Essen, by Benade, Bokelmann, Ehmke, Renz, Nowaczyk, Schmidt and Steimle. The scope of their study was to find promising working pairs for use in absorption cycles and determine the main properties of the mixture. The basis of their studies concentrated upon finding a fluid pair which had high thermal and chemical stabilities and which also exhibited a high solubility of the refrigerant in the absorbent. Their research was concentrated on organic systems.

The high solubility of a system depended upon the formation of hydrogen bonds between the molecules [114]. It was therefore, necessary to use a refrigerant which was a polar, covalent molecule with a strong electron affinity, while the absorbent had to be an electron donor.

The main refrigerant groups were: alcohols, carboxylic acids, halogenated hydrocarbons and primary/ secondary amines. The main absorbent groups were: alcohols, esters, ethers, ketones and carboxylic acids.

Pointwise measurements of the solubility of 150 fluid pairs were taken and the most promising were investigated further. These studies led to the identification of ten possible fluid pairs, which are listed in Table 2.10 ([17], [18], [19], [114]). The next stage of the project was to obtain accurate property measurements for the fluid pairs. The properties investigated were the fluid density, viscosity, heat capacity and the excess heat of mixing. The thermal stability of the systems were also investigated. Charts for the vapour pressure and phase equilibrium for these systems have also been produced.

Refrigerant (Electron acceptor)	Absorbent (Electron donor)	ΔB.Pt (degC)	Refrigerant (Electron acceptor)	Absorbent (Electron donor)	ΔB.Pt (degC)
TFE	DMPU	158	HFIP	Sul	229
TFE	NMP	127	PFPA	DMETEG	178
TFE	Pyr	171	R22	DMETEG	234
HFIP	DMPU	174	R22	DMETrEG	257
HFIP	DMETEG	217	R123a	DMETEG	281

Table 2.10: Proposed working fluid pairs by the University of Essen.

The TFE- NMP system operated very well over a wide concentration range enabling it to used at low evaporator temperatures and high generator temperatures. The vapour pressure at low temperature is below atmospheric pressure. Therefore there was a possibility of operating a two stage system without operating at too high a pressure on the high pressure side of the second stage. Another possible working fluid pair, which was proposed was the system TFE- Pyr, which could achieve an exit temperature of around 200 °C leaving the absorber [19]. This particular working pair was used in the experimental work of Westra [224] and also the simulation studies of Zhuo [232], although not at very high temperatures. The use of dimethylpropyleneurea (DMPU) as an

absorbent in combination with TFE also showed favourable results, although this combination was not a good as the fluid pairing of TFE- Pyr.

The major drawback with these systems is that TFE is highly toxic and flammable and therefore its use as a refrigerant should be discouraged. Another drawback of the TFE- NMP system is that the difference in the boiling points is only 127.4 °C, which is less than for the ammonia/ water system, making it necessary to provide a rectification stage.

Systems containing hexafluoroisopropanol (HFIP) have also been tested successfully but it is unlikely that it will be used in absorption cycles because it is toxic, see Tables 2.11 and 2.12. The same is true for pentafluoropropionic acid (PFPA). The working fluid pairs of dichlorotrifluoroethane (R123a)- DMETEG and chlorodifluoromethane (R22)- DMETEG have successfully been tested. However, the cycle performance achieved was less than that for the fluid combination of TFE- NMP. Both of the mixtures do have certain advantages over TFE- NMP as they both have low toxicities and flammabilities. Also the difference in the boiling points of both mixtures is greater than 200 degC therefore there is no need for rectification. The refrigerant R22 has also been tested with DMETrEG and the results obtained indicate that this combination is better than that of R22- DMETEG. The potential use of R22 as a refrigerant is promising but its use for high temperature applications is restricted because of the high pressures which would be required.

Abbreviation	Chemical name	B.Pt (°C)	Toxic	Flamm.
$CHCl_3$	Chloroform	61.1	High	Low
CH_3OH	Methanol	64.6	High	High
C_2H_5OH	Ethanol	78	High	High
C_3H_7OH	N- Propanol	97.2	High	High
$(CH_2NH_2)_2$	Diaminoethane or ethanediamine	118	Mod- high	Mod
HFIP	Hexafluoroisopropanol	58	High	Low
PFPA	Pentafluoropropionic acid	96- 98	High	Low
R21	Dichlorofluoromethane	9	High	Low
R22	Chlorodifluoromethane	-41	Low	Low
R123a	Dichlorotrifluoroethane	29	Low	Low
R124	Chlorotetrafluoroethane	-12	Low(?)	Low
R133a	Chlorotrifluoroethane	6	High	Unknown
TFE	Trifluoroethanol	74	High	Mod

Table 2.11: Summary of organic refrigerants.

2.5.2 Inorganic Fluid Systems.

Much of the work undertaken using inorganic fluid systems was based upon extending the operating limits of the binary fluids of ammonia/water and water/ lithium bromide by addition of one or more component. The paper by Kashiwagi [152] gives an extensive review of possible additives for both systems as well as some organic fluid mixtures.

Other electrolytic solutions.

Chaudhari et al [111] have carried out experiments using lithium chloride, calcium chloride and a composite mixture of both as an alternative to lithium bromide. These chemicals do not pose a health risk and calcium chloride is far cheaper than lithium bromide. In addition, lithium chloride is less soluble than

Abbreviation	Chemical name	B.Pt (°C)	Toxic	Flamm.
1, 4- BD	1,4- Butanediol	235	Mod	Low
APN	Acetophenone	202	High	Low
DEM	Diethylmalonate or ethylmalonate	199	Low	Low
DHB	Dihydroxybenzene or 1,4- benzenediol or hydroquinone	285	High	Low
DMA	N, N- dimethylacetamide	165	Mod	Low
DMF	N, N- dimethylformamide	153	Low- mod	Mod
DMPU	1,3- dimethyl 3,4,5,6-tetra hydro-2(1H) pyrimidinone (Dimethylpropyleneurea)	232	Low (?)	Low
DTG or DMETEG or TEGDME	Dimethyl ether tetra ethylene glycol	275	Low	Low
DTrG or DMETrEG	Dimethyl ether triethylene glycol	216	Low	Low
DMEDEG	Dimethyl ether diethylene glycol	162	Low	Low
ETFE or EFTE	Ethyl tetrahydro furfuryl ether	158	Unknown	Unknown
GLY	Glycerol or glycerine	289	Low	Low
NMP	N- methyl pyrrolidinone	201	Low- mod	Low
Pyr	Pyrrolidinone	245	Low	Low
Sul	Sulfolane (Tetramethylene sulfone)	287	Low- mod	Low
THB	1,2,3- Trihydroxybenzene Pyrogallol	309	High	Low

Table 2.12: Summary of organic absorbents.

Toxicity and flammability data taken from SAX[198].
N.B. Flammabilities were calculated from the British Standard, using the flash point (F.Pt) of the chemical:

F.Pt < 32 °C	High
32 °C < F.Pt < 60 °C	Mod
60 °C < F.Pt	Low

lithium bromide, which restricts the range of operating conditions of a cycle employing this mixture. Using these alternatives the performance of a heat pump was not as good as with the water/ lithium bromide fluid pair although the results were comparable.

Patil et al ([75], [79], [80]) carried out an experimental programme to investigate a wide range of binary electrolytic solutions. The properties examined included vapour pressure, solubility, specific gravity, heat of mixing and VLE data for the solution. The results are documented in several papers and are in a form suitable for inclusion in a computer program. Therefore these equations could be used for simulation studies, allowing comparison of different working fluid mixtures and removing the need for individual experimental studies. The vapour pressure of the each of the fluid mixtures is characterised by equation 2.4. The parameters A, B and C are concentration dependent and are defined by the Equations 2.5, 2.6 and 2.7 (concentration units: %w/w).

$$\log_{10} P(kPa) = A + \frac{B}{T(K)} + \frac{C}{T^2(K^2)} \tag{2.4}$$

$$A = A_0 + A_1.x + A_2.x^2 + A_3.x^3 \tag{2.5}$$

$$B = B_0 + B_1.x + B_2.x^2 + B_3.x^3 \tag{2.6}$$

$$C = C_0 + C_1.x + C_2.x^2 + C_3.x^3 \tag{2.7}$$

Additives for the water/ lithium bromide system.

Several studies have been carried out using a variety of salt compounds in an attempt to improve the operability and efficiency of the water/ lithium bromide system. Table 2.13 lists some of the compounds which have been used and the reasons for their use.

Iyoki [147] and Eisa et al [85] have also suggested that ethylene glycol could be added to the binary mixture for use in refrigeration equipment. The ethylene glycol would reduce the freezing temperature of the water allowing a lower temperature to be achieved in the evaporator. However, the viscosity of the ternary mixture increases as ethylene glycol is added. The mole ratio of water to ethylene glycol used by Eisa was 15:1 and that used by Iyoki was 10: 1. Eisa reported that the ternary mixture actually gave a higher COP than that of water/ lithium bromide.

Additive	Reason
Lithium iodide	Lower crystallisation temperature.
Lithium thiocyanate	Greater cycle efficiency.
Lithium nitrate	Lower cryst^{n} temp. Corrosion inhibitor. Industrial high temperature amplifier.
Lithium chloride	Greater efficiency- but reduces operating range.
Ethylene glycol	Greater efficiency. Lower crystallisation temperature.
Zinc chloride	Greater efficiency. Lower crystallisation temperature.
Lithium chloride/ lithium thiocyanate	Lower crystallisation temperature.
Lithium molybdate, Lithium chromate	Corrosion inhibitors. " "

Table 2.13: Additives for the water/ lithium bromide working fluid.

Example of a multicomponent system.

Iyoki and Uemura [148] have investigated the influence of adding other components to the binary working fluid of water/ lithium bromide in an attempt to reduce the risk of crystallisation. Initial work concentrated on the addition of zinc chloride to the binary system, which worked satisfactorily. Subsequent work involved the addition of calcium bromide to the ternary mixture. The optimum weight ratio was found to be 1.0: 1.0: 0.13 for each of lithium bromide, zinc chloride and calcium bromide respectively. The thermal and physical properties of the system were then determined experimentally and reproduced in a form which could easily be incorporated into a computer simulation program.

A comparison of the P-T-x plots for H_2O/ LiBr system (Figure 2.4) and for the H_2O/ LiBr + $ZnCl_2$ + $CaBr_2$ system (Figure 2.6) has shown that the solubility range and the maximum concentration of the solution have been increased through the inclusion of additives. The cost per kilogram for a 50 %w/w solution has been reduced from £26 (LiBr) to £18 (1.0: 1.0: 0.13- LiBr: $ZnCl_2$: $CaBr_2$).[5] It can be seen from the P-T-x diagram that for a given pressure and concentration, the temperature of the multicomponent mixture is lower than that of the binary, thereby reducing the maximum possible temperature within a cycle.

[5]The prices only serve to give an indication of the difference in costs of the two systems. The chemical were priced at 1993 levels and were taken from a commercial catalogue dealing with small quantity chemicals. The cost for bulk purchases of these chemicals would be less than this.

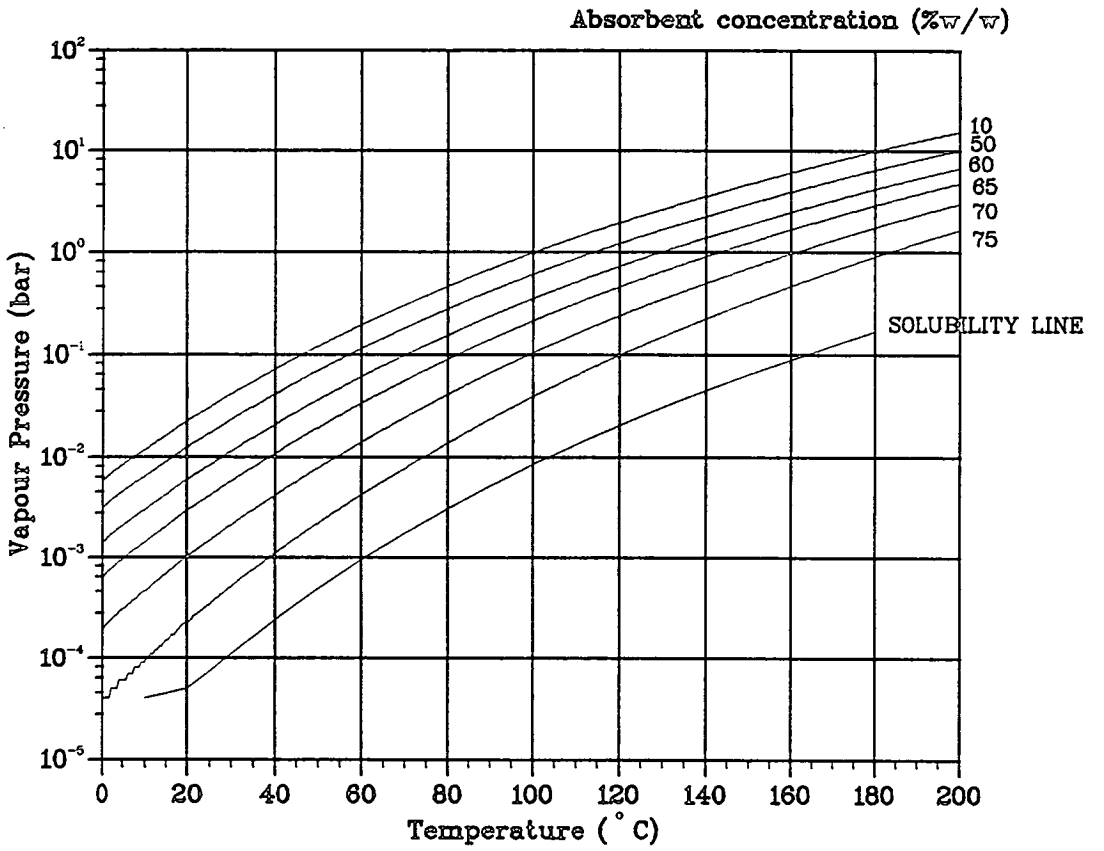

Figure 2.6: Vapour liquid equilibrium data for H_2O/ LiBr + $ZnCl_2$ + $CaBr_2$.

2.6 Computer Packages and Models.

2.6.1 Physical Property Prediction.

Property prediction for highly non- ideal mixtures of polar, H-bond and electrolytic molecules can be achieved in two ways [106]. The first method involves the interpolation/ extrapolation of experimental data, which is fitted to a suitable model. There are several models currently available to achieve this. They include methods by Margules (quadratic, cubic and 4^{th} order equations), Van Laar and Wilson. The Van Laar equations are the easiest to use and only involve two parameters.

There are other methods of property determination which are based upon the size and number of interactions between the functional groups of a compound. The ASPEN+ software utilises several of these methods- Amborse, Benson, Bondi, Joback, Lydersen, Reichenberg and UNIFAC- to estimate the pure component and mixture properties of a wide range of compounds [9]. ASPEN+ is a particularly useful computing package because as well as predicting the properties of compounds held within its own data banks, it can also be used to estimate the properties of user defined fluids, based upon the group contributions within the molecule.

The UNIFAC method makes use of the liquid phase activity coefficient to estimate the physical properties of a mixture. It is a reliable and well known computer package, however, it is only available for organic compounds and water. There are a large number of functional groups available (44) but data for interaction pairs is limited. The vapour- liquid equilibria determined by UNIFAC are generally accurate. However, the package has experienced some

problems in predicting the heat of mixing. Larsen[6] proposed a modified UNIFAC, which compromises the number of different functional groups (21) available in order to provide better temperature dependence, giving better prediction for the heat of mixing. The interaction pairings of the modified model are shown in Figure 2.7- Otter [60].

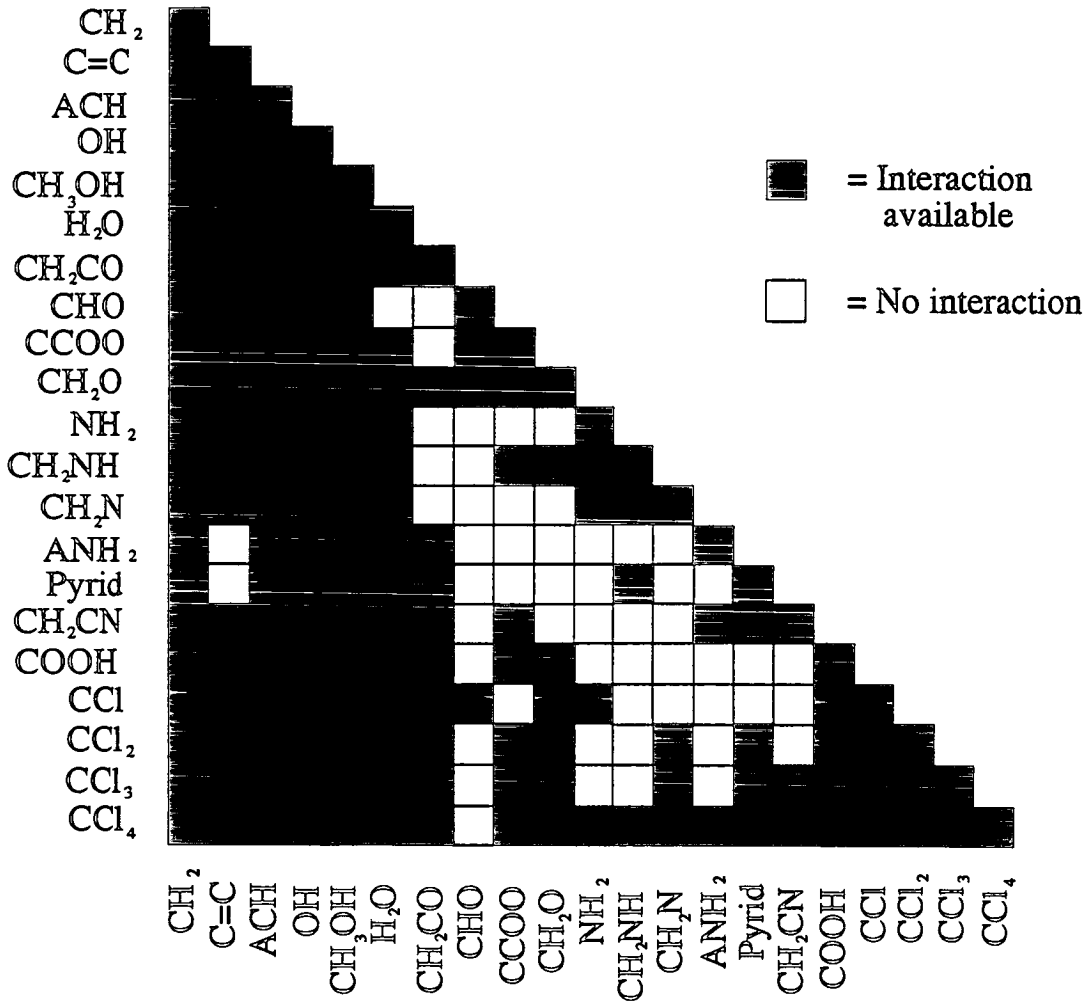

Figure 2.7: Available groups and interactions for the modified UNIFAC model.

[6]Larsen, B. L et al : Industrial Engineering Chemical Research. 1987. Volume 26. p2274

2.6.2 Water/ Ethylene Glycol Mixture Property Prediction.

An example of property prediction using the ASPEN+ computer package was carried out for the water/ ethylene glycol mixture. The mixture physical properties which were determined included the enthalpy, entropy, heat capacity and density of the liquid. In addition, the activity coefficients, viscosity and thermal conductivity for the individual components were also estimated.

P- T- x and T- x- y diagrams were constructed from the derived data and compared with actual data supplied by ICI, Figures 2.8 and 2.9. The two data sets showed slight discrepancies between the dew and bubble point curves, Figure 2.9. However, it was not felt that these differences would give a false indication of the suitability of this mixture for use in an absorption cycle. The ASPEN+ program therefore provided the preliminary data needed for the preselection of a working fluid, thereby saving time and money. Prior to the selection of water/ ethylene glycol as a working fluid pair, a detailed experimental programme would need to be undertaken to establish more accurate physical properties.

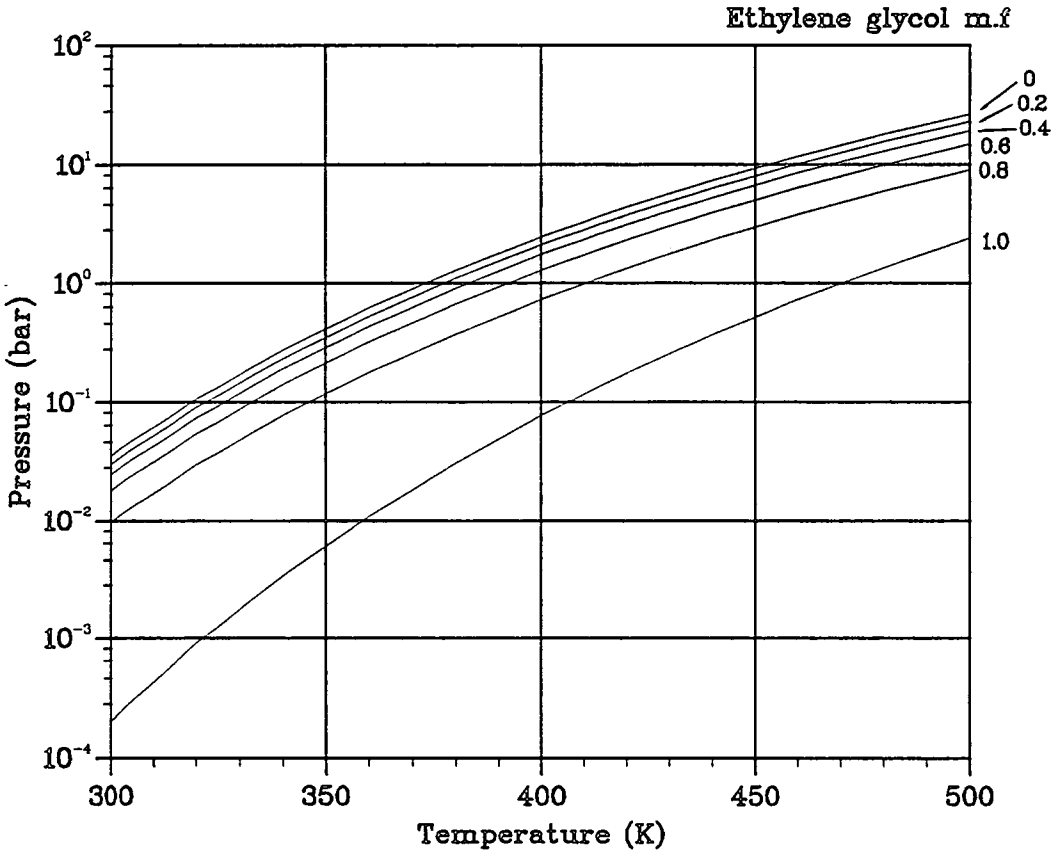

Figure 2.8: P- T- x diagram for ethylene glycol/ water.

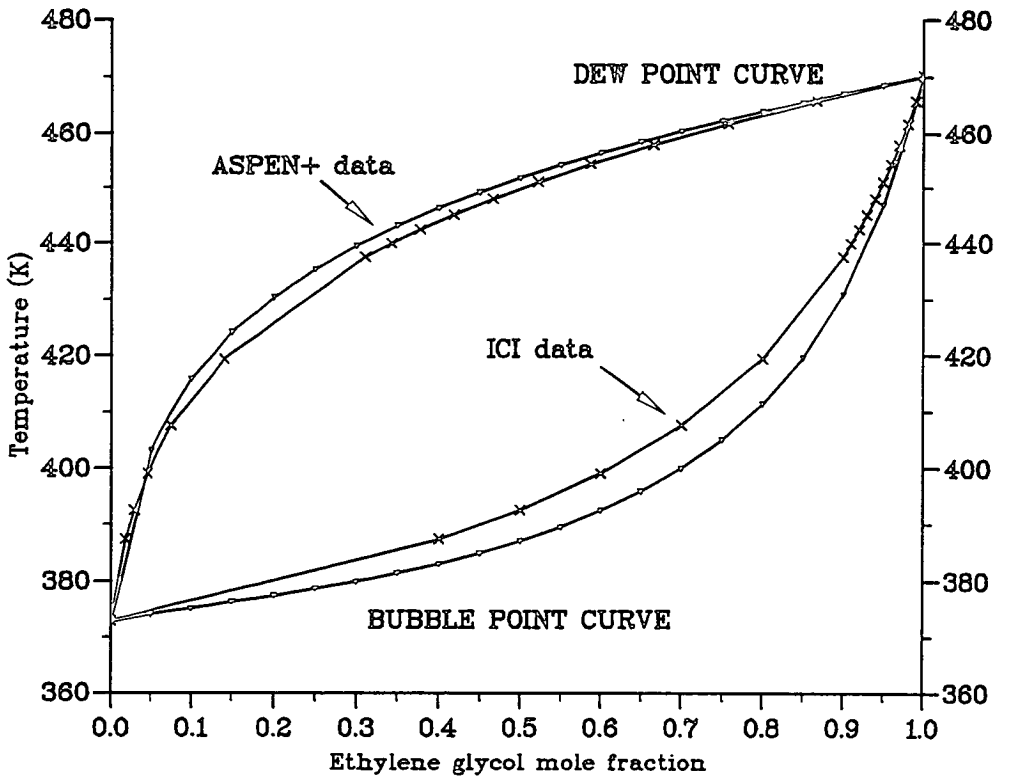

Figure 2.9: T- x- y diagram for ethylene glycol/ water at a pressure of 1 bar.

2.7 Choice of Working Fluids for Heat Recovery from Dryers.

The objectives of this project were to dehumidify and reheat humid dryer exhaust gas streams. In the current application, the absorbent used for both operations was aqueous lithium bromide. Each of the operations is discussed separately because this was felt to be the only was to achieve both requirements of dehumidifying and reheating the gas streams.

2.7.1 Open Cycle Drying and Dehumidification.

It was decided that the best way to dehumidify the humid gas stream was by direct contact with a hygroscopic solution. Two researchers have already proposed dryer- dehumidifier units which have adopted this principle ([199], [200], [201] & [207]). Scalabrin's work was based upon the drying of sensitive materials. The working fluid chosen for the absorber was aqueous lithium chloride, which did not pose as serious a health hazard as lithium bromide, while exhibiting similar thermodynamic properties (see Section 2.3.2). The other application, proposed by Snelson [207], involved the design of an absorption heat pump for a wood drying operation in Canada and utilised aqueous sodium hydroxide as the working fluid.

In choosing a working fluid to dehumidify the gas it was necessary to consider additional requirements to those given in Section 2.2. As the working fluid was in direct contact with the humid gas stream it was necessary to ensure that there was as little carry over of the absorbent into the drying process as possible. These were several reasons for this:

- The absorbent could cause contamination of the dried product, which in turn may result in product degradation.
- There would be a subsequent loss of absorbent which would require replacement. Hence the use of a cheap working fluid would be desirable.

As the dehumidification process was an open loop cycle, extreme care had be taken to ensure that the absorbent was nontoxic, nonflammable and also highly soluble in water, without risk of crystallisation at high concentrations. There were several probable candidates for use as the absorbent, these are listed in Table 2.14. Sodium hydroxide, which is widely used throughout the chemical industry, has already been suggested as a possible working fluid ([207], [58]). However, it crystallises at high concentrations and low temperatures. Therefore a study of suitable additives would need be undertaken to minimise this risk (similar to that carried out for lithium bromide). Sulphuric acid was also considered as an absorbent for use in the dehumidification process, however, because of its corrosive nature it would be necessary to use graphite as the construction material for the cycle equipment. Another possible absorbent fluid which was considered for this direct contact absorption operation was ethylene glycol. However, like sulphuric acid, it exhibits appreciable vapour pressures at the temperatures used in the process. Therefore, the absorbent would be continually passed back to the main drying process.

Absorbent	Absorbent
LiBr	$CaCl_2$
LiCl	$CaBr_2$
$LiNO_3$	$ZnCl_2$
LiI	$ZnBr_2$
NaOH	Ethylene glycol
KOH	H_2SO_4

Table 2.14: Possible absorbents for use in a direct contact dehumidifier with water as the refrigerant.

To conclude, it would appear that each of the absorbents discussed above had limitations. Therefore, the adoption of a multicomponent mixture, similar to that proposed by Iyoki [148], would best meet the dehumidification requirements needed for the recycling of humid gas streams to the main drying process.

2.7.2 High Temperature Organic Absorption Working Fluids.

The other aspect of this particular project was concerned with achieving exit temperatures from an absorption cycle of around 200 °C. The system in these studies used water- lithium bromide as the working fluid and results using this mixture were promising. However, as previously discussed, this fluid pair was prone to crystallisation problems at high concentration.

Future experimental work will endeavour to find new working fluid pairs for use in high temperature absorption systems. The fluid mixtures will need to be stable at temperatures above 200 °C. In addition, the operating pressure of the high pressure side of the cycle should be limited to a few bar, thereby removing the need for expensive, high pressure equipment. The organic working fluid

which appeared the most promising with respect to their pure component and mixture properties, as discussed previously, are listed in Table 2.15. Care should be taken when using TFE because of its toxic nature. However, as the reheat absorber was part of a closed loop system the risk of exposure was reduced.

Refrigerant	Absorbent
TFE	NMP
TFE	DMPU
TFE	Pyr
Diaminoethane	Glycerol
Diaminoethane	1,4- Butanediol

Table 2.15: Potential working fluid combinations to be tested.

2.8 Conclusions.

Most absorption systems are used for domestic and commercial air-conditioning units, in which gas is utilised as the heat source (particularly in Japan). There are also several applications in which waste heat is recovered from chemical processes and recycled for use elsewhere. Examples of these systems have been discussed earlier in this chapter, Section 2.3. In general the adoption of absorption cycle technology is limited, with the most commonly used absorption working fluids being ammonia/ water and water/ lithium bromide.

Research into new working fluid pairs and advanced cycles is currently underway in an attempt to make absorption cycles more efficient and reliable. The potential application of these new working fluids will help to extend the range of uses for absorption cycles and will overcome some of the present limitations.

Extensive searches at the University of Graz, Austria and the University of Essen, Germany have screened great number of potential working fluids. These

studies have concentrated upon the use of organic fluids. At the University of Graz the screening of these fluids was undertaken using the UNIFAC computer program. The work carried out at University of Essen involved taken pointwise solubility measurements of 150 promising fluid pairs. The most promising pairs are currently being tested further. Other studies have involved the search for additives to ammonia/ water and lithium/ bromide systems in an attempt to extend their operational limits.

A major constraint on the adoption of absorption heat pumps and transformers in industry is the lack of readily available design data, as highlighted by Macriss. This makes it difficult for the design engineer to assess the potential performance of different cycles operating with different working fluids. In an attempt to make absorption cycles more widely accepted there must be an increase in the availability of thermodynamic data on working fluids, which can be used for preliminary design calculations. This could potentially lead to an increase in the number absorption cycles used industrially.

Chapter 3

Design and Construction.

3.1 Design.

An absorption heat transformer pilot plant was designed and constructed for the purpose of recovering waste heat from humid gas streams, using a concentrated lithium bromide solution. The humid gas streams used in these studies were representative of exhaust gas streams leaving industrial spray drying units. The experimental apparatus was designed as an open loop cycle (see Chapter 1, Figure 1.16) and allowed the dehumidification and reheating of gas streams, enabling recirculation of the gas back to the spray drying chamber. Therefore, an industrial heat transformer cycle would reduce the energy consumption of the dryer by recovering the waste heat associated with the exhaust gas, which is presently vented to atmosphere.

In order to dehumidify the gas stream, it was necessary for the humid gas and concentrated lithium bromide streams to be in direct contact. It was also decided that the absorber should contain packing so as to maximise the absorption of water vapour into the absorbent solution. The temperature of the gas and liquid streams rises due to the heat released as the water vapour is absorbed, resulting in a dehumidified and reheated gas stream leaving the absorption column.

The weak lithium bromide solution, containing the absorbed water, was regenerated by flashing the solution into a low pressure generator, where the absorbed water was evaporated. Electrical heaters were used to supply extra heat to the generator in order to maintain the absorbent solution at a desired concentration. The lithium bromide solution was then recirculated to the top of the absorption column and the procedure repeated. The evaporated water from the generator was condensed at a low temperature, in this case ambient, and collected in a receiver. As the system was an open loop heat transformer cycle, there was no need for a refrigerant evaporator.

In addition to the design of the absorption cycle, it was also necessary to design a system for generating humid gas streams, similar to those created in an industrial spray drying plant (details of which are described below).

The absorbent solution used in these studies was aqueous lithium bromide solution, containing 1%w/w lithium nitrate, which was added to inhibit corrosion. However, it was prone to crystallisation at high concentrations and low temperatures. Lithium bromide was chosen because of its hygroscopic nature, exhibiting very low water partial pressures at elevated temperatures. Due to the corrosive and oxidising nature of the absorbent solution care had to be taken in its handling. The apparatus had to be constructed of stainless steel (type 316) and glass.

3.1.1 Design Basis.

The capacity of the experimental heat transformer was based on several criteria[1]:

- The heaters used to generate steam to simulate the humid airstream had a maximum power consumption of 3 kW, corresponding to a maximum steam flowrate of approximately 1.2 gs^{-1} (including heat losses).
- The diaphragm metering pump used in the studies had a maximum capacity of 4 mls^{-1}.
- The maximum superficial gas velocity in the absorber was initially set to 2 ms^{-1}- allowing the column to be sized for a given gas flowrate.
- Where possible, existing pieces of equipment were used in preference to buying or manufacturing new equipment (which would have delayed construction).

[1]See Appendix C 'Sample Calculations', Section C.1

As the profile within the absorption column was unknown it was decided that the column should be of appreciable length. It was also decided that the holdup of the working fluid should be kept to a minimum, with respect to cost and also safety. The holdup in the generator, which was also used as the main storage vessel during shut down, was approximately 4 litres.

Also, the absorbent generator had to accommodate two heating elements, which had to be covered at all times. Therefore, the diameter of the vessel was large enough to position the two heaters side- by- side, while enough working fluid was used to ensure the elements were immersed in liquid.

3.1.2 Single Stage Pilot Plant.

The initial work carried out on this project involved the design of a single stage, open loop absorption cycle consisting of a packed absorption column, a generator, a condenser/ receiver, a vacuum system and a humid gas generation system. It was preferable that the system was flexible so that it could be operated with either co- or counter- current flows of liquid and gas streams. As a direct consequence of the problems of absorbent crystallisation, the plant was designed for quick and easy dismantling to permit cleaning of the blockage.

The system was fully lagged to minimise heat losses during normal operation. The operating pressure of the generator and condenser/ receiver was typically 0.05- 0.1 bara requiring a system which could achieve the desired vacuum. The absorber and humid gas generation equipment were operated at atmospheric pressure, avoiding the need to design a system capable of operating at elevated pressures.

Generation of Humid Gas Streams.

The simulated humid gas stream was created by mixing dry air with separately generated steam. The temperature of the humid gas stream was controlled by adjusting the power input to an electrical heater, prior to its entry to the absorber. Initially a small blower was used as an air source; at a later stage a compressed air supply replaced the blower. A valve was used to control the air flowrate entering the absorber, with flowrates measured on a rotameter. Typical flowrates ranged from 1- 6 gs^{-1}.

Immediately after the rotameter, the cold air was preheated to a temperature of approximately 100 °C, so as to prevent condensation when the air and steam were mixed. The steam was generated in a lagged, glass boiler which had aluminium end plates. Electrical heaters were mounted into these end plates and used as the heat source for the boiler. The maximum power input to the heaters was 3 kW, corresponding to a maximum steam flow of about 1.2 gs^{-1}. The complete humid air generation setup is shown in Figure 3.1.

The steam flowrate was metered in three ways, allowing a comparison to be made between methods and thus validating each result. The three methods for calculating the steam flow are summarised below:

- Power input to steam generator. It was assumed that the heat of evaporation was 2557 Jg^{-1}.

$$\dot{m}_s = \frac{Power\ \ input}{2257} \qquad [gs^{-1} = W/Jg^{-1}] \qquad (3.1)$$

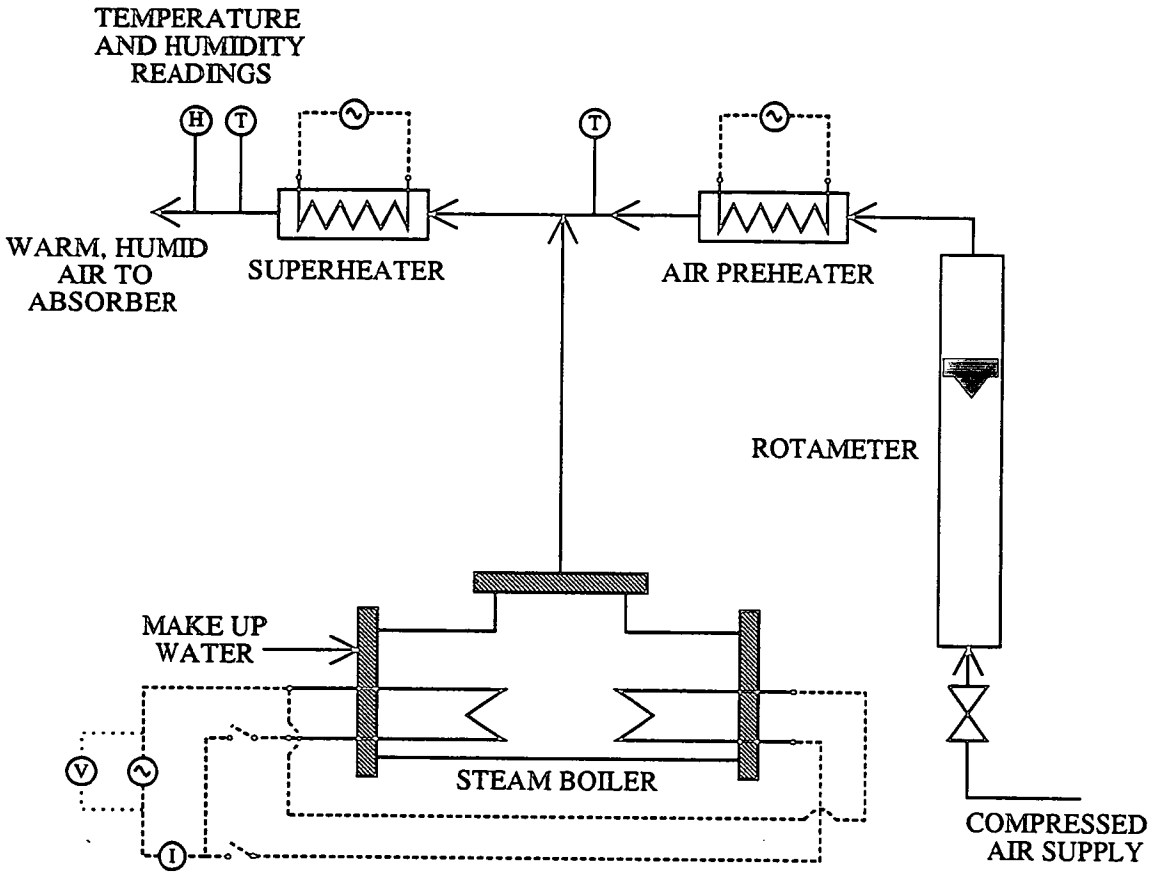

Figure 3.1: Equipment used to generate a simulated spray dryer exhaust stream.

- Inlet water head device. Fresh water was fed into the boiler when the level dropped, Figure 3.2. The amount of water entering the boiler was measured using a flowmeter. The water flowrate was measured in units of $cc.min^{-1}$.

$$\dot{m}_s = \frac{Flowrate}{\rho_w} \qquad [gs^{-1} = cc.s^{-1}/g.cc^{-1}] \tag{3.2}$$

- Humidity and temperature of the humid air stream. These were measured periodically, and allowed the calculation of steam flowrate, see Equations 3.3, 3.4, 3.5 and 3.6.

$$\%RH = \frac{p_1}{p^*(T)}\,100 \tag{3.3}$$

$$p_1 = y_1.P_T = y_1.1 = \frac{moles\ \ water}{moles\ \ water\ \ +\ \ moles\ \ air} \tag{3.4}$$

$$moles\ \ water = (moles\ \ air).\frac{p_1}{1-p_1} \qquad [mols^{-1}.(-/-)] \tag{3.5}$$

$$\dot{m}_s = 18.(moles\ \ air).\frac{\%RH.p^*(t)}{100 - \%RH.p^*(t)} \quad [gs^{-1} = (g.mol)^{-1}.mols^{-1}.(-/-)] \tag{3.6}$$

The pipework used in this section of the apparatus was mainly constructed from copper and plastic. The cold air supply was first of all routed through plastic tubing, allowing flexibility and ease of adjustment. As the pipework contained only air and water there were no problems with corrosion.

Absorption Column.

The first absorption column was constructed from stainless steel tube, 50 mm in diameter and 800 mm in length. Seven thermowells were positioned at 100 mm intervals down the length of the column; the first of which was positioned 50

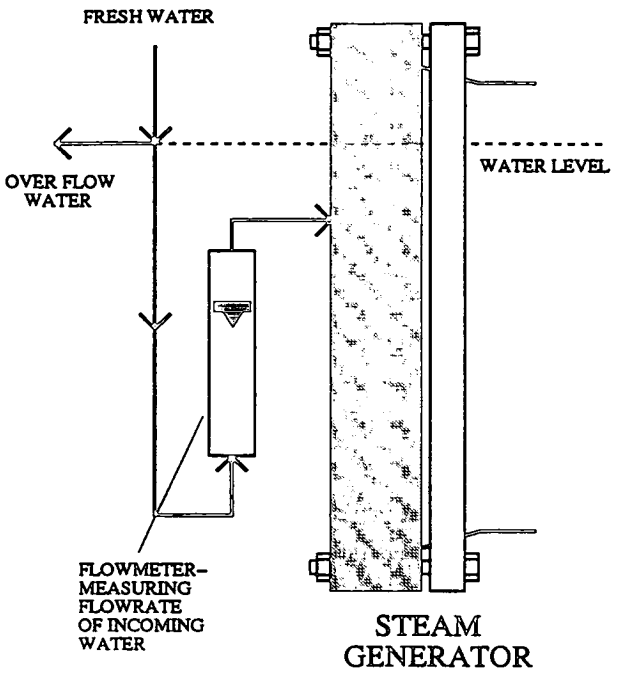

Figure 3.2: Representation of the constant head device used to measured water flow into the steam boiler.

mm from the top. The thermowells, which were made from 1.5 mm stainless steel tubing with a drop of silver solder at one end, were used to house type K thermocouples. These were used to give an indication of the temperature profile within the column. In addition to these thermocouples, the inlet and outlet temperatures of the gas and lithium bromide streams were also measured.

A glass X- piece was positioned directly beneath the stainless steel column, Figure 3.3. The bottom leg of this glass section served as a reservoir for weak lithium bromide solution, prior to its transfer to the generator. A level controller was fitted into the left- hand arm of the X- piece, which used the height of the liquid to periodically open and close a solenoid valve controlling the flow of liquid into the generator. The purpose of this device was to prevent the suction of air into the low pressure generator by ensuring that liquid was always present in the bottom section of the X- piece. The level control consisted of three electrodes, Figure 3.4, which were secured in a piece of PTFE rod, this

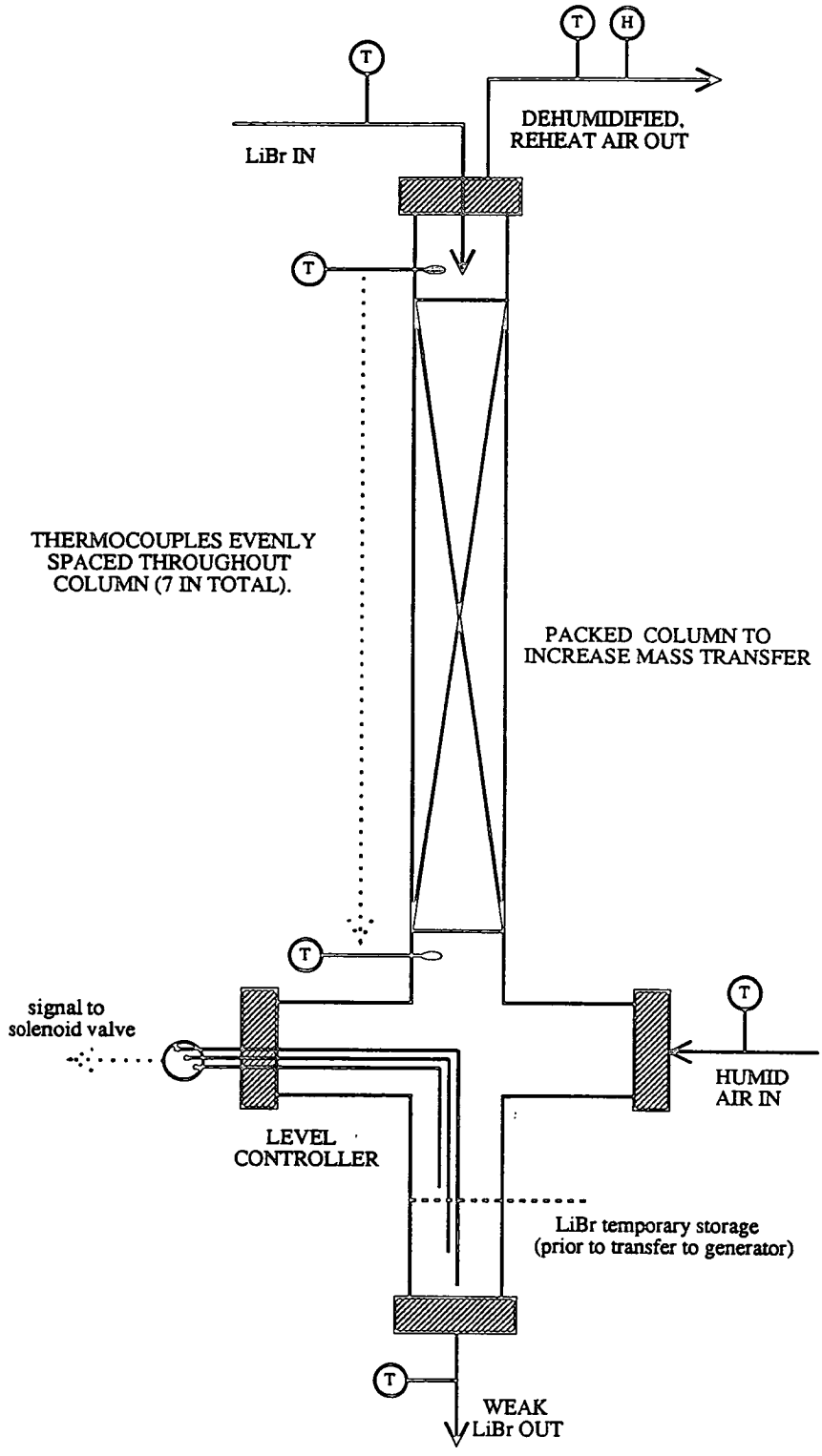

Figure 3.3: Single stage packed absorption column.

was in turn was mounted into a 12 mm Swagelok fitting. The electrodes were sheathed in a PTFE sleeving in order to prevent erroneous signals being sent to the controller and triggering the solenoid valve, caused when the liquid solution dripped onto the electrodes.

The three electrodes required for the liquid controller were:

- Common- always submerged in the liquid solution, acting as a reference electrode.
- High level- when the liquid reached this electrode a signal was sent to the controller relay, caused the solenoid valve to open. The pressure differential between the absorber and generator causes the liquid to be sucked into the generator.
- Low level cut off- when the liquid level dropped below the height of this electrode, the solenoid valve shut and stopped the transfer of liquid to the generator.

The absorber was operated in two modes allowing either the cocurrent or countercurrent flow of the gas and liquid streams, Figure 3.5. This enabled comparative studies of the dehumidification and reheating capabilities of each configuration to be assessed. In both cases, the lithium bromide and humid gas streams were in direct contact with each other to facilitate the absorption of water vapour. The column was also randomly packed with 15 mm Fenske helices, Figure 3.6, so as to enhance the mass transfer rate of water vapour between the phases.

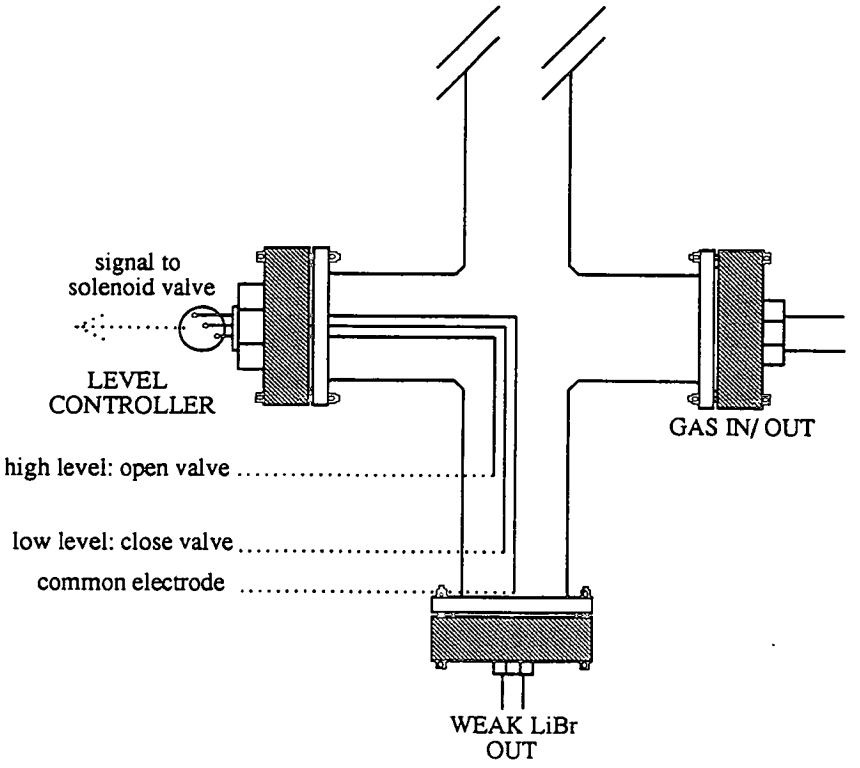

Figure 3.4: Level controller on bottom section of the absorber.

Experiments carried out using the packing indicated that the voidage of the packed column was very high, at 0.925; with an effective interfacial area of 250 m^{-1} (surface area / packed volume). One advantage of operating with such a high voidage was that the pressure drop across the column was low. Another useful measurement for assessing the packing is the equivalent spherical diameter of the packing, which was calculated to be 9 mm. This values was used to calculate mass transfer coefficients for the computer model, outlined in Chapter 5 'Computer Modelling'.

In order to ensure an even distribution of concentrated lithium bromide solution throughout the absorption column, a liquid distributor was designed. This consisted of a small piece of stainless steel rod with several angled holes drilled in it, this directed the liquid flow to all cross sections of the column, Figure 3.7.

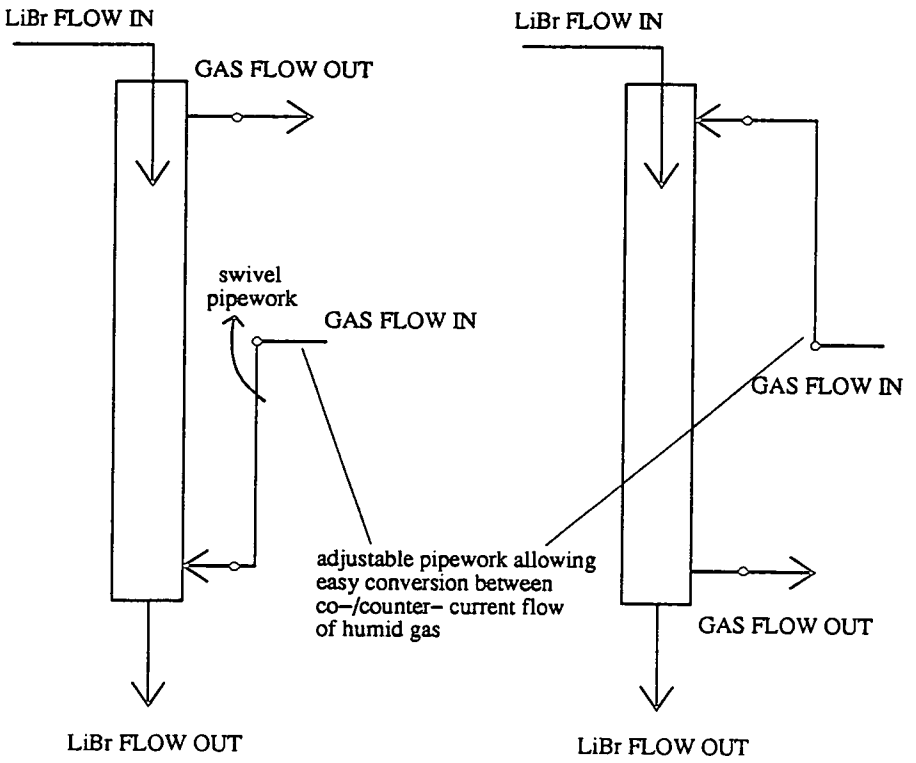

Figure 3.5: Modes of operation for the absorption column.

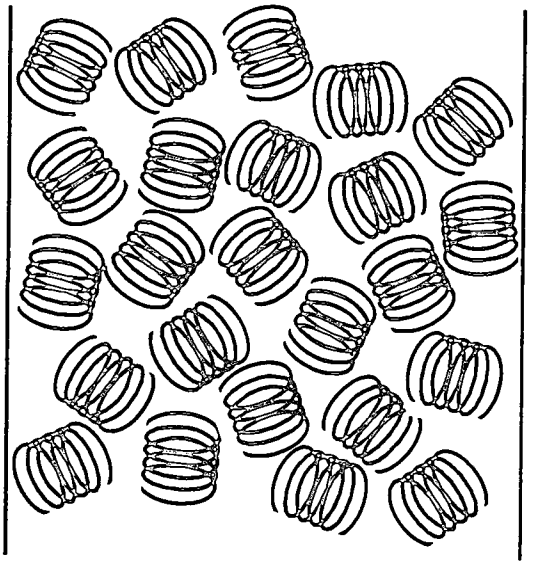

Figure 3.6: Random packing of glass Fenske helices within absorber column.

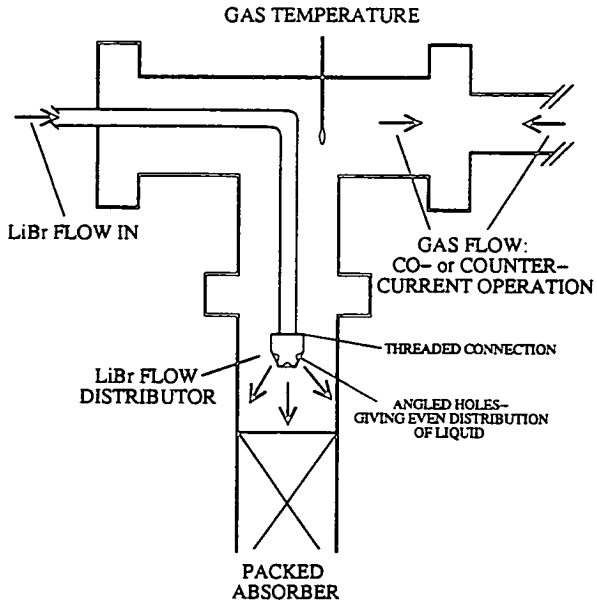

Figure 3.7: Inside the top of the absorption column.

A further design feature of the column was a packing support, which was made from a thin piece of PTFE sheet with several holes drilled in it to let the gas permeate through the column, while retaining the packing in position.

The concentrated lithium bromide solution leaving the generator was pumped into the top of the absorption column, using 6 mm stainless steel tubing. However, as a direct result of the low liquid flowrates used, typically 2- 4 mls^{-1}, the stream temperature dropped several degrees. Therefore, provision had to be made to ensure that the lithium bromide stream entering the absorber was maintained at the desired temperature. Therefore, it was necessary to heat the liquid absorbent stream using an electric heating element, which was made from Inconel 800 and could be adjusted to allow the inlet temperature of the stream to be independently controlled.

Lithium Bromide Generator.

The concentrated lithium bromide solution reservoir was made of glass, 102 mm in diameter and 600 mm in length. When the equipment was not in use, care was taken to ensure that the solution did not crystallise and solidify during storage. Therefore, the solution was diluted to a concentration of between 55-60 %w/w, at which point the crystallisation temperature is less than normal room temperature ($T_{crystallisation}$ @ 60%w/w $\sim$ 10 °C).

The vessel was operated under vacuum, typically in the range 0.05- 0.10 bara and at temperatures of between 90- 100 °C. The normal range of operating concentrations corresponding to these conditions were 60- 68 %w/w, Figure 3.8.

The purpose of this section of the apparatus was to store lithium bromide solution at the desired operating condition. Weak solution from the absorber was flashed into this vessel periodically by means of a brass solenoid valve, which was activated by the level controller, see Section 3.1.2. The flowrate of the concentrated solution leaving the generator was controlled by regulating its flow through the stainless steel diaphragm metering pump.

It was necessary to use two electric bayonet heaters to provide extra heat to the generator to ensure that the lithium bromide solution was maintained at a constant concentration during normal operation, Figure 3.8. Otherwise there would be insufficient heat to evaporate the water and the solution would become progressively weaker. The heaters consisted of an inner heating element surrounded by an outer quartz sheath (supplied by Electrothermal Engineering Ltd.). A variable power source was used to control the amount of heat supplied to the vessel, up to a maximum of 800 W. The heaters were not affected by continuous immersion in hot, concentrated lithium bromide solution. However,

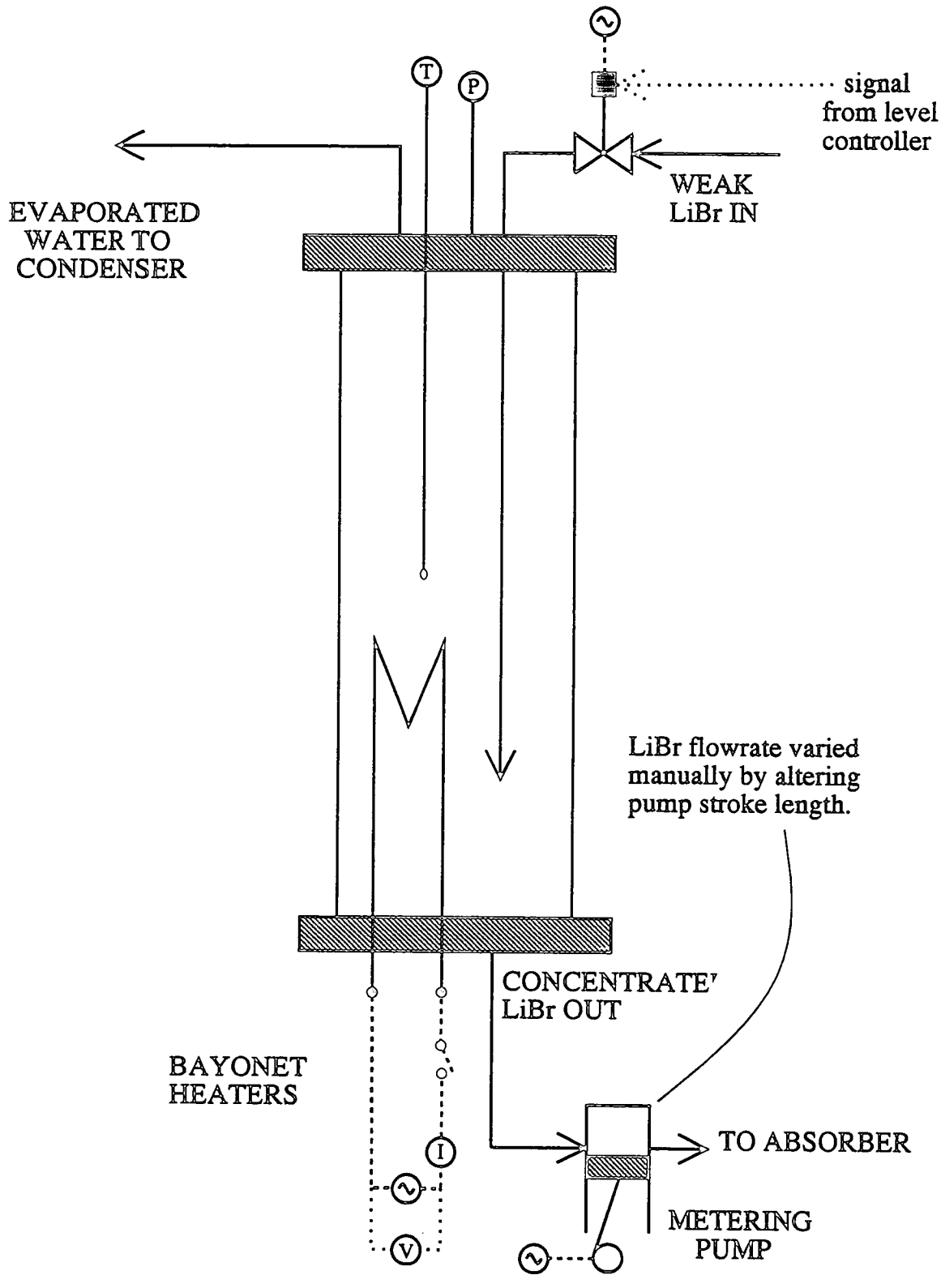

Figure 3.8: Experimental apparatus for the lithium bromide generator.

there was a potential hazard associated with diluting the hot, concentrated absorbent solution with water during shutdown of the apparatus, which could rupture the heaters or even the vessel due to thermal shock. The dilution of the concentrated lithium bromide solution and also the flushing of the absorbent pipework with water was carried out in order to minimise the risk of crystallisation.

Both ends of the glass column were sealed with stainless steel flanges, using PTFE O- rings to ensure that a good seal was obtained. As this section of the apparatus was operated under a strong vacuum it was important to remove the possibility of air leaks into the system. All pipe connections onto the flanges- flowrates into/ out of the vessel, thermowell, heater connections- were made using readily available, stainless steel Swagelok pipe connections. These fittings were screwed into holes drilled in the flanges and PTFE tape wrapped round the screwed end of each fitting to ensure that a secure and airtight connection was established.

The instrumentation on the lithium bromide generator consisted of a type K thermocouple to measure the vessel temperature and a pressure gauge which measured the vacuum within the system. The flowrate of concentrated lithium bromide solution leaving the vessel was controlled by varying the stroke length of the metering pump. It was possible to infer the inlet flowrate of the weak solution to the vessel by the summation of the flowrate of concentrated solution leaving the generator and the amount of water collected in the receiver. Finally, the power input of the electrical heaters was measured and recorded. Therefore, by knowing all the flowrates and enthalpies of the streams, as well as the extra heat input, it was possible to determine a heat balance for the vessel. This could be compared to theoretical calculations and also used to assess the performance of the equipment.

Condenser- Receiver.

The condenser used in the pilot plant was a standard Corning glass condenser with a diameter of 76 mm. The cooling medium used within the coil was water. Typical flowrates of the cooling water were between 12- 17 mls^{-1}. This corresponded to a temperature lift of only a few degrees and ensured that all of the water vapour from the generator was condensed. As the vacuum system was run continuously during normal operation, any water vapour present in the air stream after the condenser could have reduced the vacuum pump efficiency and caused operating difficulties, therefore, a high cooling water flowrate had to be maintained in the coil.

The condensed water was collected in a 500 mm length of glass, which had the same diameter as the condenser. Attached to the side of this receiver was a graduated scale, Figure 3.9. From measurements of the amount of condensate collected over a period of time, an estimation of the flowrate of water vapour from the generator and hence the amount of water absorbed from the humid gas stream could be determined. A later development to this system was the addition of a pressure differential gauge which was calibrated to measure the rate of condensate collection automatically, the data was then stored in a file for later analysis. Signals were sent directly to a PC, where the readings were converted to flowrates. When the condensate level in the receiver exceeded 400 mm, the vacuum was switched off and the valve at the bottom of the receiver opened, thereby draining the condensate from the receiver.

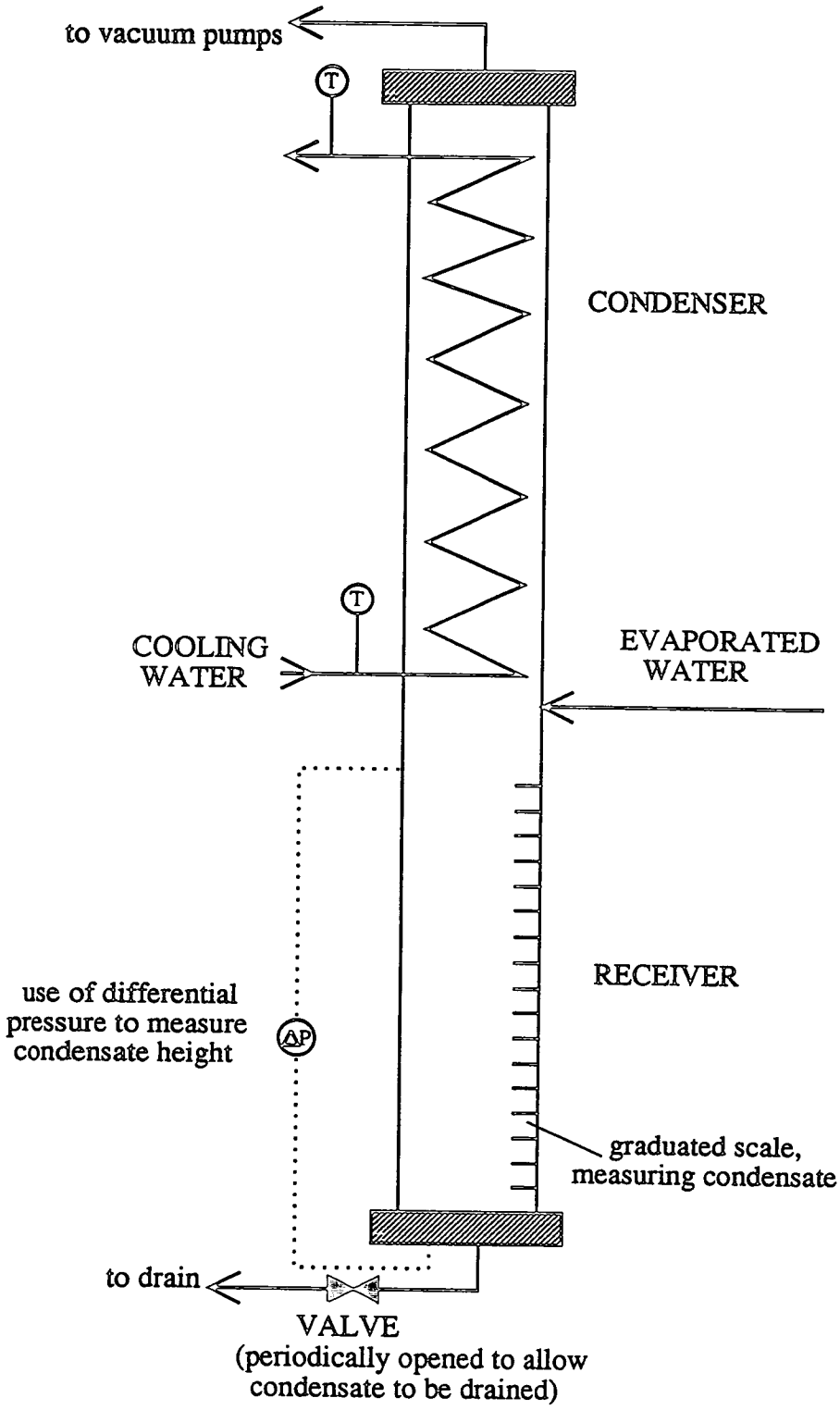

Figure 3.9: Condenser- receiver arrangement.

Ancillary Equipment.

Associated with the pilot plant were several pieces of ancillary equipment which were required for normal operation, these are described below.

Metering pump. The metering pump could accommodate three pump heads in parallel, although only two were required. The pump heads were used to deliver concentrated lithium bromide to the absorption columns, for both the single stage and double stage plants. They were manufactured from stainless steel (type 316) and were capable of flowrates of between 0- 4 mls^{-1}. The pumps were calibrated under normal operating conditions, with the vacuum system switched on, thus developing a large back pressure against which the pumps had to pull. As the low pressure generator was positioned close to the pump, problems with cavitation were experienced at the highest flowrates. However, reliable and reproducible flowrates were obtained at lower flowrates (up to a stroke length of 80 % of the maximum).

Solenoid valve. A brass solenoid valve, with 6 mm connections, was used to control the flow of weak lithium bromide solution from the absorber to the generator. The valve was actuated by an impulse from an RS liquid level sensing relay, which was triggered by a signal from one of the level control electrodes, either high (open valve) or low (close valve). The default position of the valve was closed.

Vacuum pumps. Two Edwards vacuum pumps were used to generate the high vacuum required during normal operation. Both pumps were frequently lubricated to maintain good seals between the bushes and the impeller casing,

reducing the risk of seizure. The pumps were typically operated continuously over an eight hour period, with short breaks to allow drainage of the receiver. As a result, the pumps tended to become extremely hot, causing the lubricating oil to evaporate. Therefore the pumps were 'topped- up' with oil at the end of each series of experiments.

Humidity probe. The relative humidity and temperature of the gas stream were measured using a Lee- Integer high temperature humidity probe, type CH30. Readings were fed to a meter, via a 6 pin DIN connection, where the results were displayed. Initially, using the single stage pilot plant, the readings were manually converted to give an estimate of the steam flow, using Equations 3.3, 3.4, 3.5, 3.6. In the later two stage plant, the readings were input into a PC, which automatically calculated the flow and stored the data in a file for later analysis.

The operating temperature range for the probe was -40 to +125 ^{0}C, while the specifications for the humidity sensor indicated that readings between 20- 90 %RH varied linearly. The typical operating conditions for the probe were in the range of 60- 100 °C and 10- 100 %RH. The head of the probe contained separate sensors for the humidity and temperature readings. It was protected by a metal surround with several slots, allowing the gas to flow over the sensors. A PTFE sheath, Figure 3.10, encased the head to filter out any contaminants in the stream and thus prevent damage to the humidity sensor. Indeed, malfunction while operating in a lithium bromide environment resulted in several different humidity sensors being used. The probe was received from the manufacturer precalibrated, although it was checked upon arrival against known water partial pressures generated above different concentrations of sulphuric acid solutions.

Two humidity measurements were required- before and after dehumidification- however, there was only one humidity probe requiring the transfer of the probe between sampling points. The gas stream passing through the absorption column was at an elevated temperature and as such, it could cause injury upon direct exposure to the hot stream. Therefore, the sampling port, Figure 3.10, was designed to allow the insertion of the probe, prior to exposure to the hot stream. This was achieved by securing the probe into the end of a small section of copper pipe. The probe was inserted as far as a gate valve, which was closed when not in use. Once in position, the valve could be opened and the probe pushed fully into the sample port so as to lie directly in the main flow of gas. This ensured that accurate measurements were obtained. After taking a reading, the probe was withdrawn, the valve closed and the probe removed from the sample port.

3.1.3 Two Stage Pilot Plant.

Following an extensive experimental study using the single stage heat transformer, another pilot plant was designed and constructed. The second heat transformer incorporated new ideas, which were developed as a consequence of the earlier experiments. However, the basic layout and structure of the system remained the same. The humid gas generation apparatus, the lithium bromide generator and the condenser/ receiver all remained unchanged. The only design changes were related to the absorber, which was split into two stages. These are as follows:

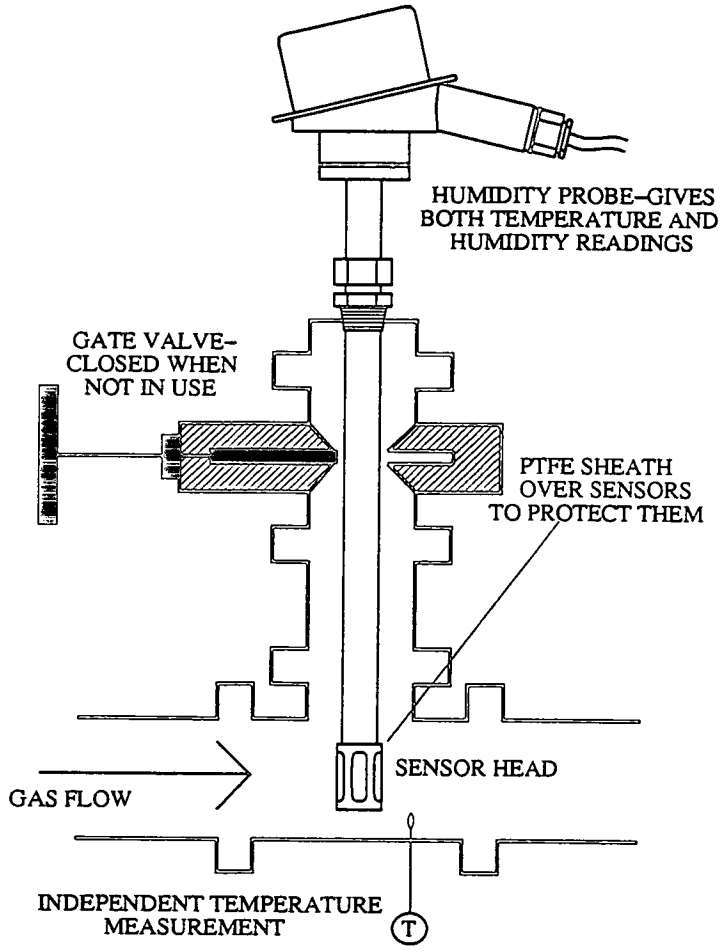

Figure 3.10: Diagram of humidity sampling point, with probe in position.

- Direct contact dehumidification of a humid gas stream. Followed by,
- Indirect reheating of the gas stream using a mixture of concentrated lithium bromide and low pressure steam.

Further developments included the automatic logging of all the temperatures onto a PC. Manually recorded data- i.e. the power input to all the heaters used, all the stream flowrates and also the vacuum on the low pressure side of the apparatus- were input to the computer. All data was stored in files, allowing analysis at a later date. (Further details of the instrumentation and the software written to log the data is contained in Section 3.2.3).

Dehumidification Column.

The design of the dehumidification column was based upon the absorption column used in the single stage plant. Several designs were investigated and their dehumidification performance assessed, details of which are summarised in Chapter 4 'Experimental Studies". Within each of the different column types five thermocouples were evenly spaced at 100 mm intervals, providing a rough temperature profile for the column. The different columns tested are discussed below in more detail:

Falling film column: A plain section of glass, with a diameter of 38 mm and length of 600 mm, was initially tested. The rationale behind this change was to test the dehumidification potential of a falling film absorber. This absorber could be operated at gas flowrates up to 5 gs^{-1} (corresponding to a superficial velocity of 4.3 ms^{-1}) without the risk of flooding. Experiments with the column were not very promising and a

redistribution plate was designed and positioned half way down the column, Figure 3.11. The aim of this modification was to improve the liquid- gas contact by redirecting the liquid flow away from the wall of the column. It was observed that the modification did improve the liquid- gas mixing above the redistributor plate.

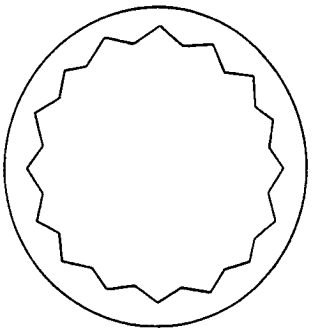

Figure 3.11: Liquid redistributor used in falling film column.

Packed column: Following tests with the falling film absorber, it was decided to fill the column with Fenske helices, Figure 3.6, and to test the dehumidification potential of a packed column. The packing helped to increase the surface area available for mass transfer. It was, however, necessary to restrict the gas flowrate to a maximum of 4 gs^{-1} due to the risk of flooding above this flowrate.

Condenser: A condenser, with the same dimensions as the previous columns, was also tested. Cooling water, flowing in a internal coil, was used to roughly control the temperature in the upper section of the column. By setting the inlet lithium bromide concentration and maintaining a set temperature at the top of the column, it was possible to gain a degree of control over the partial pressure of the exit gas. The cooling water maintained a uniform temperature throughout the column, carrying away the heat of absorption and condensation of the water. The cooling coil also increased the surface area within the column which was available for mass transfer. Problems were experienced due to flooding at higher gas

flows. It was therefore, necessary to restrict the gas flowrates through the column to a maximum of 2 gs^{-1}, corresponding to a superficial gas velocity of 1.7 ms^{-1}.

Reheat Column.

An indirect contact absorption column was designed to reheat the dehumidified gas stream and to achieve as high an exit temperature as possible. The column consisted of an inner heat pipe, which contained the hot medium; around this the dehumidified gas was circulated, Figure 3.12. High temperatures were generated within the inner tube by absorbing low pressure steam into concentrated lithium bromide solution. An important design feature of the column was the need to maximise the heat transfer to the externally flowing gas, this was achieved by placing a highly extended surface of closely packed fins on the outside of the high temperature 'absorption pipe'. The hot absorbent mixture flowed down the inner tube of the column, while the gas being heated flowed countercurrent to it, in the annular space between the inner tube and outer absorber shell.

The column was manufactured especially for this project by Cal- Gavin Ltd. of Birmingham. The inner tube of the column, the 'absorption pipe', contained a turbulence promoting insert in order to fulfill the following:

1. To help direct the flow of hot liquid to the wall and hence increase heat transfer to the external gas stream.
2. To promote turbulence within the liquid layer and thus increase the heat transfer.
3. To help maximise the contact between the liquid and steam phases with a resultant increase in mass transfer.

The inner and outer tubes and the turbulence promoting insert were made from stainless steel (type 316). The extended surface area was made from copper, as it was not subject to corrosion through contact with lithium bromide.

A later modification to the lithium bromide pipework of the reheat column, Figure 3.14, involved the addition of a bleed valve to remove inerts from the system. During experimental trials it was discovered that gases were present within the column, which led to a reduction in the steam partial pressure in the column, resulting in a decrease in the maximum obtainable gas exit temperature. As well as bleeding the column of inerts it was also necessary to ensure that no further gas could get into the system. Therefore, the liquid pipe, which delivered the weak lithium bromide solution to the X-piece of the dehumidification column, was extended to ensure that it was submerged in liquid at all times, reducing the risk of air entrainment.

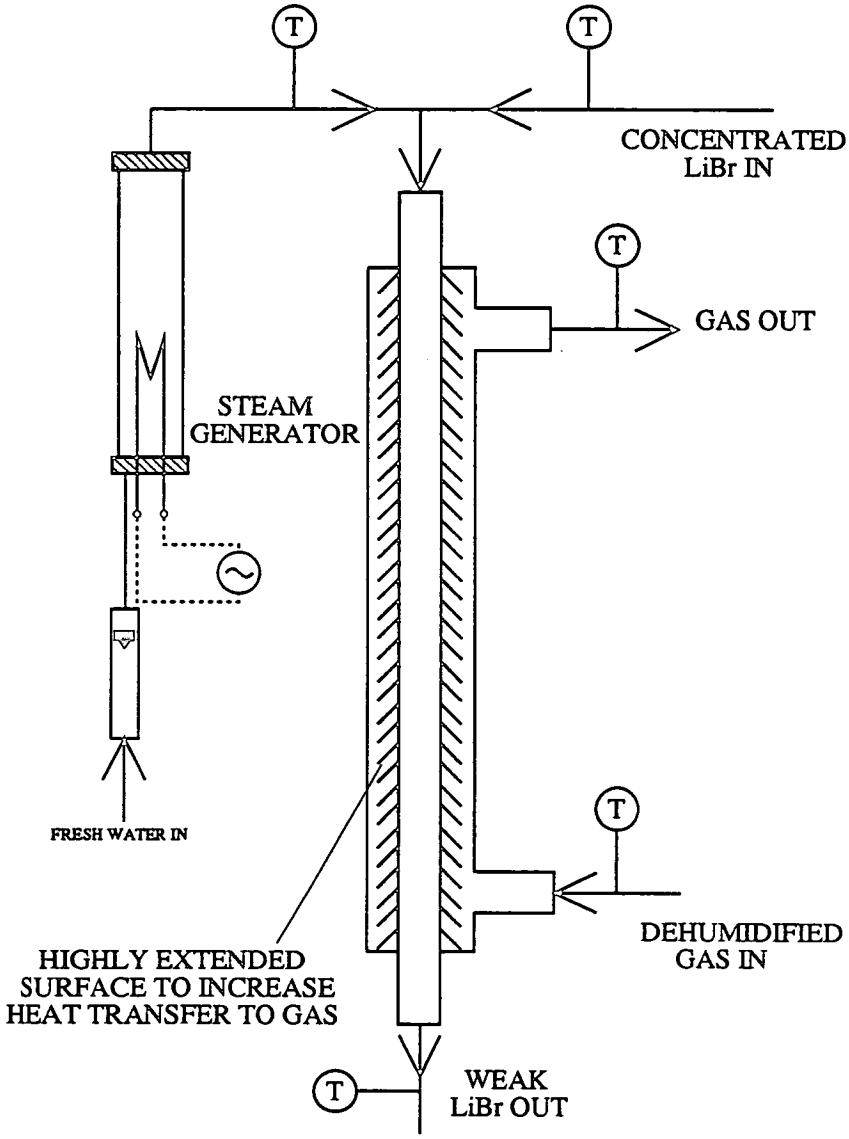

Figure 3.12: Experimental setup for the reheat column, showing the steam supply.

3.2 Construction.

3.2.1 Materials of Construction.

The experimental apparatus was constructed from glass, stainless steel (type 316) and copper. Glass was used for some of the vessels, while the stainless steel was used for all lithium bromide pipework, fittings and vessel flanges. The use of copper was restricted to areas where lithium bromide was not present, for example the steam generation system. A brass solenoid valve was used to transfer the weak lithium bromide solution from the absorber to the generator. The valve operated satisfactorily throughout the tests and did not appear to suffer from any corrosion in the presence of hot lithium bromide solution. PTFE O-rings were used to seal the surface between the glass rims of vessels and the end flanges. These O- rings were not affected by the presence of hot, concentrated lithium bromide solution and provided a good seal for the equipment when operated under vacuum.

3.2.2 Layout.

Main Framework.

The layout for the single and double stage heat transformer rig was essentially the same. The single stage process acting as the prototype for the later two stage version, which incorporated several design changes. Therefore, only the layout of the two stage process shall be discussed in this section. A compact

plant was designed and constructed to allow easy access to all parts of the apparatus. The framework for the plant was constructed using sections of Dexion. This allowed ease of construction and resulted in a frame which was flexible and easily adjusted. The final plant layout is shown in Figure 3.13.

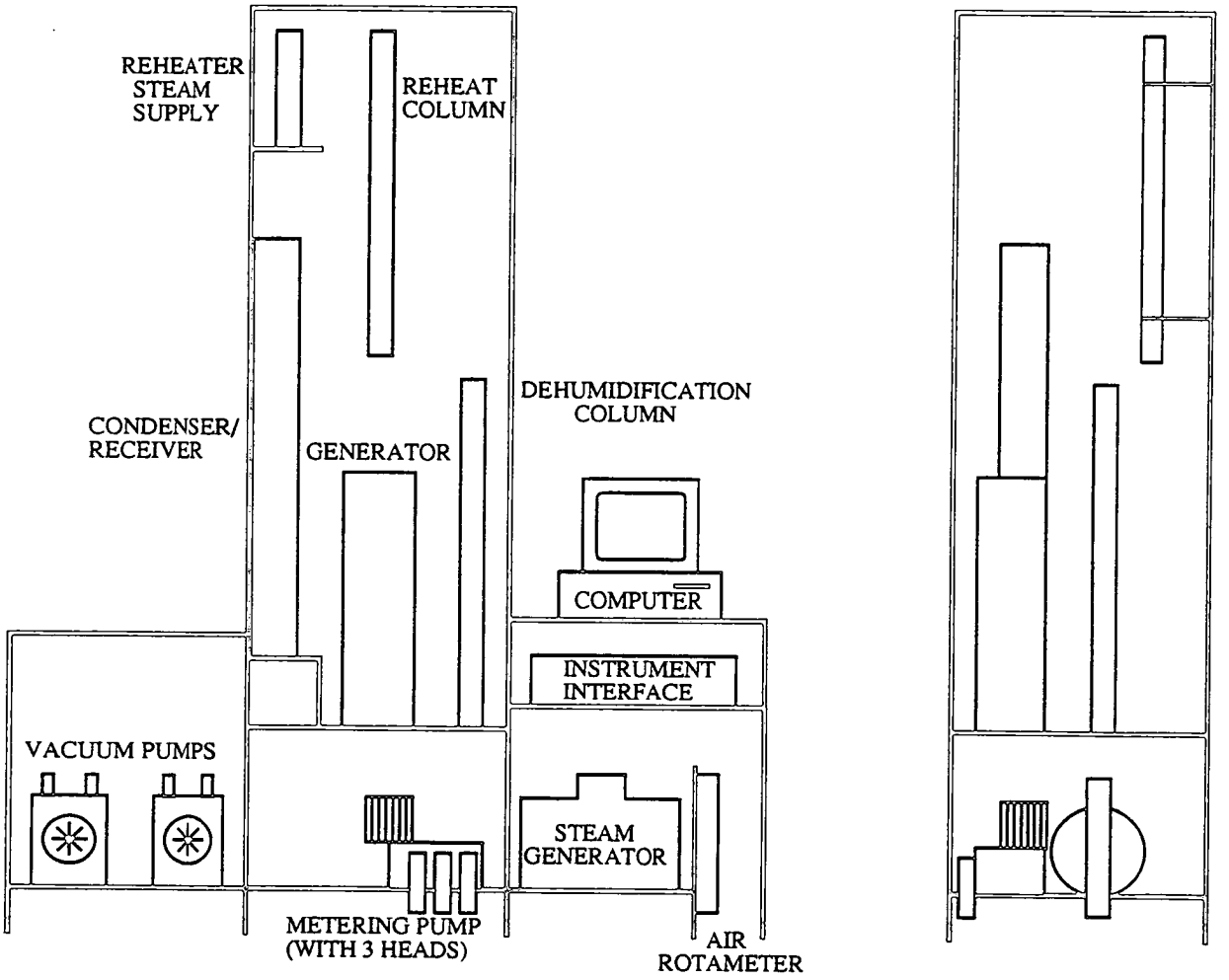

Figure 3.13: Front and end elevation showing layout of experimental apparatus (only main pieces of equipment shown.)

The position of the glass columns could be readily adjusted by altering the length of the securing bolts, which held the columns in place. Such an arrangement allowed the columns to be moved without placing undue stress on the glass sections.

All pieces of equipment and electrical connections were positioned above floor level and a plastic 'drip mat' placed beneath the rig helped to contain any spills of lithium bromide. The electrical wiring was made safe through insulation and attachment to the main frame, preventing any hazards associated with trailing cables or contact with any spilled liquid.

Lagging on the apparatus was secured using detachable tag ties, which allowed quick and easy access to individual components of the apparatus. In all cases the lagging used to minimise heat losses from the rig was a type of densely packed glass wool, approximately 20 mm thick.

Lithium Bromide Pipework.

The lithium bromide was delivered from the generator to the metering pump heads and then to each individual column via 6.3 mm stainless steel pipework. The pump was mounted above ground level to allow the liquid lines to be installed, while also providing easy access for cleaning, in case of crystallisation in the line. External heating for each of the lithium bromide lines was required in order to control and maintain a desired temperature for the lithium bromide solution, these are shown in Figure 3.14.

During shutdown, the valve below the generator was closed and the pipework flushed with hot water to minimise the risk of crystallisation. The apparatus was filled with lithium bromide solution by opening the charging valve and switching on the vacuum system, effectively sucking the solution into the generator.

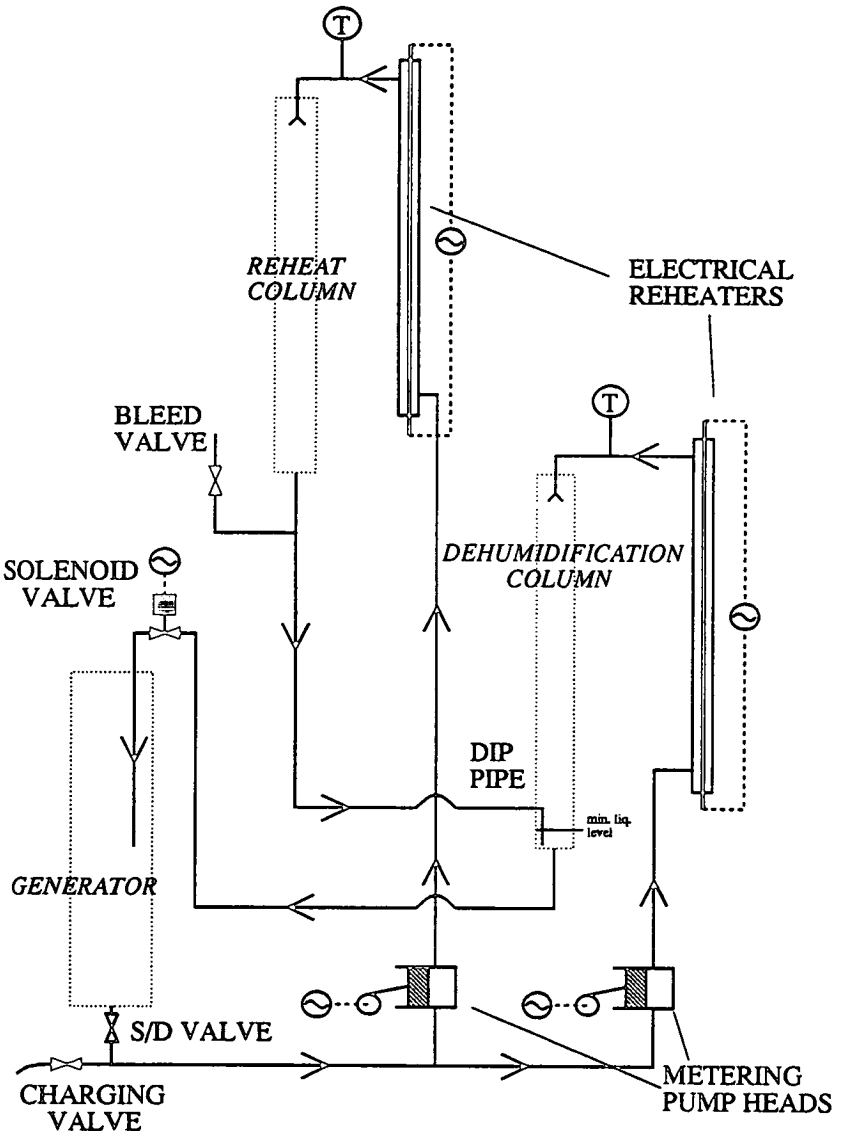

Figure 3.14: Diagram of lithium bromide pipework, including reheaters.

Assembly of Glass Sections.

Care was taken so as not to stress the joints when assembling QVF glassware as this could lead to glass failure. Figure 3.15 shows the arrangement necessary for for joining a glass section to an end flange. A similar setup was required when joining two sections of glass together.

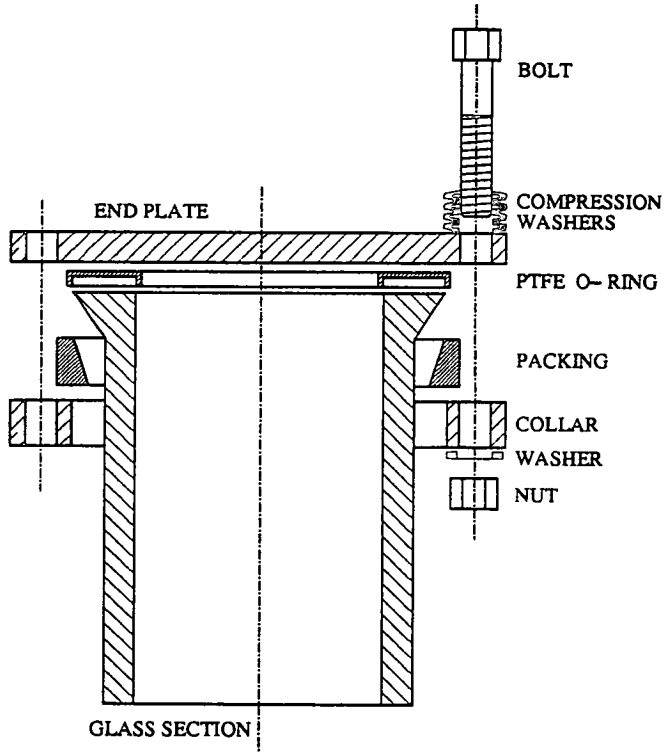

Figure 3.15: Assembly of QVF glass.

First of all, a collar, with three securing holes, and a packing ring were placed over the end of the glass. The packing secures the collar in position, over the end of the glass. It was essential that the packing was properly fitted, otherwise the collar will not lie perpendicular to the glass section, resulting in a poor seal. The end flange was held in place by three, evenly spaced, bolts. Overtightening the bolts was prevented by including several compression washers, as shown in Figure 3.15. The number of washers used was dependent upon the diameter of the glass section, details of which were taken from a QVF handbook. The

correct tension was achieved when the washers were compressed to a predetermined length, as set out in the QVF handbook. A PTFE O-ring was also used to ensure a good seal between the glass and flange.

3.2.3 Instrumentation and PC Interfacing.

The computer used for data logging and storages was a PC with a 80286 coprocessor and a PCL- 812 instrument interface. Details of the instrumentation used on the rig are provided below.

Data Readings.

The instrumentation on the rig mainly consisted of logging the temperatures in the system. A list of the temperatures measured is provided on the next page.

The temperature readings were fed into two PCLD- 889 amplifier/ multiplexer boards. Signals from the instrument box were fed through an interface box, which filtered out any noise from the signals and ensured that a clean voltage was fed to the PC- mounted PCL-812 card. The readings from PCL-812 board were converted from voltages into temperatures using TurboC program routines. The values were displayed on screen and also output to data files for future reference. The voltage range used for the temperatures was -10 to +10V (-2048 to +2048 bits), corresponding to a temperature precision of 0.12 ^{o}C bit^{-1}.

Thermocouple Number	Description/ Position
1-5	Five thermocouples placed at increasing distance down the length of the dehumidification column, giving a temperature profile.
6	Positioned after the air preheater.
7	Air inlet to dehumidification column.
8	Air outlet from dehumidification column.
9	LiBr inlet to dehumidification column.
10	Cooling water to dehumidification column.
11	Cooling water from dehumidification column.
12	LiBr outlet from dehumidification column.
13	LiBr inlet to reheat column.
14	Steam inlet to reheat column.
15	LiBr outlet from reheat column.
16	Air outlet from reheat column.
17	Temperature of weak lithium bromide stream prior to entry to the evaporator.
18	Evaporator temperature.
19	Cooling water to condenser.
20	Cooling water from condenser.

In addition to the automatic data logging of the temperatures, the amount of condensate collected in the receiver was recorded by using a differential pressure gauge. The vacuum and temperature of the generator were also recorded and used to estimate the lithium bromide concentration (using the equations given by Brunk [24]). A composition meter was also developed, which monitored and displayed the concentration of the lithium bromide solution independently to that shown on the PC. Chapter 7, 'Electronic Composition Meter', discusses the development and potential applications of this device. Measurements which were taken manually and input into the PC are listed below:

Vessel	Description of the manual data recorded
Dehumidification column:	Metering pump setting for flow of lithium bromide. Flowrate of water to the steam generator. Dry air flowrate. Pressure drop across the column. The relative humidity and temperature of the gas steam entering and leaving the column. Power input (voltage and current) to steam boiler.
Reheat column:	Metering pump setting for flow of lithium bromide. Steam flowrate to reheat column. Power (voltage and current) to steam heater. Pressure drop across the column
Generator:	Power (voltage and current) to the generator.
Miscellaneous:	Cooling water flowrate to the condenser.

Software.

A TurboC program was written to monitor and display the various temperatures, flowrates and pressures throughout the system. Figure 3.16 shows the main display screen of the data monitoring program. All of the temperatures and flows for each piece of equipment in the rig were shown. In

conjunction with the visual display of readings, all the readings taken were logged in data files, providing a comprehensive record of the operation of the system. As the apparatus operated at a steady state it was only necessary to sample data every 30 seconds.

DEHUMIDIFICATION COLUMN:= <F1> TO STOP == Mon Nov 01 09:00:30 1993

INLET:

LiBr : Flowrate	(ml/s)	= 4.53	Steam/ air : Air flow	(g/s)	= 2.00
:	(g/s)	= 7.35	: Steam flow	(g/s)	= 0.15
: Concentration	(%)	= 65.3	: Humidity	(%RH)	= 45.5
: Temperature	(°C)	= 101.1	: Temperature	(°C)	= 97.3

OUTLET:

LiBr : Concentration	(%)	= 62.2	Steam/ air : Steam flow	(g/s)	= 0.03
: Temperature	(°C)	= 135.2	: Temperature	(°C)	= 95.2

REHEAT COLUMN:

INNER TUBE:			Steam flowrate	(g/s)	= 0.16
LiBr Flowrate	(g/s)	= 6.35	Steam temp. in	(°C)	= 99.9
LiBr concentration	(%)	= 65.3	OUTER SHELL– GAS		
LiBr temp. in	(°C)	= 101.2	Inlet Temperature	(°C)	= 95.2
LiBr– steam temp. out	(°C)	= 156.3	Outlet Temperature	(°C)	= 150.4

GENERATOR :

Temperature (°C) = 97.3 Pressure (bar) = 0.075 Concentration (%) = 65.3

MISCELLANEOUS :

Amt. transferred	(g/s)	= 0.12 T_amb	(°C) = 25.3	OPERATION MODE = 2
Amt. collected	(g/s)	= 0.11		STATUS = 0

Figure 3.16: Graphical representation of data monitoring program.

The alteration of the manual readings, such as flowrates and humidities, were carried out interactively with the computer through the use of pop- up windows. Figure 3.17 shows the steps required to change the lithium bromide flowrate of the reheat column. A popup menu containing a list of options which could be changed or evaluated was activated by clicking the left hand button of the mouse, when it was positioned on the main reheat window. The arrow keys were then used to scroll through each of the options shown, before selecting the desired variable. By pressing the (RETURN) key a further window was displayed showing the current setting, this value was changed by typing in a new value and pressing (RETURN) again. The main display was restored by

pressing (ESC) to remove the pop-up windows. There were four main popup windows for each of the different sections of the main display- the dehumidification and reheat columns, the generator and some miscellaneous readings.

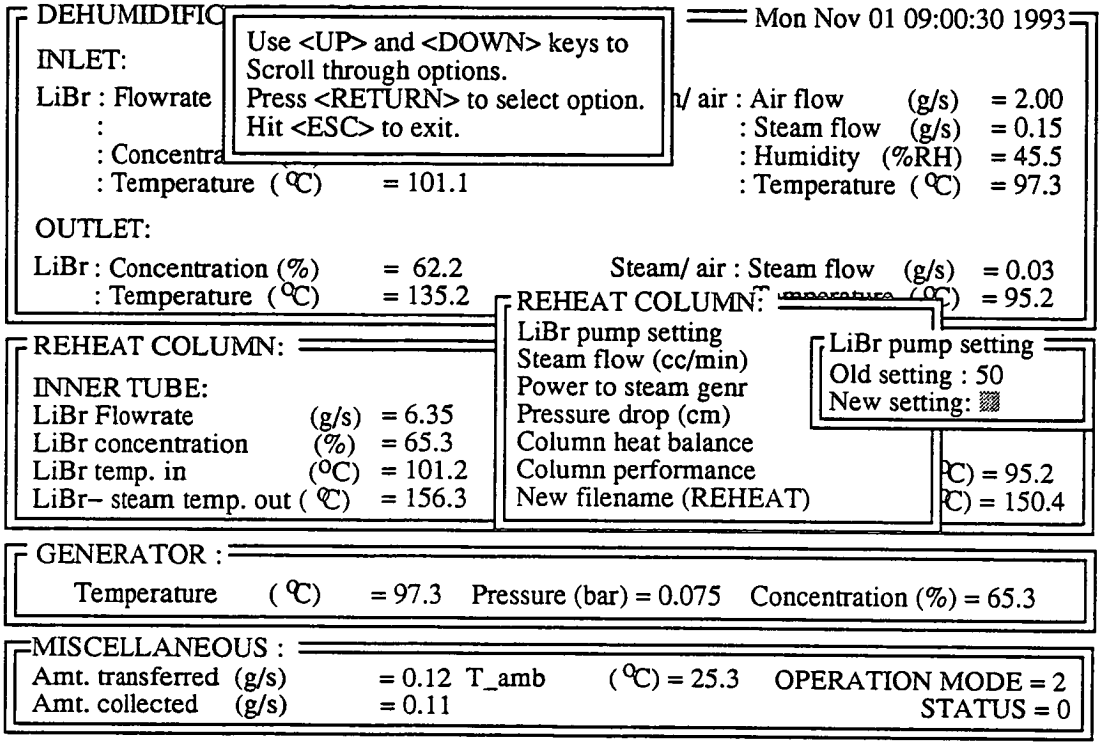

Figure 3.17: Monitoring program showing additional windows with options available for changing settings and carrying out preliminary analysis.

It can be seen from Figure 3.17 that as well as changing manual variables, the heat balance and performance of the column could also be evaluated. Once again, this data was stored in a file for later analysis. The online determination of several performance criteria was also performed, these are summarised below:

Vessel	Criteria
Dehumidification column:	Heat balance.
	Exergy balance [Base Temperature, T_O, set to 20 °C].
	Temperature change in the gas stream.
	Amount of water absorbed.
Reheat column:	Temperature change for the external gas stream and the lithium bromide flowing in the inner tube.
	Heat balance.
	Exergy balance.
Generator:	Heat balance.
	Exergy balance.
	Graphing program to display the variation in the lithium bromide concentration in the generator.
Miscellaneous:	Overall coefficient of performance of the heat transformer.
	Exergy balances for whole system- yield, effectiveness, losses.
	Graphing program to display the difference between the amount of water condensed to that transferred in the gas stream, as estimated from the difference in the gas humidity readings.

Chapter 4

Experimental Studies.

4.1 Background.

An open loop absorption heat transformer pilot plant was designed and tested for the purpose of dehumidifying and heating humid gas streams. The system was directed towards the recovery of waste heat from the humid exhaust streams of spray dryers. Conventional methods of heat recovery can not readily be applied to the recovery of energy from humid gas streams due to condensation problems and also heat transfer difficulties prevalent with gases at low temperatures. In the studies carried out, different absorption systems operating under a wide range of conditions were investigated and the performance of the cycles assessed, with respect to their dehumidification and reheating capabilities.

The design objectives were based upon recovering waste heat from a humid gas leaving a spray drying chamber at a humidity around 0.20 g-$_{H_2O}$ (g-$_{dry\ air}$)$^{-1}$ and a temperature around 100 °C. A system capable of obtaining an exit gas stream with a humidity of between 0.03- 0.05 g-$_{H_2O}$ (g-$_{dry\ air}$)$^{-1}$ and a temperature in the range 150- 200 °C was sought. The stream would then be suitable for recycle to the drying chamber and thereby, reduce the energy consumption of the drying operation.

4.1.1 Overview.

Initial experiments using a single, packed absorption column for both dehumidifying and heating duties did not achieve the objectives set out at the start of the project. This was because in order to achieve a high exit temperature, a high inlet gas humidity was required. Conversely, to achieve a low gas exit humidity, the gas exit temperature must also be low. Therefore it was decided to split the operation into two absorption stages: a direct contact dehumidification stage followed by an indirect contact reheating stage. The results obtained for both of these heat transformer cycles are discussed in the following sections. Results are presented in chronological order, see below:

- Single stage studies- influence of variables on performance [Section 4.2].
- Two stage heat transformer-
  - Dehumidification column experiments [Section 4.3].
  - Reheat column experiments [Section 4.4].
  - Prediction of gas exit temperature from inlet conditions [Section 4.5].
  - Two stage heat transformer cycle performance [Section 4.6].

The data obtained for the single stage rig was used as the basis for deciding the experiments to be undertaken using the double stage absorption cycle.
Following the presentation of the experimental results obtained for both pilot plants, a review of the performance of the two stage cycle is provided. A brief investigation of the accuracy of the results and the errors associated with the experimental trials is then discussed in Section 4.7. The last section in this chapter (Section 4.8) lists the main conclusions of these experimental studies and also outlines recommendations for future studies.

4.1.2 Operating Variables.

The single and double stage absorption cycles involved the same process streams- a gas stream and a liquid absorbent stream (aqueous lithium bromide). The two pilot plants were designed to investigate the effects of varying the operating parameters associated with the two streams. The main variables investigated are listed below.

Gas stream:	Flowrate (gs^{-1}).
	Inlet temperature (^oC).
	Humidity ($g\text{-}_{H_2O}$ $(g\text{-}_{dry\ air})^{-1}$).
Absorbent stream:	Inlet concentration (%w/w).
	Flowrate (gs^{-1}).
	Inlet temperature (^oC).

Table 4.1: Main operating variables investigated.

In addition to these operating variables, there were other factors which affected the performance of the absorption columns including the column design- packed or falling film absorber- and also the mode of operation- co/ counter current flow of the gas and liquid streams.

4.2 Single Stage Cycle: Experimental Results.

The first absorption heat transformer cycle which was designed and constructed incorporated a packed absorption column. The packing, which had an effective interfacial area of $250m^{-1}$, was used to find the best operating conditions necessary to obtain the objectives of dehumidifying and reheating a humid gas stream. Thermocouples were positioned evenly down the length of the column to give a rough indication of the temperature profile within the column, from which deductions about the absorption process were derived.

4.2.1 Programme of Experiments.

The experimental programme initially undertaken was designed to cover as broad a range of operating conditions as possible. As there were several variables of interest within the system, each one is discussed separately. Most of the experiments were operated for cocurrent operation except where indicated (Section 4.2.7).

Operating Ranges.

The range of gas flowrates used in these studies was 0.2- 2.04 gs^{-1} (dry basis), while the inlet humidity range used varied between 0.1- 3.45 $g\text{-}_{H_2O}$ $(g\text{-}_{dry\ air})^{-1}$, The inlet temperatures of the humid gas stream used were between 61- 107 °C; however, the majority were around 100 °C.

The lithium bromide concentrations used ranged between 56- 70 %w/w, while the stream flowrates were between 1- 4 mls^{-1} (approximately 1.7- 6.8 gs^{-1}). In all experiments the lithium bromide inlet temperature was kept above 100 °C in order to minimise the risk of crystallisation. In most cases the inlet temperature was set at approximately 100 °C. Some experiments were carried out using higher temperatures, up to a maximum of 138 °C, in order to determine the consequent variation of the gas exit temperature.

Operational Problems.

Much useful experimental data were obtained after initial operating problems were solved. The main problems encountered were difficulties with the humidity probe; problems with generating a reliable steam supply for the humid gas streams; and inaccurate determination of the lithium bromide concentration in the generator.

Problems with the humidity probe arose due to the condensation of water vapour on the sensor, which produced nonsensical readings which were consequently of little value. The difficulties with the steam generating system were due to leaks in the joints of the apparatus and these were easily rectified by tightening the connecting bolts between the glass sections. Lastly, the determination of the lithium bromide concentration was carried out using readings of temperature and pressure. Initially, a pressure gauge with an accuracy of ± 0.05 bar was used. This was clearly unacceptable as a huge error was obtained during normal operation because the low pressure side of the equipment was held under a vacuum of between 0.05- 0.15 bar, corresponding to an error of ± 100 - 33.3 %. Therefore, the gauge was changed to a pressure differential sensor, with an accuracy of ± 0.001 bar which allowed more

accurate values for the lithium bromide concentration to be evaluated. A full discussion of errors is covered in Section 4.7.

Following these early operating problems, it was decided to cross check the results obtained by different methods, thereby minimising measurement errors in the apparatus, ensuring that the results obtained were reasonable and that there were no problems with the pilot plant. For example, once steady state had been reached, it was possible to calculate the amount of water absorbed from the gas stream by measuring the difference between the inlet and outlet humidity readings and also directly from the amount of condensate collected in the condenser/ receiver.

4.2.2 Effect of Varying the Gas Flowrate.

Table 4.2 summarises experimental results for a limited number of runs at high and low gas humidities, over a range of gas flowrates. The influence of the gas flowrate upon the performance of the absorber, when operated at approximately constant inlet humidity, was not felt to be significant.

The range of the experimental points was limited and the readings not very consistent. However, the gas exit temperature did drop slightly when the flowrate was increased due to the extra heat required to raise the gas temperature. This is best demonstrated by the results at low gas humidities where the temperature lifts were smaller and any decrease in exit temperature was more pronounced. The effects of the variation of the inlet gas humidity and lithium bromide concentration had more effect upon the exit gas temperature than the variation of the gas flowrate. This prevented any in depth analysis of

$\dot{m}_G$ (gs^{-1})	H ($g\text{-}_{H_2O}$ $(g\text{-}_{dry\ air})^{-1}$)	$p_{H_2O_{in}}$ (bar)	$p_{H_2O_{out}}$ (bar)	$T_{G_{in}}$ (°C)	$T_{G_{out}}$ (°C)	$w_{LiBr_{in}}$ (%w/w)	F_r (-)
0.40	1.25	0.67	0.61	101	130	65	8.6
0.50	1.00	0.62	0.56	100	130	63	8.6
0.50	1.20	0.66	0.60	100	137.5	65.5	7.1
0.60	0.92	0.59	0.54	101	128	66	7.8
0.60	0.93	0.60	0.55	99.5	133	65	7.7
1.00	0.20	0.24	0.21	100	110	64	21.3
1.52	0.13	0.17	0.15	101	108	65	21.7
2.04	0.11	0.15	0.14	100	103	66	19.2

Table 4.2: Cocurrent results showing the effect of changing the gas flowrate for high/ low humidity ranges. LiBr stream conditions: Flowrate = 3.4 gs^{-1}. Inlet temperature $\sim$ 100 °C.

these results, but did highlight the importance of the inlet absorbent concentration and gas humidity. It should also be noted that, at low inlet gas humidities which were typical of spray dryer exit conditions, the exit water vapour partial pressures were still too high to permit recycling of the gas stream. In addition, the exit gas temperatures were far below expectations.

4.2.3 Effect of Varying the Gas Humidity.

As the variation of the gas flowrate did not greatly affect the exit gas stream conditions, a range of gas flowrates were used to investigate the influence of varying the inlet gas humidity upon the exit stream conditions. The results which have been summarised in Table 4.3 are grouped into three categories- very high, high and low gas humidities.

The gas streams with the highest inlet humidities produced the greatest temperature lift of 47 degC. However, the exit humidity was not reduced significantly and was still exceptionally high, making the stream unsuitable for recycling.

$\dot{m}_G$ (gs^{-1})	H ($g\text{-}_{H_2O}$ $(g\text{-}_{dry\ air})^{-1}$)	$p_{H_2O_{in}}$ (bar)	$p_{H_2O_{out}}$ (bar)	$\Delta\dot{m}_{H_2O}$ (gs^{-1})	$T_{G_{in}}$ (°C)	$T_{G_{out}}$ (°C)	F_r (-)
0.20	3.45	0.85	0.82	0.12	100	147	6.2 a)
0.40	1.25	0.67	0.61	0.11	101	130	8.6
0.40	1.90	0.75	0.71	0.15	100.5	138	5.6
0.50	1.20	0.66	0.60	0.13	100	137.5	7.2
0.60	0.92	0.59	0.54	0.11	101	128	7.8
0.60	0.93	0.60	0.55	0.10	99.5	133	7.7
1.00	0.63	0.50	0.44	0.14	100	130	6.8
0.58	0.35	0.36	0.06	0.18	99	116	21.2 b)
1.00	0.20	0.24	0.21	0.03	100	110	21.5
1.52	0.13	0.17	0.15	0.03	101	108	21.8

Table 4.3: Cocurrent results showing the effect of changing the gas humidity at different gas flowrates. LiBr stream conditions: Flowrate = 3.4 gs^{-1}. Concentration ~65 %w/w. Inlet temperature ~ 100 °C.

The dehumidification results from the high humidity runs resulted in an average amount of water of roughly 0.12 gs^{-1} being absorbed into the concentrated lithium bromide solution. The change in lithium bromide concentration was therefore only 2 %w/w. As a cross check, the equilibrium vapour pressure of water above a 63 %w/w solution of lithium bromide at 133 °C was 0.45 bar. However, the exit water vapour partial pressure from the table of results was 0.55 bar. It can be seen from Figure 4.1 that there was a sharp drop in gas temperature at the bottom of the absorption column for both temperature profiles. The reason for this was most probably a result of heat losses to the surroundings.

A closer inspection of the experiment, carried out operating with the highest inlet gas humidity, showed that if the temperature recorded within the column, which was 155 °C, was coupled with the exit absorbent concentration of 64 %w/w, the corresponding equilibrium water vapour partial pressure was 0.80 bar. This was in close agreement with the actual result obtained, 0.82 bar (see Table 4.3, Point a)), and suggested that the streams leaving the column were close to thermal and mass equilibrium. Therefore, the performance of the column agreed reasonably well with the theory, the difference in the temperatures being due to heat losses in the gas pipework.

Results for the low humidity gas streams exhibited far lower temperature lifts than the high humidity streams. This was because of a much lower equilibrium temperature between the gas and lithium bromide streams due to the low water vapour partial pressure. The exit temperatures obtained would not make an absorption heat recovery process an economical operation on an industrial scale. The exit water vapour partial pressures obtained from these results were also higher than the initial project objectives and as such the gas stream was not felt to be suitable for recycling to the drying chamber. The best dehumidification result was obtained for a gas flowrate of 0.58 gs^{-1} and an inlet humidity of 0.35 $g\text{-}_{H_2O}$ $(g\text{-}_{dry\ air})^{-1}$ (see Figure 4.1 and Table 4.3, Point b)). The result did appear to be atypical and suggested that there was an error in determining the exit gas stream conditions. This was entirely possible as the stream flowrates were quite small (see Section 4.7). It was felt, however, that the result did serve to show the difference in the exit gas conditions when the absorber was operated under different conditions.

The temperature profiles for two experimental runs a) and b) are shown in Figure 4.1. It can be seen that both profiles exhibit a rapid increase in the gas temperature over the first 20 cm of the absorption column, before the temperature levels off suggesting that thermal equilibrium was reached quite quickly.

		a)	b)
	Humidity:	High	Low
Gas conditions:	Gas flowrate	0.20 gs^{-1}	0.58 gs^{-1}
	Inlet Steam flowrate	0.69 gs^{-1}	0.20 gs^{-1}
	Inlet temperature	100 °C	99 °C
	Outlet Steam flowrate	0.55 gs^{-1}	0.03 gs^{-1}
	Outlet temperature	147 °C	116 °C
Lithium bromide	Flowrate	2gs^{-1}	2 gs^{-1}
conditions:	Concentration	67 %w/w	65 %w/w
	Inlet temperature	100 °C	105 °C

The above results clearly demonstrate that it was not possible to combine the dehumidification and reheating operations in one stage. Experiments carried out using a gas stream with a low inlet humidity only resulted in a small gas stream temperature lift . This was due to the low water vapour partial pressure and thus low equilibrium absorbent temperature generated in the absorber. Similarly, a large temperature lift was only achieved when the absorber was operated with a gas stream with a high initial humidity, which remained very high upon leaving the absorber.

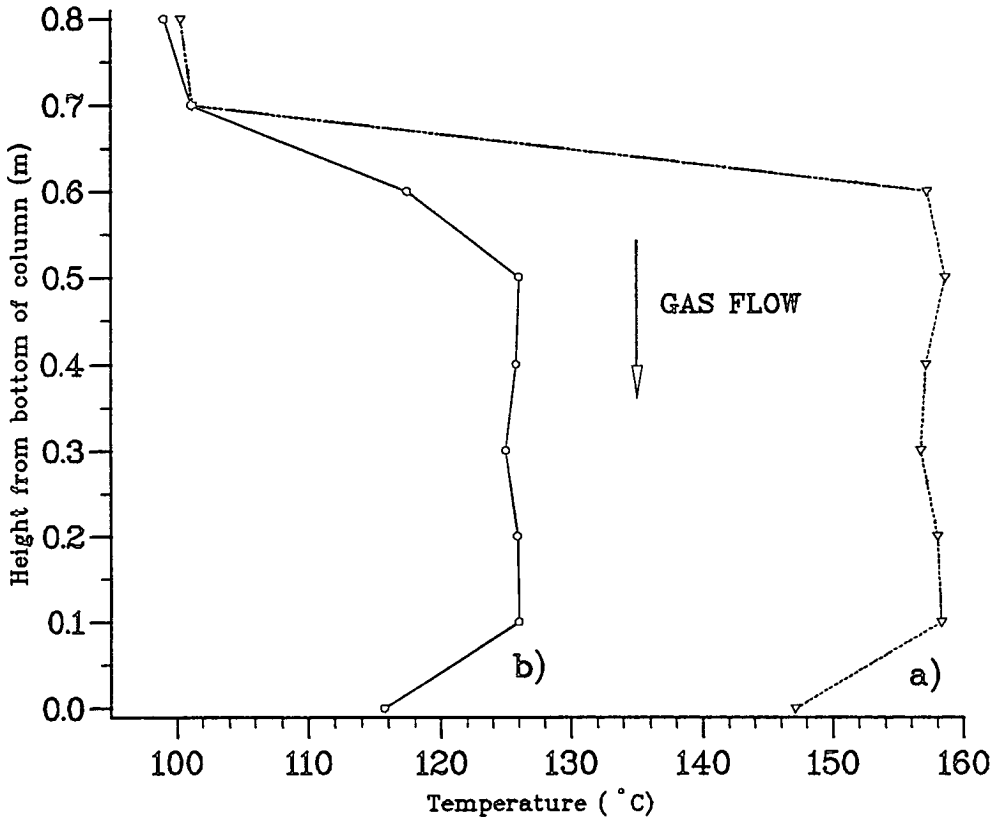

Figure 4.1: Comparison of gas temperature lifts for high and low gas humidities. Operating in cocurrent mode.

4.2.4 Effect of Varying the Lithium Bromide Concentration.

$w_{LiBr_{in}}$ (%w/w)	$\dot{m}_G$ (gs^{-1})	H ($g\text{-}_{H_2O}$ $(g\text{-}_{dry\ air})^{-1}$)	$p_{H_2O_{in}}$ (bar)	$p_{H_2O_{out}}$ (bar)	$T_{G_{in}}$ (°C)	$T_{G_{out}}$ (°C)	ΔT_G (degC)
56	0.50	1.00	0.62	0.58	103	122	19
56	0.50	1.00	0.62	0.59	100	119	19
63	0.50	1.00	0.62	0.58	104.5	136	31
63	0.50	1.00	0.62	0.56	100	130	30
65	0.60	0.93	0.60	0.55	99.5	133	34
66	0.60	0.92	0.59	0.54	101	128	27
70	0.60	0.93	0.60	0.53	103	146	43
70	1.00	1.07	0.63	0.60	105	142	37
70	1.00	1.08	0.63	0.60	103	142	39

Table 4.4: Cocurrent results showing the effect of changing the LiBr concentration. LiBr flowrate set to 3.4 gs^{-1}, inlet temperature $\sim$ 100 °C.

The concentration of lithium bromide solution was the most important variable in achieving a high temperature lift as can be seen from Table 4.4. There appears to be a linear relationship between the temperature lift and lithium bromide concentration, see Figure 4.2. However, the risk of crystallisation limited the maximum operating concentration possible with this system. The maximum absorbent concentration which was used was set to just under 70 %w/w. The crystallisation temperature of this solution was around 100 °C, which was the operating temperature of the generator.

For the most part, the exit temperatures achieved were in agreement with VLE data based upon the exit absorbent concentration and water vapour partial pressure, with the assumption that the liquid and gas streams were in equilibrium.

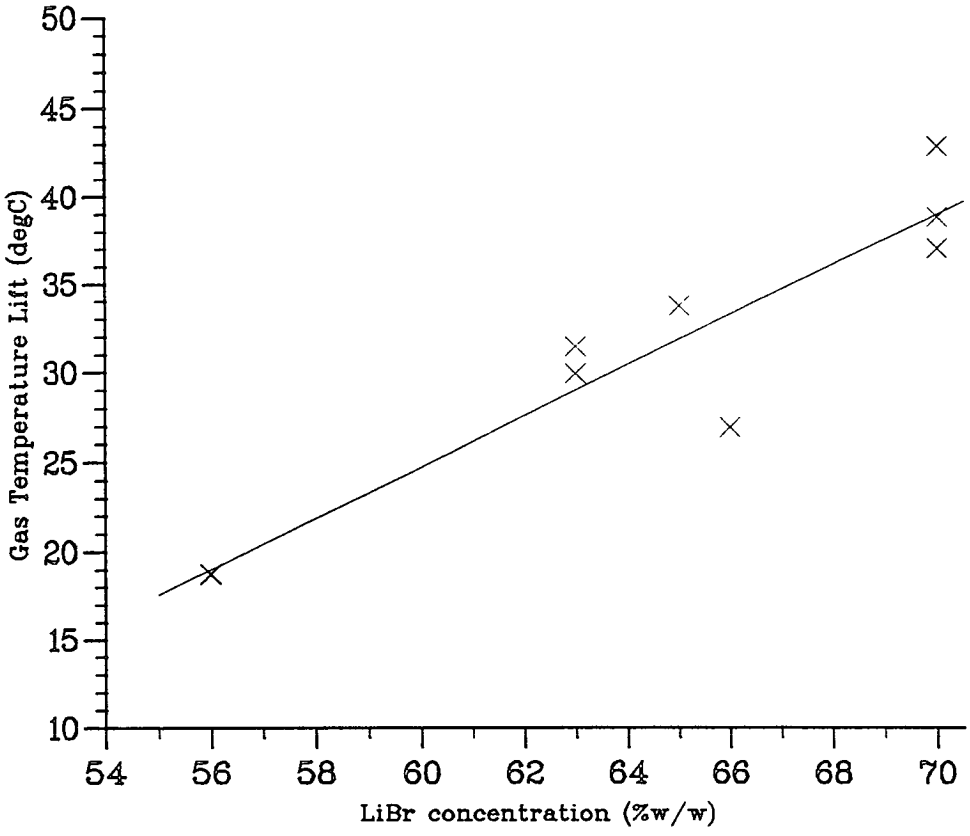

Figure 4.2: Gas temperature lift versus inlet LiBr concentration.

4.2.5 Effect of Varying the Lithium Bromide Flowrate.

$\dot{m}_{LiBr_{in}}$ (gs^{-1})	$w_{LiBr_{in}}$ (%w/w)	$\dot{m}_G$ (gs^{-1})	H ($g\text{-}_{H_2O}$ $(g\text{-}_{dry\ air})^{-1}$)	$T_{G_{out}}$ (°C)	Δw_{LiBr} (%w/w)	$\Delta\dot{m}_{H_2O}$ (gs^{-1})
3.4	67	0.20	3.45	147	2.3	0.12
5.1	67	0.20	3.45	147.5	2.8	0.22
6.8	66	0.20	3.45	144	3.0	0.33
3.4	65.5	0.50	1.20	137.5	2.4	0.13
5.1	65	0.50	1.20	131	2.4	0.20
6.8	65	0.50	1.20	137.5	2.4	0.26
1.7	65	0.98	0.26	107	1.1	0.03
2.6	64	0.98	0.18	107	0.5	0.02
3.4	64	1.00	0.20	110	0.6	0.03
3.4	65	1.52	0.13	108	0.6	0.03
5.1	65	1.50	0.13	106	0.5	0.04
6.8	65	2.00	0.20	112	0.8	0.08

Table 4.5: Cocurrent results showing the effect of changing the LiBr flowrate. Gas and LiBr inlet temperatures both approximately $\sim$ 100 °C.

There was no noticeable change in the exit gas temperatures achieved by varying the lithium bromide flowrate, Table 4.5. The data are also graphically shown in Figure 4.3. The set of points with the lowest inlet stream humidities (Line 3) showed an increase in the gas exit temperature from the absorber. There was a slight drop in gas exit temperature at the highest inlet humidities, although from the limited number of points drawn it was not possible to draw firm conclusions from the data.

Overall, the results plotted show little change in the exit temperatures for the range of conditions tested. This insensitivity in the results was attributed to two main factors. As water vapour was absorbed, at small liquid flows, there was a large decrease in the concentration of the absorbent stream, which resulted in lower equilibrium temperatures for a given water vapour partial pressure; whereas for high lithium bromide flowrates, the concentration differences were lower but the streams had larger heat flows. This meant that more heat was required to raise the temperature of the liquid stream and so the exit temperatures were much the same as for low liquid flowrates.

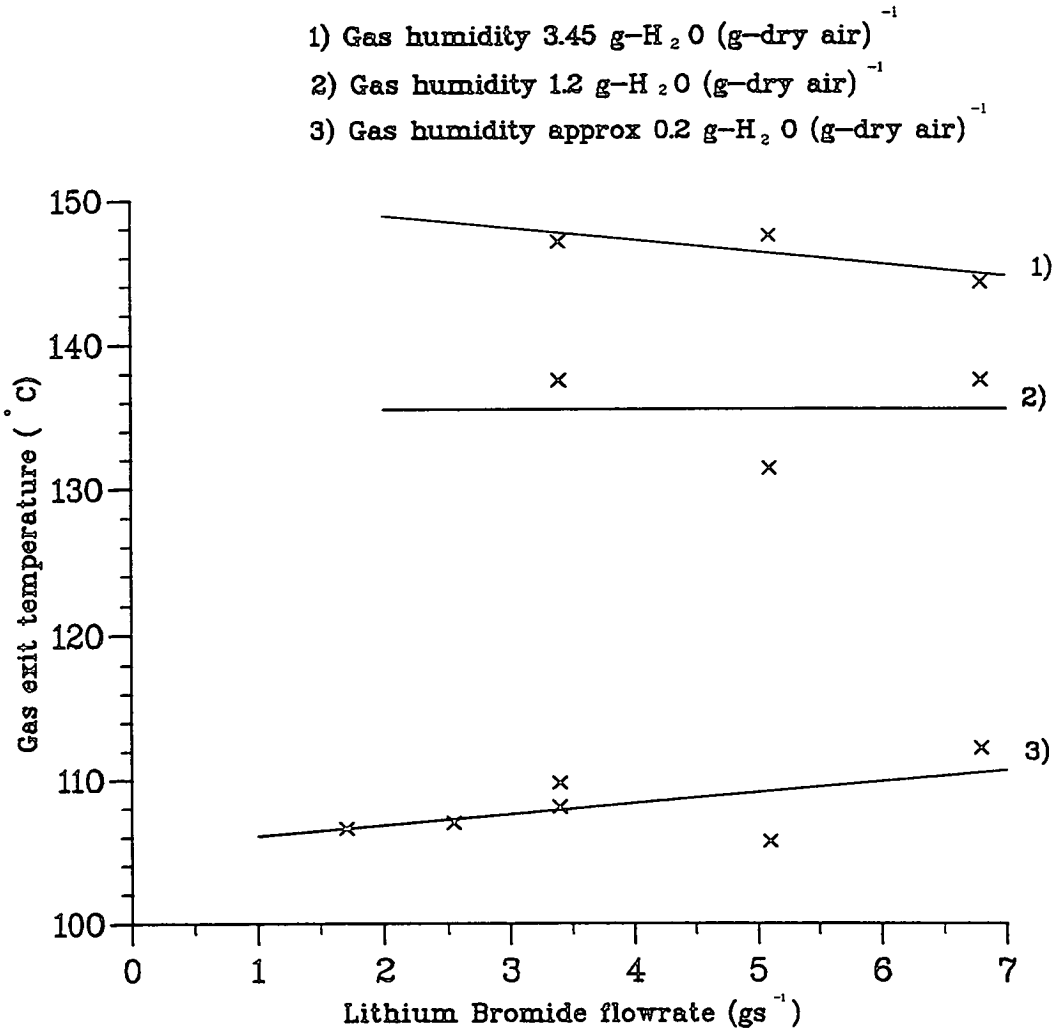

Figure 4.3: Variation of gas exit temperature with LiBr flowrate.

Figure 4.4 shows that a linear relationship existed between the amount of water absorbed and the absorbent flowrate. The effect was more pronounced for the gas streams with high inlet humidities. A look at the concentration change in the absorbent solution in Table 4.5 shows that the variation for each set of results was approximately the same. This meant that, as the lithium bromide flowrate was increased there was a corresponding rise in the amount of water transferred, thereby maintaining approximately the same exit lithium bromide concentration over the range of flowrates tested.

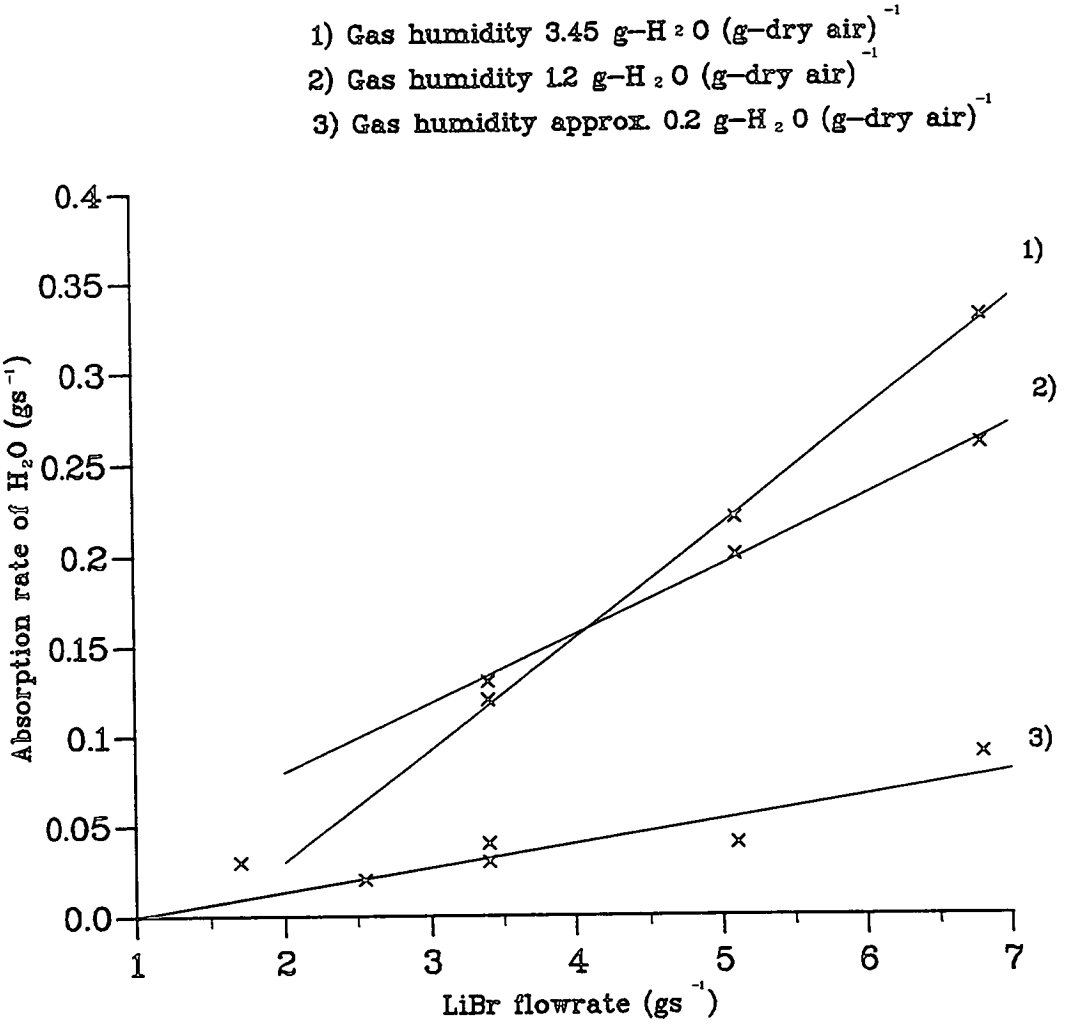

Figure 4.4: Variation in the dehumidification of humid gas streams for different LiBr flowrates.

The results obtained for gas streams with higher inlet humidities (Lines 1) and 2), Figure 4.4) were consistently higher than those of the lowest humidity streams (Line 3),Figure 4.4). This was due to the higher water vapour partial pressures present in the column, which resulted in a greater mass driving force and caused more water to be absorbed into the concentrated lithium bromide solution. In addition, the higher partial pressure meant that the equilibrium temperature within the column was also considerably higher than that obtained with a low humidity gas stream.

4.2.6 Effect of Varying the Inlet Stream Temperatures.

A few of the experimental runs, Table 4.6, were undertaken at higher inlet stream temperatures so as to evaluate the influence that the inlet temperatures exerted upon the outlet conditions.

$\dot{m}_G$ (gs^{-1})	H ($g\text{-}_{H_2O}$ $(g\text{-}_{dry\ air})^{-1}$)	T_{in} (°C)	T_{out} (°C)	$\dot{m}_{LiBr_{in}}$ (gs^{-1}	$w_{LiBr_{in}}$ (%w/w)	$T_{LiBr_{in}}$ (°C)
0.50	1.00	100	130	3.4	63	100.5
0.50	1.00	104.5	136	3.4	63	138
0.50	1.40	107	127	3.4	56	113.5
0.50	1.40	100	126	3.4	57	102
2.00	0.20	110	112	6.8	65	100

Table 4.6: Cocurrent results showing the effect of changing the LiBr inlet temperatures of the gas and liquid streams.

However, there was only a few degrees increase in the gas exit temperature, when the column was operated with an inlet gas flowrate of 0.5 gs^{-1} and an inlet lithium bromide temperature of 138 °C. Hence, only a limited increase exit gas temperature was obtained for a huge increase in the inlet stream temperature. It was concluded that the exit conditions were only dependent

upon the lithium bromide concentration and gas humidity, which determined the point of thermal and mass equilibrium. The extra heat supplied at the top of the column only served to maintain a higher temperature throughout the column, against heat losses to the surroundings.

4.2.7 Results For Countercurrent Operation.

A series of results was obtained for countercurrent operation of the absorber, Table 4.7. It was felt that by operating the column in such a mode, the dehumidification of the gas stream would be increased because the least humid gas would come into contact with the most concentrated lithium bromide solution, thus maximising the mass transfer rate at the top of the absorber.

$\dot{m}_G$ (gs^{-1})	H ($g\text{-}_{H_2O}$ ($g\text{-}_{dry\ air}$)$^{-1}$)	$p_{H_2O_{in}}$ (bar)	$p_{H_2O_{out}}$ (bar)	T_{in} (°C)	T_{out} (°C)	$\dot{m}_{LiBr_{in}}$ (gs^{-1})	$w_{LiBr_{in}}$ (%w/w)	$T_{LiBr_{in}}$ (°C)
0.50	0.80	0.56	0.52	101	105	3.4	58	102
0.50	0.80	0.56	0.52	100	116	3.4	58	130
0.50	1.00	0.62	0.59	100	112	2.6	58	101
0.50	1.00	0.62	0.58	100	110.5	3.4	58	100
0.50	1.00	0.62	0.58	100	107	3.4	58	100
1.00	0.20	0.24	0.15	106	101	5.1	65	100
1.00	0.50	0.44	0.41	107	105	3.4	58	100
1.51	0.28	0.31	0.22	104	110	6.8	65	101
1.52	0.27	0.30	0.25	100	110.5	5.1	65	99
2.00	0.12	0.16	0.14	86	102	5.1	65	101
2.00	0.12	0.16	0.13	61	99	5.1	65	100

Table 4.7: Results for countercurrent operation of the single stage absorber.

Analysis of the results clearly show that cocurrent operation gave higher temperature lifts (for a given set of operating conditions) than countercurrent operation, see Figure 4.5. This was attributed to the fact that the inlet lithium

bromide temperature was cooling the gas stream at the top of the column, prior to it leaving. The temperature profile for countercurrent operation, Figure 4.5, shows how temperature within the column was maintained at approximately 130 °C throughout the column, but dropped dramatically upon exit. It was also noted that as the gas inlet temperature was reduced the exit temperature remained approximately constant. It was therefore concluded that the exit gas temperature was dependent upon the inlet lithium bromide temperature.

		a) Counter-	b) Co- current
Gas conditions:	Gas flowrate	0.50 gs^{-1}	0.50 gs^{-1}
	Inlet Steam flowrate	0.50 gs^{-1}	0.50 gs^{-1}
	Inlet temperature	100 °C	100 °C
	Outlet Steam flowrate	0.43 gs^{-1}	0.44 gs^{-1}
	Outlet temperature	110.5 °C	119 °C
Lithium bromide	Flowrate	3.2 gs^{-1}	4.8 gs^{-1}
conditions:	Concentration	58 %w/w	56 %w/w
	Inlet temperature	100 °C	100 °C
(see Figure 4.5)			

The dehumidification of the gas stream, when the absorber was operated in countercurrent mode, did not differ greatly from the results obtained for cocurrent operation. It was difficult to obtain accurate results for the water vapour content of the inlet and outlet gas streams because the flowrates used were so small. Therefore the errors involved in trying to estimate the amount of water vapour absorbed were such that it was difficult to discriminate accurately between results. However, it can be seen that from an estimate of the VLE conditions prevalent in the absorber, that there was reasonable agreement between estimated and experimental results.

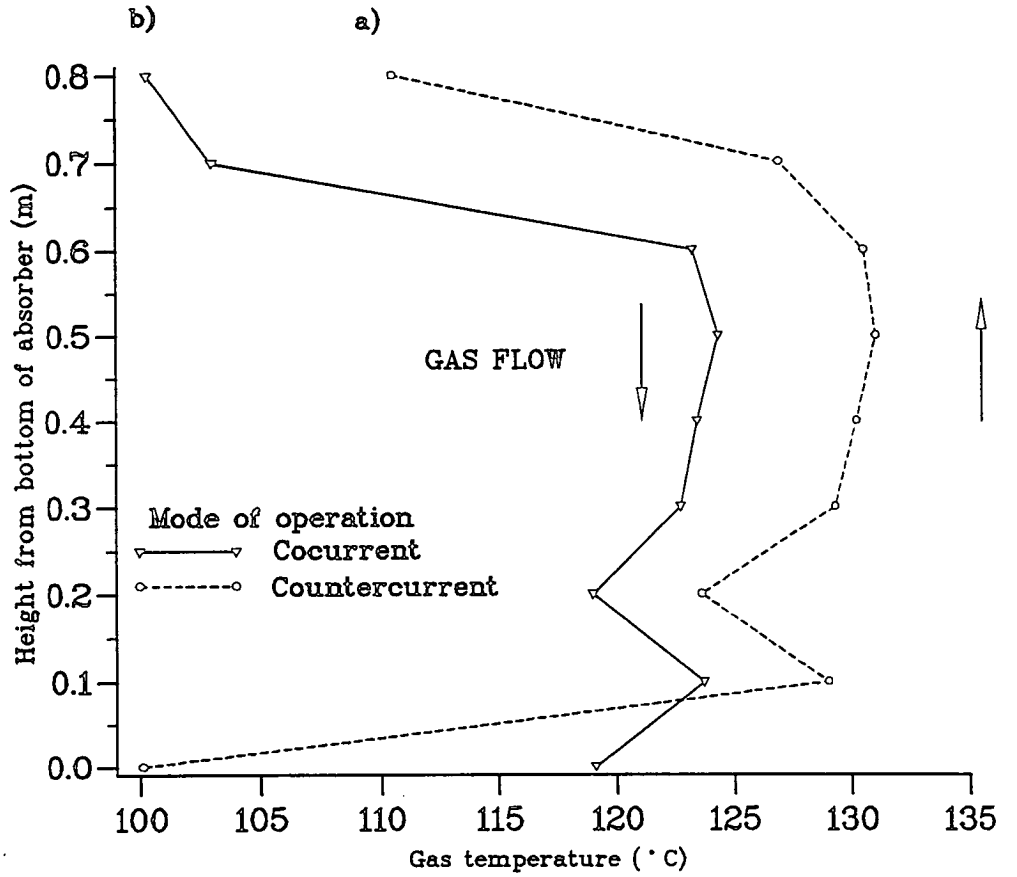

Figure 4.5: Temperature profiles through absorber column, showing differences between co- and counter- current operation.

In addition, the level of dehumidification was not very good for either co- or counter- current operations, due to the increase in temperature within the absorption column as the water vapour was absorbed. Therefore, in order to improve the dehumidification of the gas stream, it would be necessary to operate the absorber with a highly concentrated lithium bromide solution, while the temperature used was controlled so as to obtain the desired exit water vapour partial pressure. For example, if the absorption column was operated with a 65 %w/w lithium bromide solution at a temperature of 80 °C, the corresponding partial pressure, at the top of the column, would be 0.035 bar. Such a low partial pressure at the top of the column helps to maintain a large mass driving force and therefore improve dehumidification of the gas stream.

Tables 4.8 and 4.9 summarise the differences between the heat and mass transfer rates for both co- and counter- current operation. As the internal surface area of the absorption column was unknown it was necessary to define the heat and mass transfer rates using the internal volume of the absorber as a basis. The heat transfer rate was determined from the heat transferred to the gas stream, while the mass transfer rate was based on the amount of water vapour absorbed into the liquid absorbent stream. It can be seen that results for the countercurrent operation of the absorber gave better mass transfer rates, for similar operating conditions, than cocurrent operation. The heat transfer rates for the countercurrent mode of operation were low because the gas stream was effectively cooled by the inlet absorbent stream, thereby improving the dehumidification of the gas stream at the expense of reducing the overall gas temperature lift. Conversely, the cocurrent mode of operation exhibited high heat transfer rates because the gas stream was being progressively heated by the water vapour absorbing into the liquid phase. These results also illustrate the importance of using a highly concentrated lithium bromide solution to achieve a high exit temperature and therefore a high heat transfer rate (and also a high mass transfer rate), for cocurrent operation.

$w_{LiBr_{in}}$ (%w/w)	$T_{LiBr.in}$ (°C)	Gas humidity ($g\text{-}_{H_2O}$ $(g\text{-}_{dry\ air})^{-1}$)	$T_{G.in}$ (°C)	$T_{G.out}$ (°C)	Heat trans rate Q_O (kWm^{-3})	Mass trans rate M_o ($gs^{-1}m^{-3}$)
65	102	0.10	101	108	11	25
56	102	1.00	103	122	22	53
63	101	1.00	100	130	35	88
70	101	1.10	103	142	45	87

Table 4.8: Mass and heat transfer rates for cocurrent operation of the direct contact absorber.

$w_{LiBr_{in}}$ (%w/w)	$T_{LiBr.in}$ (°C)	Gas humidity ($g\text{-}_{H_2O}$ $(g\text{-}_{dry\ air})^{-1}$)	$T_{G.in}$ (°C)	$T_{G.out}$ (°C)	Heat trans rate U_O (kWm^{-3})	Mass trans rate K_o ($gs^{-1}m^{-3}$)
65	100	0.10	61	99	33	41
65	101	0.30	104	110	12	70
58	100	0.50	107	105	14	52
58	130	0.80	100	116	17	55
58	100	1.00	100	110	12	54

Table 4.9: Mass and heat transfer rates for countercurrent operation of the direct contact absorber.

4.2.8 Temperature Profiles within the Absorption Column.

The exit gas temperatures obtained for all of the results were less than the maximum temperature obtained within the column, Table 4.10. The difference was due to heat losses as the gas stream left the absorption column. It can be seen from Figure 4.6 that at the bottom of the absorber there was a X-piece, which was used for the disengagement of the liquid absorbent from the gas (for cocurrent operation). Due to difficulties in lagging this section, the heat losses from this part of the absorbent were greater than for the main absorption column. Consequently, as the exit gas temperature was measured after this point, the temperature obtained was lower than expected. It should be noted that the thermocouple used to measure the top gas temperature was situated away from the absorber and therefore showed a lower temperature than was obtained at the top of the main column, due to heat losses along the connecting pipework. This was not a serious problem for countercurrent operation as the drop in the gas temperature, due to contact with the cool inlet absorbent stream, was of greater significance.

The temperature profiles within the column were all similar to those shown in Figure 4.5, for both co- and counter- current operation, where there was a rapid rise in the gas temperature before it levelled out, indicating thermal equilibrium. It can be seen from Tables 4.10 and 4.11 that the maximum temperature obtained for cocurrent operation occurred mostly at the bottom of the absorber. By contrast, the results for the countercurrent case showed that the maximum was nearer the top of the column. Figure 4.6 shows the relative position of each thermocouple in the packed absorber and also the location of the thermocouples used to measure the inlet and outlet gas temperatures. Another observation for countercurrent operation shows how much lower the exit temperature was

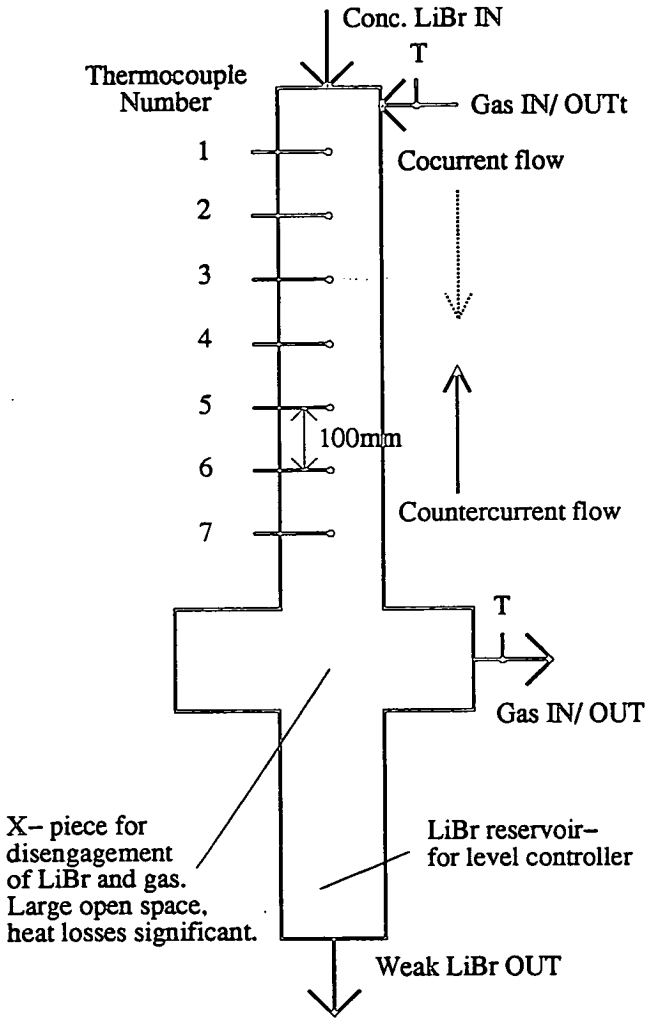

Figure 4.6: Position of thermocouples in absorption column.

$T_{G_{out}}$ (°C)	ΔT_G (degC)	$T_{G_{max}}$ (°C)	$T_{G_{max}}$ posn.	$T_{G_{out}}$ (°C)	ΔT_G (degC)	$T_{G_{max}}$ (°C)	$T_{G_{max}}$ posn.
147.5	47	160	7	128	26	133	7
147	47	159	3	122.5	21	126	7
144	44	159	7	120	20	126	7
146	43	153	7	127	20	129	5
142	39	149	7	122	19	130	7
140	39	150	7	122	19	130	5
139	39	151	7	119	19	124	7
138	38	147	7	116	17	126	7
137.5	37.5	149	7	116	16	128	7
137.5	37	149	7	116	14	129	3
142	37	149	7	115	13	118	7
133	34	142	7	110	9	114	7
131	32	149	7	108	7	112	7
136	31	142	7	106	6	110	7
130	30	144	3/4/7	107	5	116	6
130	30	137	7	107	3	115	7
130	30	135	7	103	3	106	5
128	28	132	7	103.5	2	107	5
128	27	139	7	112	2	118	5
126	27	131	7				

Table 4.10: Comparison of exit and maximum gas temperatures in absorber. Cocurrent mode. Inlet gas temperatures $\sim$ 100 °C.

$T_{G_{in}}$ (°C)	$T_{G_{out}}$ (°C)	ΔT_G (degC)	$T_{G_{max}}$ (°C)	$T_{G_{max}}$ posn.
101	105	4	129	3
100	116	16	134	2
100	110.5	10	131	3
100	112	12	132	3
100	107	7	130	2
106	101	-5	122	3
107	105	-2	120	3
104	110	6	130.5	4
100	110.5	11	127	3
86	102	16	113	3
61	99	38	107	3

Table 4.11: Comparison of exit and maximum gas temperatures in absorber. Countercurrent mode.

4.2.9 Summary of Results.

As demonstrated above, the dehumidification and reheating of a humid gas stream can not be achieved in a single absorption stage. This was a significant conclusion and outlined the way forward for this project. Separate operations must be used in order to achieve the project aims of dehumidifying a gas stream to 0.03- 0.05 g-$_{H_2O}$ (g-$_{dry\ air}$)$^{-1}$ and raising its temperature to 150- 200 °C. The most important variable in obtaining this was the absorbent concentration, which had be as high as possible.

For the dehumidification stage, which would involve the direct contact of the gas and lithium bromide streams, flowing countercurrent to each other, the temperature of the lithium bromide stream would need to be controlled so as to maintain the desired exit water vapour partial pressure. However, care must be taken to minimise the risk of crystallisation of the solution.

Secondly, the reheating of the 'dry' gas stream would be carried out in an indirect reheater. The heating medium used would again be a concentrated solution of lithium bromide into which steam would be absorbed. The resultant stream would generate temperatures in the range of 170- 190 °C. The exit temperatures were taken directly from the lithium bromide VLE diagram where solutions in the range 65- 70 %w/w, exerting a water vapour partial pressure of 1 bar, result in the above temperatures.

4.3 Two Stage Cycle: Dehumidification Studies.

Separate studies were carried out for each of the absorption processes- dehumidification and reheating- in the two stage heat transformer cycle, allowing independent control of the operating conditions in each stage. The dehumidification operation was investigated first using three different absorbers with the dehumidification capabilities of each one being assessed in turn. The three columns used were:

- Falling film absorber.
- Packed column.
- Condenser column with internal heat removal using cooling water.

Each column used will be explained in detail in the following sections. The experimental programmes undertaken investigated the influence of the main variables upon the performance for each of the absorbers, as discussed in Section 4.1.2 (Table4.1). The absorbers were operated for the countercurrent flow of the gas and liquid streams. The maximum operating concentration used in the absorbers was limited to 65- 66 %w/w so as to minimise the risk of crystallisation. The crystallisation temperature of a 66 %w/w solution of lithium bromide was 60 °C, which was lower than the normal operating temperature in the absorbers.

Figure 4.7 shows the arrangement for injecting lithium bromide into the top of each of the absorbers. Using of the average absorbent stream concentration in the column and the temperature T5, an estimate of the exit water vapour

pressure could be made. The average absorbent concentration was used in preference to inlet concentration as it was felt that this was more representative of the absorption conditions near the top of the column, where most of the dehumidification occurred. The temperature was measured from the thermocouple positioned at the top of the column (T5), just below the point where the lithium bromide stream was injected. The calculated water vapour pressure was then compared with the actual water vapour exit partial pressure in the gas stream. The exit gas humidity was determined by two methods. Firstly, a high temperature humidity probe was used to measure the gas humidity directly. The second method involved recording the difference between the inlet steam flowrate and the amount of condensate collected in order to determine the exit steam flowrate in the gas and hence the exit humidity and steam partial pressure. The average of these two results was taken to be representative of the exit gas stream.

4.3.1 Falling Film Absorber.

In this absorber, concentrated liquid absorbent was sprayed into the top of a glass column with the humid gas streams rising from the bottom. The range of gas flowrates used to test the falling film absorber was between 2- 5 gs^{-1}, while the humidity of the streams was similar to those encountered on industrial spray drying operations (typically 0.15 $g\text{-}_{H_2O}$ $(g\text{-}_{dry\ air})^{-1}$ [0.19 bar]). There were no significant differences between each of the results for the different operating conditions used, Table 4.12. However, the result taken using a low lithium bromide flowrate was slightly worse than the other results. This may have been due to several factors: poor gas- liquid contact or incomplete wetting of the absorption column.

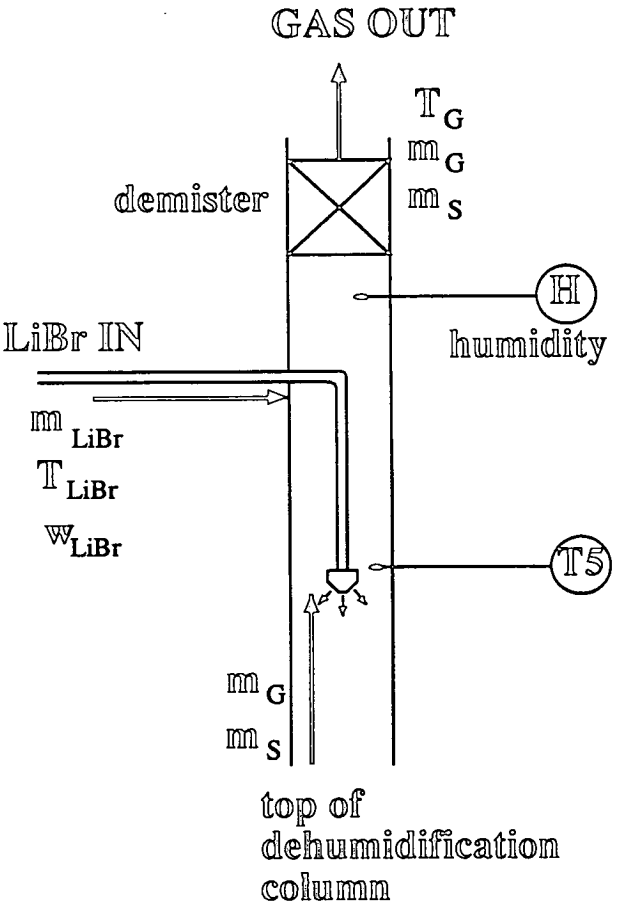

Figure 4.7: Top of dehumidification column: LiBr inlet.

In addition, there was also a larger concentration drop in the absorbent solution, giving a lower average concentration and hence a higher vapour pressure at T5. The important criteria for assessing the dehumidification performance of the column was the exit water vapour partial pressure and the agreement between this value and the estimated vapour pressure above lithium bromide solution. Figure 4.8 shows that the results for the falling film absorber were very scattered and above the equilibrium line. Therefore, although the gas streams were being dehumidified, the results were not very good as equilibrium was not being achieved, due to poor gas- liquid contact in the column. This phenomenon was observed during normal operation since most of the liquid ran down the sides of the absorber, as expected. In addition, the liquid flow was felt to be laminar and so there was not a great deal of surface renewal within the column, which resulted in poor mass transfer.

$\dot{m}_G$	$\dot{m}_{H_2O_{in}}$	$T_{G_{in}}$	$\dot{m}_{H_2O_{out}}$	$T_{G_{out}}$	$P_{H_2O_{out}}$	$\dot{m}_{LiBr_{av}}$	$w_{LiBr_{av}}$	T5	$P_{LiBr_{av}}$
(gs^{-1})	(gs^{-1})	(°C)	(gs^{-1})	(°C)	(bar)	(gs^{-1})	(%w/w)	(°C)	(bar)
2.00	0.27	72	0.17	75	0.12	8.46	65	94	0.055
3.00	0.45	97	0.33	76	0.15	4.05	59	86	0.09
3.00	0.40	90	0.28	84	0.13	6.46	65	94	0.06
3.00	0.41	91	0.23	73	0.11	7.90	58	81	0.08
3.00	0.45	94	0.21	74	0.10	8.05	59	87	0.10
3.00	0.42	98	0.27	83	0.13	8.28	63	90	0.075
3.00	0.40	96	0.21	83	0.10	8.55	65	93	0.06
4.00	0.56	100	0.42	90	0.14	8.32	64	85	0.055
5.00	0.62	79	0.29	95	0.09	8.37	62	90	0.08

Table 4.12: Performance data for the falling film dehumidification column.

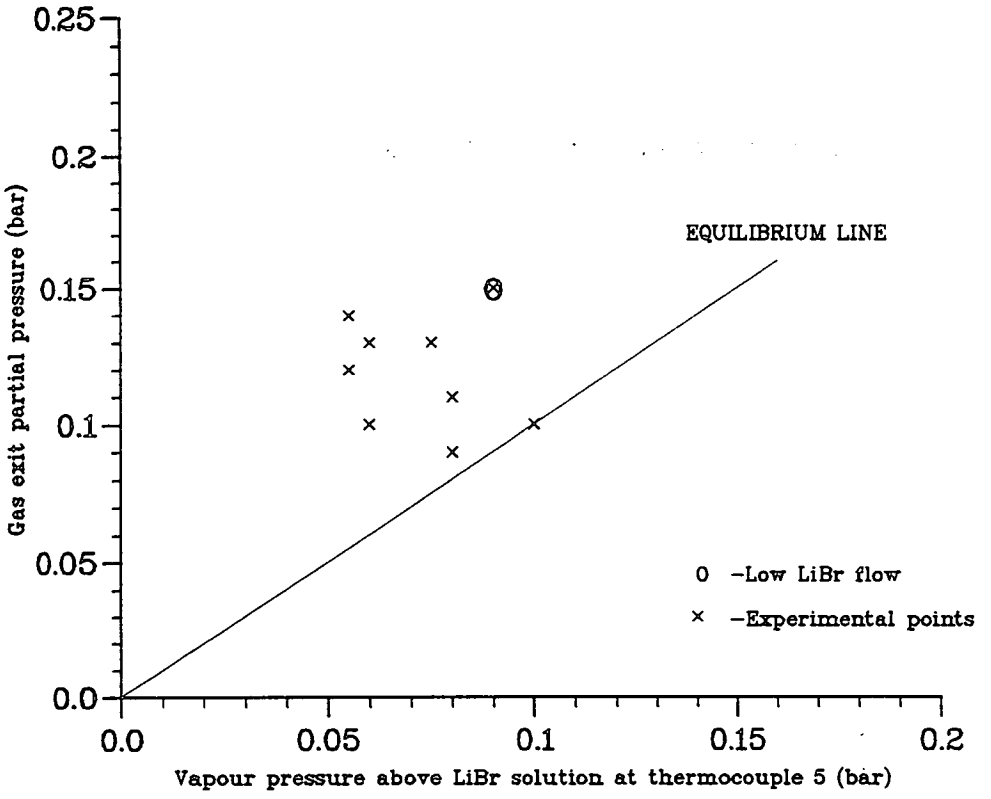

Figure 4.8: Exit water vapour partial pressure versus vapour pressure for the falling film absorber.

4.3.2 Packed Column.

Following the experiments with the falling film absorber, the column was packed with 15mm Fenske helices, which helped to improve the gas- liquid contact and hence the amount of water absorbed, Table 4.13. The gas flowrate for the packed absorber runs was limited to 4 gs^{-1} due flooding problems within the column at higher flows. The range of inlet humidities was widened to between 0.10- 0.26 $g\text{-}_{H_2O}$ $(g\text{-}_{dry\ air})^{-1}$ [0.14- 0.29 bar]. This allowed the effects of operating the column with a high humidity gas stream to be monitored. Figure 4.9 shows that the modification to the column did increase the dehumidification of the gas stream and also helped reduce the scatter of the results as the majority of the points were closer to the equilibrium line.

$\dot{m}_G$ (gs^{-1})	$\dot{m}_{H_2O_{in}}$ (gs^{-1})	$T_{G_{in}}$ (°C)	$\dot{m}_{H_2O_{out}}$ (gs^{-1})	$T_{G_{out}}$ (°C)	$P_{H_2O_{out}}$ (bar)	$\dot{m}_{LiBr_{av}}$ (gs^{-1})	$w_{LiBr_{av}}$ (%w/w)	T5 (°C)	$P_{LiBr_{av}}$ (bar)
2.00	0.32	101	0.15	88	0.11	8.29	62	97	0.10
2.00	0.23	100	0.12	84	0.09	8.30	63	92	0.075
2.00	0.40	99	0.24	91	0.16	8.31	63	99	0.12
3.00	0.35	96	0.21	87	0.10	4.08	60	95	0.11
3.00	0.35	69	0.23	79	0.10	4.09	61	84	0.065
3.00	0.57	72	0.35	84	0.16	4.12	60	91	0.11
3.00	0.35	67	0.16	80	0.08	8.11	61	85	0.07
3.00	0.57	71	0.27	84	0.13	8.17	61	90	0.09
3.00	0.31	98	0.18	89	0.09	8.27	63	95	0.09
3.00	0.32	100	0.17	90	0.08	8.28	63	96	0.095
3.00	0.77	99	0.50	100	0.21	8.33	62	105	0.16
3.00	0.54	100	0.30	95	0.14	8.36	63	101	0.12
4.00	0.66	98	0.43	89	0.13	8.15	60	95	0.12
4.00	0.38	100	0.25	89	0.09	8.17	62	93	0.09
4.00	0.65	96	0.42	96	0.14	8.22	61	100	0.14
4.00	0.38	71	0.23	83	0.08	8.23	62	85	0.07

Table 4.13: Performance data for the packed dehumidification column.

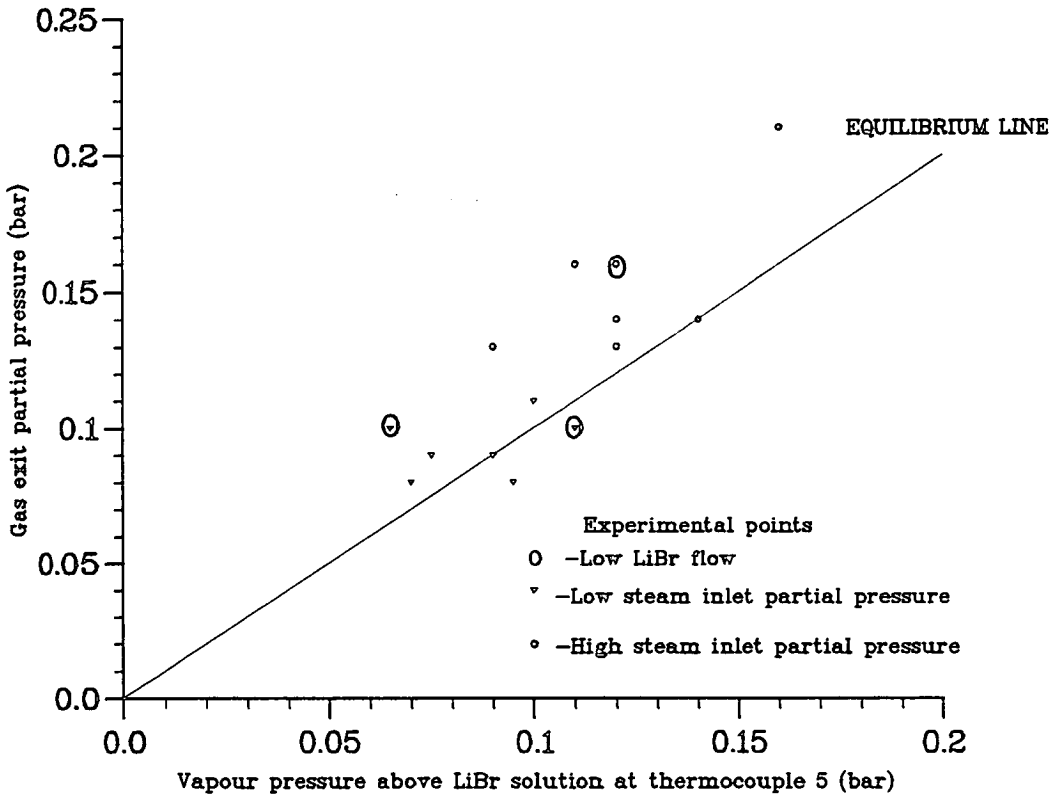

Figure 4.9: Exit water vapour partial pressure versus vapour pressure for the packed column.

Experiments carried out using high humidity gas streams resulted in exit conditions which were furthest from the equilibrium line, indicating a high exit water vapour partial pressure. A closer inspection of both Table 4.9 and Figure 4.9 show that these gas streams exhibited higher temperatures at T5 and therefore higher exit partial pressures. This was due to the increase in the water vapour content in the gas, causing an rise in the amount of absorption into the lithium bromide solution. This in turn resulted in an increase in the gas and liquid temperatures and therefore decreased the *proportion* of the vapour absorbed because of the increased vapour pressure above the lithium bromide solution.

A few of the experiments were undertaken using lower lithium bromide flowrates; the resulting effect was a drop in the dehumidification of the gas stream. This was attributed to the larger concentration change in the absorbent stream. It was also noted that the lowest outlet vapour pressures were obtained at the highest lithium bromide solution concentrations.

4.3.3 Condenser.

Further improvements in dehumidification were achieved by replacing the packed absorber with a column containing an internal cooling coil, which removed the heat of absorption from the absorber and allowed the temperature at the top of the column to be controlled. This had the effect of maintaining the water vapour pressure above the LiBr solution as low as possible. Therefore, the rate of absorption of water into the LiBr solution was increased, reducing the exit water vapour partial pressure and improving the gas dehumidification. Experiments were carried out varying the same parameters as listed in Table 4.1 as well as controlling the cooling water flowrate to the condenser.

Due to the large heat transfer surface area of the cooling coil within the condenser it was necessary to restrict the maximum gas flowrate to 1.8 gs^{-1} to avoid the column flooding at higher flowrates. All the experiments were carried out for gas streams with of relatively low inlet humidities, between 0.13- 0.24g-$_{H_2O}$ $(g\text{-}_{dry\ air})^{-1}$ [0.17- 0.28 bar]. The corresponding steam flowrates used varied between 0.15- 0.41 gs^{-1}, which was close to the limits of accurate measurement with the apparatus used. Therefore, errors in the results were larger than in the previous column. However, the consistency and reproducibility of the results obtained validates the conclusions drawn.

$\dot{m}_G$ (gs^{-1})	$\dot{m}_{H_2O_{in}}$ (gs^{-1})	$T_{G_{in}}$ (°C)	$\dot{m}_{H_2O_{out}}$ (gs^{-1})	$T_{G_{out}}$ (°C)	$P_{H_2O_{out}}$ (bar)	$\dot{m}_{LiBr_{av}}$ (gs^{-1})	$w_{LiBr_{av}}$ (%w/w)	T5 (°C)	$P_{LiBr_{av}}$ (bar)
1.00	0.23	98	0.07	60	0.10	4.14	58	66	0.04
1.00	0.15	80	0.03	65	0.045	8.39	64	70	0.03
1.00	0.23	98	0.06	61	0.09	8.05	59	68	0.04
1.00	0.23	73	0.05	60	0.07	8.07	59	66	0.035
1.20	0.17	78	0.03	65	0.04	8.38	64	70	0.025
1.20	0.24	87	0.04	67	0.05	8.37	63	73	0.03
1.40	0.18	84	0.05	66	0.05	8.38	64	72	0.025
1.60	0.23	70	0.05	68	0.05	8.44	62.5	72	0.035
1.60	0.24	83	0.04	68	0.04	8.40	64	73	0.03
1.60	0.33	83	0.05	72	0.05	8.47	62	77	0.045
1.80	0.28	77	0.13	83	0.10	4.12	60	92	0.10
1.80	0.28	93	0.15	88	0.12	4.12	60	96	0.12
1.80	0.28	95	0.16	85	0.12	4.09	61	93	0.10
1.80	0.43	78	0.26	86	0.19	4.11	59	94	0.13
1.80	0.26	93	0.08	82	0.07	8.19	61	90	0.08
1.80	0.26	96	0.06	85	0.05	8.38	62.5	93	0.08
1.80	0.27	78	0.07	62	0.06	8.18	61	68	0.03
1.80	0.27	96	0.07	72	0.06	8.02	59	79	0.065
1.80	0.27	102	0.08	61	0.07	8.04	59	66	0.04
1.80	0.28	71	0.07	82	0.06	8.14	61	91	0.085
1.80	0.28	71	0.06	87	0.05	8.31	63	94	0.08
1.80	0.28	71	0.07	85	0.06	8.46	64	93	0.07
1.80	0.41	98	0.12	88	0.10	8.40	62	96	0.10

Table 4.14: Performance data for the condenser.

The lowest exit gas humidities obtained using the condenser were suitable enough to allow the recycling of the 'dried' gas stream. The best results were obtained at high cooling water and lithium bromide flowrates, Figure 4.10. The highest exit water vapour partial pressures occurred using low flowrates of lithium bromide. This was due to a greater drop in the concentration of the absorbent stream, as a result the partial pressure above the solution was higher. Also, at lower absorbent flowrates, the liquid distribution throughout the column was poor. This contributed to higher exit water vapour partial pressures due to poor gas- liquid contact which in turn led to a reduction in the mass transfer rate.

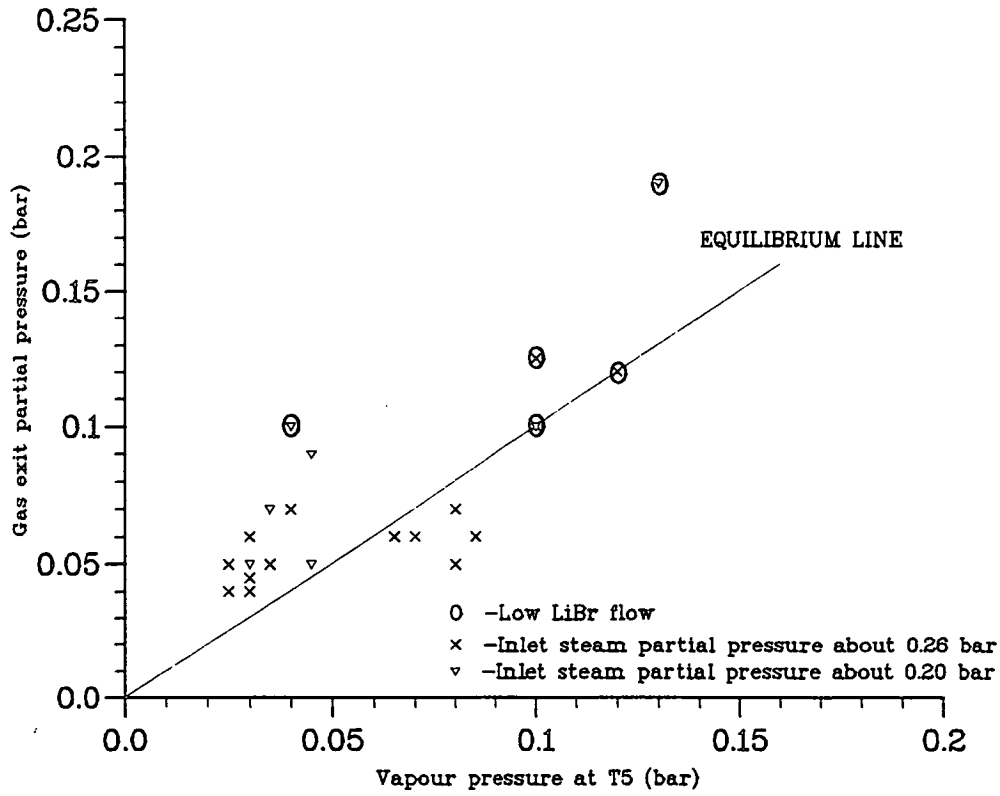

Figure 4.10: Exit water vapour partial pressure versus vapour pressure for the condenser.

The cooling water flowrates used in the experimental trials varied between 0.5-8.9 gs^{-1}. It can be seen from Table 4.15 that at the lowest cooling water flowrates, the exit temperatures of the cooling streams were nearly at boiling point, therefore very little heat was being transferred at the top of the column. In fact, the cooling water exit temperatures were higher than the gas temperatures, suggesting that heat was being transferred to the gas stream instead of the other way round. Therefore, it can be concluded that at low water flowrates very little cooling was achieved with this system. However, even at low cooling water flowrates there was an improvement in the dehumidification of the gas stream compared to the other columns tested. This was because of better gas- liquid contact due to the large cooling surface area.

Conversely, for high flowrates, the exit cooling water temperatures were lower than the gas temperatures, which was as expected, Table 4.15. This indicated that heat was being continually removed from the top of the column, where it was most needed. Thereby, ensuring that low exit water vapour pressures were obtained. It was therefore concluded that the removal of heat from the absorber did improve the absorption of water vapour into the lithium bromide stream.

Lastly, the temperatures obtained for T5 were consistently higher than the actual gas exit temperatures recorded. This was due to heat losses between two measurement points, the point T5, near the top of the column and the gas exit. As the gas flowrates were small and the heat capacity of the stream was low this represented losses of only a few watts.

$\dot{m}_G$ (gs^{-1})	$T_{G_{in}}$ (°C)	$T_{G_{out}}$ (°C)	T5 (°C)	$\dot{m}_{CW}$ (gs^{-1})	$T_{CW_{in}}$ (°C)	$T_{CW_{out}}$ (°C)
1.00	98	60	66	8.4	47	58
1.00	80	65	70	8.9	52	55
1.00	98	61	68	7.5	48	61
1.00	73	60	66	9.8	46.5	58.5
1.20	78	65	70	8.7	53	57
1.20	87	67	73	8.5	53	57
1.40	84	66	72	8.9	55.5	56.5
1.60	70	68	72	8.7	54	59
1.60	83	68	73	8.6	53	57
1.60	83	72	77	8.5	51	59
1.80	77	83	92	0.5	24.5	96
1.80	93	88	96	0.5	25	97
1.80	95	85	93	0.5	24.5	96
1.80	78	86	94	0.5	24.5	95.5
1.80	93	82	90	0.5	22.5	96
1.80	96	85	93	0.5	25	97
1.80	78	62	68	7.1	49	62
1.80	96	72	79	4.0	47	79
1.80	102	61	66	7.1	49	62
1.80	71	82	91	0.5	23.5	95
1.80	71	87	94	0.5	24.5	96
1.80	71	85	93	0.5	24.5	96
1.80	98	88	96	0.5	26	96

Table 4.15: Influence of C.W flowrate upon exit gas conditions.

4.4 Two Stage Cycle: Reheat Column Studies.

Experiments with the reheat column were directed towards obtaining as high a temperature within the absorber as possible. This was achieved by mixing a concentrated lithium bromide solution with a low pressure steam source. The heat generated from this absorption process was then transferred to a countercurrent flowing gas stream. The gas stream being heated flowed in the annular space between the outer absorber shell and the inner absorption tube, while hot lithium bromide- steam mixture flowed down the inside of the absorption tube. A highly extended surface on the absorption pipe helped to maximise the rate of heat transfer to the gas.

The primary operating variables in these studies were the gas and lithium bromide flowrates and the LiBr concentration (as detailed in Table 4.1) with the addition of a separate steam source. Secondary variables which were also studied were the inlet temperatures of the process streams. It was assumed that the gas entering the column had previously been dehumidified, in the direct contact absorber (Section 4.3), and so the gas humidity was ignored in the tests carried out. An important operating criterion used to measure the performance of the reheat absorber was the circulation ratio. This was defined as the ratio between the lithium bromide and steam mass feeds in the inner tube of the column (F_r). This ratio was used in preference to quoting separate flowrates for both streams, allowing easier classification and discussion of the experimental results.

Medium	Operation	Gas flow	$T_{G_{bot}}$	$T_{G_{top}}$	$T_{I_{top}}$	$T_{I_{bot}}$	U_O
		(gs^{-1})	(^oC)		(^oC)		(W/m^2K)
LiBr	Heating	2.00	21	68	70	58	140 ±150
LiBr	Heating	3.00	21	71	73	59	220 ±295
LiBr	Heating	3.00	26	96	100	77	210 ±80
LiBr	Heating	5.00	23	81	88	62	285 ±85
LiBr	Heating	6.00	23	73	83	57	280 ±70
LiBr	Cooling	5.00	98	55	53	55	290 ±180
LiBr	Cooling	6.00	98	68	63	77	295 ±95
Steam	Heating	2.67	69	98	101	100	120 ±70
Steam	Heating	3.00	21	96	98	97	200 ±385
Steam	Heating	3.00	19	95	100	100	150 ±40
Steam	Heating	4.00	25	101	104	103	240 ±350
Steam	Heating	4.00	32	97	101	100	210 ±240
Steam	Heating	4.00	23	97	100	100	240 ±200
Steam	Heating	4.00	15	99	102	100	250 ±100
Steam	Heating	4.00	11	93	104	100	160 ±20
Steam	Heating	4.00	20	95	101	100	190 ±190

Table 4.16: Experimental results for the determination of the overall heat transfer coefficient for the reheat column.

4.4.1 Heat Transfer Characteristics of the Reheat Absorber.

Prior to carrying out absorption experiments with the heat exchanger, it was necessary to determine the column's heat transfer characteristics. Two modes of operation were investigated in this experimental programme, namely the heating and cooling of the column. The heating trials were carried out using either steam or lithium bromide, flowing in the inner tube of the column, to heat externally flowing gas streams. The cooling experiments were achieved by removing heat from hot gas streams using cold lithium bromide, Tables 4.16 and 4.17. The two process streams flowed countercurrent to each other to maximise the heat transfer.

Gas flow	$T_{G_{av}}$	k_G	k_{H_2O}	k_{av}	h_G (*)	Re_G	Nu_G
(gs^{-1})	(^oC)	($Wm^{-1}K^{-1}$)			($Wm^{-2}K^{-1}$)	(-)	(-)
2.00	45	2.75	N/A	2.75	150	1800	155 ±180
3.00	46	2.76	N/A	2.76	250	2600	255 ±350
3.00	61	2.87	N/A	2.87	230	2600	225 ±90
5.00	43	2.73	N/A	2.73	320	4400	330 ±100
6.00	40	2.70	N/A	2.70	320	5300	330 ±90
5.00	76	2.99	N/A	2.99	330	4400	310 ±200
6.00	83	3.03	N/A	3.03	340	5300	315 ±100
2.67	84	3.05	2.40	2.89	125	2370	120 ±80
3.00	59	2.86	N/A	2.86	220	2600	215 ±435
3.00	57	2.85	N/A	2.85	160	2600	160 ±45
4.00	63	2.89	N/A	2.89	270	3500	260 ±395
4.00	65	2.90	N/A	2.90	230	3500	225 ±270
4.00	60	2.87	N/A	2.87	260	3500	255 ±210
4.00	57	2.85	N/A	2.85	280	3500	270 ±115
4.00	52	2.81	N/A	2.81	170	3500	170 ±30
4.00	57	2.85	N/A	2.85	210	3500	210 ±210

Table 4.17: Nusselt and Reynolds numbers for the gas stream, used to determine the heat transfer characteristics of the reheat column.

* As the majority of the heat resistance in the column was on the gas side (constituting approximately 95% of the total heat transfer resistance), an inner heat transfer coefficient (h_I) of $3000 Wm^{-2}K^{-1}$ was assumed. Hence knowing U_O, h_I and $^x/_k$, it was possible to determine the outside gas heat transfer coefficient (h_G). It should also be noted that the gas heat transfer coefficient was based on the external, smooth tube area and neglected the extended surface which was used to enhance the heat transfer.
(see Appendix C 'Sample Calculations', Section C.2.1.)

Using dimensional analysis, the data collected was manipulated to give Nusselt and Reynolds numbers for the gas streams (Table 4.17). The most general expression relating the two dimensionless groups is given in Equation 4.1. The constants 'm' and 'c' were determined by plotting Nusselt number against Reynolds number on log- log paper, Equation 4.2, where 'm' represented the gradient of the line, while the y- intercept was $\log_{10}(c)$.

It was also shown by Reynolds that the Nusselt number was dependent upon the Prandtl number [1] according to $Pr^{1/3}$. However, the variation of Pr in these tests was minimal, Table 4.18, it was therefore considered to be constant and was incorporated into the 'c' term of Equation 4.1.

$$Nu = c.Re^{m} \tag{4.1}$$

$$log(Nu) = log(c) + m.log(Re);\ where\ c = c'.Pr^{1/3} \tag{4.2}$$

Flowrates		Prandtl Number(*)			
Gas	Vapour	Gas	Vapour	Average	$Pr^{1/3}$
(gs^{-1})		(-)			(-)
2.00	0.00	0.70	-	0.70	0.89
2.00	0.17	0.70	0.92	0.72	0.90
2.00	0.67	0.70	0.92	0.76	0.91

Table 4.18: Variation of the gas Prandtl number with humidity.
(* assuming average Prandtl numbers over the temperature range 25- 85 °C.)

[1] The refinement was due to the influence of molecular diffusion across the boundary layer within the fluid being studied, causing a reduction in the rate of heat transfer. However, experiments using gases gave good predictions for the HTCs because the rate of heat transfer was almost the same as the rate of momentum transfer, implying a Pr of approximately one and so its effect upon Nu was omitted.

Line (1), Figure 4.11 shows that a linear relationship existed between the Nusselt number (for the outside gas heat transfer coefficient in the absorber) and the Reynolds number (based on the annular gas flowrate). The method of least squares was used to perform a linear regression on the experimental points, resulting in a constant of proportionality (c) of 1.28, while the coefficient 'm' was 0.78, see Equation 4.3. The standard Nu- Re relationship for turbulent flow in pipes, as proposed by Sieder- Tate [2], was also drawn on Figure 4.11, Line (2). It can be seen from Figure 4.11 that there was an increase in the gas heat transfer coefficient of 12 to 14- fold as a result of the highly extended surface on the outside of the inner tube. (see Appendix C 'Sample Calculations', Section C.2.2.).

$$Nu = 0.41.\ Re^{0.78} \tag{4.3}$$

It should be noted that in most of the experiments performed, the gas outlet temperature was very close to the inlet inner tube temperature. This was a consequence of the extended surface on the absorption tube, which gave high gas heat transfer coefficients and resulting in close temperature approaches between the two process streams at the top of the column. Therefore, the errors in the log mean temperature differences, the gas heat transfer coefficients and hence the Nusselt numbers were very large. However, because the final data points were consistent, the expression given in Equation 4.3 was felt to be valid.

[2]Sieder, E. N. and Tate G. E.; Ind. Eng. Chem., 28, pp1429- 1436 (1936).
$Nu = 0.027.\ Re^{0.8}.\ Pr^{1/3}$

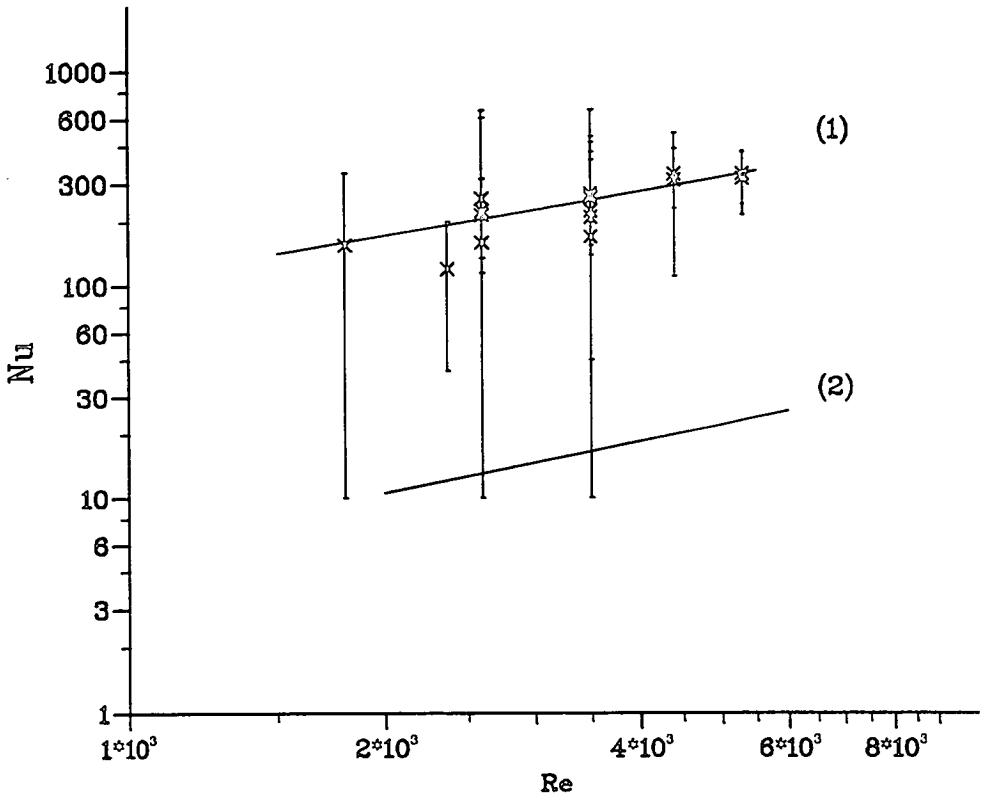

Figure 4.11: Determination of the overall heat transfer coefficient for heat transfer to the external gas stream.

4.4.2 Early Absorption Trials.

The first absorption experiments carried out using the reheat column were very promising. Reasonable gas exit temperatures were achieved using relatively high concentrations of lithium bromide solutions. However, the temperatures obtained were not as high as expected. This was attributed to the presence of inerts within the inner tube of the absorber, which reduced the steam partial pressure in the absorber and therefore lowered the maximum absorption temperature.

It was therefore necessary to completely remove or, at the very least, significantly reduce the inerts from the absorption column. The modifications carried out, as described in Chapter 3 'Design and Construction', Figure 3.14, involved the addition of a bleed valve to the lithium bromide pipework leaving the reheat column; and the extension of the pipe which delivered the weak lithium bromide to the liquid reservoir at the bottom of the dehumidification column. The bleed valve served to remove inerts at the start of the experiment, and replaced them with steam. The dip pipe ensured that the lithium bromide solution flowed in a closed circuit and thus prevented any air being sucked up into the reheat column.

$\dot{m}_{LiBr_{in}}$	$w_{LiBr_{in}}$	$\dot{m}_{RS}$	Inner tube temperature		Gas temperature		
			Top	Bottom	Bottom	Top	ΔT_G
(gs^{-1})	(%w/w)	(gs^{-1})	(°C)	(°C)	(°C)	(°C)	(degC)
4.30	60	0.10	104	121	91	132	41
4.30	60.5	0.10	100	116	91	126	35
4.30	62	0.10	99	115	91	126	35
5.93	61	0.10	99	116	92	127	35
2.95	61	0.10	96.5	117	95	132	37
4.51	58	0.12	98	111	71	124	53
4.51	59	0.12	99	111.5	71	125.5	55
2.90	60	0.12	98	113	71	134	63
2.90	61	0.12	99	115	72	137	65
2.33	61	0.12	103	121	72	140	67
2.33	61	0.12	98	117	72	138	66
4.41	61.5	0.16	105	129	103	138	35

Table 4.19: a) Reheat data for the absorption column before the modifications.

$\dot{m}_{LiBr_{in}}$	$w_{LiBr_{in}}$	$\dot{m}_{RS}$	Inner tube temperature		Gas temperature		
			Top	Bottom	Bottom	Top	ΔT_G
(gs^{-1})	(%w/w)	(gs^{-1})	(°C)	(°C)	(°C)	(°C)	(degC)
2.06	59	0.12	101	118	62	135	73
2.06	60	0.12	102	117	62	137.5	76
2.06	61	0.12	103	118	62	139	77
2.06	61	0.12	103	120	62.5	141.5	79
2.06	61	0.16	104	139	58	142	84
2.06	61	0.16	102	145	82	143.5	62
2.06	61.5	0.16	103	147	90	145	55
1.48	62	0.16	93	143	101	147	45
1.48	62	0.16	103	139	73	147	74
2.11	58	0.16	106	132	79	131	52
2.11	59	0.16	101	134	86	130	44
2.11	60	0.16	102	136	88	133.5	45
2.11	61	0.16	101.5	139	96	136	40
2.12	63	0.16	101	140	99	136	37
2.82	59.5	0.14	100	136	92	131	38
2.82	61.5	0.14	99	136.5	93	135.5	43
2.82	63	0.14	99	139	92	138	45

Table 4.20: b) Reheat data for the absorption column after the modifications.

Figure 4.12 shows that the modifications to the pipework did improve the gas exit temperatures. Despite the fact that several of the operating parameters were varied during these runs, there was a definite increase of a few degrees in the exit gas temperatures obtained throughout the concentration range used. The 'VLE TEMPERATURE' line was drawn based upon the exit lithium bromide concentration and assumed a vapour pressure of 1 bar. The exit concentration was chosen this was representative of the maximum achievable absorption temperature after the steam has been absorbed. After establishing a reliable operating system the operability of the system was investigated.

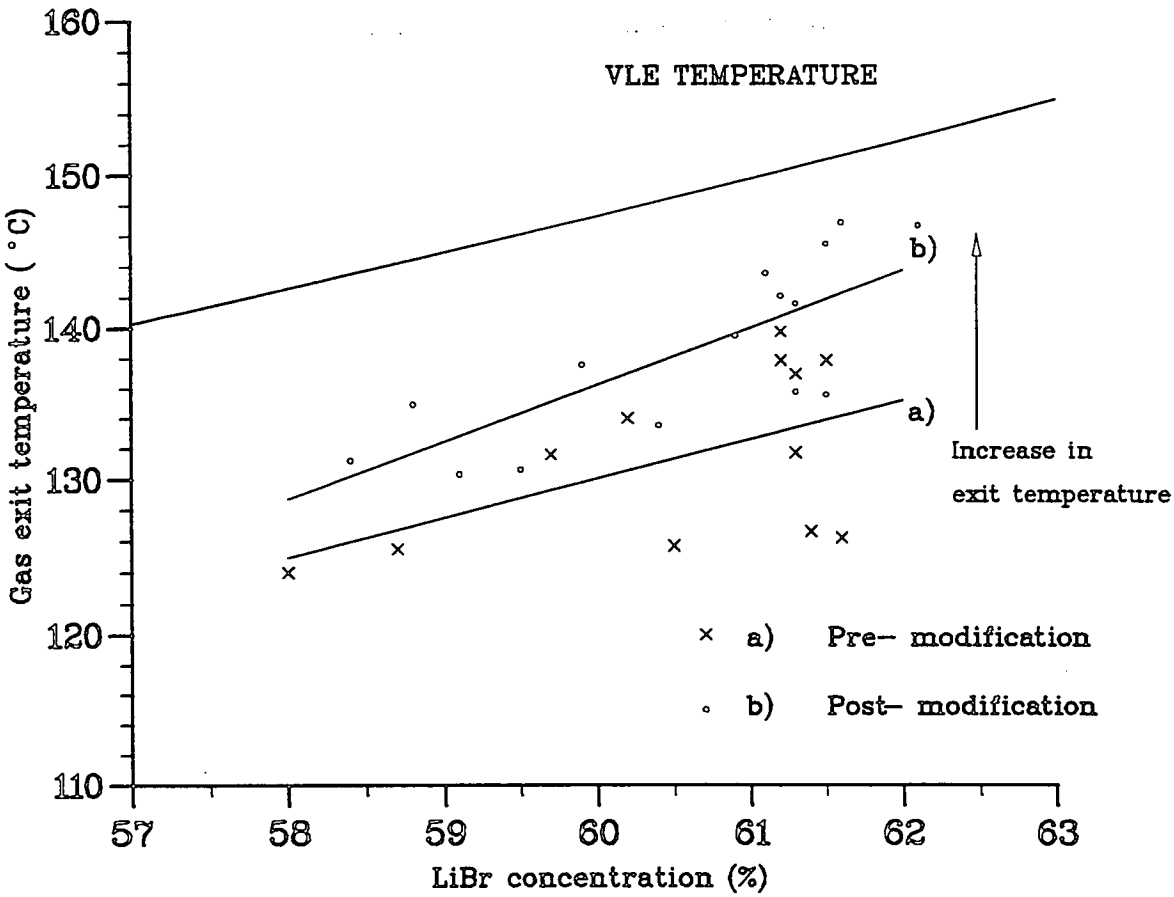

Figure 4.12: Improvement in gas exit temperature after modification to the reheat column.

4.4.3 Effect of Varying the Gas Flowrate.

Several gas flowrates were used in the experimental runs in order to determine the influence of the flowrate upon the operation of the absorber and the exit gas temperatures achieved. It can be seen from Figure 4.13 that although the highest gas outlet temperatures were obtained at the highest lithium bromide inlet concentrations, a peak in the outlet temperature occurred in each case at a gas flowrate of 3 gs^{-1}.

Figure 4.13 shows that as the gas flowrate increased between 2- 3 gs^{-1} there was initially a rise in the gas exit temperature, before gradually decreasing as the flowrate was increased to 6 gs^{-1}. The initial increase in exit temperature was due to an increase in overall heat transfer coefficient, increasing the rate of heat transferred to the gas stream. Another factor which influenced the exit temperatures was the rate of heat loss to the surroundings, which accounted for a larger proportion of the total heat transferred at the lowest gas stream flowrates. For example, assuming a 20 W heat loss over the column and the associated pipework, the corresponding drop in temperature for a gas at 2 gs^{-1} would be 10 degC, whereas if the flow were 3 gs^{-1} it would only be 6.7 degC.

The subsequent drop in the exit temperature above gas flowrates of $3gs^{-1}$ was a result of the increased heat content (C_G) of the gas stream. Therefore, despite an increase in the gas heat transfer coefficient as the Reynolds number rose, according to Equation 4.3, there was also a corresponding and greater increase in the heat required to raise the temperature of the stream by one degree.

$\dot{m}_G$ (gs^{-1})	$\dot{m}_{LiBr}$ (gs^{-1})	w_{LiBr} (%w/w)	$\dot{m}_{RS}$ (gs^{-1})	F_r (-)	$T_{G_{in}}$ (°C)	$T_{G_{out}}$ (°C)	ΔT_G (degC)	Q (W)	Q_{input} (W)	COP (-)
2.00	2.81	57	0.16	17.6	66	123	57	114	578	0.20
2.00	2.82	57	0.16	17.6	93	128	35	71	555	0.13
3.00	2.06	55	0.12	17.2	81	131	51	152	570	0.27
3.00	2.81	56	0.16	17.6	85	132	47	141	561	0.25
3.00	2.82	57	0.16	17.6	82	133	51	152	561	0.27
4.00	2.11	57	0.12	17.6	93	131	38	152	470	0.32
5.00	2.82	57	0.16	17.6	80	128	48	238	561	0.42

Table 4.21: Experimental data showing the influence of the gas flowrate upon the gas exit temperature. LiBr concentration range 55- 57 %w/w.

$\dot{m}_G$ (gs^{-1})	$\dot{m}_{LiBr}$ (gs^{-1})	w_{LiBr} (%w/w)	$\dot{m}_{RS}$ (gs^{-1})	F_r (-)	$T_{G_{in}}$ (°C)	$T_{G_{out}}$ (°C)	ΔT_G (degC)	Q (W)	Q_{input} (W)	COP (-)
2.00	2.90	60	0.16	18.1	79	128	49	98	621	0.16
2.00	2.93	60	0.16	18.3	81	129	48	96	621	0.15
2.00	2.92	60	0.16	18.3	82	130	49	97	621	0.16
3.00	2.82	59	0.14	20.1	92	131	38	115	585	0.20
3.00	2.06	59	0.12	17.2	62	135	73	218	570	0.38
3.00	2.06	60	0.12	17.2	62	138	76	228	570	0.40
4.00	2.86	58	0.16	17.9	76	127	50	201	647	0.31
4.00	2.86	58	0.16	17.9	77	129	52	209	667	0.31
4.00	2.88	59	0.16	18.0	76	128	52	208	681	0.31
4.00	2.20	60	0.12	18.3	93	134	41	164	530	0.31
5.00	2.84	58	0.16	17.8	80	129	49	246	561	0.44
5.00	2.88	59	0.16	18.0	80	130	50	252	611	0.41
5.00	2.92	60	0.16	18.3	80	132	52	261	611	0.43
6.00	2.87	59	0.16	17.9	75	128	53	319	561	0.57
6.00	2.91	60	0.16	18.2	79	131	51	308	621	0.50

Table 4.22: Experimental data showing the influence of the gas flowrate upon the gas exit temperature. LiBr concentration range 58- 60 %w/w.

$\dot{m}_G$ (gs^{-1})	$\dot{m}_{LiBr}$ (gs^{-1})	w_{LiBr} (%w/w)	$\dot{m}_{RS}$ (gs^{-1})	F_r (-)	$T_{G_{in}}$ (°C)	$T_{G_{out}}$ (°C)	ΔT_G (degC)	Q (W)	Q_{input} (W)	COP (-)
2.00	2.97	62	0.16	18.6	82	131	49	98	611	0.16
3.00	2.82	61	0.14	20.1	93	136	43	128	585	0.22
3.00	2.33	61	0.12	19.4	72	138	66	198	540	0.37
3.00	2.82	63	0.14	20.1	93	138	45	136	585	0.23
3.00	2.06	61	0.12	17.2	62	139	77	232	570	0.41
3.00	2.33	61	0.12	19.4	72	140	67	203	540	0.37
3.00	2.06	61	0.12	17.2	62	141	79	237	570	0.42
4.00	2.22	61	0.12	18.5	93	137	44	178	530	0.33
4.00	3.00	62	0.16	18.8	82	137	55	222	722	0.31
4.00	2.25	62	0.12	18.8	93	140	47	188	550	0.34
5.00	2.98	62	0.16	18.6	80	136	56	278	611	0.46
6.00	2.95	61	0.16	18.4	79	131	52	313	621	0.50
6.00	3.00	62	0.16	18.8	79	134	55	329	621	0.53

Table 4.23: Experimental data showing the influence of the gas flowrate upon the gas exit temperature. LiBr concentration range 61- 63 %w/w.

$\dot{m}_G$ (gs^{-1})	$\dot{m}_{LiBr}$ (gs^{-1})	w_{LiBr} (%w/w)	$\dot{m}_{RS}$ (gs^{-1})	F_r (-)	$T_{G_{in}}$ (°C)	$T_{G_{out}}$ (°C)	ΔT_G (degC)	Q (W)	Q_{input} (W)	COP (-)
2.00	2.90	64	0.16	18.1	82	135	53	105	647	0.16
3.00	2.82	64	0.14	20.1	91	139	48	143	585	0.24
3.00	2.82	65	0.14	20.1	92	144	52	156	585	0.27
3.00	2.82	66	0.14	20.1	92	145	53	158	585	0.27
3.00	2.82	66	0.14	20.1	92	146	54	162	585	0.28
3.00	2.82	66	0.14	20.1	92	147	55	164	585	0.28
3.00	2.29	66	0.12	19.1	88	149	61	183	570	0.32
4.00	2.28	64	0.12	19.0	94	142	49	195	570	0.34
4.00	2.31	64	0.12	19.3	94	144	51	202	570	0.35
5.00	3.04	64	0.16	19.0	80	138	58	289	641	0.45
5.00	3.08	64	0.16	19.3	80	139	59	297	661	0.45
5.00	3.01	65	0.16	18.8	79	140	61	305	661	0.46
5.00	3.02	66	0.16	18.9	80	142	63	313	661	0.47
6.00	3.05	64	0.16	19.1	78	135	57	344	641	0.54
6.00	3.02	65	0.16	18.9	76	137	61	364	661	0.55
6.00	3.04	65	0.16	19.0	77	138	61	366	661	0.55
6.00	3.00	66	0.16	18.4	76	139	63	377	661	0.57

Table 4.24: Experimental data showing the influence of the gas flowrate upon the gas exit temperature. LiBr concentration range 64- 66 %w/w.

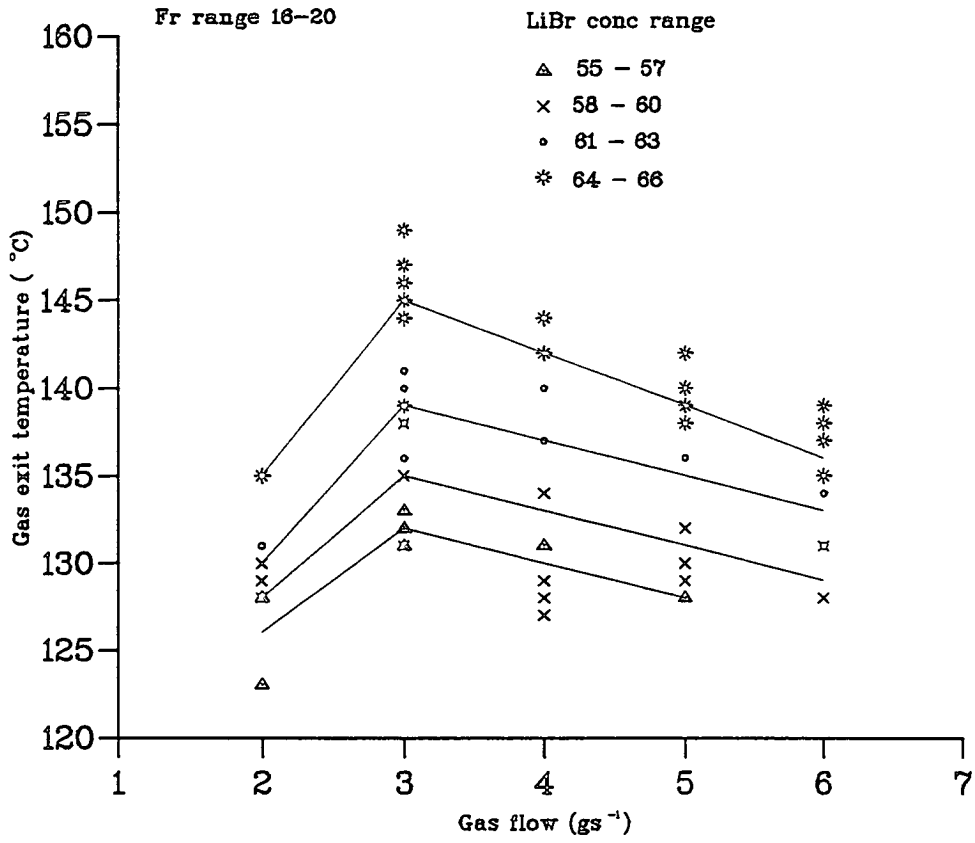

Figure 4.13: Effect of gas flowrate upon the exit gas stream temperature.

The circulation ratio used in these tests ranged between 16 and 20, implying a relatively high steam mass flows and low lithium bromide flowrates. Therefore, the inner tube steam heat capacity was kept low, while the steam partial pressure remained high, resulting in high absorption temperatures and hence higher gas exit temperatures.

4.4.4 Effect of Varying the Absorption Conditions.

In addition to the extended surface on the outside of the absorption pipe, a turbulence promoting device was inserted to the inside of the tube. The promoter helped both mass and heat transfer within the liquid absorbent:

- Diversion of the flow of hot absorbent liquid to the wall to improve heat transfer to the gas.
- Increase in mixing between the liquid and steam phases, thus increasing mass transfer and the absorption of steam into the absorbent.
- Promotion of turbulence within the liquid stream, increasing heat transfer.

It proved extremely difficult to instrument the absorber so as to determine the individual phase heat transfer coefficients or the influence of the promoter upon heat transfer. As discussed earlier, most of the heat transfer resistance was on the gas side and so the effects of the liquid side heat resistances ignored and were considered to be constant. The heat transfer coefficient assumed for the liquid side was 3000 $Wm^{-2}K^{-1}$, which was in close agreement to the empirical value determined in the computer simulation model (Chapter 5, Section 5.4.2).

The main variables influencing the performance of the column are the inlet lithium bromide concentration and the circulation ratio. Table 4.25 summarises data from the reheat column operating with gas flows of 3 gs^{-1} and inlet inner stream temperatures of approximately 100 °C.

Variation of the Lithium Bromide Concentration. It can be clearly seen from Figure 4.14 that the highest gas exit temperatures were obtained when operating the absorber at the lowest circulation ratios (F_r) and highest absorbent concentrations. Each of the data sets shows a linear relationship between exit gas temperature and lithium bromide concentration, which was also seen in the single stage studies (Section 4.2.4).

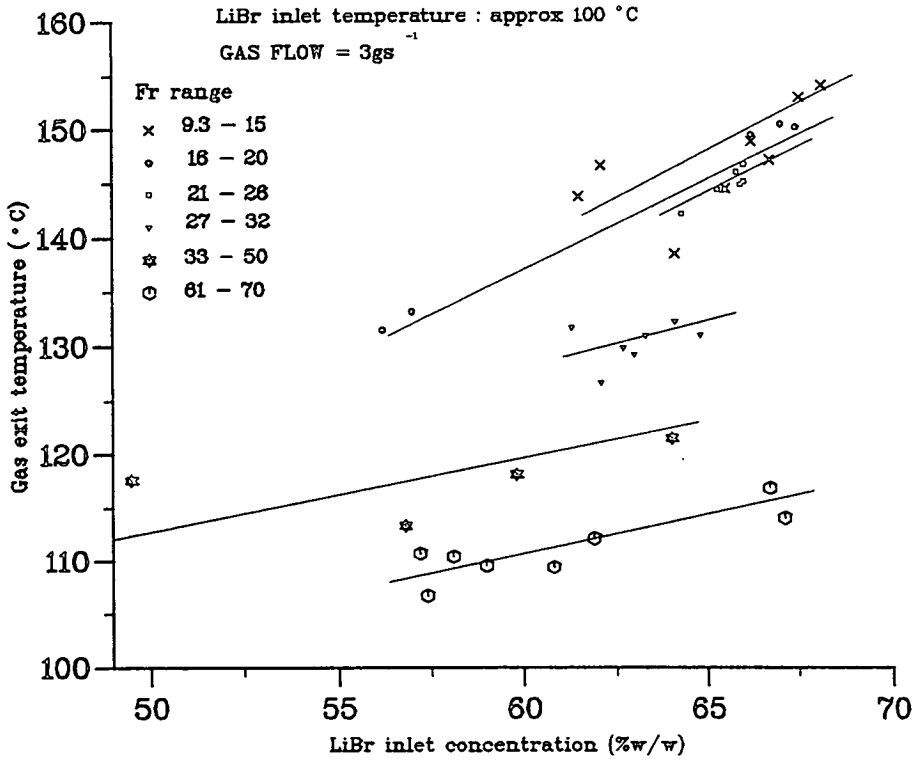

Figure 4.14: Performance data for the reheat column.

F_r	$\dot{m}_{LiBr_{in}}$	$w_{LiBr_{in}}$	$\dot{m}_{RS}$	$T_{G_{in}}$	$T_{G_{out}}$	ΔT_G	Q_G	Q_{input}	COP	ζ
(-)	(gs^{-1})	(%w/w)	(gs^{-1})	(°C)	(°C)	(degC)	(W)	(W)	(-)	(-)
9.3	1.48	62	0.16	101	147	45	137	661	0.21	0.39
13.3	2.12	64	0.16	99	139	39	118	644	0.18	0.39
13.9	2.22	62	0.16	89	144	55	165	661	0.25	0.60
14.3	2.29	66	0.16	86	149	63	189	701	0.27	0.73
14.6	2.34	68	0.16	86	153	67	202	701	0.29	0.80
14.7	2.35	66	0.16	78	145	66	198	666	0.30	0.65
14.8	2.36	68	0.16	86	154	68	204	701	0.29	0.80
14.9	2.39	67	0.16	92	147	55	165	703	0.24	0.64
15.1	2.41	67	0.16	93	150	57	170	717	0.24	0.68
17.6	2.81	56	0.16	85	132	47	140	561	0.25	0.54
17.6	2.82	57	0.16	83	133	51	152	561	0.27	0.57
19.1	2.29	66	0.12	89	149	61	183	570	0.32	0.79
19.3	2.32	67	0.12	88	150	62	187	610	0.31	0.75
20.1	2.82	66	0.14	92	144	52	156	585	0.27	0.92
20.1	2.82	66	0.14	92	146	54	162	585	0.28	0.90
20.1	2.82	66	0.14	92	145	53	158	585	0.27	0.93
25.3	3.04	65	0.12	88	144	57	169	570	0.30	0.70
25.6	3.07	66	0.12	88	147	58	175	570	0.31	0.72
25.7	3.08	64	0.12	90	142	52	156	570	0.27	0.68
27.3	2.18	63	0.08	77	130	53	159	480	0.33	0.61
27.3	2.18	63	0.08	77	131	54	163	480	0.34	0.68
27.3	2.18	65	0.08	77	131	54	163	480	0.34	0.62
27.9	2.23	62	0.08	94	127	33	98	480	0.20	0.46
27.9	2.23	63	0.08	94	129	35	104	480	0.22	0.48
27.9	2.23	64	0.08	94	132	38	113	480	0.24	0.53
29.5	2.95	61	0.10	95	132	37	112	495	0.23	0.55
35.2	4.22	50	0.12	83	118	35	105	570	0.18	0.49
41.1	2.47	57	0.06	82	113	31	93	415	0.23	0.50
42.2	2.53	64	0.06	83	122	39	117	435	0.27	0.63
42.3	2.54	60	0.06	82	118	36	109	435	0.25	0.58
70.8	4.25	57	0.06	93	107	14	42	435	0.10	0.22
70.8	4.25	57	0.06	93	111	18	54	435	0.12	0.31
70.8	4.25	58	0.06	94	110	16	48	435	0.11	0.24
70.8	4.25	59	0.06	72	110	38	114	435	0.26	0.46
73.0	4.38	67	0.06	83	117	34	102	385	0.26	0.72
73.3	4.40	67	0.06	83	114	31	93	385	0.24	0.63
73.5	4.41	61	0.06	86	109	23	69	385	0.18	0.36
74.5	4.47	62	0.06	85	112	27	81	385	0.21	0.36

Table 4.25: Performance data for the reheat column for increasing the circulation ratio.

Variation of the Circulation Ratio. The highest gas exit temperatures were obtained when operating the absorber with low circulation ratios. The reason for this can be attributed to lower liquid stream heat capacities, resulting in greater heat transfer to the gas stream. The gas temperature lifts for the lowest ratios vary between 50 and 70 degC, while the maximum temperature lift was 72 degC, when the inlet temperature of the gas stream was 86 °C and the inlet lithium bromide temperature was 112 °C.

The lowest circulation ratio achievable in these experiments was 9.3, which occurred using a steam flowrate of 0.16 gs^{-1} (the maximum possible with the heaters used) and a lithium bromide flowrate of 1.48 gs^{-1}. It was not possible to obtain reliable or steady absorbent flows below this. This was probably because of the slow or incorrect seating of the non-return valves on the diaphragm pump head used for these experiments and also because of the short stroke length of the pump. There may also have been problems due to cavitation in the pipework because of the small bore pipe used and because the generator was positioned quite close to the actual pump, i.e the NPSH was low. However, as the lithium bromide solution flowrate decreases towards zero, the influence of the steam would become dominant and the maximum gas exit temperature will drop to 100 °C. By contrast when the column was operated at high circulation ratios there was insufficient steam present in the inner tube to cause a large rise in the temperature of the gas stream. At low steam flowrates the presence of inerts in the absorber become dominant resulting in a low equilibrium vapour pressure and thus a low absorbent maximum temperature (see Chapter 5, Section 5.6.2).

4.4.5 Effect of Varying the Inlet Stream Temperatures.

There was no distinct improvement in the exit gas temperature as a result of varying the inlet temperature of either the gas or lithium bromide streams. This indicated that there was a close temperature approach at the top of the column.

The highest gas exit temperature obtained was 160 °C, when operating with a 68 %w/w lithium bromide solution, flowing at 2.36 gs^{-1} with an inlet temperature of 112 °C and a steam flowrate of 0.16 gs^{-1} (F_r = 14.8). For comparison, the exit temperature obtained when operating under similar conditions, but with an inlet lithium bromide temperature of 100 °C was 154 °C. As the operating conditions were the same in both cases, the maximum absorption temperature, estimated from the average absorbent concentration and a partial pressure of 1 bar, was 170 °C. The LMTDs were 28 ±4 degC and 31 ±4 degC respectively. showing a negligible difference between the results considering the errors involved. A slightly higher exit temperature was obtained in the first run because of the extra heat input at the top of the column ((2.36 x 1.5 x 12) = 40 W).

The independence of the gas inlet temperature upon the exit temperature is shown in Table 4.26, where the inlet temperature varied between 79- 102 °C. As the exit gas temperatures were approximately constant over this range, it was concluded that there was a close temperature approach at the top of the absorber. The exit gas temperature was therefore dependent solely upon the absorbent concentration and steam partial pressure in the inner absorption tube The close temperature approach was due to the extremely high gas heat transfer coefficients (see Section 4.4.1) generated as a result of the highly extended surface area available for heat transfer within the absorption column.

$\dot{m}_{LiBr_{in}}$	$w_{LiBr_{in}}$	F_r	$T_{G_{in}}$	$T_{G_{out}}$	ΔT_G	Q_G	Q_{input}	COP	ζ
(g s^{-1})	(%w/w)	(-)	(°C)	(°C)	(degC)	(W)	(W)	(-)	(-)
1.48	62	9.3	102	148	46	139	661	0.21	0.34
2.06	62	12.9	95	148	52	158	661	0.24	0.47
2.11	58	13.2	79	131	52	156	620	0.25	0.39
2.33	65	14.6	82	146	64	193	666	0.29	0.49
2.36	68	14.8	86	158	72	216	701	0.31	0.70
2.36	68	14.8	97	160	63	188	701	0.27	0.59

Table 4.26: Performance data for the reheat column. Inlet LiBr temperature range 111-119 °C, steam flowrate 0.16 gs^{-1}.

4.5 Prediction of Exit Temperatures.

In order to predict the temperature of the gas stream leaving the top of the reheat column, it was first of all necessary to establish the maximum absorption temperature within the inner tube. The absorption temperature was easily determined from the absorbent concentration and steam partial pressure within the inner tube. However, as this maximum temperature did not occur at the top of the absorption column, Figure 4.15, the available heat transfer area was unknown and so the heat transfer calculation was more difficult. However, by combining the overall heat transfer coefficient and the heat transfer area in one term called $(U.A)_O$ [3], the exit stream conditions were determined, providing that $(U.A)_O$ could be calculated. The method used to find the gas outlet temperature is discussed in Section 4.5.2.

[3] Analogous to absorption in packed beds where the mass transfer coefficient and the loading area, which is variable and thus unknown, are coupled together.

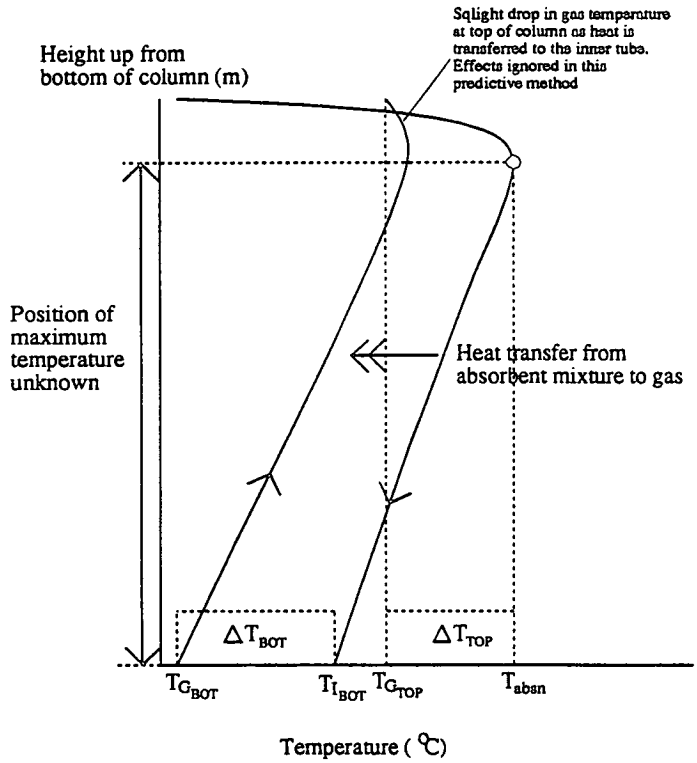

Figure 4.15: Graphical representation of the absorption process with heat transfer to an external gas stream.

As discussed in the previous sections, the primary variables required to achieve a high gas exit temperature were the gas flowrate, the circulation ratio in the inner tube and the lithium bromide inlet concentration. Therefore, in order to obtain an empirical correlation for $(U.A)_O$, the effects of each of these variables must be investigated in turn. The equation for $(U.A)_O$ can be expressed in terms of the individual heat transfer resistances within the absorber, Equation 4.4.

$$\frac{1}{(U.A)_O} = \frac{1}{h_G.A_O} + \frac{1}{h_I.A_I} + \frac{x}{k.A_{LM}} \tag{4.4}$$

The absorbent concentration and circulation ratio were felt to have a minimal effect upon the inside heat resistance, therefore the term h_I was considered to be a constant. In addition, the wall thermal conductivity did not vary and so the third term of Equation 4.4 was also considered to be constant. Therefore, both the inside and wall heat transfer resistances were grouped in a single term 'B'. Finally, the outside heat resistances, h_O, were dependent upon the gas Reynolds number (see Section 4.4.1) and so the Equation 4.4 was simplied to a correlation relating $(U.A)_O$ with Re_G (determined from the gas flowrate), Equation 4.5.

$$\frac{1}{(U.A)_O} = B + C.Re_G^x \tag{4.5}$$

It should be noted that a separate correlation was developed to the one expressing Nu_G (and hence h_G) and Re_G (Section 4.4.1) because the previous relationship was for simple heating/ cooling of the absorber, whereas this correlation was related to the absorption experiments. As mentioned earlier, the heat transfer area was not known and so the relationship between the combined term $(U.A)_O$ and Re_G was assumed to be different.

4.5.1 Influence of Gas Flowrate upon $(U.A)_O$.

The experimental values for $(U.A)_O$ were determined using the standard heat transfer Equations 4.6 and 4.7. The results combining the gas Reynolds number and $(U.A)_O$ are summarised in Table 4.27, for approximately constant inlet lithium bromide concentrations and circulation ratios. As the highest exit temperatures were only obtained when the absorber was operating with low circulation ratios and high inlet concentrations, only data collected under these conditions was considered valuable in establishing a correlation for $(U.A)_O$ and Re_G.

$$(U.A)_O = \frac{Q_G}{\Delta T_{LM}} \tag{4.6}$$

$$Where\ \Delta T_{LM} = \frac{(T_{absn} - T_{G_{top}}) - (T_{L_{bot}} - T_{G_{bot}})}{ln(\frac{T_{absn} - T_{G_{top}}}{T_{L_{bot}} - T_{G_{bot}}})} \tag{4.7}$$

(T_{absn} is the estimated maximum absorption temperature in the absorber.)

A plot of $\log_{10}$ [$(U.A)_O^{-1}$ -B] versus $\log_{10}$ Re_G, Figure 4.16, shows that a straight line relationship does exist between the two variables. The correlation relating the two variables was determined from linear regression, Equation 4.8.

$$(U.A)_O^{-1} = 0.0077 + 3965.\ Re^{-1.3} \tag{4.8}$$

The results for $(U.A)_O$ and Re_G, Table 4.27, do not show any great variation over the range of gas flows investigated. Therefore, the previous assumption of omitting w_{LiBr} and F_r from the empirical relationship was justified. Indeed the relationship obtained yielded a very good correlation coefficient, based upon the line of best fit through the points, of 0.98, indicating a strong linear relationship between [$(U.A)_O^{-1}$ - B] and Re_G.

4.5.2 Summary of Method to Predict Exit Temperatures.

The prediction of the exit temperatures for both the gas and absorbent streams can be achieved by using the heat exchanger effectiveness, which was first proposed by Nusselt [4]. The method was modified for this particular application in order to account for absorption occurring within the inner tube of the exchanger. It was assumed that the area available for heat transfer was the area between T_{absn} (which was determined from a function expressed in terms of the absorbent concentration and steam partial pressure) and the bottom of the exchanger, Figure 4.15. The region above this, which was quite small as the

[4] W. Nusselt, Tech Mechanik and Thermodynamik, 12 (1930)

Re_G	F_r	$w_{LiBr_{top}}$	T_{abs_n}	$T_{G_{top}}$	$T_{I_{bot}}$	$T_{G_{bot}}$	ΔT_{LM}	Q_G	$(U.A)_O$
(-)	(-)	(%w/w)	(°C) (*)	(°C)	(°C)	(°C)	(degC)	(W)	(WK^{-1})
1680	18.1	63.8	154	135	141	82	35	106	3.0
1680	14.4	64.4	154	141	145	82	32	118	3.7
1680	14.6	65.3	158	146	148	82	31	128	4.1
2520	14.9	65.5	158	144	137	78	31	198	6.4
2520	14.6	65.2	158	146	143	82	30	192	6.4
2520	14.9	66.7	160	147	146	92	29	165	5.7
2520	14.0	64.5	155	147	149	87	26	180	6.9
2520	14.3	66.2	160	149	151	86	30	189	6.3
2520	14.6	67.5	162	153	152	86	29	201	6.9
3360	14.2	63.1	150	142	141	94	22	192	8.7
3360	15.3	63.6	153	142	140	91	25	204	8.2
3360	15.3	63.7	153	143	141	92	24	204	8.5
3360	15.4	64.2	155	144	142	92	26	208	8.0
3360	15.5	65.0	157	144	142	92	27	208	7.7
4200	13.8	63.3	150	134	120	78	27	280	10.4
4200	13.9	64.1	153	136	117	78	27	290	10.7
4200	14.1	65.2	157	136	121	79	30	285	9.5
4200	14.5	67.1	161	143	121	79	28	320	11.4
5040	14.1	62.9	150	136	116	78	24	348	14.5
5040	13.9	64.1	153	136	112	77	25	354	14.2
5040	14.2	65.6	158	140	112	77	26	378	14.5
5040	14.3	66.3	159	140	114	77	27	378	14.0

Table 4.27: Summary of results showing a selection of results for $(U.A)_O$ at varying gas flowrates for high inlet absorbent concentrations and low circulation ratios.

(*- The inner tube temperature at the top of the column was estimated from the lithium bromide VLE equations, using an estimate of the average concentration in the column- see Appendix C 'Sample Calculations', Section C.2.1.)

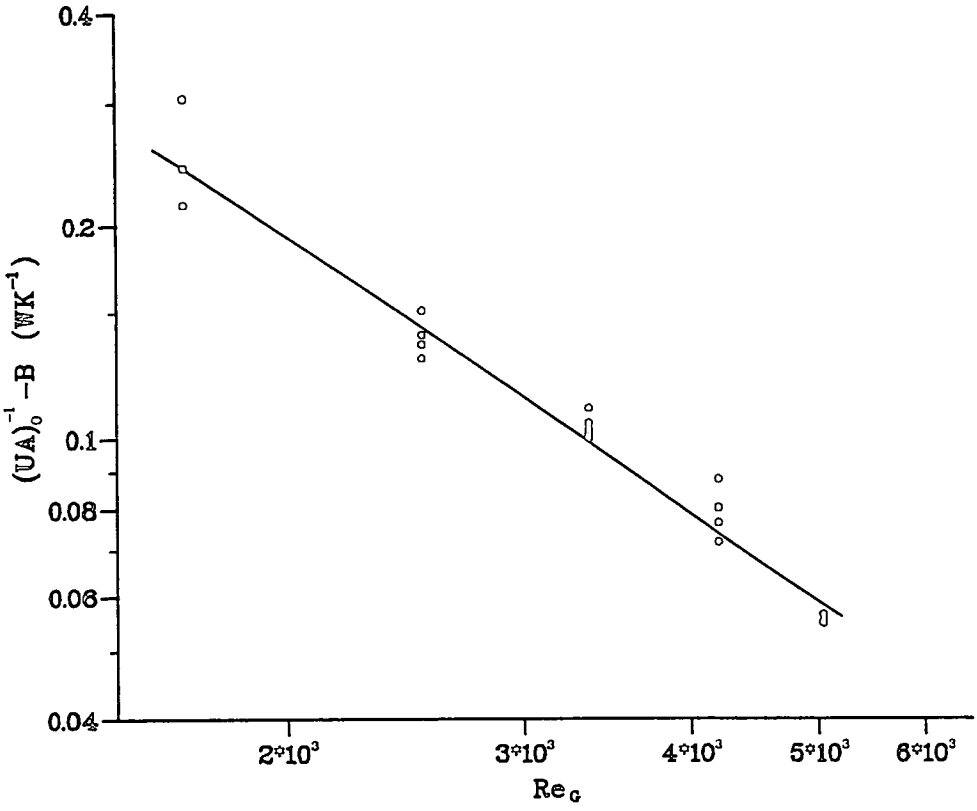

Figure 4.16: Graph of $[(U.A)_O^{-1}$ - B] versus Re_G.

absorption process was extremely rapid, did involve the slight cooling of the gas stream as heat was returned to the absorbent mixture in the inner tube. However, this was ignored in order to simplify the prediction of the gas exit temperature.

The Nusselt method states that the heat exchanger effectiveness is the ratio of the actual heat transferred in the exchanger to the maximum heat that could theoretically be transferred between the streams fed, Equation 4.9.

$$\varepsilon = \frac{Actual\ Heat\ Transfer}{Maximum\ Heat\ Transfer} \tag{4.9}$$

The effectiveness can also be expressed in terms of the stream capacities, Equation 4.10. In a normal heat transfer problem, the stream with the smallest capacity (C_{min}) would undergo the greatest change in temperature. Therefore, the maximum rate of heat transfer, the denominator in Equations 4.11 and 4.12, could be expressed in terms of the maximum temperature change in the stream[5] and C_{min}. Similarly, the actual heat transferred was determined from the capacity of the other stream multiplied by its corresponding temperature change.

$$C_L = \dot{m}_{L_{bot}} . c_{P_L}; \quad C_G = \dot{m}_G . c_{P_G}; \tag{4.10}$$

The exit absorbent stream conditions were used in determining C_L. This was because above the point where the maximum absorption temperature occurred, the flowrate of the absorbent stream changed significantly as the majority of the

[5](T_{absn} - $T_{G_{in}}$)- Maximum absorption temperature less the gas inlet temperature.

steam was absorbed. Therefore, an extra term would need to be included for the steam flow. However, the variation in the absorbent flowrate after the maximum absorption temperature had been reached was small. Indeed the only part of the absorption column which was of interest in this method was the region between the maximum absorption temperature and the bottom of the column. Therefore although the absorbent stream conditions- flowrate and concentration- varied after the maximum temperature had been reached, the changes were ignored in this predictive method in order to make calculations simpler.

The exchanger effectiveness can be expressed in two different forms, relating the stream temperatures and capacities, Equations 4.11 and 4.12, depending on which stream has the smallest capacity. Hence, if ε were known, then the exit stream temperatures could be estimated. If the gas stream had the smallest capacity, it would first of all be necessary to determine the exit absorbent temperature and then solve a heat simple heat balance to find the outlet gas temperature.

$$\varepsilon = \frac{C_G \cdot (T_{G_{out}} - T_{G_{in}})}{C_{min} \cdot (T_{absn} - T_{G_{in}})} \quad when\ C_L = C_{min} \tag{4.11}$$

$$\varepsilon = \frac{C_L \cdot (T_{absn} - T_{L_{out}})}{C_{min} \cdot (T_{absn} - T_{G_{in}})} \quad when\ C_G = C_{min} \tag{4.12}$$

A theoretical equation defining ε for a single pass, countercurrent exchanger was given by Welty ([117], p395) and is reproduced in Equation 4.14. The term NTU (Number of Transfer Units) is defined in Equation 4.13, where $(U.A)_O$ was evaluated from Equation 4.8. Therefore, knowing the stream capacities and NTU, an estimate of the exchanger effectiveness can be made. Once ε has been

determined, the exit stream conditions can be found, as discussed previously.

$$NTU = \frac{(U.A)_O}{C_{min}} \tag{4.13}$$

$$\varepsilon = \frac{1 - e^{-NTU(1-\frac{C_{min}}{C_{max}})}}{1 - (\frac{C_{min}}{C_{max}})\, e^{-NTU(1-\frac{C_{min}}{C_{max}})}} \tag{4.14}$$

In summary, the exit stream conditions can easily be determined by following the steps outlined in Equation 4.15.

$$m_G \rightarrow Re_G \rightarrow (U.A)_O \, \alpha \, C_{min} \rightarrow NTU \, \alpha \, \frac{C_{min}}{C_{max}} \rightarrow \varepsilon \rightarrow T_{G_{top}} \, or \, T_{L_{bot}} \tag{4.15}$$

4.5.3 Comparison between Experimental and Predicted Exit Temperatures.

In order to verify the validity of the predictive method described in the previous section, Section 4.5.2, a series of experimental results was compared with those determined numerically. Table 4.28 summarises the data obtained; while the second group of results ($w_{LiBr_{in}}$ = 59/60 %w/w) were plotted in Figure 4.17.

The first set of gas exit temperatures obtained using this predictive method were estimated assuming an ideal system with no heat losses. However, more realistic

results were then calculated which incorporated heat losses to the surroundings. The overall heat transfer coefficient for heat losses to the surroundings was assumed to be 1 $Wm^{-2}K^{-1}$, while the heat transfer area was assumed to be 0.32 m^2. Hence, it was necessary to first of all estimate the gas exit temperature for ideal conditions. This temperature was then used to determine the log-mean temperature difference between the gas stream and the surroundings and hence the heat loss term. The exit gas temperature was then refined.

Experimental						Predicted		
$\dot{m}_G$	$\dot{m}_{LiBr_{in}}$	$\dot{m}_{RS}$	$w_{LiBr_{in}}$	$T_{G_{bot}}$	$T_{G_{top}}$	ε	$T_{G_{IDEAL}}$	$T_{G_{LOSSES}}$
(gs^{-1})	(gs^{-1})	(gs^{-1})	(%w/w)	(°C)	(°C)	(-)	(°C)	(°C)
2.00	2.82	0.16	57	66	123	0.81	128	115
3.00	2.82	0.16	57	82	133	0.79	129	121
5.00	2.82	0.16	57	80	128	0.73	125	120
2.00	2.90	0.16	60	79	128	0.81	136	123
3.00	2.82	0.14	59	92	131	0.78	135	126
4.00	2.88	0.16	59	76	128	0.77	131	124
5.00	2.88	0.16	59	80	130	0.74	130	124
6.00	2.87	0.16	59	75	128	0.76	125	120
2.00	2.97	0.16	62	82	131	0.81	140	127
3.00	2.82	0.14	61	93	136	0.79	141	132
4.00	3.00	0.16	62	82	137	0.78	138	132
5.00	2.98	0.16	62	80	136	0.74	135	129
6.00	3.00	0.16	62	79	134	0.74	132	127
2.00	2.90	0.16	64	82	135	0.81	146	132
3.00	2.82	0.14	64	91	139	0.79	146	137
5.00	3.04	0.16	64	80	138	0.75	141	135
6.00	3.05	0.16	64	78	135	0.74	137	133

Table 4.28: Comparison of experimental and predicted gas exit temperatures using exchanger effectiveness model.

(see Appendix C 'Sample Calculations', Section C.2.3.)

It can be seen from the results that the experimental exit gas temperatures analysed lay consistently between the temperatures predicted for the 'ideal' and 'heat loss' cases. This suggested that the predictive method could be used as a design tool to size and estimate the performance of the reheat absorber operating under any conditions.

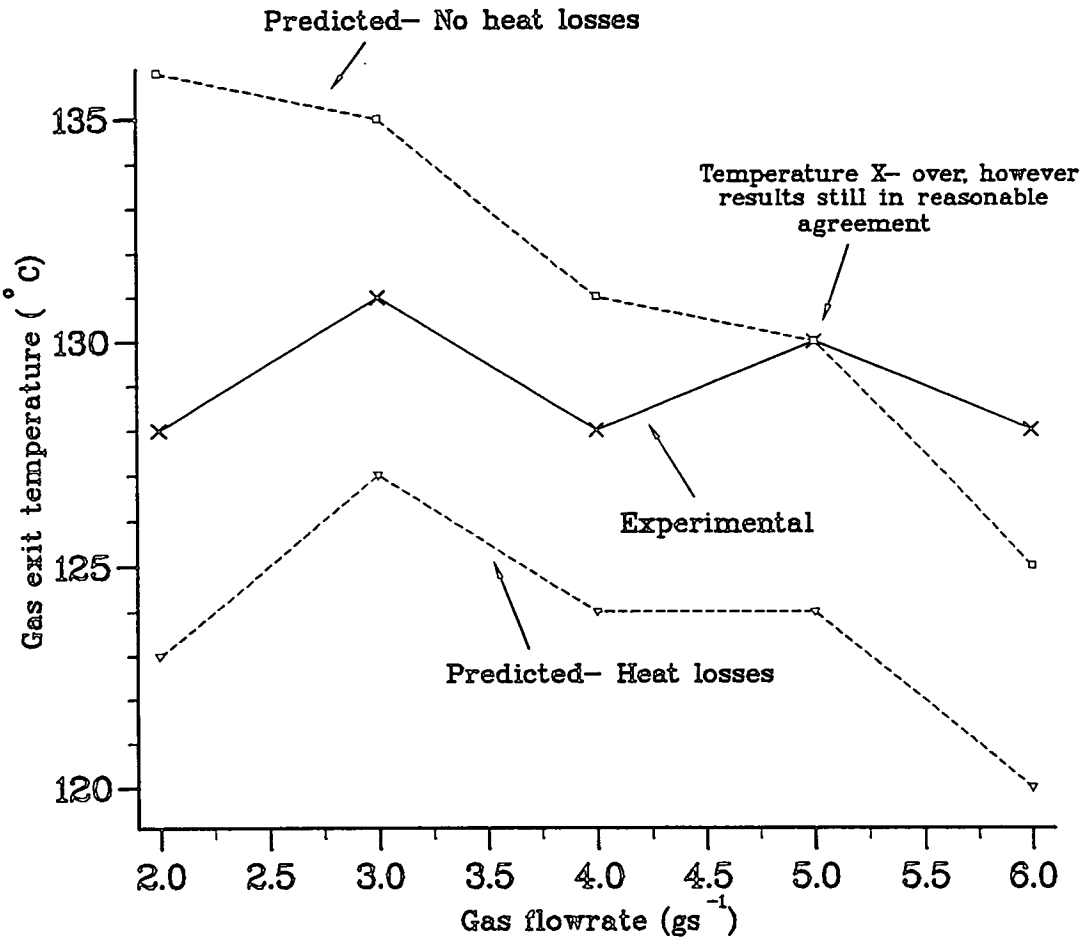

Figure 4.17: Variation of gas exit temperatures for experimental and predicted results, with inlet LiBr concentration 59- 60 %w/w.

The 'ideal' results generally show that the maximum exit temperature was obtained at the lowest flowrate, in this case 2 gs^{-1}, when the exchanger was at its most effective (ϵ at its maximum). However, the effect of introducing heat losses to the system caused the position of the maximum exit temperature to shift to a gas flowrate of 3 gs^{-1}. This agreed with the results for the maximum exit temperatures which were obtained in the reheat experiments carried out in these studies (Section 4.4.3). This confirmed the conclusion that heat losses at 2 gs^{-1}s affected the temperature of the gas stream more than at 3 gs^{-1}s. The predicted decrease above 3 gs^{-1} also confirmed that the heat content of the gas stream increased at a greater rate than $(U.\ A)_O$.

Table 4.29 summaries the data obtained for the reheat absorber by operating it with a wide range of gas flowrates, while keeping the remainder of the parameters constant (see below).

LiBr flowrate	= 4.00 gs^{-1}
Steam flowrate	= 0.20 gs^{-1}
Inlet concentration	= 68 %w/w
Maximum absorption temperature	= 174 °C
Inlet gas temperature	= 80 °C
Assuming U_{losses}	= 1 $Wm^{-2}K^{-1}$;
and A_{losses}	= 0.32 m^2

Figure 4.18 shows how the position of the maximum exit gas temperature was affected by heat losses from the gas side. When exit gas temperatures were determined for the absorber, operating with no heat losses, the maximum exit temperature was obtained at gas flows of 2 gs^{-1}. Below this flowrate, the overall heat transfer coefficient was so low that the heat transferred was also small, despite the stream having a small heat capacity. At higher flowrate, the stream heat capacity increased faster than $(U.\ A)_O$, resulting in a drop in temperature. The position of the maximum exit temperature changed to 4- 5 gs^{-1} when heat losses were introduced to the equations. The drop in the exit temperature was

$\dot{m}_G$ (gs^{-1})	$(UA)_O$ (WK^{-1})	NTU (-)	ε (-)	Q_G (W)	$T_{G_{toP_{IDEAL}}}$ (°C)	$T_{G_{toP_{LOSSES}}}$ (°C)
1.00	1.80	1.80	0.81	76	156	128
2.00	4.14	2.07	0.79	160	160	146
3.00	6.74	2.25	0.77	234	158	148
4.00	9.52	2.38	0.74	308	157	150
5.00	12.44	2.49	0.76	376	155	150
6.00	15.48	2.58	0.75	434	152	148
7.00	18.63	2.66	0.74	494	150	146
8.00	21.86	2.88	0.81	543	148	144

Table 4.29: Effect of varying gas flowrate on the predicted gas exit temperature.

because the rate of heat losses to the surroundings was greater than the heat being transferred to the gas from the inner absorption tube.

4.6 Performance of Two Stage Cycle.

In a heat transformer, a quantity of energy at a moderate temperature level is upgraded to a higher level, at the expense of downgrading a proportion of the heat supply, usually to ambient temperature. In this particular application, the medium grade energy input was supplied to the generator and to the steam source for the reheat absorber, which both operated around 100 °C. The high temperature side of the process was the reheat absorber, which transferred heat to the externally flowing gas stream, resulting in exit gas temperatures up to 150- 160 °C. The low grade energy stream was produced in the condenser where cooling water extracted the heat from the water vapour leaving the generator.

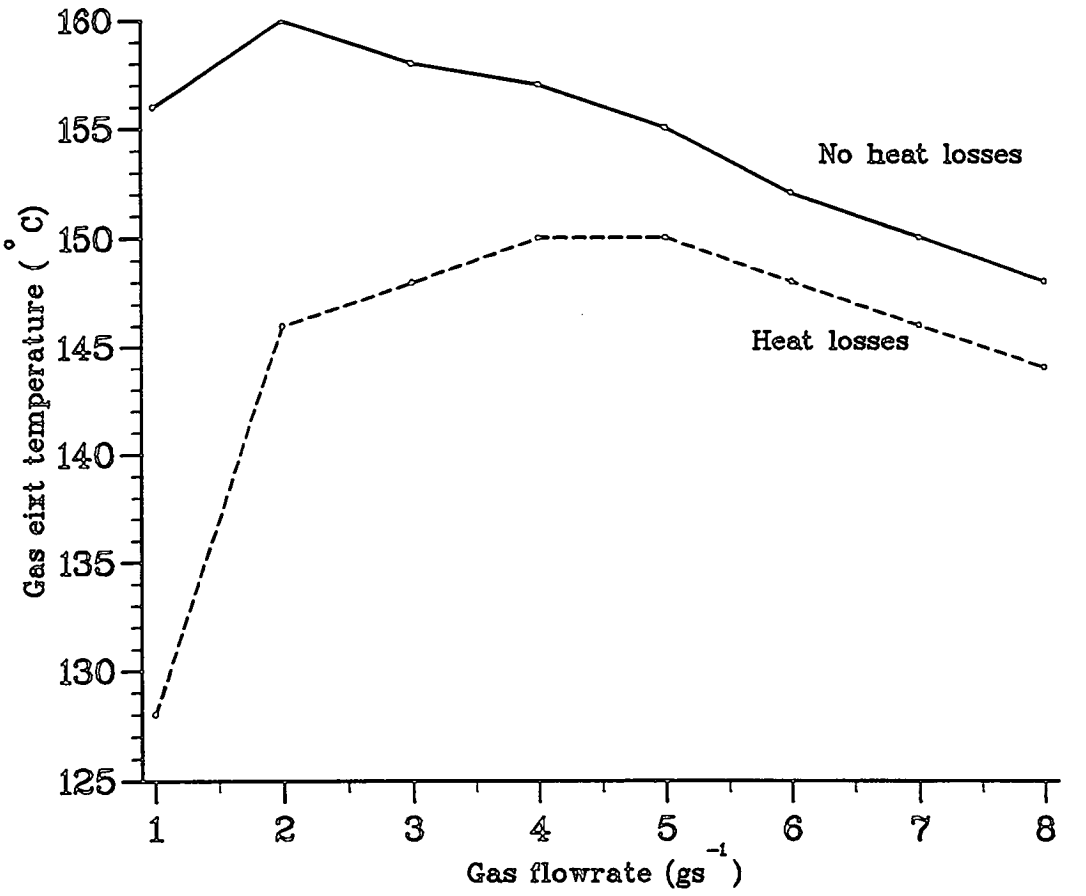

Figure 4.18: Variation of predicted gas exit temperatures for a range of gas flowrates. Inlet LiBr concentration = 68 %w/w.

The heat transformer used in these studies was designed to obtain the maximum exit gas temperature from the reheat absorber. The best results were obtained operating with high absorbent concentrations and low circulation ratio, which resulted in a high temperature of absorption within the inner tube of the reheat column, maximising the rate of heat transfer to the gas stream. Typical gas temperature lifts achieved operating with these conditions were of the order of 50- 70 degC, corresponding to heat outputs of 100- 350 W, depending on the gas flowrate used. The heat input to the generator and steam supply was typically 600 W.

In assessing the performance of the transformer, it should be noted that although electrical power, which is considered a primary energy source, was used on this experimental rig this was solely for convenience. On an industrial unit the energy source could be any low-grade heat available at temperatures up to 100 °C, for example, waste steam which could be extremely cheap.

An interesting feature of this particular absorption heat transformer application was that as the heat source required in the generator could be waste heat, the operating costs of the cycle would be low. Therefore, the efficiency of the cycle was not considered such an important a factor as achieving a high exit temperature from the reheat column. However, in order to upgrade the energy of the waste stream to as high (and useful) an energy level as possible, the capital cost of the system increases. Consequently, the efficiency of the cycle can not be ignored when designing the capacity and operating conditions of the equipment.

4.6.1 Coefficient of Performance.

The coefficient of performance (COP) of the cycle was determined from the useful heat produced (the heat transferred to the gas stream), divided by the heat input. The heat removed in the condenser was ignored as it was of no practical use because the temperature was so low. It can be seen from Tables 4.21, 4.22, 4.23, 4.24, 4.25 and 4.26 that the heat input to the generator and also the steam flow in the absorber remains approximately the same for all the experimental runs, around 600W. The variation in COP can therefore be seen in the heat output from the system, Q_G (Equation 4.16).

$$Q_G = m_G . c_{P_G} . \Delta T_G \tag{4.16}$$

The lowest COPs of approximately 0.15 were obtained when the rig was operated at a gas flow of 2 gs^{-1}, while the COPs obtained when operating at 6 gs^{-1} were as high as 0.5- 0.55. However, the gas temperature lift when operating at a gas flow of 6 gs^{-1} was lower than at 3 gs^{-1}. Therefore, although more heat was being transferred to the gas, the quality of the heat was lower. The corresponding COPs for gas flowrates of 3 gs^{-1} were around 0.2- 0.3, depending on the operating conditions.

As previously mentioned a high absorbent concentration and low circulation ratio were necessary to achieve a high exit gas temperature, thereby improving the system COP ($Q_G \alpha \Delta T_G$). Therefore, for a constant gas flowrate, the lowest COPs coincided with low exit temperatures, because of unfavourable inner tube conditions.

4.6.2 Exergy Balances.

The COP of the transformer, although highest when operating at the highest gas flows, took no account of the quality of energy delivered, only its quantity. A better performance criterion for the reheat column is the exergetic efficiency, ζ. This is the increase in the exergy of the gas stream divided by the exergetic loss of the lithium bromide/ steam mixture, Equations 1.4 and 1.5.

Tables 4.25 and 4.26 show the effect on ζ of increasing the circulation ratio. As the circulation ratio in the reheat column increased, ζ was found to rise to a peak value of around 0.9 and then subsequently decreased. Closer inspection of the extremities showed that at low circulation ratios (high steam flows, while the lithium bromide flow was approximately constant) more heat was required for the generation of steam and also in the generator. A large heat load was necessary in the generator because more steam had to be evaporated in order to restore the absorbent stream to its original concentration. At the other extreme, when the heat transformer was operated with high lithium bromide and low steam flows (very high circulation ratios), there was a drop in the exergetic efficiency of the system. This was because there was insufficient steam in the absorption column to generate a high equilibrium absorption temperature. Consequentially, there was only a small temperature increase in the gas stream, and so the exergy change in the reheat column was small. The highest exergy efficiencies occurred when there was sufficient steam present in the absorber to give a moderate temperature lift in the gas stream of 40- 50 degC and the heat input to the system was around 500 W.

It was therefore concluded that high gas exit temperatures could be achieved only at the expense of increased exergy loss from the lithium bromide/ steam mixture. More heat was input to the system for diminishing returns.

4.7 Experimental Errors.

All of the variables measured in the apparatus were subject to errors of one form or another, e.g instrument precision, system fluctuations, operator error. The precision of various instruments was assessed prior to operation. For example, the thermocouples and metering pumps were calibrated and the accuracy of the readings determined. However, the normal fluctuations experienced when measuring a variable and operator errors could not be predetermined. Therefore, it was necessary to estimate their influence upon results in order to assess the validity of the experimental data.

The errors for derived quantities were estimated using simple error rules based upon a) the addition of the absolute errors of two values when adding/ subtracting; b) the sum of relative errors when multiplying/ dividing two quantities; c) errors in log values estimated from the values obtained at their limits, based on individual component errors.[6]

4.7.1 Instrument Precision.

The main readings taken during an experimental run were the temperatures of the process stream at various places in the equipment, the vacuum in the generator, the stream flowrates and the power inputs to the various heaters.

[6]See Appendix C 'Sample Calculations', Section C.2.1)

Instrument	Error
Temperature readings	± 0.1 °C
Pressure readings	± 0.05 bar (or ± 1 "H_2O)
	[pressure gauge used in single stage experiments]
	± 0.005 bar
	[pressure transducer used in two stage experiments]
Main steam generator:	(To generate vapour for simulation of humid gas streams)
Voltage	± 5 V
Current	± 0.4 A
Power	± 130 W (For a steam flow of 0.6 gs^{-1}- Q = 1.3 kW;
Error in steam flow	± 0.05 gs^{-1} assuming λ_{H_2O} = 2257 Jg^{-1})
Steam flowmeter	± 0.04 gs^{-1}
LiBr generator :	(N.B There were two ammeters in the generator, one for each heater)
Voltage	± 5 V
Current	± 0.01 A
Reheat steam boiler:	
Voltage	± 5 V
Current	± 0.01 A
Power	± 9 W (For a steam flow of 0.16 gs^{-1}- Q = 361 W;
Error in steam flow	± 0.005 gs^{-1} assuming λ_{H_2O} = 2257 Jg^{-1})
Steam flowmeter	± 0.04 gs^{-1}
Rotameter flowrate	± 0.1 $l.min^{-1}$
Metering pump	± 1 % of stroke length
	± 0.04 mls^{-1}
	± 0.06 gs^{-1} (approx, depends on ρ)

Table 4.30: Instrument precision for the AHT.

4.7.2 Temperatures.

The most important readings were the temperatures, which were measured using Type- K thermocouples. In the single stage heat transformer cycle, the temperatures were measured manually using a Comark, a precalibrated electronic thermometer. The two stage cycle involved an automatic data collection system, which stored the measured the temperatures at set intervals and stored to the readings to a file.

The temperatures measured on the Comark were accurate to ± 0.1 degC, as were the readings measured using the PC. However, fluctuations in the temperature readings were experienced during normal operation. This was probably because the lithium bromide solution dripped over the thermowells in the absorber, causing the temperature to rise and fall. As a result the readings were only recorded to ± 1 degC. But, as these results were readily reproduced, it was felt that this level of accuracy was sufficient in assessing the performance of the cycle.

4.7.3 Flowrates.

Lithium Bromide flowrates.

The variation in lithium bromide flowrate was controlled by varying the stroke length of the metering pump, which was measured in increments of 1 %. The resultant accuracy in the stream flowrate was approximately 0.06 gs^{-1}, as determined from the calibration chart.

It should be noted that during the calibration of the metering pump, the liquid flowrate decreased as the vacuum in the generator was increased, for a given pump stroke length. This could have been a result of the non-return valves on the pump head not seating properly, causing a backward suction of liquid at high vacuums. However, as the results obtained were taken at the normal operating vacuum of the generator (0.10 bar) and that the flowrates obtained were reproducible, it was felt that the calibration chart determined was accurate.

Humid Gas Flowrates.

The measurement of the gas flowrate was carried out at ambient temperature using a precalibrated rotameter, which was accurate to $\pm$ 1 l.min^{-1} (0.01 gs^{-1} air). During normal operation, the flowrate was periodically checked to ensure that it did not vary much.

The steam flow, used to generate the humid gas streams, was measured in three ways:

- Flowrate measured on a precalibrated flowmeter. Accuracy $\pm$ 2.5 cc.min^{-1} (0.04 gs^{-1})
- Power consumption of the heaters. Accuracy $\pm$ 0.05 gs^{-1} of steam produced for a power input of 1.3 kW.
- Humidity readings using the humidity probe. Accuracy $\pm$ 3 %RH (including fluctuations) [$\equiv$ 0.01 gs^{-1}, for an inlet humidity of 0.25 g-$_{H_2O}$ (g-$_{dry\ air}$)$^{-1}$).

It should be noted that a lot of problems were experienced with the humidity probe. However, when it did operate well, the readings obtained did fluctuate by a few percent. The readings obtained for the steam flowrate were therefore an average of all three measurements, in order to reduce the likelihood of a large error.

In addition, the amount of water absorbed into the absorbent stream was measured in two ways- condensate collection and direct humidity measurement. These were averaged, again to reduce the errors.

Reheat Steam Flowrates.

The steam flowrate in the reheat column was measured using two methods- power consumption in the heater (taking into account heat losses) and the input water flowrate to the boiler. The readings for both measurement techniques were consistent and in close agreement to each other, therefore an average reading was taken for the reheat steam flow.

4.7.4 Other Measurements.

The other measurements taken during an experimental runs were the power consumption of the lithium bromide generator and the pressure in the generator. The error in the power consumption in the generator was $\pm$ 13 W, which was typically 4 % of the heat load to the generator. Of great importance in determining the concentration of the strong lithium bromide solution was the pressure, which was accurate to $\pm$ 0.005 bar and temperature, accurate to $\pm$ 1

degC, of the generator. The resultant accuracy in the lithium bromide concentration estimated from the VLE chart was ± 1 %w/w,

Although cooling water was used to remove heat from the condenser, the flow of water was not accurately recorded. (The project was principally concerned with the high temperature side of the process and not the low, ambient temperature side).

4.8 Conclusions.

Extensive experimental programmes were carried out using, first of all, a single stage absorption heat transformer cycle, followed by a double stage operation. Considerable data were obtained from both cycles, and these were used to establish the best operating conditions necessary to achieve the highest gas exit temperature from the absorber.

4.8.1 Single Stage Heat Transformer.

The single stage absorption cycle was initially constructed to simultaneously dehumidify and reheat a humid gas stream, by direct contact with a concentrated lithium bromide solution. It became evident that it was not possible to achieve both objectives in one stage.

In order to dehumidify the gas stream, countercurrent operation was found to be superior to cocurrent operation, as the 'driest' gas came in contact with the most concentrated absorbent solution at the top of the absorption column.

The highest gas exit temperatures were achieved when operating in cocurrent mode. At the top of the column there was a rapid increase in the temperature of both process streams as the water from the gas was absorbed into the lithium bromide solution. The streams quickly reached thermal and mass equilibrium, before exiting at a higher temperature. A linear relationship was found to exist between the gas exit temperature and absorbent concentration, which could be increased to 70 %w/w before encountering crystallisation problems.

4.8.2 Two Stage Heat Transformer.

Following the experience of using the single stage absorber, it was decided to separate the process into two stages- a dehumidification stage, followed by a reheating stage. Results from the dehumidification process indicate that the exit water vapour partial pressure can be controlled by maintaining a high absorbent concentration and low temperature at the top of the column. A heat exchanger, using cooling water to remove the heat of absorption from the process streams, resulted in a water vapour exit partial pressure of 0.04 bar being obtained.

The gas stream flowed in an annulus, countercurrent to a hot absorbent mixture of lithium bromide/ steam (in the inner pipe). The heat which was released by the absorption process was transferred to the gas stream. Exit gas temperatures in the range 150- 160 °C were attainable in the reheat column when operating with a lithium bromide solution of 68 %w/w. A design method for predicting

the gas exit temperature from known inlet conditions, was also proposed based upon experimental findings.

4.8.3 Future Work and Developments.

The experiments undertaken in this project provided a comprehensive study of the potential benefit of heat transformers for dehumidifying and reheating humid gas streams using aqueous lithium bromide as the absorbent working fluid. Future work would involve the application of new working fluids to further extend the results obtained here. Of greatest significance is the improvement in the maximum exit temperature possible in a single, or even double, stage absorption cycle. The upgrading of medium grade, waste energy to higher levels extends the uses to which absorption cycles can be applied.

The current application could be modified in several ways to give a more integrated cycle. As the maximum inlet absorbent concentration in the dehumidification column was less than that used in the reheat column, there would be a conflict when trying to operate both absorption stage from a single absorbent feed source. It was therefore proposed to use the absorbent solution leaving the reheat stage to dehumidify the humid gas streams in the direct contact absorber. However, the temperature of the solution would be too high to provide any reasonable dehumidification of the gas stream. It would therefore be necessary to first of all cool this absorbent stream prior to entry to the dehumidification column. The strong lithium bromide solution leaving the generator could be exchanged with this stream, effectively preheating the concentrated lithium bromide solution fed to the reheat column, while also cooling the weaker solution going to the dehumidification column.

Another change to the current operation would be the pumping of the condensate to the steam generator, attached to the reheat column. Therefore, should any lithium bromide carry over into the condensate, it would be retained in the cycle and not release to the surroundings. These proposed modifications are illustrated in Figure 4.19.

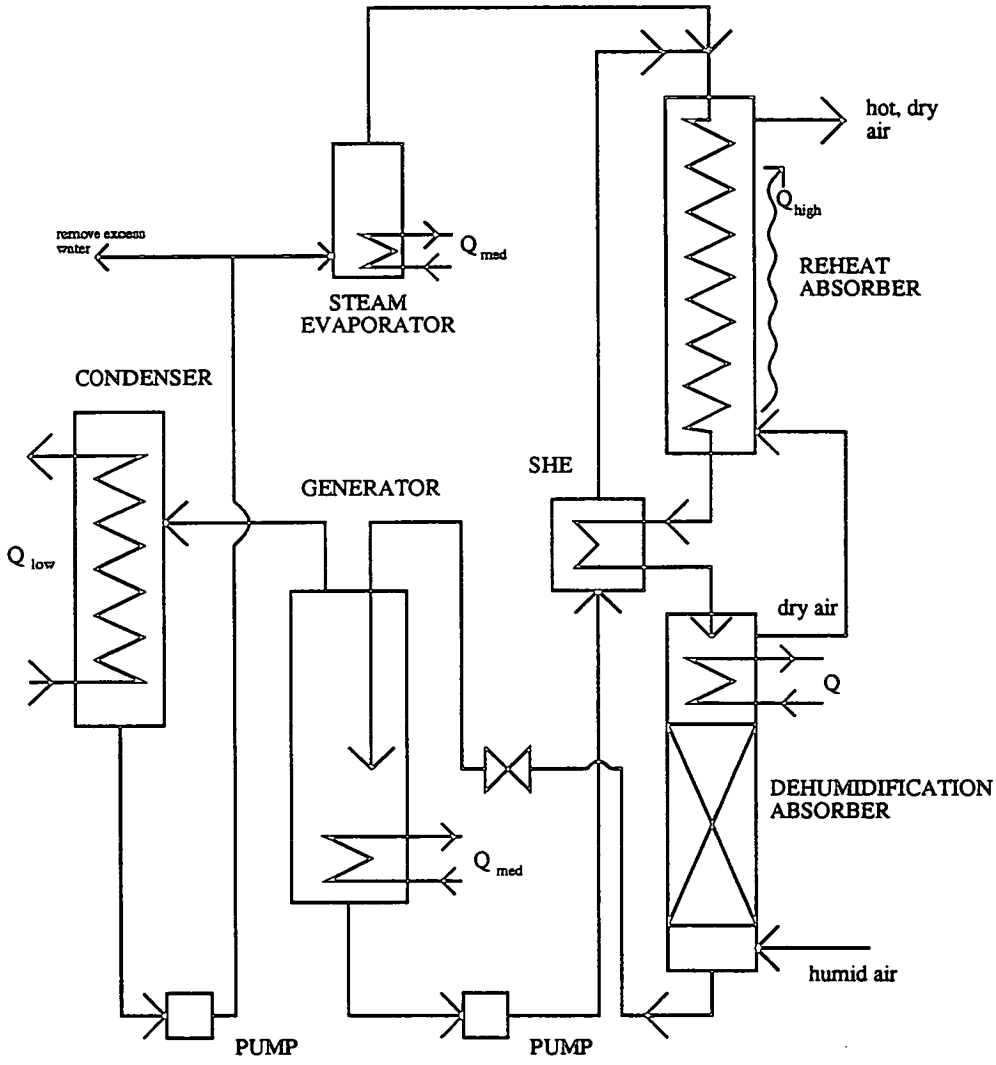

Figure 4.19: Proposed modification to the two stage absorption heat transformer cycle.

Chapter 5

Computer Modelling.

5.1 Introduction.

Simulation models of the experimental absorption column were developed to provide an insight into the absorption process. A similar model was developed by Manole [54] which detailed the temperature profiles and the heat and mass fluxes within a falling film absorber, operating with ammonia/ water. Another computer model written at the University of Lund [1] looked at different absorption cycle configurations, treating the components as 'black boxes', and evaluated the performance of the cycles operating under different conditions. The working fluid pairs examined using this model were water/ sodium hydroxide or water/ lithium bromide.

The aims of this particular study were to investigate the effects of interfacial conditions upon the rate of absorption and the resultant temperature increase in the refrigerant and absorbent streams. The absorption fluid working pair used was water/ lithium bromide, for which physical data was readily available ([24], [165]).

Results from the simulations are represented graphically in the form of temperature profiles for each of the process streams, as well as a profile for the interfacial temperature. In some cases mass flow profiles for the refrigerant stream have been presented (see Sections 5.5, 5.7 and 5.8). The results obtained were also compared to experimental data collected on the test facility (Chapter 4, 'Experimental Studies') so as to validate the model.

5.2 Model Development.

The simulation programs were written in the turbo-C programming language. The first program to be written investigated the simple cocurrent absorption of steam into a concentrated lithium bromide solution. As the vapour was absorbed into the liquid stream there was a release of heat, which caused the temperature of both the streams to increase. The absorption process was extremely rapid, with a sharp increase in temperature of both streams in the upper (inlet) region of the column. This finding was confirmed from early simulation runs (see Section 5.5). It was also shown that the streams leaving the column were in thermal and mass equilibrium.

After establishing this basic absorption model, the principles were extended to include simultaneous heat removal to an externally flowing gas stream. The program was written so that the external gas stream could flow either co- or counter- current to the hot absorbent/ refrigerant mixture. Each variant of the program produced a similar gas temperature profile because the temperature of the hot absorbent stream remained approximately constant throughout the length of the column (see Figure 5.5).

Lastly, the model was used for the purpose of investigating the dehumidification of humid gas streams by direct contact with concentrated liquid absorbent solutions. Two modes of operation were considered, namely the co- or counter-current flow of the humid gas and absorbent streams.

5.2.1 Absorption Column Representation.

The absorption column used in the simulation model was based upon the experimental apparatus used in the project. The length of the absorber was 800mm, with an internal diameter of 25mm. In order to provide an accurate representation of the temperature and flow profiles, it was necessary to divide the column length into cross- sectional slices of equal thickness, Figure 5.1a). The thickness of each slice was 0.1mm, which gives a total of 8000 slices for the column. Each slice was split into three sections, as shown in Figure 5.1b) for cocurrent operation. These were namely refrigerant vapour phase, liquid phase and the interface, which was the boundary between the phases.

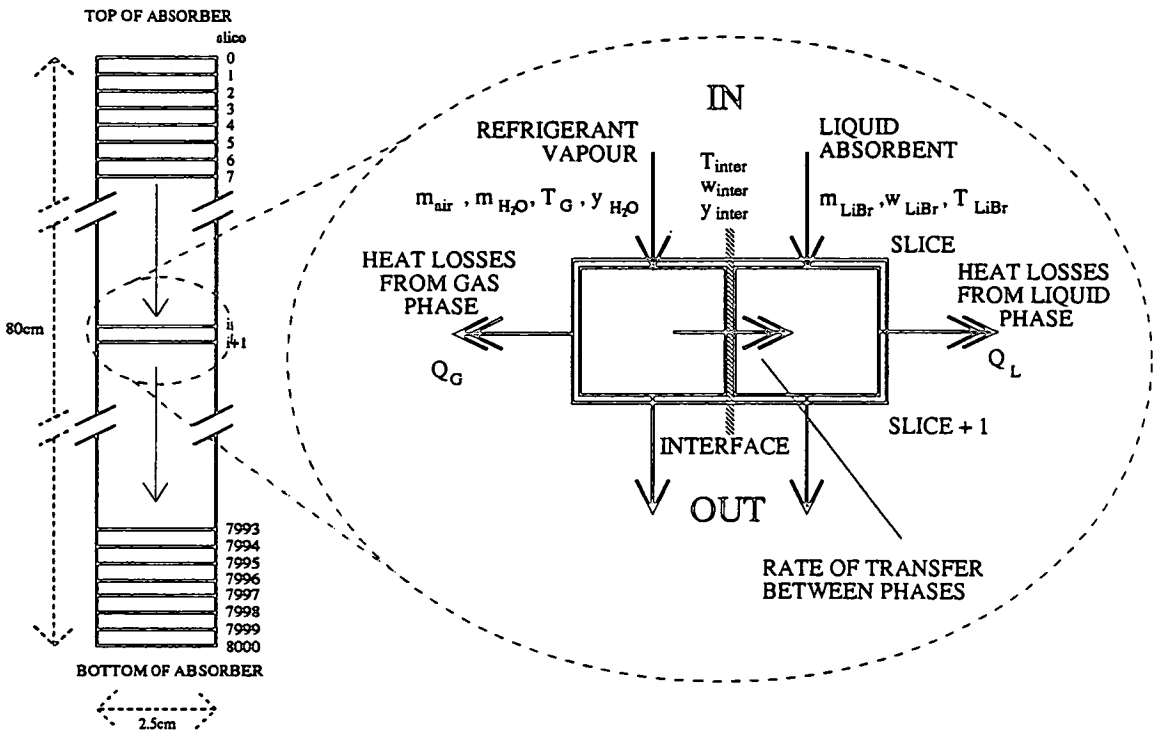

Figure 5.1: a) Overall column representation b) Representation of individual slice for cocurrent absorption.

Figure 5.2 is a schematic representation of the absorption process, showing how the partial pressure of the water vapour in the bulk gas phase was greater than the interfacial pressure, ensuring continued transfer of the refrigerant into the liquid phase. The interfacial concentration was higher in refrigerant than in the bulk absorbent (and was therefore a weaker solution). The absorbed refrigerant was thus transferred to the bulk liquid absorbent down a concentration gradient. As well as mass transfer between the phases, heat transfer also occurred. Assuming that the interface was in thermal and mass equilibrium, it was possible to calculate the interfacial temperature from the interfacial pressure and concentration using the equation provided in the paper by Brunk [24]. Using the interfacial temperature, the exit temperatures of the bulk gas and liquid were then calculated.

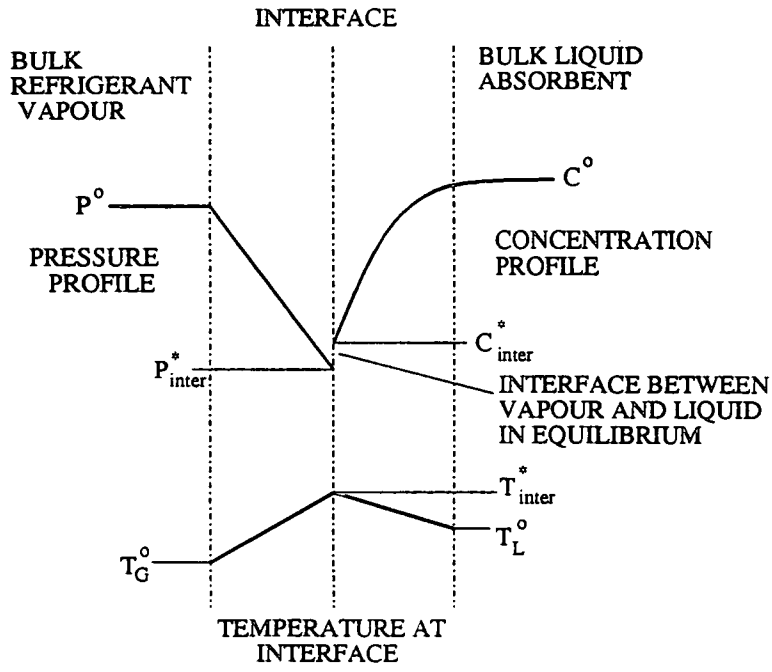

Figure 5.2: Refrigerant and absorbent conditions at interface.

The computation for each model was from the top of the column to the bottom. For the models where the gas streams flowed countercurrent to absorbent stream (i.e absorption with countercurrent heat removal; countercurrent dehumidification), it was necessary to assume a set of exit gas conditions at the top of the column. In such cases, it was first of all necessary to estimate conditions for the gas streams at the top of the column and then continue with the simulation process as normal. At the end of the run, when the bottom of the column was reached, the stream exit conditions were compared to the initial values. If the outlet values were within a specified tolerance the run was complete, otherwise the estimated exit conditions of the stream, at the top of the column, were adjusted and the run repeated.

In order to calculate the exit conditions from a slice (temperatures and flows) it was necessary to solve a series of equations based upon the mass and heat transfer in each of the phases in addition to an overall energy balance for each slice. When the heat and mass balances converged to a specified tolerance the

model progressed to the next slice and the procedure repeated. Progression through the column continued until profiles had been completed for all 8000 slices.

5.2.2 Model Basis.

Each of the models was based upon well established heat and mass transfer relationships. The heat and mass transfer coefficients for the gas and liquid streams were obtained from empirical equations proposed by Treybal [215]. The paper was an investigation of the adiabatic absorption of a solute from a carrier gas into an liquid absorbent solution. In an attempt to make the computational stages of the model simpler and less time consuming, several assumptions were made:

- The amount of refrigerant transferred to the liquid absorbent was chosen as the independent variable.
- There was no axial dispersion within either the gas or liquid phases. The transfer of refrigerant was assumed to be solely perpendicular to the bulk flow of the streams.
- The gas and liquid phases were each well mixed radially and thus the bulk conditions were representative of the whole phase.
- The column packing was completely irrigated, with no stagnant zones.
- There was thermal and mass equilibrium at the interfacial boundary between the gas and liquid phases.

The procedure used to determine the exit conditions from a slice, given the inlet conditions, initially involved the determination of the exit flows. This was achieved by simply varying the flow of each stream by the amount of transferred (water) vapour. The interfacial pressure and concentration were then calculated from a knowledge of the mass transfer rates in each phase, based upon Equations 5.7 and 5.8.

As the local vapour and liquid at the interface were assumed to be in equilibrium it was possible to determine the interfacial temperature, using the equations given by Brunk [24], Equations 5.1, 5.2, 5.3 and 5.4 (N.B All the constant values are contained in the paper). The interfacial temperature was dependent upon the both the interfacial pressure and concentration. Equation 5.1 was used to calculate a pseudo temperature (T') which was dependent on the pressure. Next the concentration terms (α and β) were calculated. Finally, the interfacial temperature was determined by combining each of the terms (T', α and β, Equation 5.4.

$$T' = \frac{k_1 - [(4.k_2.(log_{10}(14.5038.P) - k_0)) + k_1^2)]^{1/2}}{2.(log_{10}(14.5038.P) - k_0)} - 491.67 \qquad (5.1)$$

$$\alpha = \Sigma_{i=0}^{3}\Sigma_{j=0}^{3} a_{ij}.x^j \qquad (5.2)$$

$$\beta = \Sigma_{i=0}^{3}\Sigma_{j=0}^{3} b_{ij}.x^j \qquad (5.3)$$

$$T = \alpha.\frac{T'}{1.8} + \beta \qquad (5.4)$$

The newly calculated interfacial temperature was then used to determine the rate of heat transfer within in each phase. It was then possible to determine the exit temperature of the liquid and gas streams from a knowledge of the heat transferred within each phase. The effects of heat losses to the surroundings were also included in the model. Finally, it was then necessary to carry out an overall heat balance for the whole slice, using Equation 5.5. If the heat balance was not within a specified tolerance, as in Equation 5.6, it was necessary to adjust the amount of water transferred and repeat the above procedure. This was repeated until the specified tolerance was met, at which point, the height was incremented and the same steps repeated for the next slice.

$$(m_{G_{in}}.h_{G_{in}}) + (m_{LiBr_{in}}.h_{L_{in}}) = (m_{G_{out}}.h_{G_{out}}) + (m_{LiBr_{out}}.h_{L_{out}}) + Q_{losses} \quad (5.5)$$

$$|HEAT\ IN - HEAT\ OUT| < tolerance \quad (5.6)$$

The core of the problem, which was essentially the same for each of the programs, is itemised in below for the absorption of steam into a concentrated lithium bromide solution with simultaneous heat removal to an externally flowing fluid. A detailed flowsheet of this program is shown in Figure 5.3. When considering the simple case of the absorption of steam into the absorbent solution, the transfer of heat to the externally flowing fluid was removed.

Algorithm for absorption of steam into lithium bromide, with simultaneous heat removal to an external fluid.

Step 1: *Set initial amount of refrigerant to be transferred.*

Step 2: *Estimate outlet flows of steam and lithium bromide.*

Step 3: *Initial guess at the vapour pressure above the absorbent solution at the interface.*

Step 4: *Calculate mass transfer coefficients for both refrigerant (steam) and absorbent (lithium bromide) streams.*

Step 5: *Use mass transfer equations to find the interfacial pressure and concentration.*

Step 6: *Repeat Step 4 & 5 until convergence of the "interfacial pressure".*

Step 7: *Calculate heat transfer coefficients for both streams.*

Step 8: *Determine the interfacial temperature, assuming that the interface is at equilibrium-* $T_{interface} = fn(p_{interface}, w_{interface})$.

Step 9: *Calculate the rate of heat transfer to the external fluid, based on the temperatures of the absorption fluid pair, also including heat losses to the surroundings* ($U_{losses} = 3Wm^{-2}K^{-1}$). *The overall heat transfer coefficient was determined using an empirical equation based upon the flowrate of the external gas stream.*

Step 10: *Use interfacial temperature and external heat transfer to calculate outlet temperatures of both gas and liquid phases.*

Step 11: *Convergence of the interfacial temperature.*

Step 12: *Perform an overall enthalpy balance on the slice.*

Step 13: *Vary amount vapour absorbed if heat into/ out of slice is not equal to the heat out. Repeat procedure*

Step 14: *Write results to file. Increment height- continue down through column.*

The individual mass transfer equations used in the computer program are given below, Equation 5.7 for the gas phase and Equation 5.8 for the liquid phase. It should be noted that the transfer of water from the gas phase was taken as being positive. In addition, as the paper by Treybal was written in 1969 all the variables used were in imperial units and so it was necessary to convert all the parameters to SI units. The mass transfer coefficients used in the two mass transfer equations were based upon Colburn- Drew relations, Equations 5.9 and 5.10, for the gas and liquid phases respectively.

$$Moles\ transferred = F_G.ln(\frac{1-y_{inter}}{1-y_{H_2O}}).a_{inter}.\delta z \tag{5.7}$$

$$Moles\ transferred = -F_L.ln(\frac{1-x_{H_2O}}{1-x_{inter}}).a_{inter}.\delta z \tag{5.8}$$

Specific interfacial surface, a_{inter} [$ft^2\ ft^{-3}$]; Slice thickness, δz [ft].

$$F_G = \frac{1.195.G}{Sc_G^{2/3}}(\frac{d_s.G'}{\mu_G(1-\epsilon_{wet})})^{-0.36} \tag{5.9}$$

Total gas mass flow, G [(lb.mol) $hr^{-1}ft^{-2}$]; Gas mass velocity, G' [lb $hr^{-1}ft^{-2}$]; Gas Schmidt number, Sc_G [-]; Equivalent spherical diameter of packing, d_s [ft]; Gas viscosity, μ_G [lb ft^{-1} hr^{-1}; Wetted voidage, ϵ_{wet} [-].

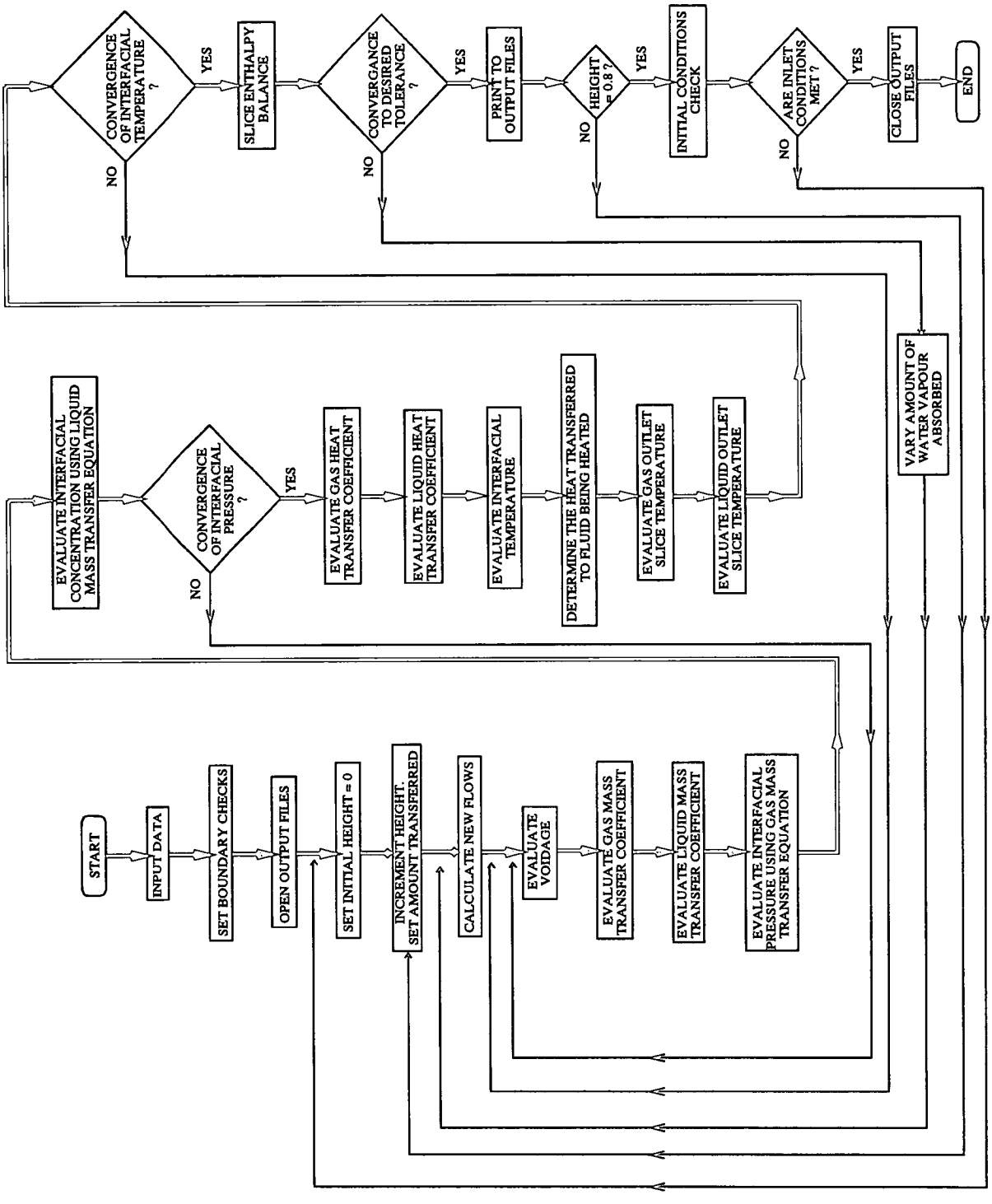

Figure 5.3: Flowsheet for absorption of steam into a concentrated LiBr solution, with countercurrent heat removal.

$$F_L = \frac{25.1.D_L.\rho_L}{d_s.M_L} .(\frac{d_s.L'}{\mu_L})^{0.45}.Sc_L^{0.5} \quad (5.10)$$

Liquid diffusivity, D_L [$ft^2\ hr^{-1}$]; Liquid density, ρ_L [lb ft^{-3}]; Average molecular weight, M_L [lb $(lb.mol)^{-1}$]; Liquid viscosity, μ_L [lb $ft^{-1}\ hr^{-1}$]; Schmidt number, Sc_G [-];

5.2.3 Data Sources.

Most of the physical properties of aqueous lithium bromide solutions were taken from work done by M^{c}Neely [172], Brunk [24] and Liu [165]. The heat capacity, enthalpy, thermal conductivity and vapour pressure were all determined from equations provided by Brunk, while the liquid solution density and viscosity were determined from Liu. The correlation for the lithium bromide heat capacity was only valid for temperatures up to 100°C. Above this temperature, the correlation behaved oddly. Therefore, it was necessary to assume a constant value for the stream heat capacity above this temperature based upon the concentration of the solution.

However, data on the diffusivity of the concentrated lithium bromide solutions was not readily available. Initially, a constant value for the liquid diffusivity of $3x10^{-9}m^2s^{-1}$ was used, which had been suggested by Le Goff (in a private communication). Later, a concentration dependent relationship (based on a temperature of 25°C) was used, Equation 5.11. In conjunction with this equation, the effects of temperature variation were also considered, Equation 5.12. Both of the relationships were taken from work carried out by Gierow [129]. Indeed the differences in the diffusivities obtained using these two methods was not significant.

The diffusivity was only used to calculate the liquid mass transfer coefficient, Equation 5.10. This equation was only dependent upon the square root of the diffusivity, thereby reducing any effects of the approximations used in determining the liquid solution diffusivity. It should also be noted that the liquid mass transfer coefficient (12- 16 (lb.mol) hr^{-1} ft^{-2}) was four to eight times that of the gas mass transfer coefficient (2- 3 (lb.mol) hr^{-1} ft^{-2}). Thus the liquid coefficient was not limiting with respect to the mass transfer of refrigerant vapour into the absorbent.

$$D = [(-0.0713.w) + 5.2665].10^{-7} \qquad [cm^2 s^{-1}] \qquad (5.11)$$

$$\frac{D_1.\mu_1}{T_1} = \frac{D_2.\mu_2}{T_2} \qquad (5.12)$$

Finally, the properties of water vapour and air were taken from 'Perry', the Chemical Engineers' Handbook [186] and also Harwoods' Steam Tables [139]. The diffusivity of the water- air mixture was calculated from a dimensional equation[1] provided in 'Perry' (p3.285), Equation 5.13, which predicts the diffusivity to within ±5 - 10%, based upon the atomic diffusion volumes of each component. The mixture enthalpy and heat capacity were also determined using the pure component properties and combining them by taken the weighted average of the mixture (assumed to be 79% N_2 and 21%O_2)

$$D = \frac{10^{-3}.T^{1.75}.[(M_A + M_B)/(M_A.M_B)]^{0.5}}{P.[(\Sigma v)_A^{1/3} + (\Sigma v)_B^{1/3}]^2} \qquad (5.13)$$

T [K]; P [atm]; D [cm^2s^{-1}]; M is the molecular weight and Σ v the atomic diffusion volume. Finally, the wetted voidage of the packed column was calculated using Equation 5.14, where h_t refers to the total liquid holdup in the column and ϵ_{dry} the dry column voidage. The dry voidage was determined from experiment, whilst the total holdup was calculated from Equations 5.15 and

[1] From papers by: Fuller, E. N and Giddings, J. C. *J. Gas Chromatography*, **3**, 222 (1965). Fuller, E. N et al. *Ind. Eng. Chem.*, **58**(5), 18 (1966)

5.16, which were taken from a paper by Shulman et al. [66]. The constants (α, γ and θ) are all empirical constants and are dependent on the packing used in the column. It should be noted that Fenske helices were not included in the table of values and so the values associated with Raschig rings of a similar size were used, giving values of 2.5x10^{-5}, 0.965 and 0.376 (see paper), for each of the constants respectively.

$$\epsilon_{wet} = \epsilon_{dry} - h_t \tag{5.14}$$

$$\beta = \gamma . d_s^{\theta} \tag{5.15}$$

$$h_t = \frac{\alpha . L^{\beta}}{d_s^2} \tag{5.16}$$

Equivalent spherical diameter of packing, d_s [ft]

5.3 Cocurrent Absorption Model.

5.3.1 Absorption of Steam into Lithium Bromide.

The first program to be written was used to investigate the absorption of steam into concentrated lithium bromide solution. The operating conditions which were input were:

- Steam flowrate (gs^{-1}).
- Steam inlet temperature (°C).
- Lithium bromide inlet concentration (%w/w).
- Lithium bromide inlet flowrate (gs^{-1}).

- Lithium bromide inlet temperature (°C).
- Partial pressure of inerts present in absorption tube (bar).

All the data was fed into the program automatically, via data files, and the results obtained stored in a similar manner. The main operating variables were the steam and lithium bromide flowrates and the lithium bromide concentration. Each of these variables was investigated in turn and their resultant effects on the performance of the absorption column monitored (see Section 5.5). A further development to the program allowed a range of operating conditions to be input which resulted in an array of results being generated and thus provided a more extensive investigation of the absorber performance. The inlet temperature of each stream was also varied but the effects were secondary. Further to this, an investigation of the presence of inerts within the absorption column was also carried out. The inerts would effectively lower the steam partial pressure, and hence lower the maximum temperature achievable within the column for the given inlet absorbent concentration.

5.3.2 Cocurrent Absorption with External Heat Removal.

In addition to the inlet conditions required for the simple absorption program, it was also necessary to include data for the external stream being heated. The additional data which was input was:

- Gas flowrate (gs^{-1}).
- Gas inlet temperature (°C).

- Mode of operation- either co- or counter- current heat removal

In the countercurrent heat removal case, where the external gas stream flowed countercurrent to the absorbent/ refrigerant mixture, it was necessary to estimate exit temperature of the gas stream, at the top of the absorber. This was achieved by multiplying the inlet gas stream temperature by a constant, determined from the Equations 5.17, which was based upon a correlation relating actual experimental exit temperatures with the inlet temperatures of gas streams at a flowrate of $3gs^{-1}$. Next, the constant was refined to take into account the variation of the gas exit temperature with the stream flowrate, Equation 5.18, which was again based on experimental observations.

$$k' = (0.000168.T_{G_{in}}) + 1.005201; \tag{5.17}$$

$$k = k'.e^{\dot{m}_G}.e^3 \tag{5.18}$$

In order to evaluate the rate of heat transfer to the external gas accurately, it was necessary to know the overall heat transfer coefficient (HTC). This was determined by first of all correlating experimental values for the gas side heat transfer coefficient with the external gas flow. The experiment involved the heating of a gas stream using an inner heat source of known flowrate and inlet and outlet temperatures (see Chapter 4, Section 4.4.1 'Heat Transfer Characteristics of the Reheat Absorber' for details), from which accurate data could be obtained for the gas side heat transfer coefficient. The correlation obtained, Equation 5.19, expresses the gas side heat transfer coefficient as a function of the gas side Reynolds number, Re, and Prandtl number, Pr. Equation 5.19 was expressed in a form similar to the correlation quoted by

Sieder and Tate for turbulent flow in a plain tube (see Chapter 4, Section 4.4.1).

$$Nu = 0.41.\ Re^{0.78} \tag{5.19}$$

In order to determine the overall heat transfer coefficient it was also necessary to estimate the liquid side heat transfer coefficient and also the heat resistance through the tube wall, which were assumed to be small in comparison to the gas side heat resistance. It was therefore assumed that the liquid heat transfer coefficient should be 3 $kWm^{-2}K^{-1}$ and that the wall resistance was negligible (This assumption was verified within the program, where the liquid HTC was estimated from an empirical equation to range between 2.2- 3.5 $kWm^{-2}K^{-1}$). In fact the inside HTC could be larger because of the turbulence promoter inserted inside the tube to aid heat transfer, again reducing the heat transfer resistances on the absorption side. Results obtained indicate that the gas side resistance was dominant and accounted for about 95% of the total resistance.

The overall heat balance for a slice was similar to the simple absorption program except that, instead of heat losses to the surroundings from the absorption tube, heat was transferred to the gas stream, Equations 5.20 and 5.21.

$$\textit{Change in heat load in inner absorption tube} = \textit{Heat to gas stream} \tag{5.20}$$

$$[(m.h)_{LiBr}+(m.\lambda)_{RS}]_{i+1}-[(m.h)_{LiBr}+(m.\lambda)_{RS}]_i = (m.c_P)_G.(T_i-T_{i+1}) \tag{5.21}$$

The Section 5.6 discusses the results obtained for this particular program and compares the simulated profiles with experimental data. As with the simple absorption program, the effect of inerts on the column performance was also investigated.

5.3.3 Cocurrent Dehumidification of a Humid Gas Stream.

Another variant of the model was the dehumidification of a humid gas stream. This particular program investigated the cocurrent flow of humid gas and concentrated lithium bromide streams, which was essentially the same as that described in section 5.3.1. The variables are once again the same, with the addition of the gas flowrate.

The humidities of the gas stream which were considered ranged between 0.10-0.25 g-$_{H_2O}$ (g-$_{dry\ air}$)$^{-1}$. This particular range was typical of an industrial spray dryer outlet streams. Again, the procedure for calculating results was the same as previously discussed and included the loss of heat to the surroundings.

5.4 Countercurrent Dehumidification Model.

In this particular model the humid gas stream flowed up through the absorption column, while the concentrated lithium bromide solution flowed by gravity down through the column. As previously mentioned, it was necessary to estimate the exit conditions of the gas stream at the top of the absorber and then proceed with the absorption process, working from the top of the column to the bottom. At the bottom, the gas conditions were then compared to the initial conditions input. If the flowrate of the water vapour or the calculated temperature were not within a specified tolerance they were varied and the absorption process was repeated with the new exit conditions.

5.4.1 Rough Profile.

In order to run this particular program, it was first of all necessary to determine the exit stream conditions of both the gas stream, at the top of the absorber, and the lithium bromide, at the bottom of the column. This was achieved by initially calculating overall heat and mass balances for the column, using the following assumptions:

- The interfacial pressure at the top of the column was determined from the VLE equation, using the inlet lithium bromide concentration and temperature to find the corresponding vapour pressure. It was then assumed that the exit water vapour and interfacial pressures were not in equilibrium. The water vapour partial pressure was then estimated from:

  $$(\text{Partial pressure})_{H_2O} = \text{c.} \quad (\text{Interfacial vapour pressure})_{H_2O}$$

  In this equation 'c' was a factor which varied depending on the overall heat balance of the column. Initially, the factor was set to 1.1.

- The amount of water absorbed into the lithium bromide solution was equal to the difference between the inlet and outlet water vapour flows in the gas stream. Therefore, the exit lithium bromide stream conditions were determined once the exit water vapour flowrate (and amount of absorbed vapour) had be calculated.

- Finally, the lithium bromide exit temperature was assumed to be equal to the interfacial temperature, at the bottom of the absorber. Where the temperature was determined from the interfacial pressure, assumed equal to the gas inlet partial pressure, and the interfacial concentration, equal to the exit lithium bromide concentration.

Once the mass balance for the absorber had been determined, it was possible to calculate the overall heat balance for the system. The equation for the heat balance was rearranged in terms of the exit gas temperature, which was still unknown. After the exit gas temperature had been estimated, it was necessary to confirm that the result was valid. If for example, the final exit gas temperature was less than zero or else greater than the exit absorbent temperature, the amount of water transferred was varied and the procedure repeated.

The next stage in this procedure, involved the subdivision of the column into eight equal sections. Heat and mass balances for each of the sections were then determined, assuming that the amount of water absorbed in each stage was the same. Each section was evaluated in succession, starting at the top and working down. As, the top temperatures and the flowrates of each stream were known it was only necessary to find the exit temperatures.

First of all, the exit interfacial temperature was calculated from a knowledge of the exit water vapour partial pressure and exit lithium bromide concentration for the slice. The exit temperature of each stream was then estimated by taking a weighted average of the inlet stream and the interfacial temperatures. The actual weightings were not important as accurate exit temperatures were determined for each stream at each cross sectional slice within the model. Initially the weighting was 60:40 (T_{inter}: T_G), for the gas stream and 95:5 (T_{inter}: T_{LiBr}), for the liquid phase. The determination of the exit gas temperature was weighted towards the inlet gas temperature because of the low heat transfer coefficient (HTC) between the gas and the interface. Similarly, the exit LiBr temperature was set almost equal to the interfacial temperature because the HTC between the liquid and interface was large.

The program varied the factor controlling the gas temperature. However, if this factor was greater than one or fell below zero then the value was reset and the liquid 'fudge factor' varied. This procedure was repeated until the heat balance had converged to a specified tolerance. The algorithm used for estimating the gas and liquid stream flows and temperatures in the absorber is detailed below.

Algorithm for estimating rough exit flows and temperatures for the countercurrent dehumidification of a humid gas stream.

Step 1: *Find interfacial vapour pressure above the concentrated lithium bromide solution at the top of the absorber.*

$$p_{interface} = fn(\ T_{LiBr_{top}},\ w_{LiBr_{top}}).$$

Step 2: *Set exit gas partial pressure, at top of column, equal to interfacial vapour pressure multipied by a factor, which was used because the streams were not in equilibrium with each other.*

Step 3: *Estimate the amount of water vapour transferred from the difference between the inlet and estimated exit flowrates.*

Step 4: *Find outlet lithium bromide flowrate and concentration.*

Step 5: *Assume that the interfacial vapour pressure, at the bottom of the absorber, was in equilibrium with inlet water vapour partial pressure. Similarly, the interfacial concentration was assumed to be equal to the exit lithium bromide concentration. Hence, find the interfacial temperature and set it equal to the exit temperature of the lithium bromide stream.*

Step 6: *Perform an overall energy balance on the column and find the exit gas temperature.*

Step 7: *Check validity of estimated temperature, vary the amount of water absorbed into the absorbent stream if necessary (Repeating Steps 2-6). Else continue...*

Step 9: *Split column into eight sections.*

Step 8: *Assume equal absorption of water vapour in each section. Determine mass flowrates of each stream through the column.*

Step 9: *For each section, perform a heat balance. Vary gas exit temperature as necessary until the difference in the heat transferred between phases is less than a specified tolerance.*

Step 10: *Progress to next section, setting the inlet conditions equal to exit conditions of previous section.*

Step 11: *After establishing the rough temperature and mass profiles within the absorber for each section, interpolate for each cross sectional slice, thus providing initial estimates of all variables and making computation of the precise absorption model easier.*

Once the rough temperature and flows profiles for each of the column sections were completed it was possible to estimate the temperature and flow of each stream for each slice of the column, by means of linear interpolation. The determined values were stored in large data files and used as the initial data sets when carrying out the rigorous calculation of the absorption profiles. Figure 5.4 illustrates the gas and lithium bromide temperature profiles within the absorption column operating with the following conditions.

Gas conditions:	Gas flow = 2.00 gs^{-1}.	
	Steam flow = 0.23 gs^{-1}.	Inlet temperature = 86 °C.
Lithium bromide conditions:	Flow = 5.31 gs^{-1}.	Inlet temperature = 101 °C.
		Inlet concentration = 65 %w/w.

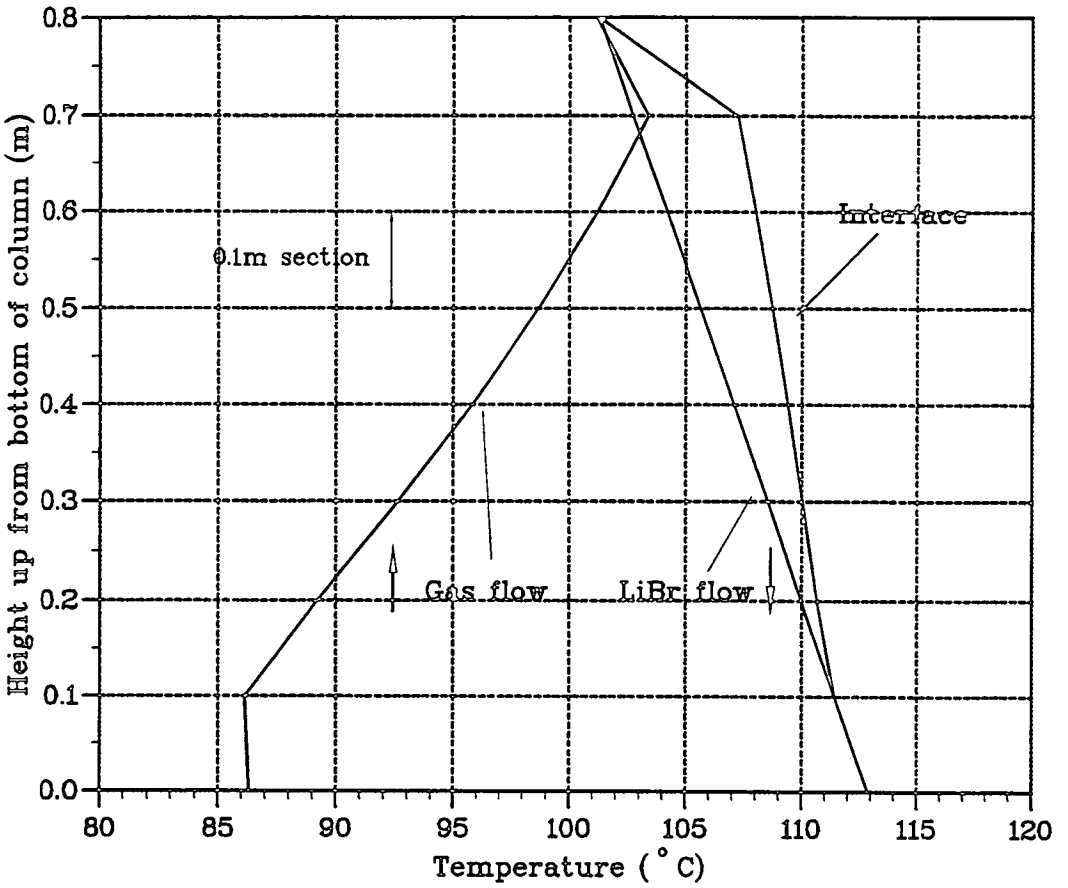

Figure 5.4: Approximate stream temperature profiles for the countercurrent dehumidification process.

5.5 Simple Cocurrent Absorption Results.

Results for the absorption of steam (the refrigerant vapour) into a concentrated lithium bromide solution indicated that the temperature of the lithium bromide stream rapidly reached a maximum near the top of the column, while the temperature of the refrigerant stream lagged behind. Over the lower half of the column, the temperatures of both streams remained approximately constant, with the refrigerant temperature only slightly less than that of the liquid temperature, Figure 5.5. The steam temperature did not increase as rapidly as the liquid temperature because the film heat transfer coefficient (HTC) of the refrigerant phase was far smaller than that of the liquid phase. The liquid phase HTC was approximately 1200- 2000 BTU $hr^{-1}ft^{-2o}F^{-1}$ (2.2- 3.5 $kWm^{-2}K^{-1}$), indicating a low heat transfer resistance. This was reflected in the temperature profile obtained, which showed that bulk stream temperature rose quickly to that of the interfacial temperature, while the HTC for the steam was only around 2- 3 BTU $hr^{-1}ft^{-2o}F$ (3.5- 5.4 $Wm^{-2}K^{-1}$), resulting in a more gradual increase in the steam temperature.

The sharp increase in temperature of the lithium bromide was also reflected in the rapid absorption of steam into the absorbent solution at the top of the column, followed by a more gradual linear decline at the bottom of the absorber, Figure 5.6. The exit steam flowrate was approximately 0.035 gs^{-1}, indicating that 0.125 gs^{-1} had been absorbed. An approximate calculation indicated that the maximum temperature achieved corresponded to the equilibrium temperature occurring at the average lithium bromide concentration, assuming a steam partial pressure of 1 bar (i.e 66 %w/w $\rightarrow$ 169 °C).

Absorption Tube:-

Steam conditions:	Flow = 0.16 gs^{-1}.	Inlet temperature = 100.3 °C.
Lithium bromide conditions:	Flow = 2.36 gs^{-1}.	Inlet temperature = 111.7 °C.
	Inlet concentration	= 68.4 %w/w.

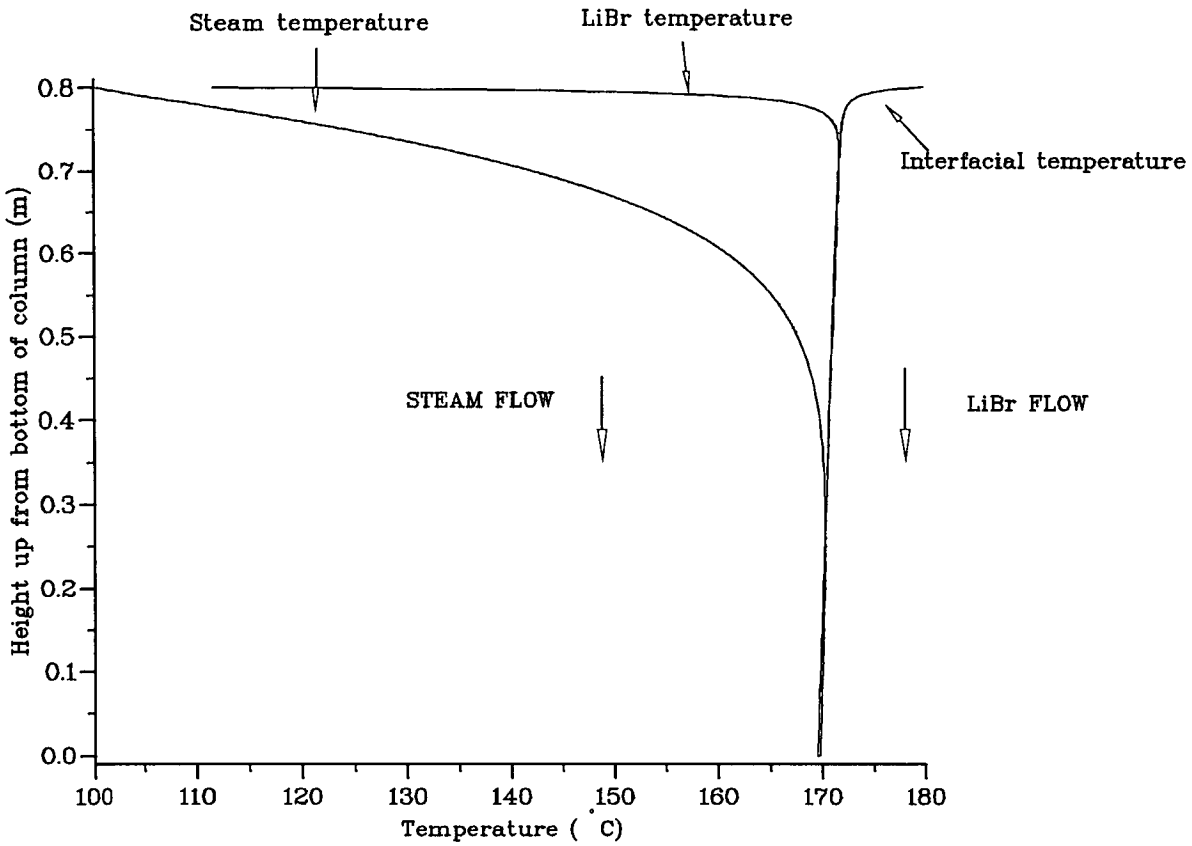

Figure 5.5: Temperature profiles for the absorption of steam into a concentrated LiBr solution, no inerts present.

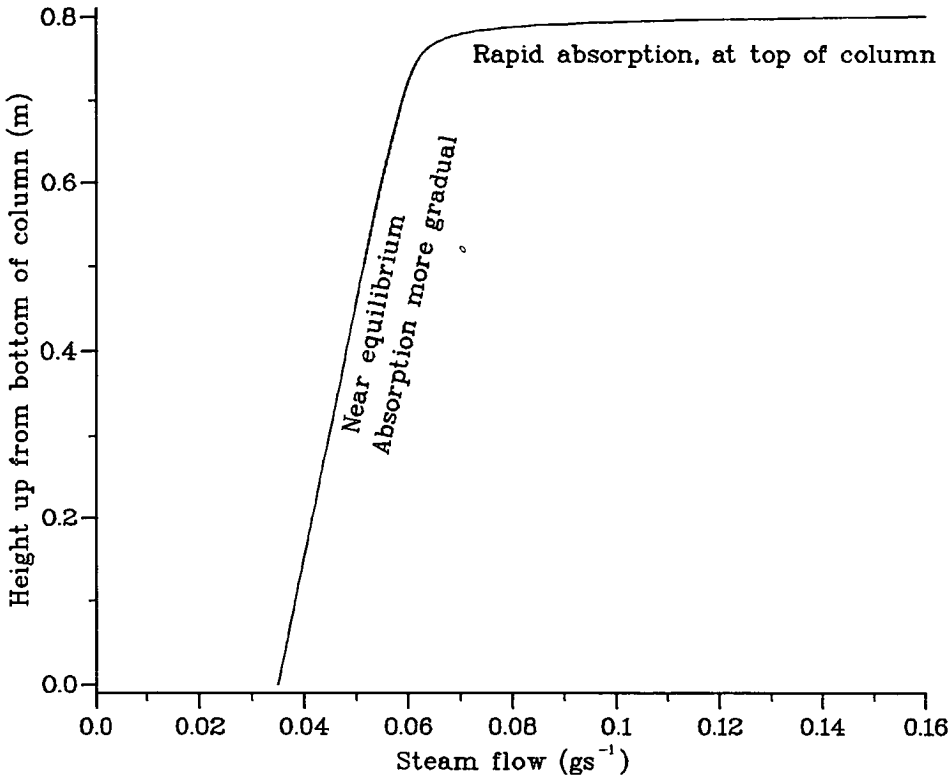

Figure 5.6: Mass profile of steam flowrate through column, no inerts.

Figures 5.5 and 5.6 illustrate the ideal case of steam absorption into a concentrated lithium bromide solution. It would be more realistic to assume that there were inerts present in the system. The operation of the absorber with inerts present is presented below, with the same inlet stream conditions as the previous example with the addition of an inert stream. The initial partial pressure of steam was set to 0.7 bar, with the inerts accounting for the other 0.3 bar.

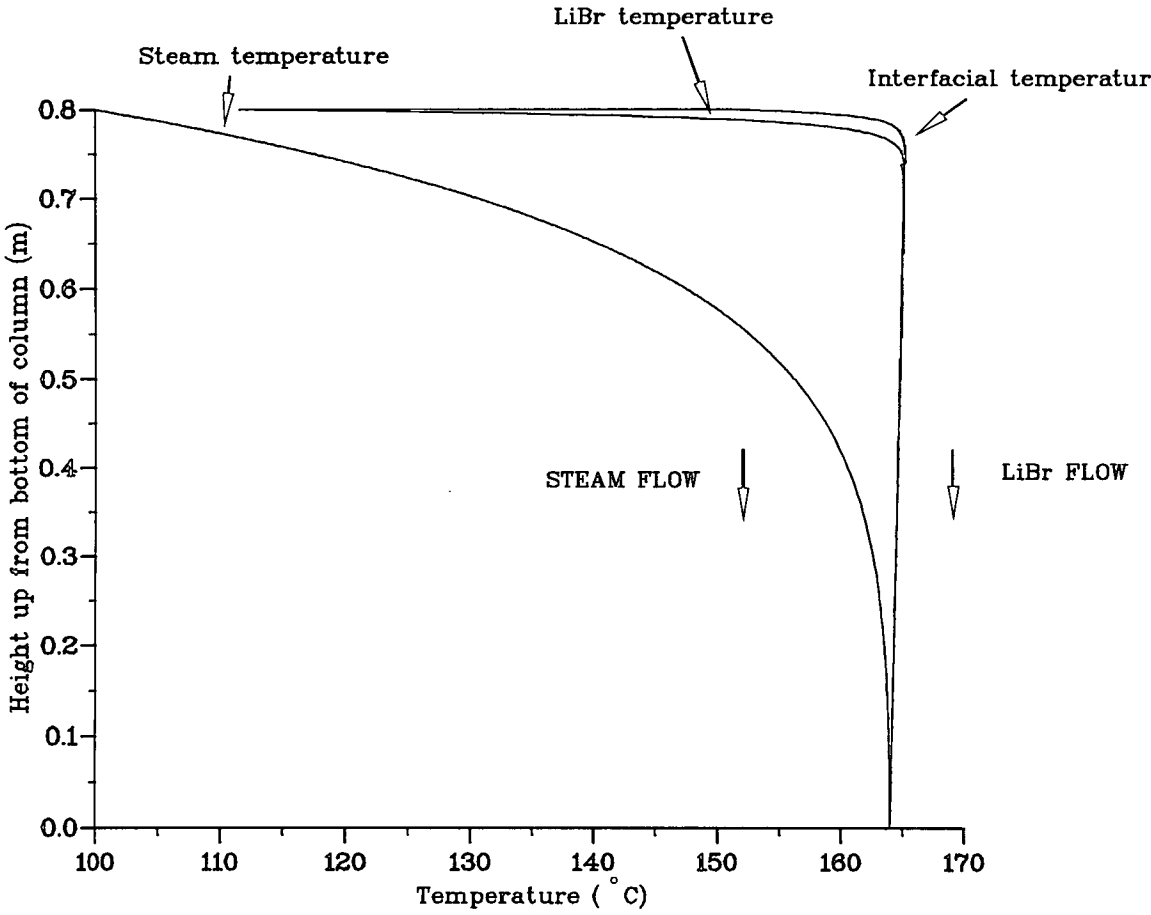

Figure 5.7: Temperature profiles for the absorption of steam into a concentrated LiBr solution, inerts present.

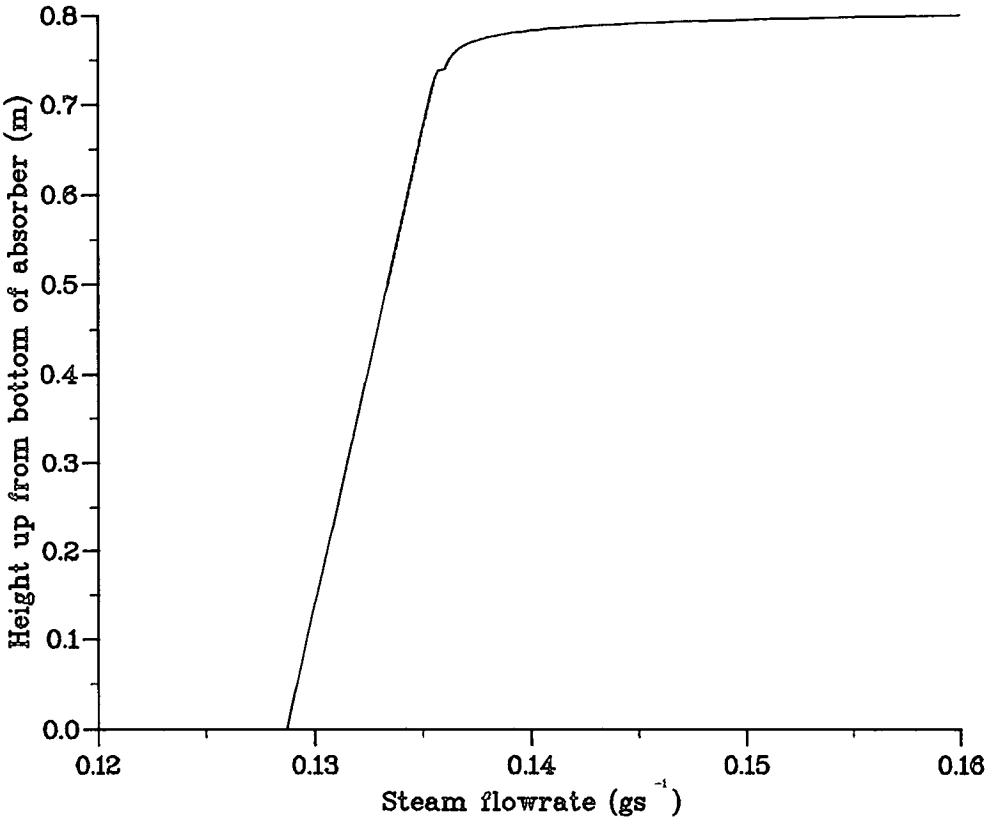

Figure 5.8: Mass profile of steam flowrate through column, with inerts (0.7bar initial partial pressure of stream).

It can be seen from Figure 5.7 that the exit gas temperature was reduced by the presence of inerts in the absorption column. The inerts reduced the partial pressure of steam in the column and as result reduced the maximum achievable temperature. For example, if the steam pressure was reduced to 0.7 bar, the maximum absorption temperature was reduced by 7 degC to 162 °C. The model also predicted a corresponding decrease in the amount of steam absorbed into the absorbent solution, Figure 5.8.

5.5.1 Effects of Varying the Stream Flowrates.

In the simple absorption model there were only two process streams- refrigerant vapour (steam) and liquid absorbent (concentrated lithium bromide solution). The following section investigates the effect of varying the flowrate of each of the streams upon the exit temperatures from the absorber. A useful parameter in quantifying the capacity of the absorber is the circulation ratio, which is the ratio between the inlet lithium bromide and steam flowrates.

Steam Flow.

A similar range of steam flowrates was tested in the model assuming constant absorbent conditions. The inlet solution flowrate was 2.3 gs^{-1}, with a concentration of 66 %w/w. The inlet temperature of both streams were 100 °C. Two different setups were analysed: one without any inerts present in the absorber; the other with an assumed initial inerts partial pressure of 0.3 bar.

In the ideal absorption case with no inerts present, it can be seen that increasing the steam flowrate, for a constant lithium bromide flow, resulted in a decrease in the exit lithium bromide temperature. The lowest steam flowrate, 0.06 gs^{-1}, gave the highest exit lithium bromide concentration, 64.3 %w/w, and thus the highest equilibrium temperature, 167.5 °C.

$\dot{m}_{RS_{top}}$ (gs^{-1})	$w_{LiBr_{bot}}$ (%w/w)	$\dot{m}_{RS_{bot}}$ (gs^{-1})	$T_{I_{bot}}$ (°C)
0.06	64.3	0.00	167.5
0.08	63.8	0.00	165.8
0.10	63.3	0.00	164.1
0.12	62.7	0.00	162.5
0.14	62.5	0.01	161.8
0.16	62.5	0.03	161.8
0.18	62.5	0.05	161.8
0.20	62.5	0.07	161.7
0.22	62.5	0.09	161.6
0.24	62.5	0.11	161.4
0.26	62.5	0.12	161.3
0.28	62.5	0.14	161.2
0.30	62.5	0.16	161.2

Table 5.1: Effect of varying the steam flowrate on the exit LiBr temperature.

Table 5.1 shows that all the steam, up to 0.13 gs^{-1} was absorbed, for a system with no inerts. Any increase above this only resulted in a further decrease in the exit lithium bromide temperature due to an increased heat load on the system. In comparison Table 5.2 shows that under the same operating conditions there was a significant decrease in the amount of steam absorbed when inerts were present, due a reduction in the steam partial pressure (initial inerts pressure was set to 0.3 bar in each case).

The simulation results show that when the simple absorption model was tested with a range of increasing steam flowrates, when no inerts were present in the system, the exit lithium bromide temperature initially decreased by a few degrees. At the highest steam flowrates, the exit temperatures were

approximately constant. The initial decrease in temperature was attributed to the decrease in absorbent concentration as more steam was absorbed into the liquid phase. Above a steam flowrate of $0.13 gs^{-1}$, the amount of steam absorbed did not increase, therefore the exit absorbent concentration remained constant [2]. The exit stream temperature continued to decrease slightly as the steam flowrate increased, this was due to the presence of excess steam in the absorber, which also required heating.

$\dot{m}_{RS_{top}}$ (gs^{-1})	$\dot{m}_{Inerts}$ (gs^{-1})	$w_{LiBr_{bot}}$ (%w/w)	$\dot{m}_{RS_{bot}}$ (gs^{-1})	$T_{I_{bot}}$ (°C)	Exit steam p.p (bar)
0.06	0.04	65.2	0.03	142.8	0.55
0.08	0.05	65.2	0.05	151.3	0.62
0.10	0.07	65.2	0.07	153.3	0.62
0.12	0.08	65.2	0.09	154.6	0.64
0.14	0.10	65.2	0.11	155.1	0.64

Table 5.2: Effect of varying the steam flowrate on the exit LiBr temperature with inerts present. Initial inerts partial pressure 0.3 bar.

By comparison, when the model was operated under the same conditions but with inerts present in the gas phase, the exit stream temperature was higher for the highest steam flowrates, Table 5.2. When the program was operated with inerts present in the gas phase, it was assumed that the phase was well mixed and that the inerts did not accumulate at the interface (see Section 5.2.2). This was a fair assumption because the absorption model was based on a packed column, which gave a large mass transfer area and also served to mix each phase. At the lowest steam flows, once the steam has been absorbed into the liquid phase the effect of the inerts increased far more than at higher steam flows. It was concluded that the equilibrium absorption temperature was lowered due to the increased effect of inerts in the system. The exit steam partial pressure at the lowest steam flowrate was 0.55 bar, whereas at the highest steam flowrate the partial pressure drops to only 0.64 bar.

[2] A good estimate of the exit absorption temperature could be made solely from the average lithium bromide concentration and the steam partial pressure.

It was also noted that in the system with inerts, the exit absorbent concentration remained constant over the range of steam flowrates investigated, as did the maximum absorption temperature obtained in the column. This suggested that the same amount of steam was absorbed independent of the initial flowrate because the absorbent stream conditions were the same for all the runs carried out. Therefore, the interfacial conditions remained the same for each run. Indeed in all cases tested with inerts present in the gas phase, the amount of steam absorbed was only $0.03 gs^{-1}$, compared to $0.13 gs^{-1}$ when there are no inerts present.

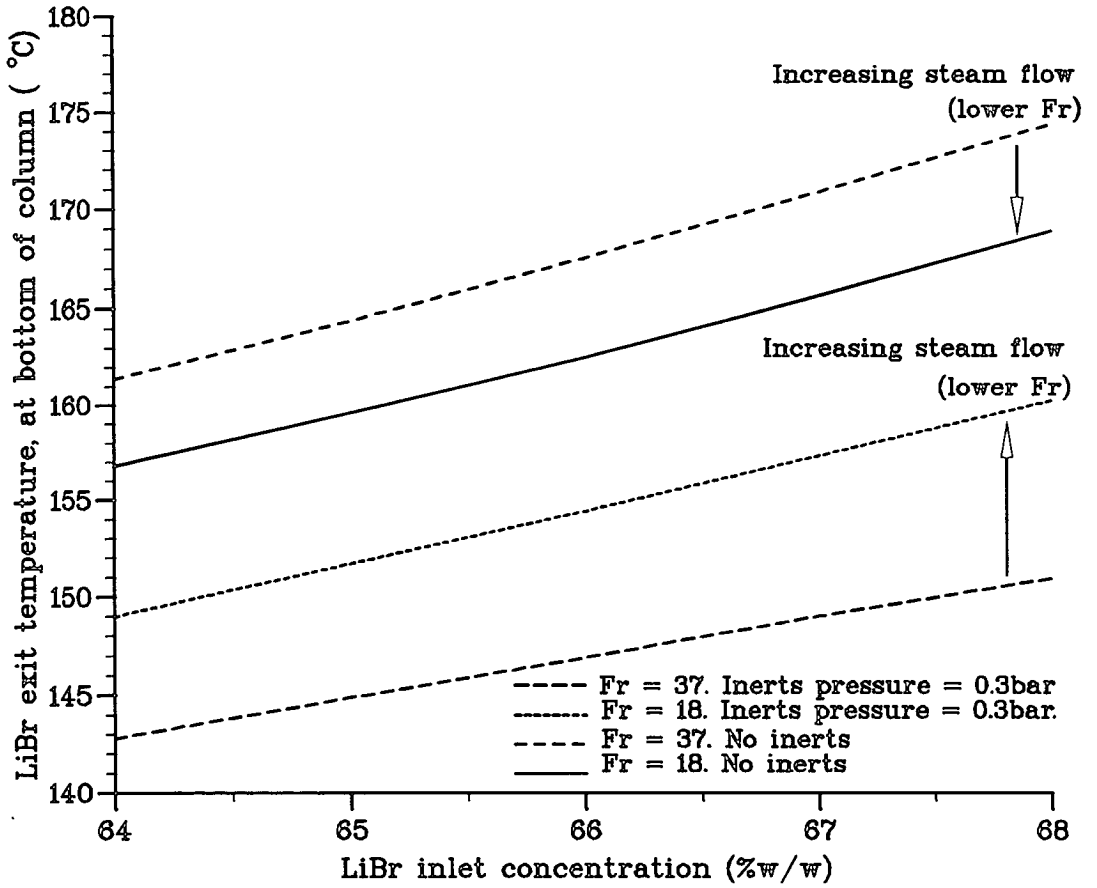

Figure 5.9: Effect of inerts on the exit LiBr temperature, for the simple absorption model.

The same effects were reproduced over a range of inlet absorbent concentrations, see Figure 5.9. Two different circulation ratios were examined, assuming constant lithium bromide flow and varying steam flow. All of the conditions tested exhibited an increase in exit stream temperature with increased absorbent concentration, with the ideal systems (no inerts) performing better. Again, it can be seen that increasing the steam flow in the ideal system decreases the exit temperature, while the opposite was true for the case with inerts present.

Lithium Bromide Flow.

The influence of varying the inlet lithium bromide flowrate on the exit stream temperature is shown in Figure 5.10. The diagram illustrates the variation in exit temperature for four inlet liquid flows over a range of circulation ratios[3], in each case the inlet concentration was 66 %w/w. As expected, the lowest exit temperatures occurred at the lowest absorbent flowrate, where there was the greatest change in the lithium bromide concentration due to the absorption of steam.

In Figure 5.10 there exist plateau regions (Lines c) and d)). This appeared to indicate that this was the point where the maximum amount of steam had been absorbed into the liquid phase. Subsequent increases in the steam flowrate (decreasing the circulation ratio) caused a further drop in temperature as the heat load of the system was further increased without any further absorption occurring.

[3]Circulation ratio (F_r = Lithium bromide flowrate / Steam flowrate ($\dot{m}_{LiBr}$ / $\dot{m}_{RS}$)

It can also be seen from Figure 5.10 that the exit temperature profiles for different inlet lithium bromide flowrates were the same for the same circulation ratios (i.e there was an overlap in results, see Lines a) and b)). The lines a) and b) also appear to be approaching an asymptotic value of approximately 171 °C, which is the equilibrium temperature of a 66 %w/w solution of lithium bromide at 1 bar (i.e as the steam flow was decreased (increasing F_r, the concentration change in the absorbent decreased to zero). It can therefore be concluded the effect of varying the circulation ratio in the absorber had a significant effect on the exit temperature obtained in the absorber, independent of the absolute value of the lithium bromide flowrate (providing all the steam was absorbed). The maximum stream exit temperature was solely dependent on the equilibrium conditions between the refrigerant and absorbent phases.

5.5.2 Effects of Varying the Lithium Bromide Concentration.

The previous sections have highlighted the importance of the absorbent concentration in achieving a high exit stream temperature. There was effectively a step increase in the exit lithium bromide solution temperature for each incremental change in absorbent concentration, over a range of circulation ratios, Figure 5.11.

It can also be seen from Figure 5.11 that the same temperature profiles to those of Lines c) and d) in Figure 5.10 were obtained. In addition, the position of the constant temperature region experienced for each absorbent concentration shifted. The onset of the constant temperature region varied from a circulation ratio of 19 when the concentration was 64 %w/w to 17 at 68 %w/w. This

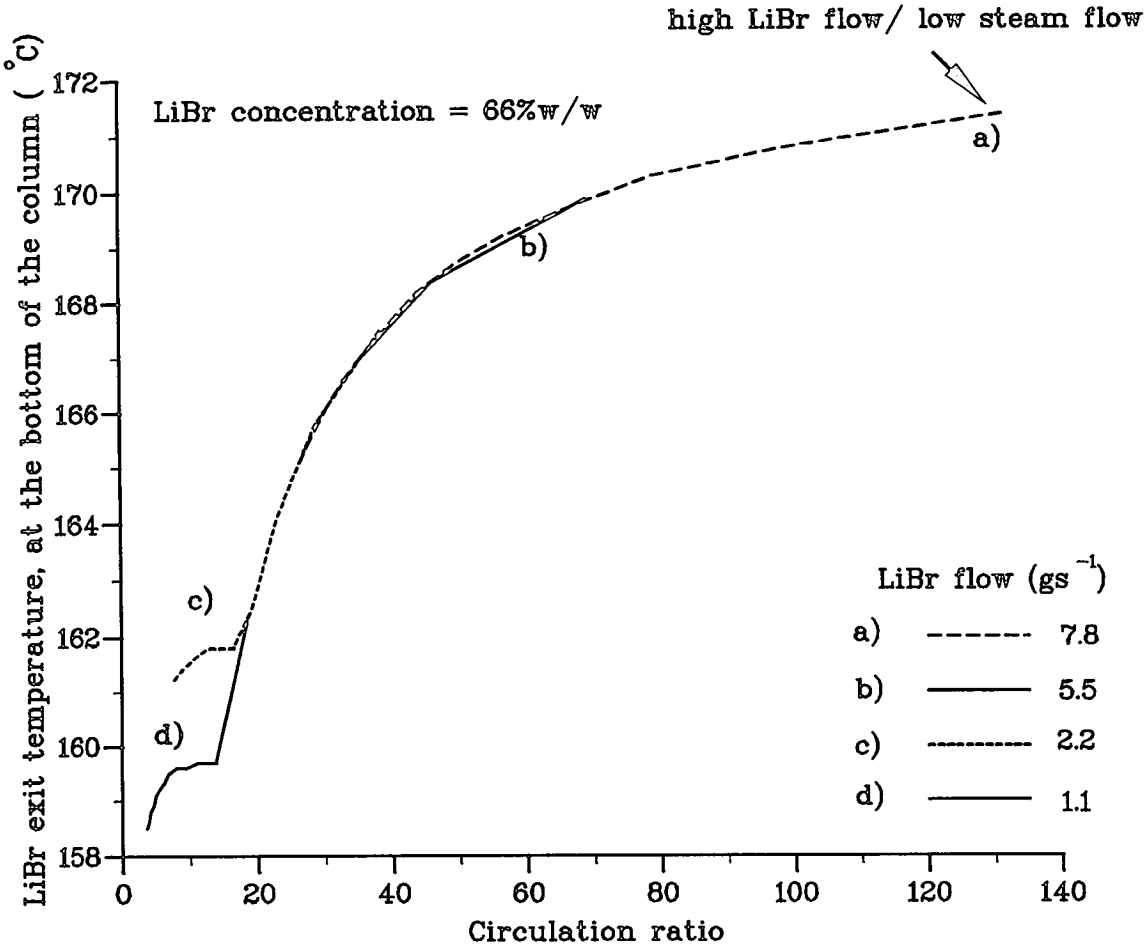

Figure 5.10: Effect of varying LiBr inlet flowrate at different inlet concentrations on the LiBr exit temperature.

observation was as expected because as the inlet concentration of the lithium bromide stream increased, the absorption driving force also increased and therefore more steam could be absorbed into the liquid before effective saturation. The saturation occurred when no more steam could be absorbed despite the increase in the steam flowrate (lowering the circulation ratio).

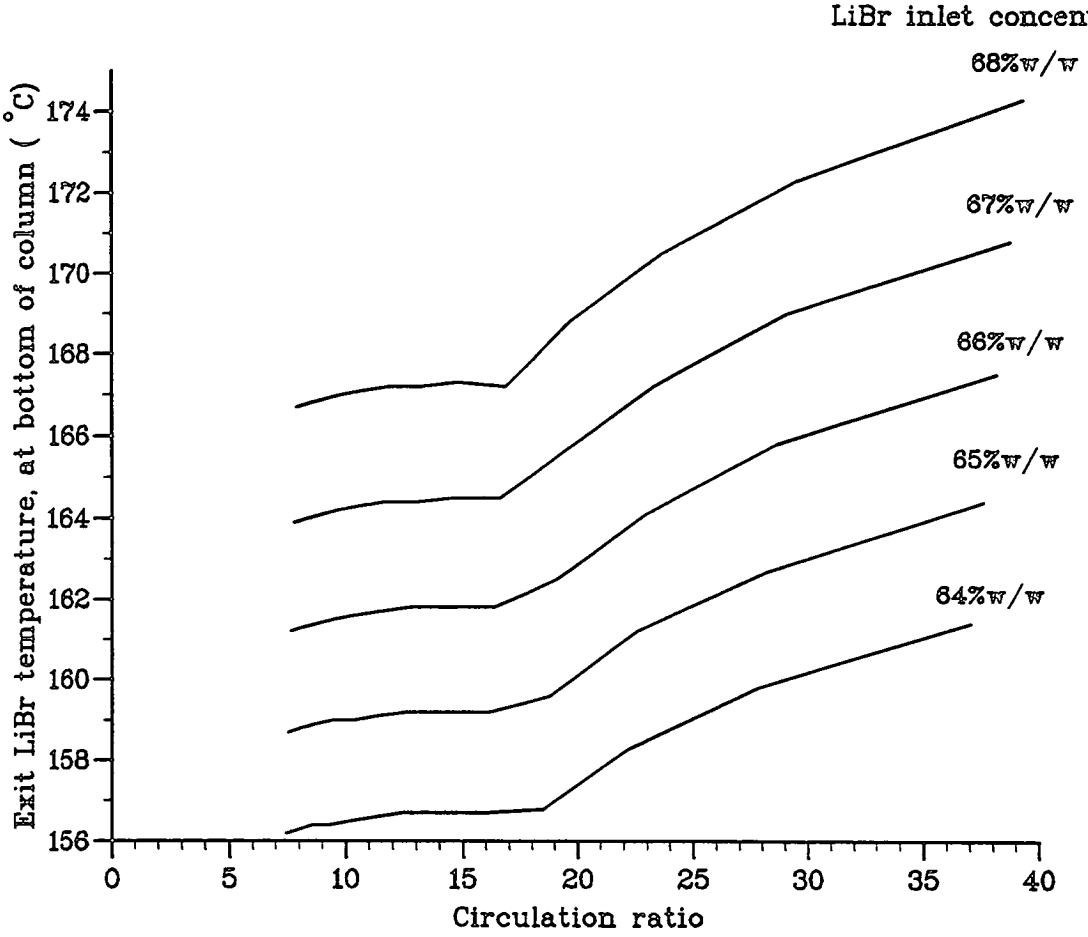

Figure 5.11: Effect of varying the inlet LiBr concentration on the exit LiBr temperature.

5.5.3 Effects of Varying the Stream Inlet Temperatures.

The variation of the stream inlet temperatures did not affect the exit absorption temperature when the absorber was operated at the lowest steam flowrate of 0.06 gs^{-1}, Figure 5.12. This can be attributed to the low concentration change in the absorbent stream resulting in an extremely high absorption temperature. Indeed because the rate of absorption of steam into the lithium bromide was so rapid, the temperature of the bulk absorbent stream quickly increased to approximately the same as that of the interface. As the interfacial temperature was solely dependent on the interfacial concentration and steam partial pressure, the effect of varying the inlet stream temperatures were negligible.

However, as the steam flowrate was increased, there was a distinct increase in the exit stream temperatures obtained as the inlet stream temperatures were increased. The increase was due to the extra heat added to the system at the inlet, allowing a closer approach to the maximum absorption temperature to be achieved. The improvement in the exit temperature, for each steam flow, was approximately 1 degC for each 10 degC increase in the initial temperature.

The exit stream temperature was previously shown to increase as the inlet absorbent concentration increased. It can be seen from Figure 5.12 that the relationship between these variables was linear. The change in the exit stream temperature as the absorbent concentration increases does not depend upon the initial stream temperature or the refrigerant (steam) flowrate. The increase in the exit temperature was approximately 2 degC per percent.

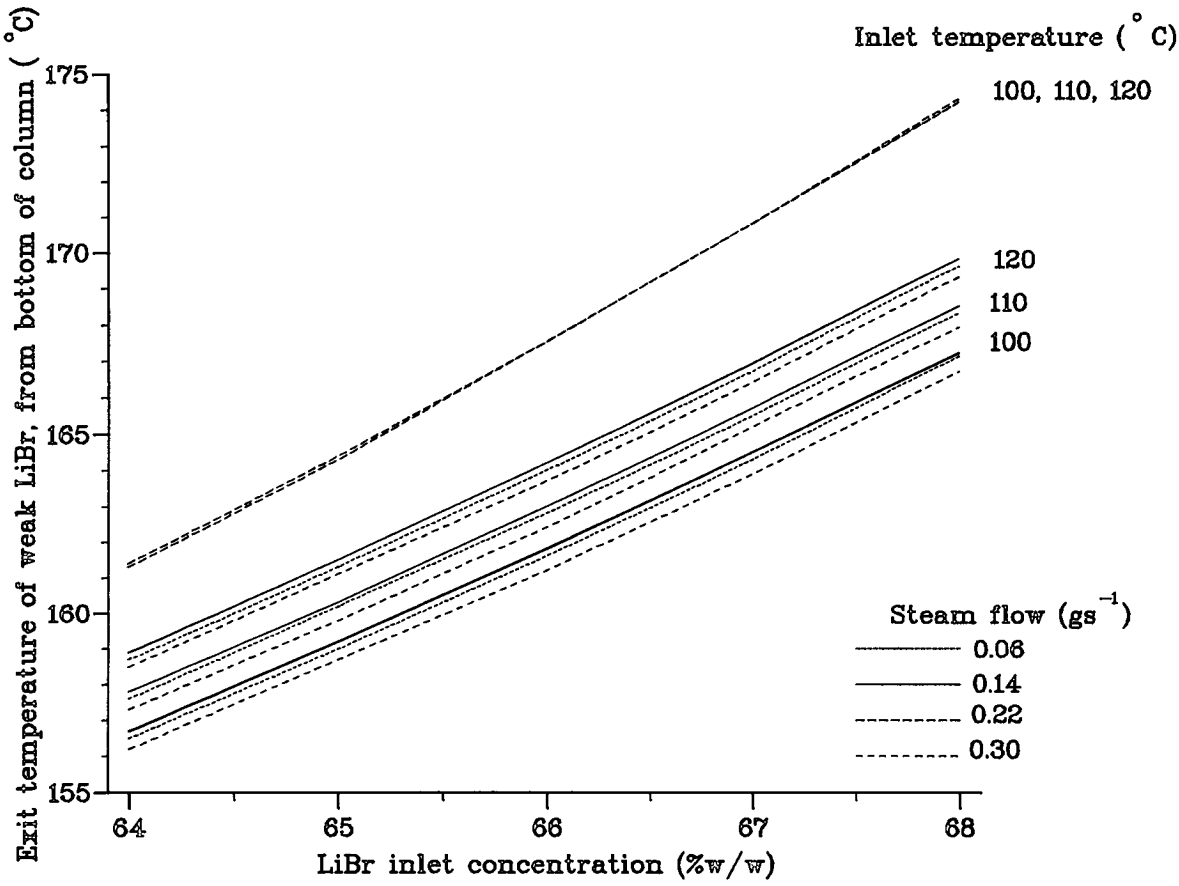

Figure 5.12: Effects of varying the steam flowrate and the inlet stream temperatures upon the LiBr exit temperature.

5.6 Results for Cocurrent Absorption with External Heat Removal.

After successfully modelling the absorption of steam into a concentrated solution of lithium bromide adiabatically, the computer program was extended to investigate the effects of heat removal from the hot absorbent fluid. An externally flowing gas stream was used to remove heat from the absorption tube. Figure 5.13 shows the setup for countercurrent heat removal. The following sections present results for both cocurrent and countercurrent heat removal.

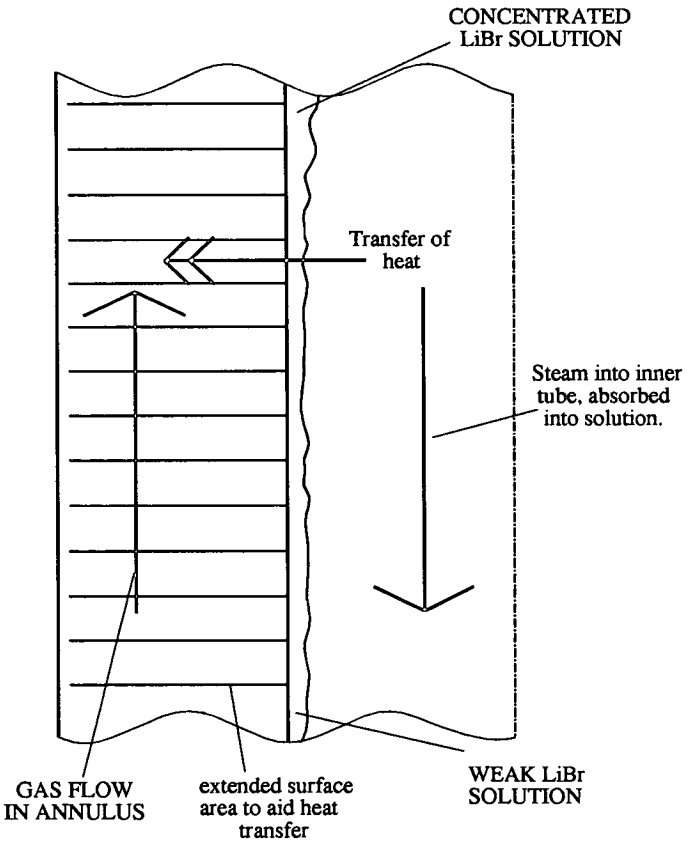

Figure 5.13: Schematic representation of steam absorption into LiBr solution, with simultaneous heat removal by a countercurrent stream of gas.

5.6.1 Countercurrent Heat Removal.

All of the experiments carried out using the reheat absorber involved the use of countercurrent gas streams to remove the heat from the absorption tube. The first simulations were carried out using experimental operating conditions, enabling a direct comparison to be made between the theoretical and experimental results, thereby validating the model. Following a description of this, each of the process variables will be discussed in turn with respect to gaining a detailed insight of the reheat process.

Comparison between Experimental and Theoretical Results.

The experimental apparatus permitted measurements of only the inlet and outlet stream temperatures, however, the theoretical results obtained from the simulation model were in reasonable agreement with these points. Figure 5.14 illustrates the temperature profiles of both the external gas stream and of the inner absorbent stream. As with the simple absorption model, the lithium bromide stream temperature rapidly increased to a maximum as the steam was absorbed into the liquid, and then remained at approximately this temperature throughout the column.

Absorption tube:-		
Steam conditions:	Flow = $0.16 gs^{-1}$.	Inlet temperature = 100 °C.
Lithium bromide conditions:	Flow = $2.36 gs^{-1}$.	Inlet temperature = 112°C.
		Inlet concentration = 68%w/w.
Outer annulus:-		
Gas conditions:	Flow = $3.00 gs^{-1}$.	Inlet temperature = 97°C.
Experimental Results:-	Gas exit	temperature = 160°C
	LiBr exit	temperature = 159°C

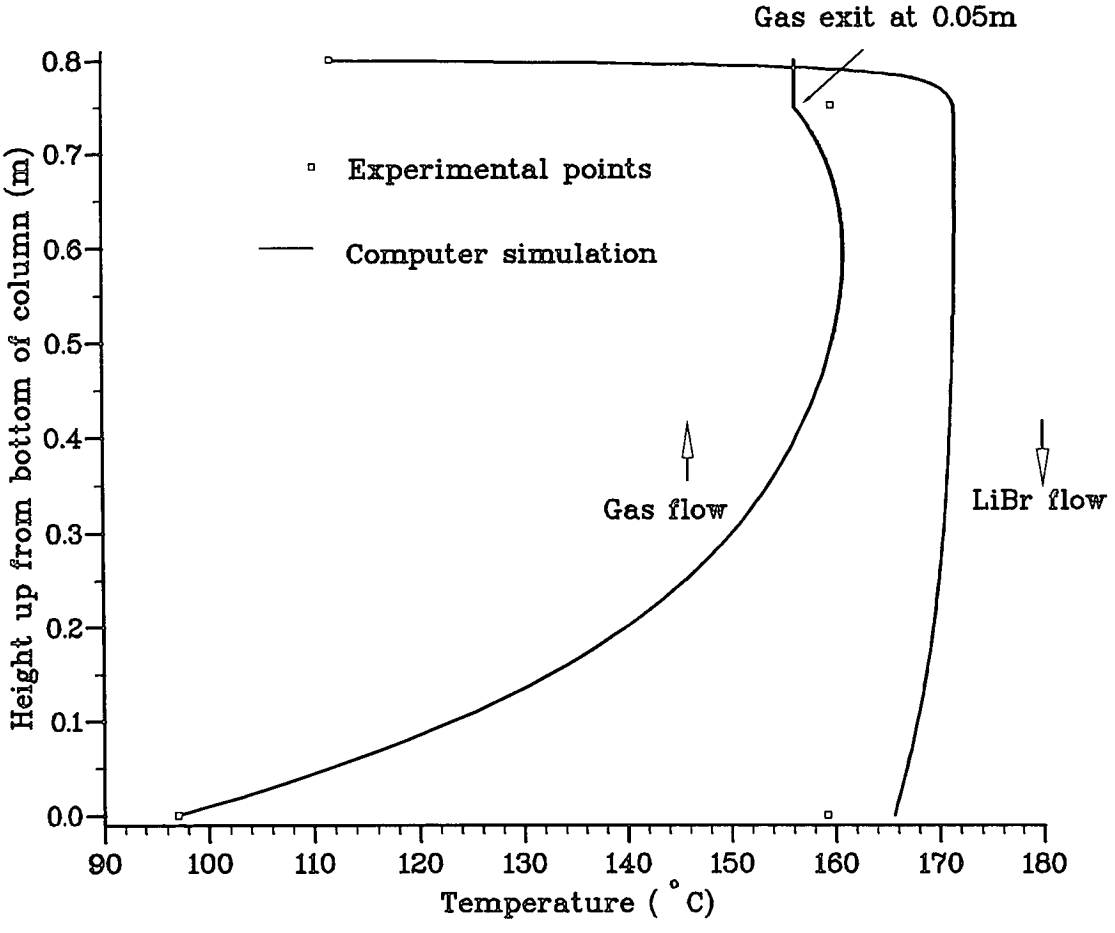

Figure 5.14: Temperature profiles for cocurrent absorption of steam into LiBr, with countercurrent heat removal by an external gas stream.

It can also been seen from Figure 5.14 that the gas temperature drops slightly

before exiting at the top of the column. This was due to heat being transferred back into the inner absorption tube. As was seen from the simple absorption case, Figure 5.5, the steam temperature did not increase as rapidly as the liquid phase and so resulted in the transfer of heat from the gas stream.

Table 5.3 compares the results from the simulation program, for a range of gas flowrates, with actual experimental data. The gas exit temperatures predicted in most cases agree well with the experimental values. However, the liquid exit temperatures were consistently higher than obtained experimentally. It was felt that although the VLE data for the lithium bromide was accurate at high concentrations, around the temperatures 160- 175°C, the thermodynamic properties calculated for the absorbent stream were used at the limits of their validity. For example, although the absorbent stream concentration and flowrate were measured accurately, the stream density and heat capacity were only estimated from the correlations provided by Brunk and Liu. It was therefore concluded that the differences in the measured and predicted temperature was because the predicted absorbent streams had larger heat capacities and/ or densities than the actual streams used in the experiments. Hence, the results obtained for the simulation model resulted in higher exit absorbent stream temperatures because the predicted heat loads of the streams were greater than actually used during the experimental trails.

The gas exit temperatures were in reasonable agreement because the overall heat transfer coefficient used to determine the rate of heat transfer to the gas stream was based on an empirical value from the experimental absorber; and the fluid properties of gases were well characterised over the temperatures used. In addition, the maximum absorbent temperature was felt to be accurate as it was based upon the absorbent stream partial pressure and concentration, which were both measured. Hence the rate of heat transfer between the inner absorption tube and the gas stream were in close agreement for both the experimental and predicted results.

						Experimental		Simulation	
$\dot{m}_G$	$T_{G_{bot}}$	$\dot{m}_{LiBr_{in}}$	$w_{LiBr_{in}}$	$\dot{m}_{RS}$	$T_{I_{top}}$	$T_{G_{top}}$	$T_{I_{bot}}$	$T_{G_{top}}$	$T_{I_{bot}}$
(gs^{-1})	(°C)	(gs^{-1})	(%w/w)	(gs^{-1})	(°C)	(°C)	(°C)	(°C)	(°C)
2.00	82	2.30	64	0.16	102	141	145	146	158
2.00	79	2.90	60	0.16	101	128	134	136	146
3.00	89	2.22	62	0.16	101	144	145	142	150
3.00	92	2.82	66	0.14	101	144	146	151	162
3.00	93	2.41	67	0.16	100	150	150	155	164
3.00	97	2361	68	0.16	112	156	165	160	159
4.00	94	2.27	63	0.16	101	142	141	145	152
4.00	92	2.48	65	0.16	100	144	142	149	156
5.00	79	2.08	56	0.16	107	130	129	130	137
5.00	78	2.21	61	0.16	100	134	120	138	147
6.00	78	2.21	61	0.16	102	131	113	138	145
6.00	77	2.25	63	0.16	101	135	116	141	149

Table 5.3: Comparison of experimental and computer results.

Effect of Inerts on the Absorber Performance.

As previously discussed in Section 5.5, the presence of inerts in the absorption tube lowered the maximum equilibrium temperature because the steam partial pressure was effectively reduced. This particular problem was also identified in Chapter 4 'Experimental Studies', Section 4.4.2 'Early Absorption Trials',

where the maximum achievable gas exit temperature was affected by inerts in the vapour space of the absorption tube.

Figure 5.15 shows that similar temperature profiles were obtained for simulations where a gas stream was being heated, with/ without inerts present in the absorption tube. The lower portions of the profiles were virtually identical, as the gas was heated from its initial temperature. As the temperature of the absorbent stream in the inner absorption tube was far hotter than either gas stream, the temperature difference between the gas streams and the hot absorbent fluid were similar, resulting in a similar rate of increase in the temperature of the gas streams. The greatest variation in temperature profile occurred at the top of the column, where most of the steam was absorbed. A lower maximum absorption temperature occurred when inerts were present in the absorption tube because the partial pressure of the steam was reduced. This resulted in a lower exit gas temperature for the case with inerts present, Figure 5.15.

Absorption tube:-		
Steam conditions:	Flow = 0.16 gs^{-1}.	Inlet temperature = 100 °C.
Inerts:	a) Initial partial pressure	= n/a
	b) Initial partial pressure	= 0.3 bar
Lithium bromide conditions:	Flow = 2.36 gs^{-1}.	Inlet temperature = 100 °C.
		Inlet concentration = 68 %w/w.
Outer annulus:-		
Gas conditions:	Flow = 3.0 gs^{-1}.	Inlet temperature = 90 °C.

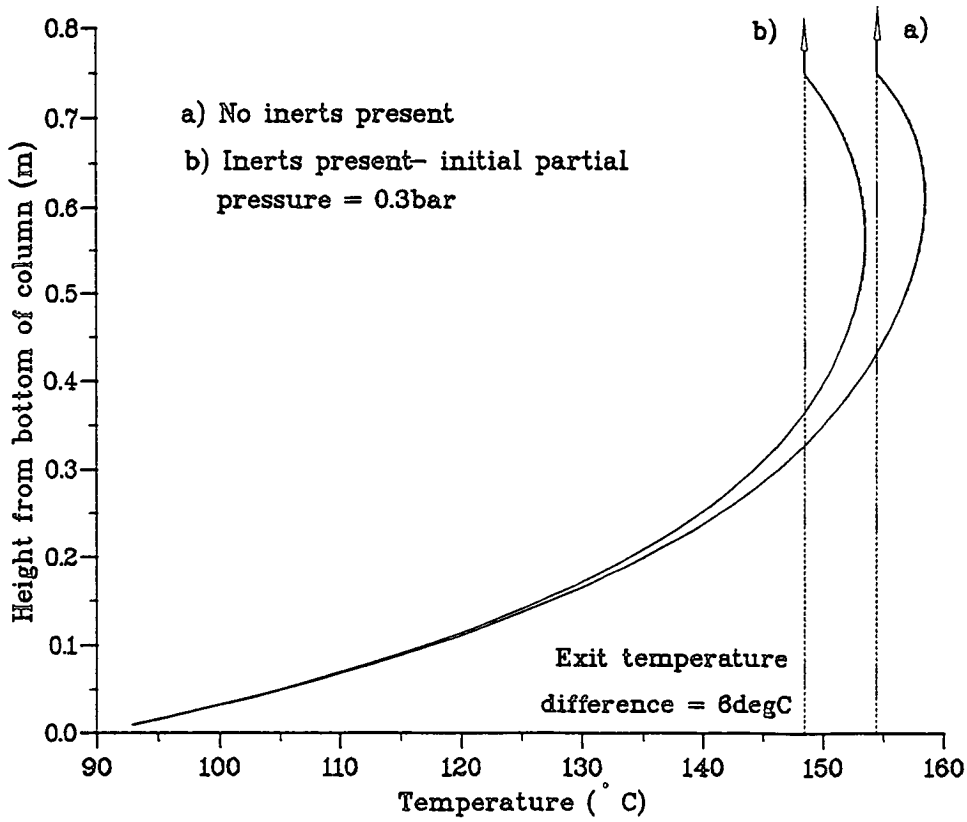

Figure 5.15: Effects of inerts, present in the absorption tube, on the gas temperature.

Absorption tube:-		
Steam conditions:	Flow = 0.16 gs^{-1}.	Inlet temperature = 100 °C.
Lithium bromide conditions:	Flow = 2.36 gs^{-1}.	Inlet temperature = 100 °C. Inlet concentration range = 65- 68 %w/w.
Outer annulus:-		
Gas conditions:	Flow = 3.0 gs^{-1}.	Inlet temperature = 90 °C.

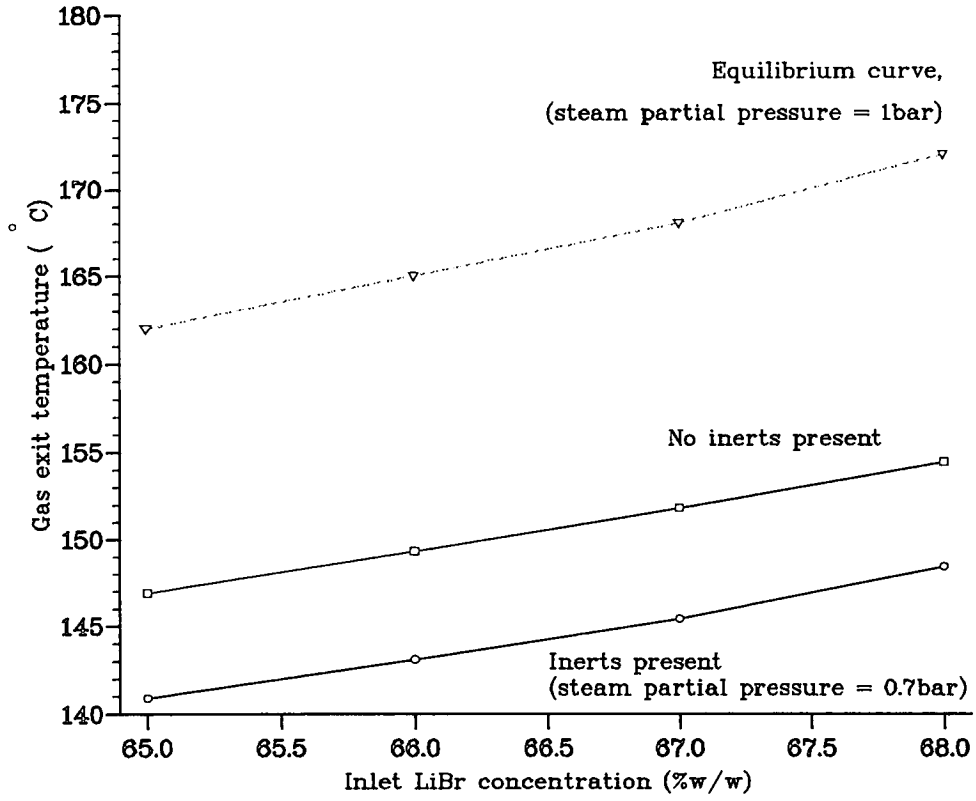

Figure 5.16: Effect of inerts on the gas exit temperature for varying LiBr concentration.

Figure 5.16 illustrates the variation of the exit temperature over a range of concentrations. It can be seen that the exit gas temperature was consistently lower by approximately 6 degC when inerts were present in the system. The linear dependency of the results on the lithium bromide concentration is again evident in the results for the system with and without inerts present. For comparison, a line representing the maximum VLE temperature has also been drawn (assuming a partial pressure of 1bar and an "average" lithium bromide concentration). The difference between the actual expected exit temperatures and this line was due to the heat transfer resistances in the gas phase.

The presence of inerts in the absorption tube created a problem when trying to maximise the gas exit temperature because of the lower steam partial pressure in the absorption tube. It should also be noted that there was a reduction in the amount of steam absorbed into the lithium bromide stream because of the reduction in the mass driving force. Therefore, the exit lithium bromide concentration remained higher when inerts were present in the absorption tube. However, this was not enough to offset the reduction in the equilibrium partial pressure caused by the inerts and so a lower absorption temperature being obtained. As a result, the log- mean temperature difference between the gas and absorbent streams at the top of the column was also reduced, for simulations carried out with inerts present in the absorption tube. Consequently, there was a reduction in the exit gas temperature obtained, for a given inlet absorbent concentration.

Effect of Varying the Absorption Mixture Stream Conditions.

The principal variables within the absorption tube which will be discussed, are:

- Steam flowrate.
- Lithium bromide flowrate.
- Lithium bromide concentration.

The results tabulated below also illustrate the influence of the circulation ratio upon the gas exit temperature, which depended upon both the steam and lithium bromide flowrates. As the most important system variable was the inlet absorbent concentration, a range of inlet concentrations were studied within each of the following sections.

Steam Flowrate. As with the simple absorption model, the effect of increasing the steam flowrate in the reheat absorber was investigated. Figure 5.17 summarises the results obtained for simulation model operating over a wide range of inlet lithium bromide concentrations with a gas stream of 3 gs^{-1} and an inlet temperature of 90 °C. The results show that there was no appreciable difference between exit gas temperatures obtained for the different steam flows, over the lower concentrations. There was a slight improvement in the gas exit temperature for the lowest steam flowrate over the other results, at the highest absorbent concentration. Inspection of the results in Table 5.4 shows that for inlet steam flowrates of between 0.16 and 0.20 gs^{-1}, there was an excess of steam at the bottom of the absorber. This resulted in exit lithium bromide concentrations which were approximately the same, and consequently

the maximum absorption and gas exit temperatures were constant. However, as the absorbent concentration increased, there was a greater mass driving force which resulted in more steam being absorbed into the liquid phase. As a result there was a reduction in the exit absorbent concentrations for the higher steam flowrates. The lower exit lithium bromide concentration corresponded to a decrease in the maximum absorption temperature achieved in the absorber and hence resulted in lower exit gas temperatures.

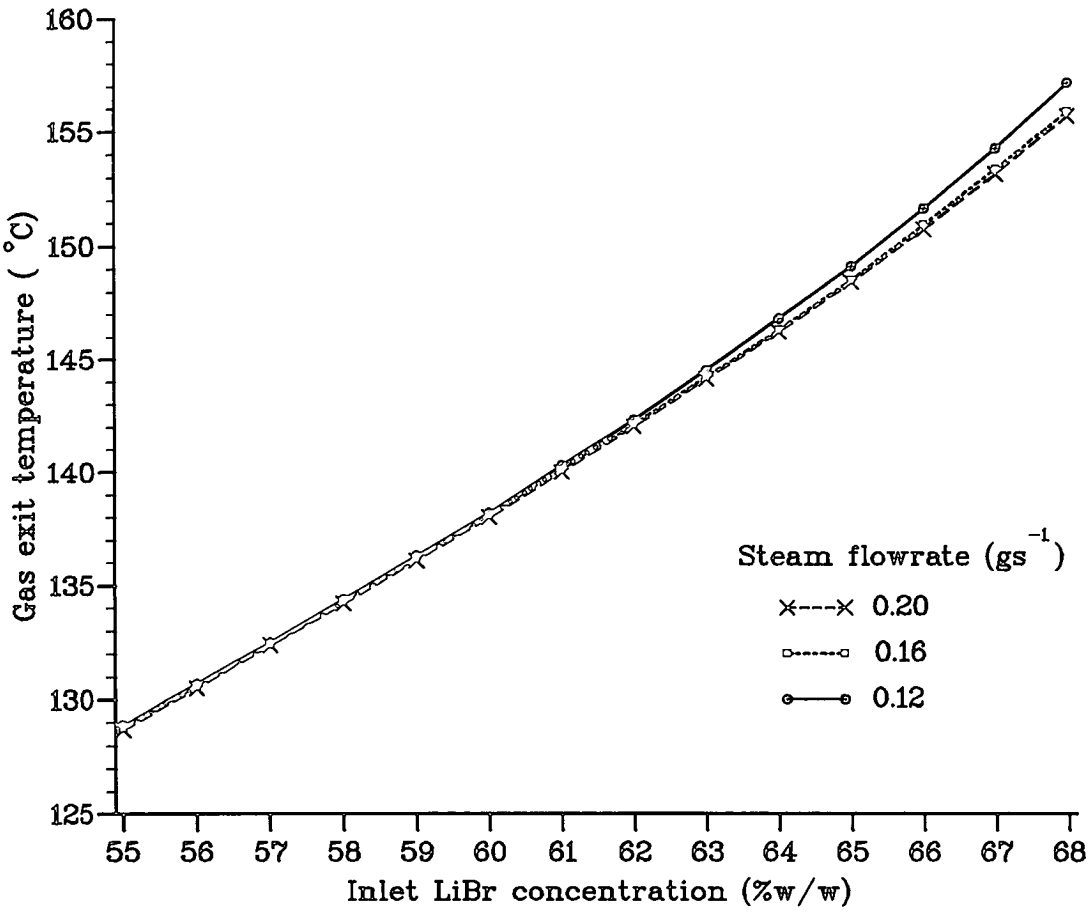

Figure 5.17: Effect on the gas exit temperature of varying the initial steam flow and LiBr concentration.

$w_{LiBr_{top}}$ (%w/w)	$\dot{m}_{RS_{top}}$ (gs^{-1})	F_r (-)	$w_{LiBr_{bot}}$ (%w/w)	$\dot{m}_{RS_{bot}}$ (gs^{-1})	$T_{I_{bot}}$ (°C)	$T_{G_{top}}$ (°C)
55	0.12	17.3	52.0	0.00	135	129
56	0.12	17.6	53.0	0.00	137	131
57	0.12	17.8	54.0	0.00	140	132
58	0.12	18.0	55.0	0.00	142	134
59	0.12	18.2	56.0	0.00	144	136
60	0.12	18.5	56.9	0.00	146	138
61	0.12	18.7	57.9	0.00	149	140
62	0.12	18.9	58.9	0.00	151	142
63	0.12	19.2	59.9	0.00	153	145
64	0.12	19.4	60.9	0.00	156	147
65	0.12	19.6	61.9	0.00	159	149
66	0.12	19.9	62.9	0.00	162	152
67	0.12	20.1	63.8	0.00	164	154
68	0.12	20.3	64.8	0.00	168	157
55	0.16	13.0	51.9	0.03	135	129
56	0.16	13.2	52.8	0.03	137	131
57	0.16	13.3	53.6	0.03	139	132
58	0.16	13.5	54.5	0.02	141	134
59	0.16	13.7	55.4	0.02	143	136
60	0.16	13.9	56.2	0.01	145	138
61	0.16	14.0	57.1	0.01	146	140
62	0.16	14.2	57.9	0.00	149	142
63	0.16	14.4	58.9	0.00	151	144
64	0.16	14.5	59.9	0.00	154	146
65	0.16	14.7	60.9	0.00	156	149
66	0.16	14.9	61.9	0.00	159	151
67	0.16	15.1	62.9	0.00	162	153
68	0.16	15.2	63.8	0.00	164	156
55	0.20	10.4	51.8	0.07	135	129
56	0.20	10.5	52.7	0.07	137	131
57	0.20	10.7	53.6	0.06	139	132
58	0.20	10.8	54.4	0.06	140	134
59	0.20	10.9	55.3	0.05	142	136
60	0.20	11.1	56.1	0.05	144	138
61	0.20	11.2	57.0	0.04	146	140
62	0.20	11.4	57.8	0.04	148	142
63	0.20	11.5	58.7	0.03	150	144
64	0.20	11.6	59.5	0.02	152	146
65	0.20	11.8	60.3	0.01	154	148
66	0.20	11.9	61.2	0.01	156	151
67	0.20	12.1	61.9	0.00	159	153
68	0.20	12.2	62.9	0.00	162	156

Table 5.4: Data summarising the influence of the steam flowrate on the exit gas temperature, for a range of inlet LiBr concentrations.

The ideal absorption model showed improvement in the exit gas temperature for decreasing steam flowrate. However, this system would not be practical in a real absorption cycle as there would be inerts present in the system, which would have a greater effect on the performance of the absorber when the refrigerant flowrates were smaller (see previous discussion).

LiBr Flowrate in Absorption Tube. The following section investigates the effect upon the exit gas temperature of varying the inlet lithium bromide flowrate. As previously mentioned when the absorption tube flowrates are varied the circulation ratio in the column also varies. Therefore, two cases were analysed: one assuming a constant steam flowrate in the column; the other, constant circulation ratio. It should be noted that the circulation ratio did vary slightly, this was due to the density of the absorbent solution rising for increasing inlet concentration. As the inlet lithium bromide flowrate was input 'mls^{-1}', the mass flowrate of the liquid stream rose as the density increased. However, this was thought not to affect the results greatly.

Figure 5.18 shows that increasing the lithium bromide flowrate, while maintaining a constant steam flowrate (increasing the circulation ratio), considerably increased the gas exit temperature for a range of inlet lithium bromide concentrations. As the steam flowrate was constant in each case, the concentration change of the absorbent stream was less than for the case where the circulation ratio was kept constant. This resulted in higher exit absorbent concentrations being obtained at the higher circulation ratios and hence higher absorption and exit gas temperatures, see Table 5.5. This observation agrees with the earlier result for the simple absorption model. However, by increasing the lithium bromide flowrate, there would be an increase in the pumping requirements of the system.

$\dot{m}_{LiBr_{top}}$ (gs^{-1})	$w_{LiBr_{top}}$ (%w/w)	$\dot{m}_{RS}$ (gs^{-1})	F_r (-)	$w_{LiBr_{bot}}$ (%w/w)	$T_{I_{bot}}$ (°C)	$T_{GT_{top}}$ (°C)
2.30	64	0.12	19.1	60.8	156	147
2.33	65	0.12	19.4	61.8	159	149
2.37	66	0.12	19.7	62.8	161	152
2.40	67	0.12	20.0	63.8	164	154
2.44	68	0.12	20.3	64.8	168	157
4.98	64	0.12	41.5	62.5	161	151
5.05	65	0.12	42.1	63.5	164	153
5.13	66	0.12	42.7	64.5	167	156
5.20	67	0.12	43.4	65.5	170	159
5.28	68	0.12	44.0	66.5	174	162
4.98	64	0.26	19.1	60.8	156	147
5.05	65	0.26	19.4	61.8	159	149
5.13	66	0.26	19.7	62.8	162	152
5.20	67	0.26	20.0	63.8	165	154
5.28	68	0.26	20.3	64.8	168	157

Table 5.5: Results for varying the LiBr flowrate with constant steam flowrate and approximately constant circulation ratio.

The results of the simulations with constant circulation ratio and with increasing lithium bromide flowrate were essentially the same. The exit absorbent concentrations were the same for low and high stream flowrates. The resultant effect was that the gas exit temperatures were also the same.

Another important feature of Figure 5.18 was the increase in exit temperature as the inlet absorbent concentration increased. However, there was a physical constraint on the maximum lithium bromide concentration within the system due to crystallisation problems. Maximum concentration used in these studies was therefore set to 68 %w/w, which has a crystallisation temperature around 82 °C.

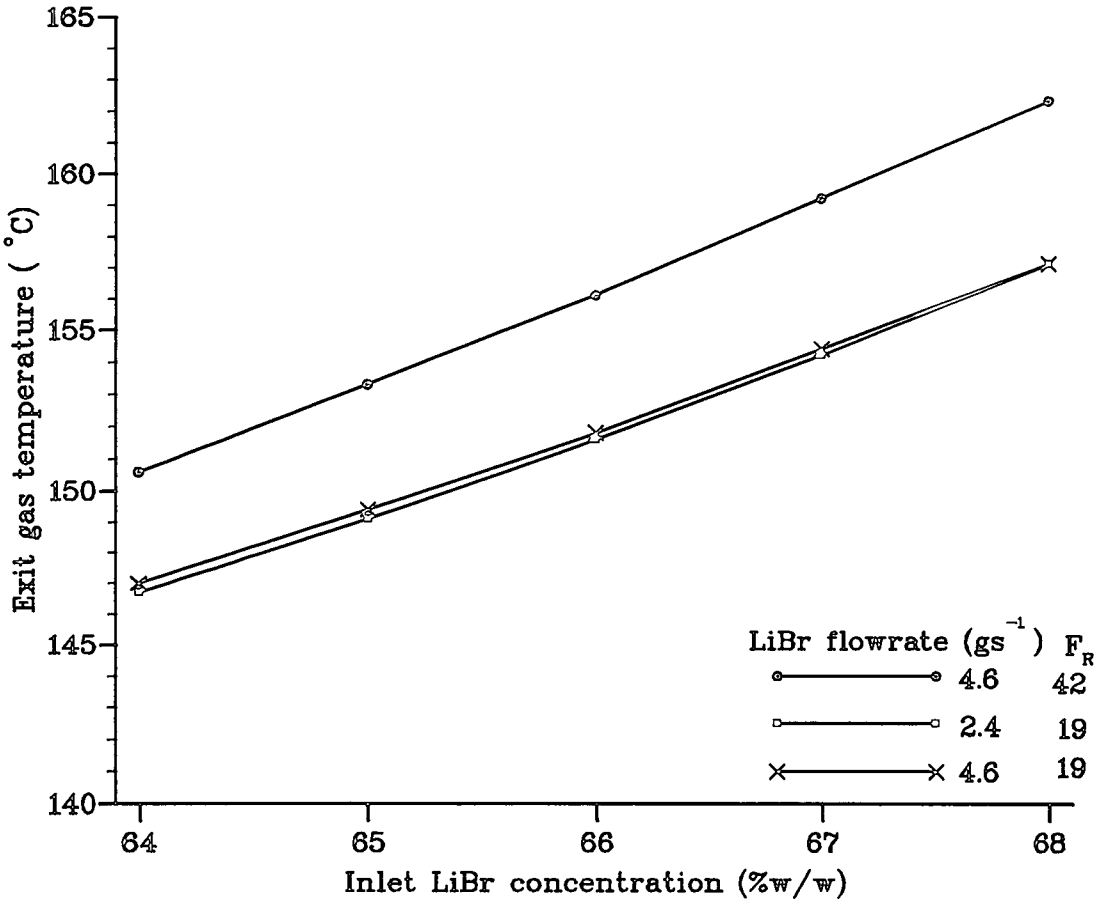

Figure 5.18: Effect on the gas exit temperature of varying the LiBr flowrate.

Influence of Gas Conditions on Absorber Performance.

The primary aim of the reheat column was to maximise the exit temperature of the gas stream. The outside shell variables which were studied were the gas flowrate and temperature.

Influence of Gas Flowrate. Increasing the flowrate of the external gas stream improved the rate of heat transfer to the stream (Equation 5.19), thereby increasing the gas exit temperature. However, counterbalancing this effect was the increase in the heat load of the gas stream as the flowrate was increased. This resulted in more heat being required to raise the temperature of the gas by 1 degC, thus reducing the maximum exit temperature. Therefore it was necessary to optimise the gas flowrate in the absorption column in order to achieve as high an exit stream temperature as possible. The range of gas flowrates used in these studies was 1- 6 gs^{-1}. In all cases the inlet gas temperature was set to 90 °C while the inlet steam and lithium bromide temperatures were 100 °C. The inlet lithium bromide flowrate was set to approximately 1.53 mls^{-1}, although the actual mass flowrate did vary slightly because the liquid density increased as the absorbent concentration increased (In addition the mass flowrate of absorbent through the column increased as steam was absorbed).

The results obtained for the simulation model show that there was an initial increase in the exit gas temperature as the gas flowrate was increased from 1 to 3 gs^{-1}. This improvement was due to an increase in overall heat transfer coefficient (HTC_o). The rate of heat transfer increased more than the heat capacity ($\dot{m}_G . c_P$) of the gas stream. Above gas flowrates of 3 gs^{-1} the heat capacity of the stream became dominant and increased faster than the HTC_o,

which resulted in the exit gas temperatures dropping. These observations agree well with those obtained in Chapter 4, Section 4.4.3 'Effect of Varying the Gas Flowrate', where there was similar peak in the gas exit temperatures at a gas flowrate of 3 gs^{-1}, Figure 5.19, again indicating a cross over between the dominance of the heat transfer rate of the absorber and the heat capacity of the gas stream.

However, the variation in the predicted exit gas temperatures was not as great as the experimental results. This pattern of behaviour was repeated for different inlet absorbent concentrations over the range 65- 68 %w/w. It was felt that the heat losses to the surroundings were higher than predicted, which resulted in better exit temperatures for the simulation model.

Figure 5.19 also shows that increasing the inlet absorbent concentration increases the exit gas temperature by 2degC per percent. It was also shown that as the steam flowrate to the absorption tube increased, the gas exit temperature decreased due to lower equilibrium absorbent concentrations, Tables 5.6 and 5.7. In all the simulation runs, for different inlet steam flowrates, the exit steam flowrates was zero, indicating that all the steam had been absorbed into the absorbent stream. This highlighted the fact that the maximum amount of steam absorbed into the lithium bromide was greater than that obtained in the simple absorption model. In this particular model, as heat was being continuously removed from the absorption tube by the external gas stream, the refrigerant and absorbent phases were constantly shifted from an equilibrium state. As a result, more steam was absorbed into the liquid phase, resulting in lower equilibrium concentrations and also lower gas exit temperatures.

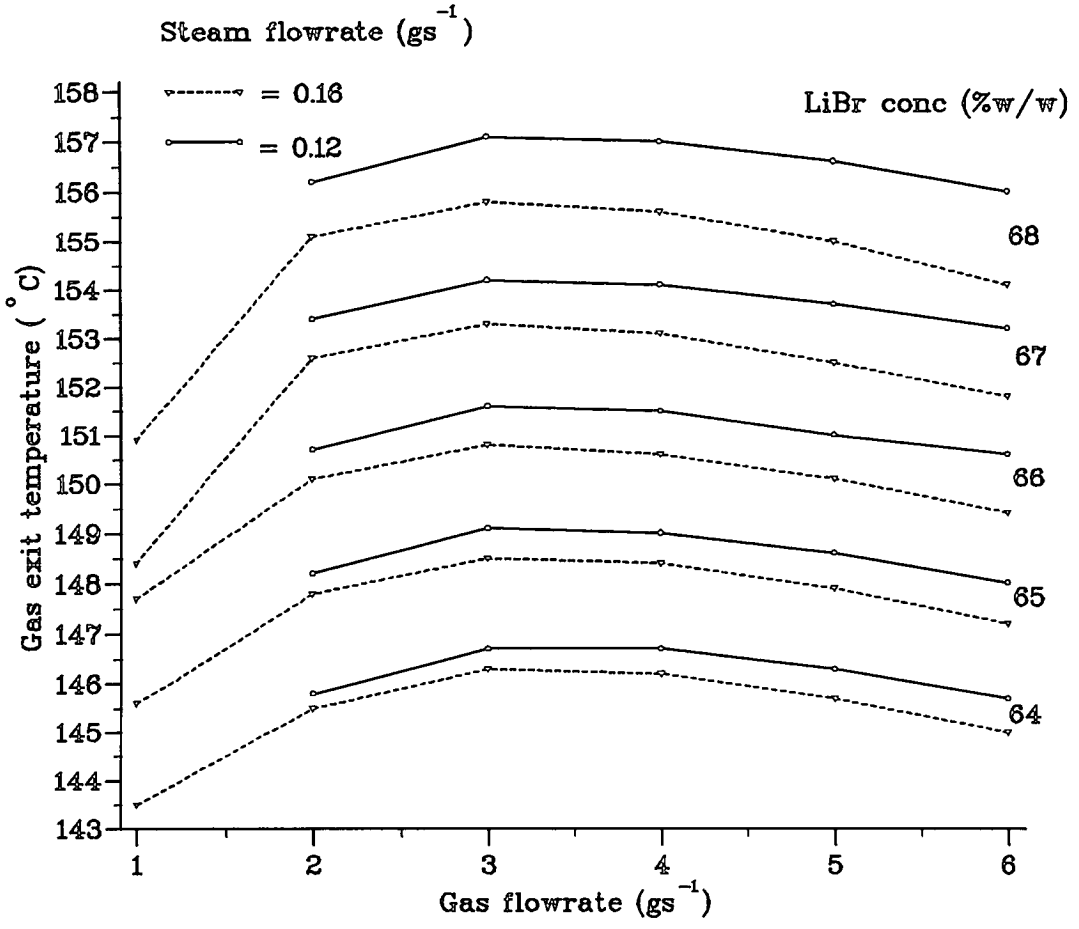

Figure 5.19: Variation of the gas exit temperature with gas flowrate, for counter-current heat removal, over a range of inlet LiBr concentrations.

$\dot{m}_G$ (gs^{-1})	$\dot{m}_{RS_{top}}$ (gs^{-1})	$w_{LiBr_{top}}$ (%w/w)	F_r (-)	$w_{LiBr_{bot}}$ (%w/w)	$T_{G_{bot}}$ (°C)	$T_{I_{bot}}$ (°C)
1.00	0.16	64	14.4	60.6	144	157
1.00	0.16	65	14.6	61.5	146	159
1.00	0.16	66	14.8	62.3	148	161
1.00	0.16	67	15.0	62.8	148	162
1.00	0.16	68	15.2	63.8	151	165
2.00	0.12	64	19.1	60.8	146	156
2.00	0.12	65	19.4	61.8	148	159
2.00	0.12	66	19.7	62.8	151	162
2.00	0.12	67	20.0	63.8	153	165
2.00	0.12	68	20.3	64.8	156	168
2.00	0.16	64	14.4	59.9	146	154
2.00	0.16	65	14.6	60.8	148	156
2.00	0.16	66	14.8	61.8	150	159
2.00	0.16	67	15.0	62.8	153	162
2.00	0.16	68	15.2	63.8	155	165
3.00	0.12	64	19.1	61.8	147	156
3.00	0.12	65	19.4	61.8	149	159
3.00	0.12	66	19.7	62.8	152	161
3.00	0.12	67	20.0	63.8	154	164
3.00	0.12	68	20.3	64.8	157	168
3.00	0.16	64	14.4	59.9	146	153
3.00	0.16	65	14.6	60.8	149	156
3.00	0.16	66	14.8	61.8	151	159
3.00	0.16	67	15.0	62.8	153	161
3.00	0.16	68	15.2	63.8	156	164
4.00	0.12	64	19.1	61.8	147	156
4.00	0.12	65	19.4	61.8	149	158
4.00	0.12	66	19.7	62.8	152	161
4.00	0.12	67	20.0	63.8	154	164
4.00	0.12	68	20.3	64.8	157	167
4.00	0.16	64	14.4	59.9	146	153
4.00	0.16	65	14.6	60.8	148	156
4.00	0.16	66	14.8	61.8	150	158
4.00	0.16	67	15.0	62.8	153	161
4.00	0.16	68	15.2	63.8	156	164

Table 5.6: Results for the simulation model with countercurrent heat removal to externally flowing gas stream (1- 4 gs^{-1}).

$\dot{m}_G$ (gs^{-1})	$\dot{m}_{RS_{top}}$ (gs^{-1})	$w_{LiBr_{top}}$ (%w/w)	F_r (-)	$w_{LiBr_{bot}}$ (%w/w)	$T_{G_{bot}}$ (°C)	$T_{I_{bot}}$ (°C)
5.00	0.12	64	19.1	61.8	146	155
5.00	0.12	65	19.4	61.8	149	158
5.00	0.12	66	19.7	62.8	151	161
5.00	0.12	67	20.0	63.8	154	164
5.00	0.12	68	20.3	64.8	157	167
5.00	0.16	64	14.4	59.9	146	153
5.00	0.16	65	14.6	60.8	148	155
5.00	0.16	66	14.8	61.8	150	158
5.00	0.16	67	15.0	62.8	152	161
5.00	0.16	68	15.2	63.8	155	164
6.00	0.12	64	19.1	61.8	146	155
6.00	0.12	65	19.4	61.8	148	158
6.00	0.12	66	19.7	62.8	151	161
6.00	0.12	67	20.0	63.8	153	164
6.00	0.12	68	20.3	64.8	156	167
6.00	0.16	64	14.4	59.9	145	153
6.00	0.16	65	14.6	60.8	147	155
6.00	0.16	66	14.8	61.8	149	158
6.00	0.16	67	15.0	62.8	152	161
6.00	0.16	68	15.2	63.8	154	164

Table 5.7: Results for the simulation model with countercurrent heat removal to externally flowing gas stream (5- 6 gs^{-1}).

It can be seen from Figure 5.19 that there was a significant improvement in the exit gas temperature as the gas flowrate was increased from 1 to 2 gs^{-1}, for a steam flow of 0.16 gs^{-1}. This was due to a low heat transfer coefficient obtained when operating at a gas flow of 1 gs^{-1}, which reduced the rate of heat transfer to the fluid. The results for 1 gs^{-1} also show a slight drift at the higher concentrations: this was probably due to the program not converging to desired conditions within the normal duration of the program cycle. At a flowrate of 1 gs^{-1}, the heat load of the gas stream was extremely sensitive to changes and took longer to converge than the flowrates. However, the results obtained were reasonably consistent and continued to exhibit the expected trends despite the poor results obtained for a gas flowrate of 1 gs^{-1}.

Conversely, results obtained for the absorber when operating with a gas flowrate of 1 gs^{-1} and an absorption steam flowrate of 0.12 gs^{-1} were highly unstable. This was due to the difficulty in obtaining convergence with the calculation method used. For countercurrent flows, it was first of all necessary to predict the gas temperature at the top of the column before executing the program. The program then proceeded to calculate the stream temperature profiles, starting at the top of the column and working to the bottom. Once the program had reached the bottom of the column, it was necessary to test the final gas stream conditions to see if they agreed with the input values. In the case of operating with gas flows of 1 gs^{-1}, the rate of convergence was slow, thus resulting in incorrect predicted profiles.

Gas Inlet Temperature. There was little variation in the exit gas temperature as the inlet gas stream temperature was varied, Figure 5.20, which was also observed in the experiments carried out with the reheat absorber (Chapter 4, Section 4.4.5 'Effect of Varying the Inlet Stream Temperatures'). This indicated that gas streams were only dependent upon the inner absorption

conditions for achieving high gas exit temperatures.

It was therefore concluded that any reasonable inlet temperature could be used to achieve a exit gas temperature of between 140- 150 °C, depending on the inlet absorbent concentration. Indeed, boosting the inlet temperature from 90 °C, a typical temperature for a dryer exhaust stream, to 120 °C (achieved through preheating with LP steam for example) would only result in an improvement of around 1 degC in the exit temperature achieved. Therefore, it was felt that preheating of the gas stream was not worth while. Indeed the LPS would be better used to provide extra heat within the absorption cycle, where a proportion of the heat would be upgraded to around 140- 150 °C.

Absorption tube:-		
Steam conditions:	Flow values = 0.16 gs^{-1}.	Inlet temperature = 100 °C.
Lithium bromide conditions:	Flow = 2.36 gs^{-1}.	Inlet temperature = 100 °C. Inlet concentration range = 65- 68 %w/w.
Outer annulus:-		
Gas conditions:	Flow = 3.0 gs^{-1}.	Inlet temperature = 40, 90, 120 °C.

Of greater significant was the influence of inerts, upon the exit temperature which was also shown on Figure 5.20 for comparison. It would be of greater importance to ensure that there were no inerts present in an actual absorption cycle, than to worry about preheating the process heat sink stream. Finally, a linear relationship was again shown to exist between the gas exit temperature and the inlet absorbent concentration.

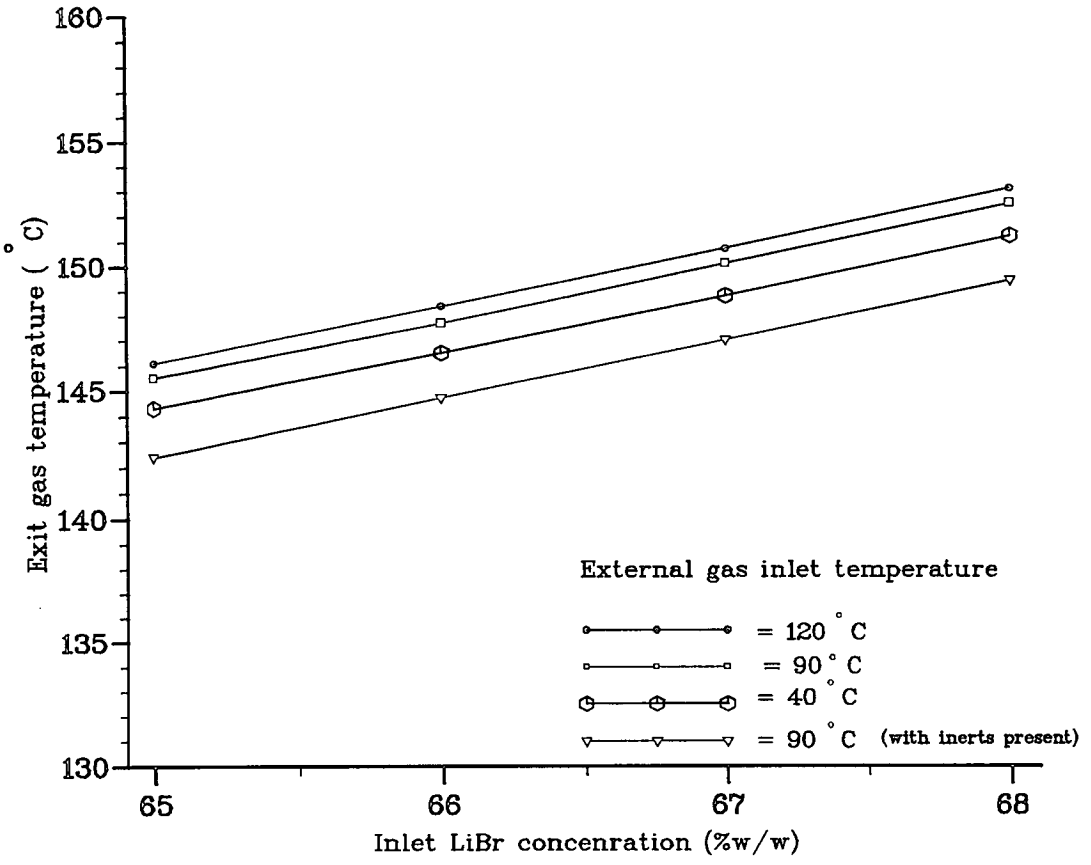

Figure 5.20: Effects on the gas exit temperature for varying its inlet temperature.

5.6.2 Cocurrent Heat Removal.

Another variant of the simulation model was the cocurrent absorption of steam into a concentrated lithium bromide solution with external heat removal to a cocurrent gas stream. Similar absorbent stream temperature profiles were obtained for this model as for the countercurrent case, Figure 5.21.

Once again, the interfacial temperature was seen to increase rapidly until it reached an equilibrium state as determined from the interfacial concentration and pressure. The subsequent dip in temperature occurred as the gas was introduced to the column and the transfer of heat to the outer shell began. As heat was being continuously transferred to the external gas stream, more steam was being absorbed into the liquid phase. Over the bottom portion of the column, the absorbent stream temperature levels off as rate of heat transfer to the gas stream decreases. The temperature of the absorbent stream then remained approximately constant, as the last of the steam was absorbed, balancing the rate of heat transfer to the heat of relase from the absorption of the steam.

Absorption tube:-		
Steam conditions:	Inlet temperature =	100 °C
	Flow value =	0.16 gs^{-1}
Lithium bromide conditions:	Flow =	2.36 gs^{-1}
	Inlet temperature =	100 °C
	Inlet concentration =	66 %w/w
Outer annulus:-		
Gas conditions:	Flow = 3.0 gs^{-1}.	Inlet temperature = 90 °C.

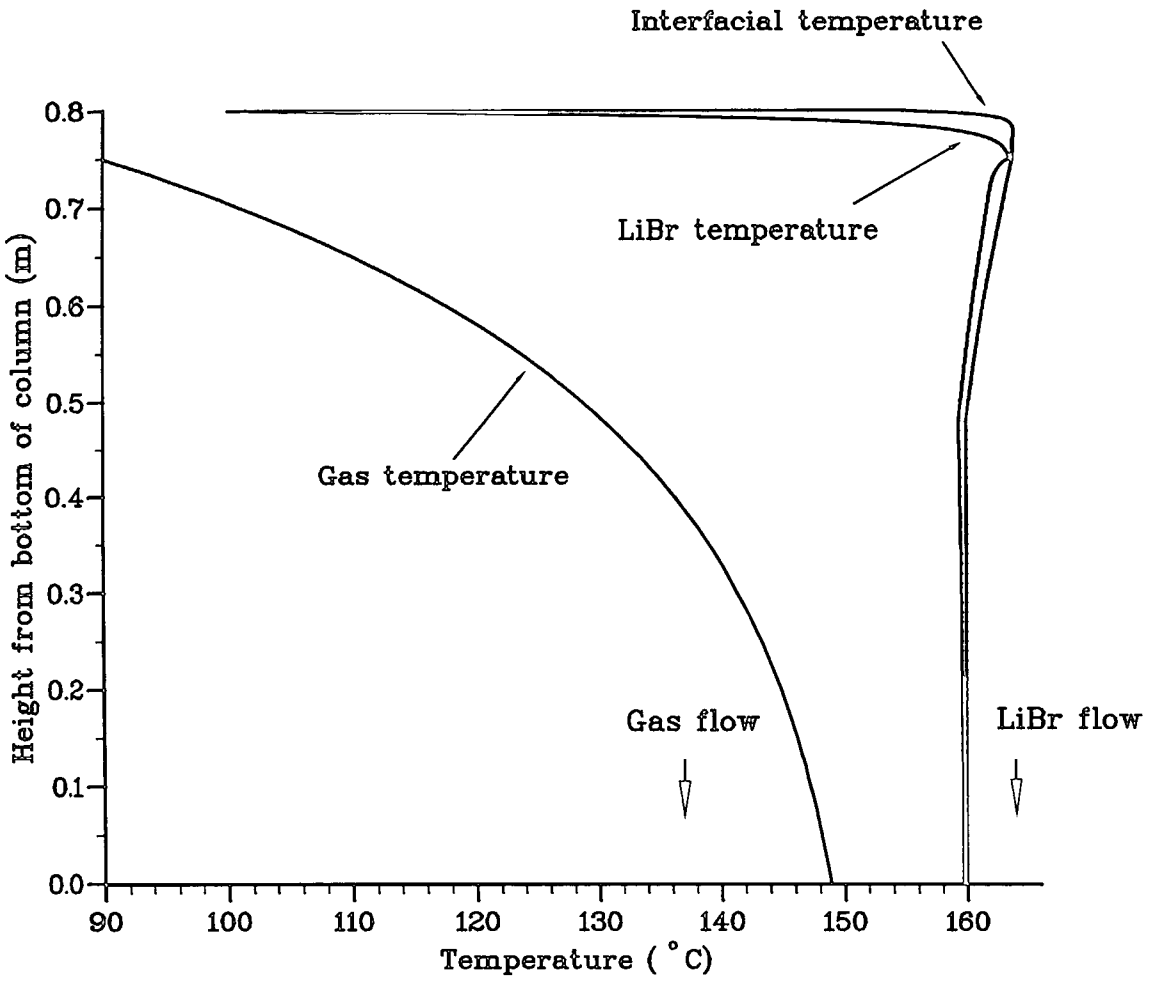

Figure 5.21: Temperature profiles in absorption column, for cocurrent heat removal.

Influence of Lithium Bromide Flowrate.

The following section deals with the effect of increasing the lithium bromide stream flowrate, for constant steam flowrate and constant circulation ratio. The tests were carried out assuming an external gas stream with a flowrate of 3 gs^{-1} and an inlet temperature of 90 °C. Similar results were obtained as with the countercurrent heat removal model. Figure 5.22 again shows the linear increase in the gas exit temperature with absorbent concentration. Again, the cases with the low steam and high absorbent flows show higher exit temperatures due to the higher exit absorbent concentrations, see Table 5.8.

$\dot{m}_{LiBr_{top}}$ (gs^{-1})	$w_{LiBr_{top}}$ (%w/w)	F_r (-)	$w_{LiBr_{bot}}$ (%w/w)	$T_{G_{bot}}$ (°C)	$T_{I_{bot}}$ (°C)
2.30	64	14.4	59.9	144	154
2.33	65	14.6	60.8	146	157
2.37	66	14.8	61.8	149	160
2.40	67	15.0	62.8	152	163
2.44	68	15.2	63.8	154	166
4.59	64	38.3	62.4	150	161
4.66	65	38.9	63.4	153	164
4.73	66	39.5	64.4	156	168
4.80	67	40.0	65.4	159	171
4.87	68	40.6	66.4	162	174
4.59	64	14.4	60.1	145	155
4.66	65	14.6	61.0	147	157
4.73	66	14.8	61.8	149	160
4.80	67	15.0	62.8	152	163
4.87	68	15.2	63.8	155	166

Table 5.8: Results for the simulation model with cocurrent heat removal to externally flowing gas stream, with varying LiBr flowrate.

For comparison, the constant circulation ratio case showed a very slight improvement in exit temperature when operating with at higher lithium bromide flowrates. The difference was due to the higher absorbent stream heat capacity which meant that the absorbent stream maintained a higher temperature through the absorption column, as heat was transferred to the gas

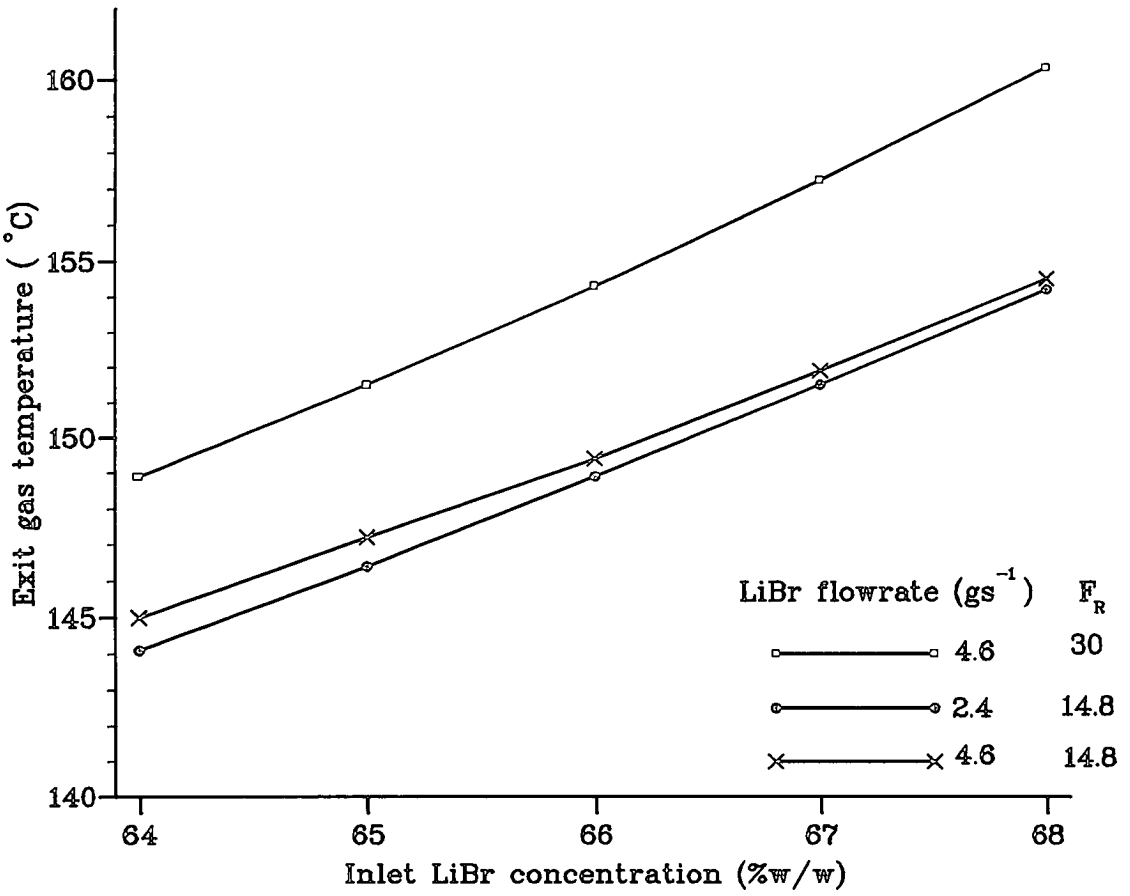

Figure 5.22: Variation of the gas exit temperature with inlet LiBr flowrate, for a range of inlet LiBr concentrations.

stream. Therefore, the temperature difference between the absorbent and gas streams was higher than when operating with a smaller absorbent flow (which would lose its heat more quickly). As the inlet absorbent stream concentration was increased, corresponding to an increase in the maximum absorption temperature, there was a similar increase in the heat transferred to the gas stream, thereby decreasing the influence of the absorbent stream heat capacity on the exit gas temperature.

Effect of Varying the Gas Stream Conditions.

As with the countercurrent heat removal model, the influence of the gas flowrate was studied, while operating with an absorbent flowrate of approximately 1.3 mls^{-1} ($\sim$ 2.4 gs^{-1}). In all cases the inlet gas temperature was 90 °C.

The results obtained for the cocurrent mode of operation again show the same trends as obtained in both the countercurrent heat removal studies-experimental and theoretical. The cocurrent profiles for the cases with a steam flowrate of 0.16 gs^{-1} almost exactly follow those of the cases with 0.12 gs^{-1} but with an inlet absorbent concentration which was 1 %w/w lower. Indeed, inspection of Table 5.9 shows that the exit absorbent concentrations were shifted by 1 % for the higher steam flowrate. A direct comparison between the modes of operation for selected results (see following Table) was drawn on Figure 5.24,

Absorption tube:-				
Steam conditions:	a)	b)	c)	d)
Flowrate	0.12 gs^{-1}	0.12 gs^{-1}	0.16 gs^{-1}	0.16 gs^{-1}
Inlet T_{RS} = 100 °C				
Lithium bromide conditions:				
Flowrate =	2.33 gs^{-1}	2.44 gs^{-1}	2.33 gs^{-1}	2.44 gs^{-1}
Inlet w_{LiBr} =	65 %w/w	68 %w/w	65 %w/w	68 %w/w
Inlet T_{LiBr} = 100 °C				

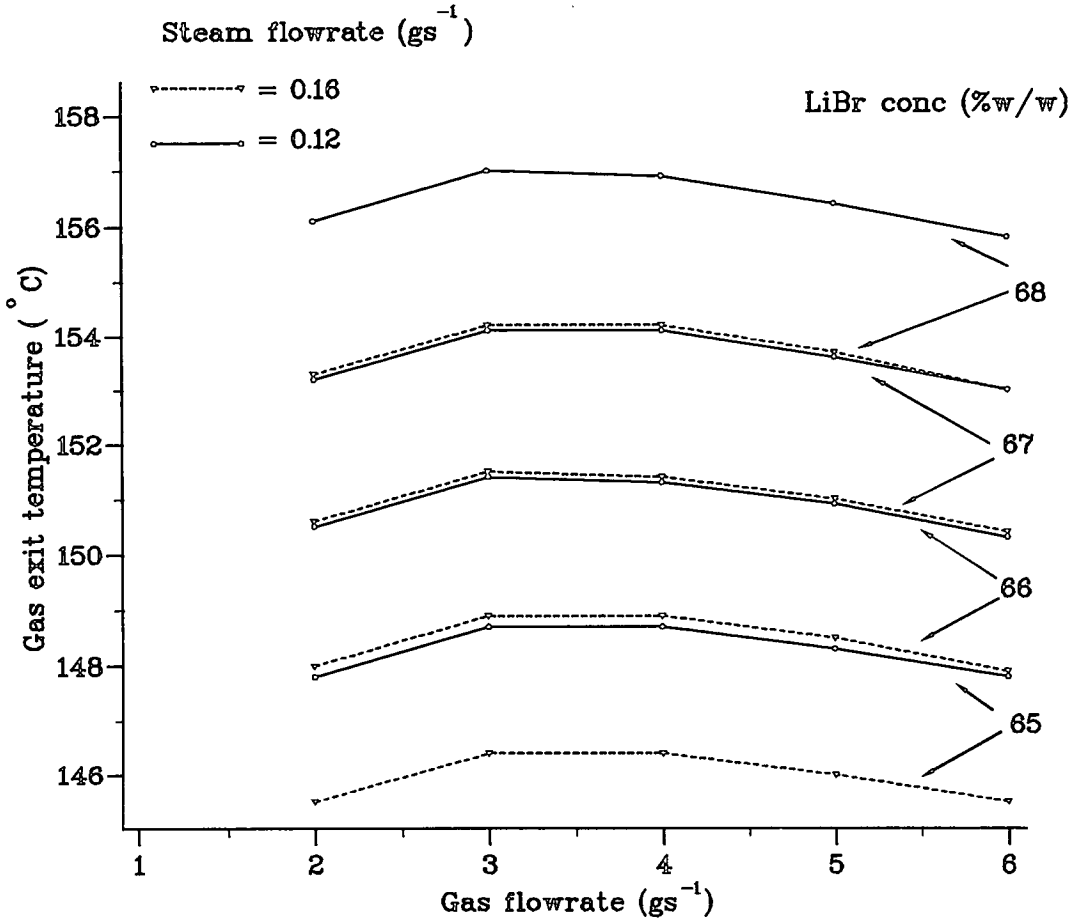

Figure 5.23: Variation of the gas exit temperature with gas flowrate, for cocurrent heat removal, over a range of inlet LiBr concentrations.

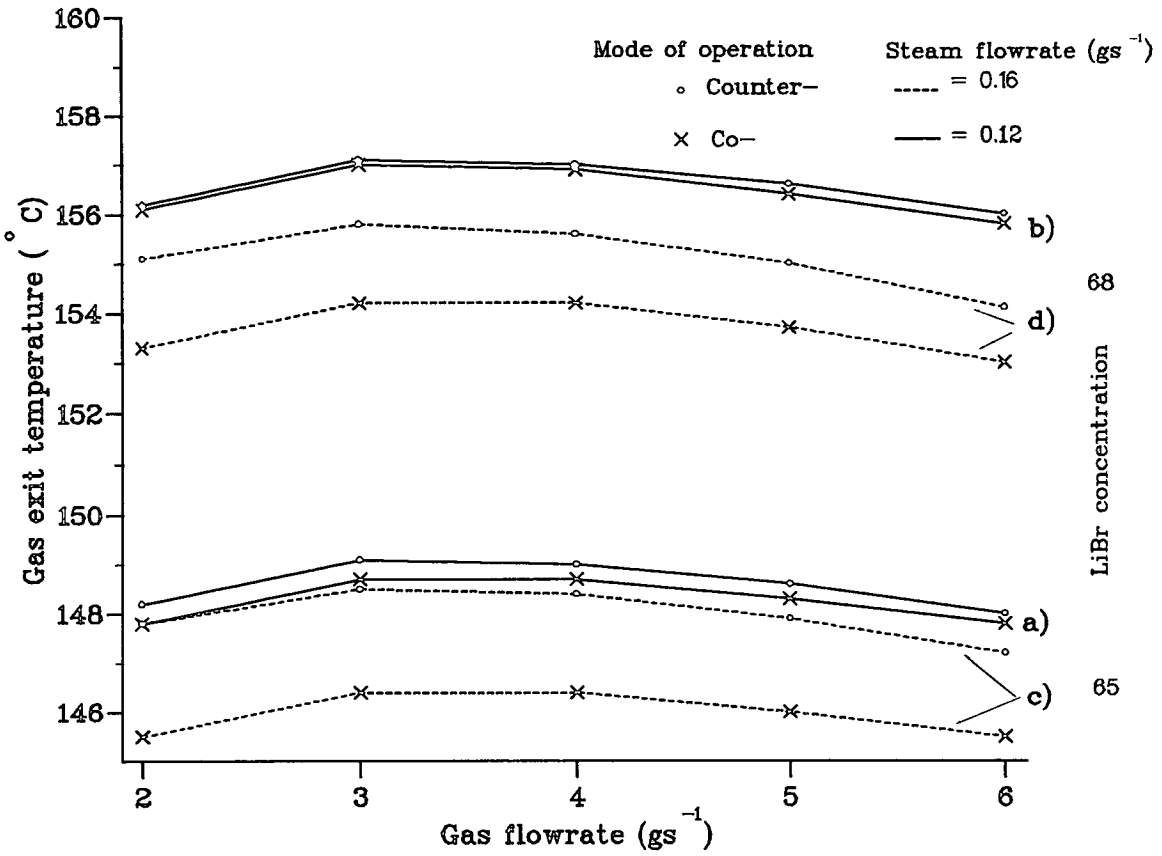

Figure 5.24: Comparison between heat removal modes for range of operating conditions.

Figure 5.24 shows very little improvement in the exit temperature for the countercurrent model over the cocurrent model, when operating with a steam flowrate of 0.12 gs^{-1}, for both concentrations (65 and 68 %w/w). However, when the absorber was operated with an initial steam flowrate of 0.16 gs^{-1}, there was a greater improvement in the exit gas temperature for the countercurrent model.

In the countercurrent model, the gas came into contact with the most concentrated absorbent stream at the top of the column, resulting in higher gas exit temperatures. However, in the cocurrent mode, heat was progressively transferred to a gas stream which was increasing in temperature. Therefore the 'hottest' gas only came into contact with the weakest lithium bromide solution, the absorption temperature of which was lower than that for the countercurrent model.

5.6.3 Comparison of Results for Co-/ Counter- Current Heat Removal.

The studies of the simulation model with co- and counter- current heat removal have exhibited similar results when operating under the same conditions. There was a slight improvement in gas exit temperature in the countercurrent model, simply because the hottest gas was being heated by the most concentrated, and thus hottest, absorbent stream. The similarities arose because of the approximately constant temperature profile within the absorption column. As shown in the simple absorption model, the steam was quickly absorbed into the liquid phase, resulting in a rapid increase in the absorbent temperature. Therefore, in both cases the gas stream was being heated by a stream which

$\dot{m}_G$ (gs^{-1})	$\dot{m}_{RS_{top}}$ (gs^{-1})	$w_{LiBr_{top}}$ (%w/w)	F_r (-)	$w_{LiBr_{bot}}$ (%w/w)	$T_{G_{bot}}$ (°C)	$T_{I_{bot}}$ (°C)
2.00	0.12	65	19.4	61.8	148	160
2.00	0.12	66	19.7	62.8	151	163
2.00	0.12	67	20.0	63.8	153	166
2.00	0.12	68	20.3	64.8	156	169
2.00	0.16	65	14.6	60.8	146	157
2.00	0.16	66	14.8	61.8	148	160
2.00	0.16	67	15.0	62.8	151	163
2.00	0.16	68	15.2	63.8	153	166
3.00	0.12	65	19.4	61.8	149	160
3.00	0.12	66	19.7	62.8	151	163
3.00	0.12	67	20.0	63.8	154	166
3.00	0.12	68	20.3	64.8	157	169
3.00	0.16	65	14.6	60.8	146	157
3.00	0.16	66	14.8	61.8	149	160
3.00	0.16	67	15.0	62.8	152	163
3.00	0.16	68	15.2	63.8	154	166
4.00	0.12	65	19.4	61.8	149	160
4.00	0.12	66	19.7	62.8	151	163
4.00	0.12	67	20.0	63.8	154	166
4.00	0.12	68	20.3	64.8	157	169
4.00	0.16	65	14.6	60.8	146	157
4.00	0.16	66	14.8	61.8	149	160
4.00	0.16	67	15.0	62.8	151	163
4.00	0.16	68	15.2	63.8	154	166
5.00	0.12	65	19.4	61.8	148	160
5.00	0.12	66	19.7	62.8	151	163
5.00	0.12	67	20.0	63.8	154	166
5.00	0.12	68	20.3	64.8	156	169
5.00	0.16	65	14.6	60.8	146	157
5.00	0.16	66	14.8	61.8	148	160
5.00	0.16	67	15.0	62.8	151	163
5.00	0.16	68	15.2	63.8	154	166
6.00	0.12	65	19.4	61.8	148	160
6.00	0.12	66	19.7	62.8	150	163
6.00	0.12	67	20.0	63.8	153	166
6.00	0.12	68	20.3	64.8	156	169
6.00	0.16	65	14.6	60.8	145	157
6.00	0.16	66	14.8	61.8	148	160
6.00	0.16	67	15.0	62.8	150	163
6.00	0.16	68	15.2	63.8	153	166

Table 5.9: Results for the simulation model with cocurrent heat removal to externally flowing gas stream.

had a reasonably constant temperature.

The exit gas temperature was primarily dependent on the conditions within the absorption column- absorbent concentration, flowrate and circulation ratio.

On a computational note, the cocurrent heat removal model was considerably faster than the countercurrent model, in which it was necessary to continue the computation cycle until the inlet gas stream conditions were achieved.

5.7 Results for the Cocurrent Dehumidification Model

The other aspect of the research undertaken as part of the project was the dehumidification of humid gas streams. The dehumidification process was carried out by direct contact with a concentrated lithium bromide solution. The computer model developed previously for the reheating operation was easily adapted to model the dehumidification process. The following section investigates the performance of the absorber when operated under a range of conditions for the cocurrent flow of humid gas and concentrated absorbent solution streams. Attention was paid to both the exit temperature and the exit humidity of the gas stream.

As an initial verification of the accuracy of the model, the computer program was input with actual experimental values. The conditions input were obtained from early absorption experiments, where the temperature profile within the column was recorded at regular intervals. The profiles obtained for the

experimental and simulation runs were in reasonable agreement, although the simulation liquid temperature remained consistently higher than actually measured. The reason for this was probably due to the to inaccuracies in predicting the absorbent stream properties.

<u>Dehumidification column</u>;-	
Lithium bromide conditions:	Flow = 6.8 gs^{-1}.
	Inlet temperature = 100.0 °C.
	Inlet concentration = 64 %w/w.
Gas conditions:	Gas Flow = 2.0 gs^{-1}.
	Inlet temperature = 110.0 °C.
	Inlet water vapour flow = 0.40 gs^{-1}.
	(Humidity = 0.20 $g\text{-}_{H_2O}$ $(g\text{-}_{dry\ air})^{-1}$).
	Outlet water vapour flow= 0.31 gs^{-1}.
	(Humidity = 0.15 $g\text{-}_{H_2O}$ $(g\text{-}_{dry\ air})^{-1}$).
<u>Experimental Result</u>:-	Outlet water vapour flow = 0.31 gs^{-1}
	Exit gas temperature = 112 °C

It can be seen from Figure 5.25 that the temperature of the absorbent stream quickly rose to a maximum as the water vapour was absorbed. Figure 5.26 confirms that there was a sharp decrease in the humidity of the gas stream as the gas and liquid phases approached equilibrium. Thereafter the rate of absorption of the water vapour declined. The absorption process continued due to heat losses from the system, thereby maintaining a thermal imbalance between the phases. As a result more water vapour was absorbed as the interfacial temperature dropped. At the bottom of the column the gas, whose temperature had been lagging behind that of the liquid phase due to a lower heat transfer coefficient, was essentially in equilibrium with the liquid stream, indicating that further absorption was not possible.

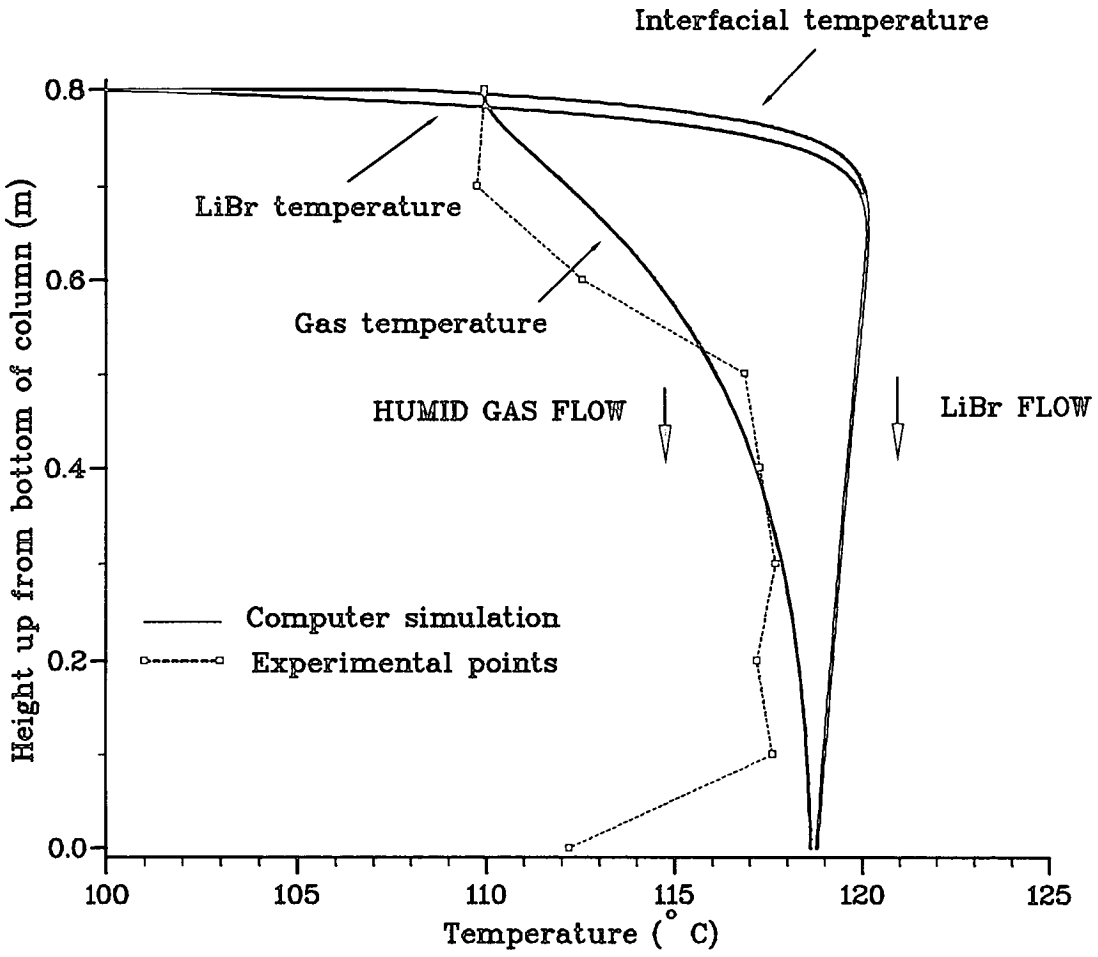

Figure 5.25: Temperature profile in absorber for cocurrent dehumidification of a humid gas stream.

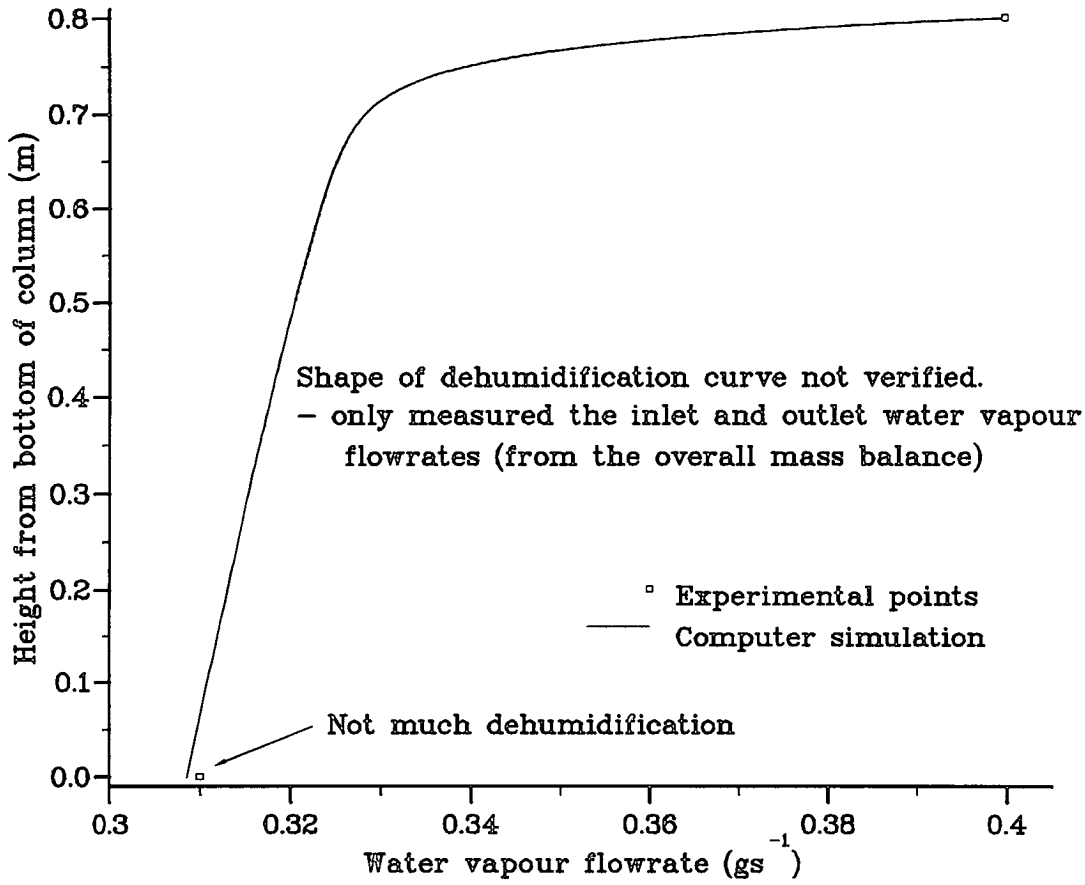

Figure 5.26: Mass profile of water vapour through the absorber for cocurrent dehumidification.

5.7.1 Influence of Gas Flowrate on Dehumidification Performance.

Simulation trials were carried out assuming constant absorbent conditions and a constant inlet gas humidity of 0.18 g-$_{H_2O}$ (g-$_{dry\ air}$)$^{-1}$ for a range of gas flowrates. Figure 5.27 shows that there was no significant difference between the exit stream temperatures at different gas flowrates, as the absorbent concentration increased. Inspection of Table 5.10 shows that for all the gas flowrates tested the exit absorbent concentrations remained constant, resulting in consistent exit gas temperatures because the equilibrium temperature for a particular inlet concentration was the same for each flowrate.

Further inspection of Table 5.10 also shows that the amount of water vapour absorbed was the same for all the gas flowrates, despite the increase in the initial water vapour flow necessary to maintain a constant inlet stream humidity. As a result the exit humidities were progressively higher as the gas flowrate increased, see Figure 5.28, because the amount of water vapour absorbed was a decreasing proportion of the initial water content of the gas stream. It was therefore concluded that the dehumidification capabilities of the absorber were dependent upon the absorbent conditions. A high inlet concentration ensured that the amount of water vapour absorbed increased. Therefore, the overall vapour absorption would be improved by maintaining a high absorption concentration which would be possible by operating the column with a higher absorbent flowrate (see Section 5.7.3).

The results for the dehumidification of a range of gas flowrates, with constant inlet humidity, were not very good. The change in gas stream humidity was only around 0.01- 0.04 g-$_{H_2O}$ (g-$_{dry\ air}$)$^{-1}$. The reason for this can be seen from Figure 5.27 which shows an increase in the exit gas temperature in comparison

$\dot{m}_G$ (gs^{-1})	$\dot{m}_{H_2O_{top}}$ (gs^{-1})	$w_{LiBr_{top}}$ (%w/w)	$\dot{m}_{H_2O_{bot}}$ (gs^{-1})	$w_{LiBr_{bot}}$ (%w/w)	$T_{G_{bot}}$ (°C)	$T_{I_{bot}}$ (°C)
2.00	0.36	60	0.32	59.2	107	107
2.00	0.36	61	0.32	60.1	109	109
2.00	0.36	62	0.31	61.1	111	111
2.00	0.36	63	0.31	62.0	113	113
2.00	0.36	64	0.30	62.9	115	115
2.00	0.36	65	0.30	63.8	117	117
2.00	0.36	66	0.30	64.7	119	119
2.00	0.36	67	0.29	65.6	121	121
3.00	0.54	60	0.50	59.2	108	108
3.00	0.54	61	0.49	60.1	109	110
3.00	0.54	62	0.49	61.0	111	112
3.00	0.54	63	0.48	61.9	113	114
3.00	0.54	64	0.48	62.8	115	116
3.00	0.54	65	0.47	63.7	117	118
3.00	0.54	66	0.47	64.6	119	120
3.00	0.54	67	0.46	65.4	121	122
4.00	0.72	60	0.68	59.1	108	108
4.00	0.72	61	0.67	60.0	109	110
4.00	0.72	62	0.67	60.9	111	112
4.00	0.72	63	0.66	61.8	113	114
4.00	0.72	64	0.65	62.7	115	116
4.00	0.72	65	0.65	63.6	117	118
4.00	0.72	66	0.64	64.4	119	121
4.00	0.72	67	0.64	65.3	121	123
5.00	0.90	60	0.85	59.1	107	108
5.00	0.90	61	0.85	59.9	109	110
5.00	0.90	62	0.84	60.8	111	112
5.00	0.90	63	0.84	61.7	113	114
5.00	0.90	64	0.83	62.6	115	116
5.00	0.90	65	0.82	63.5	116	118
5.00	0.90	66	0.82	64.3	118	121
5.00	0.90	67	0.81	65.2	120	123

Table 5.10: Results for the dehumidification simulation model for varying gas flowrate.

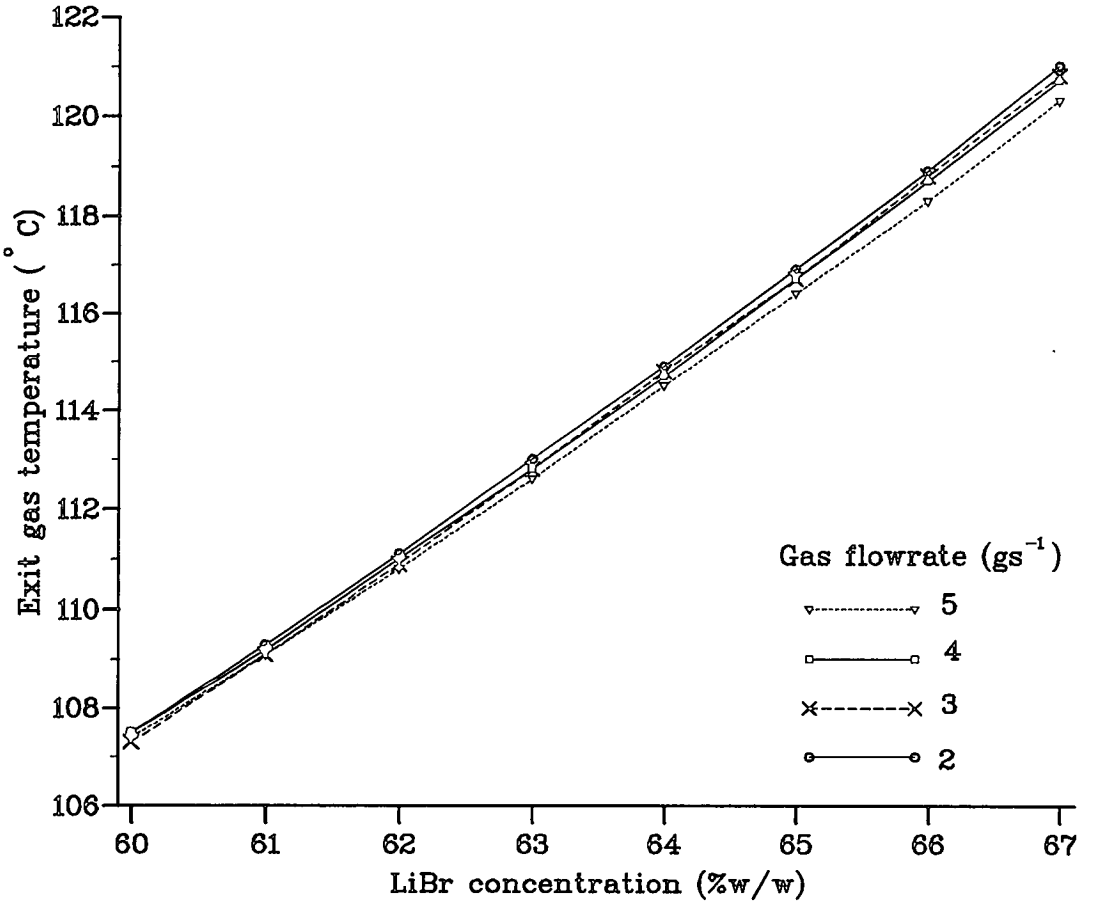

Figure 5.27: Variation of gas exit temperature, with different gas flowrates for a constant inlet humidity.

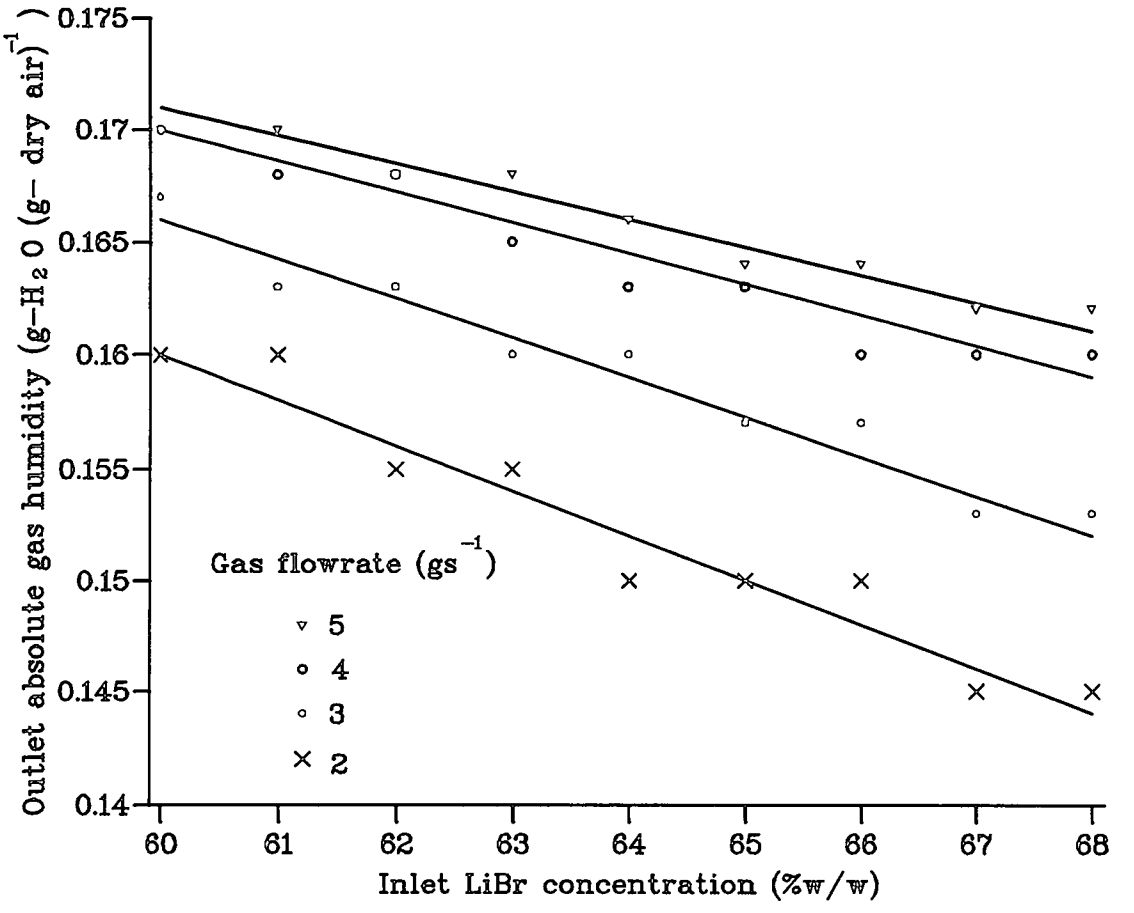

Figure 5.28: Dehumidification capabilities of the absorber column for varying gas flowrate.

to the inlet stream temperature. The change in the gas temperature increases for increasing inlet absorbent concentration. As a result, the partial pressure above the absorbent solution increased, effectively reducing the amount of water vapour which was be absorbed into the liquid phase. An improvement to the dehumidification system would be to remove the excess heat from the system and maintain the rate of absorption (see Chapter 4, Section 4.3.3 'Condenser')

5.7.2 Influence of Gas Humidity on Dehumidification Performance.

For a constant gas flowrate, the influence of the inlet gas humidity was determined, assuming constant absorbent conditions. As with the previous section, the dehumidification of the gas stream was slight and the amount of vapour absorbed only increased a little with increased absorbent concentration. Figure 5.29 again illustrates the increase in the exit stream temperature due to the absorption of the water vapour into lithium bromide.

As the amount of water vapour absorbed was essentially the same, the decrease in the gas stream humidity was also the same for the range of conditions applied. Hence, the dehumidification performance of the absorber was effectively reduced as the inlet gas humidity was increased.

$\dot{m}_G$ (gs^{-1})	$\dot{m}_{H_2O_{top}}$ (gs^{-1})	$w_{LiBr_{top}}$ (%w/w)	$\dot{m}_{H_2O_{bot}}$ (gs^{-1})	$w_{LiBr_{bot}}$ (%w/w)	$T_{G_{bot}}$ (°C)	$T_{I_{bot}}$ (°C)
3.00	0.42	64	0.37	62.9	111	111
3.00	0.42	65	0.36	63.8	112	113
3.00	0.42	66	0.36	64.7	114	115
3.00	0.42	67	0.35	65.6	116	117
3.00	0.46	64	0.40	62.9	112	113
3.00	0.46	65	0.40	63.8	114	115
3.00	0.46	66	0.39	64.7	116	117
3.00	0.46	67	0.39	65.6	118	119
3.00	0.50	64	0.44	62.8	114	114
3.00	0.50	65	0.44	63.7	116	116
3.00	0.50	66	0.43	64.6	118	119
3.00	0.50	67	0.43	65.5	120	121
3.00	0.54	64	0.48	62.8	115	116
3.00	0.54	65	0.47	63.7	117	118
3.00	0.54	66	0.47	64.6	119	120
3.00	0.54	67	0.46	65.4	121	122
3.00	0.58	64	0.52	62.7	116	117
3.00	0.58	65	0.51	63.6	118	120
3.00	0.58	66	0.51	64.5	120	122
3.00	0.58	67	0.51	65.5	121	121

Table 5.11: Results for the dehumidification simulation model, with varying humidity

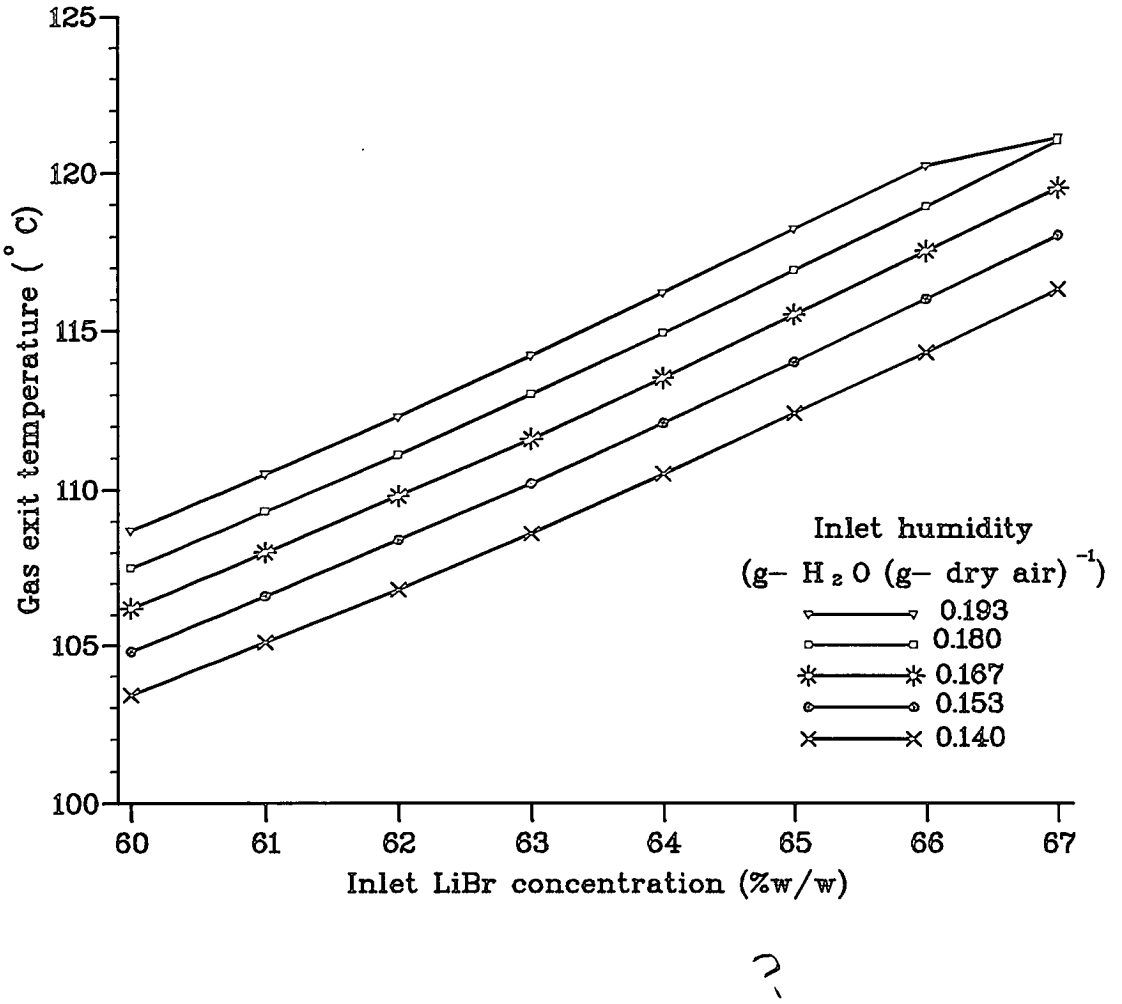

Figure 5.29: Variation of gas exit temperature and humidity for increasing gas inlet humidity.

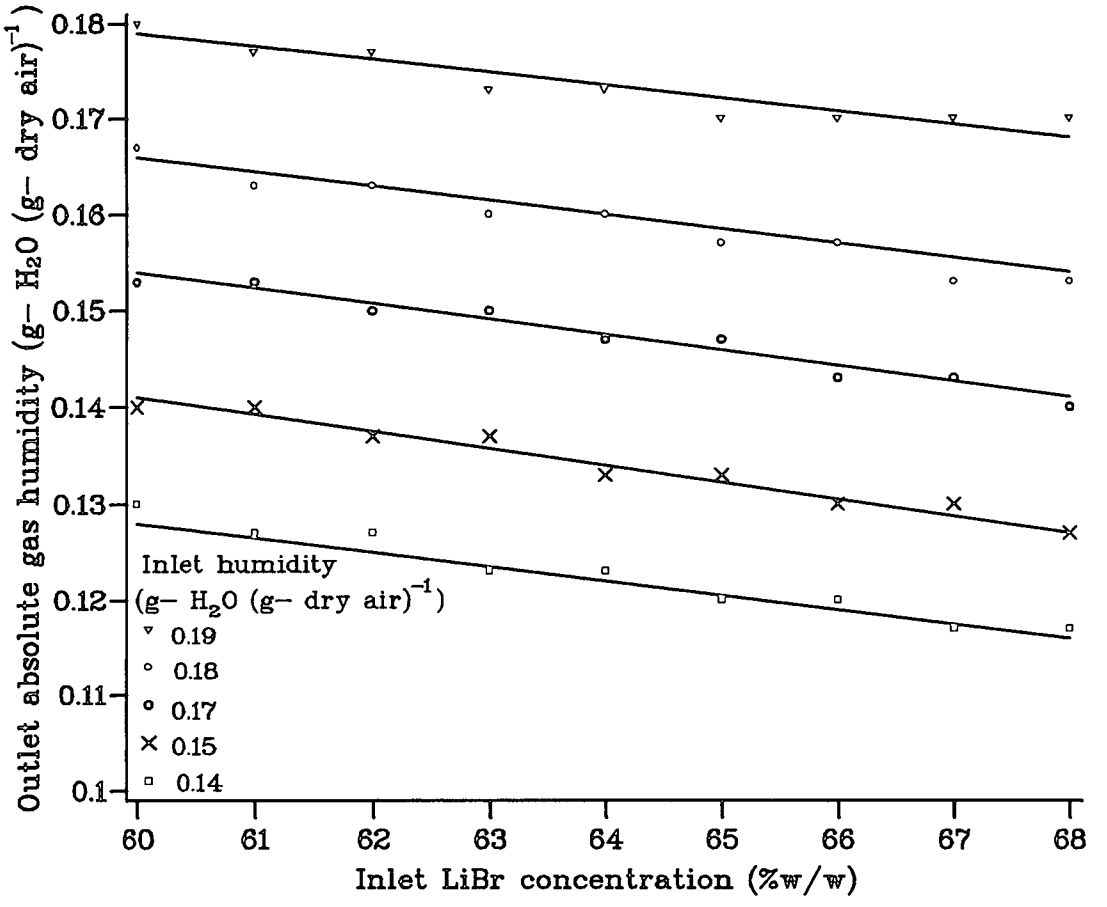

Figure 5.30: Variation in dehumidification performance of the absorber for a range of inlet humidities.

5.7.3 Influence of Lithium Bromide Flowrate.

The previous sections have indicated that the absorbent stream conditions primarily affect the amount of absorption into the liquid phase. Increasing the absorbent concentration did slightly increase the amount of water absorbed. However, as previously explained the increased absorbent concentration also resulted in an increase in the stream temperature.

Simulations were carried out using constant gas stream conditions- temperature of 90°C and an inlet humidity of 0.18 $g\text{-}_{H_2O}$ $(g\text{-}_{dry\ air})^{-1}$, at two different lithium bromide flowrates. The temperature profiles which were obtained for the two flowrates were approximately constant, Figure 5.31, although the exit temperature obtained with the higher flowrate was slighter lower due to the increased heat load of the lithium bromide stream.

$\dot{m}_G$	$\dot{m}_{LiBr_{top}}$	$w_{LiBr_{top}}$	$\dot{m}_{H_2O_{bot}}$	$w_{LiBr_{bot}}$	$T_{G_{bot}}$	$T_{I_{bot}}$
(gs^{-1})	(gs^{-1})	(%w/w)	(gs^{-1})	(%w/w)	(°C)	(°C)
3.00	2.93	60	0.50	59.2	108	108
3.00	2.97	61	0.49	60.1	109	110
3.00	3.01	62	0.49	61.0	111	112
3.00	3.06	63	0.48	61.9	113	114
3.00	3.10	64	0.48	62.8	115	116
3.00	3.14	65	0.47	63.7	117	118
3.00	3.18	66	0.47	64.6	119	120
3.00	3.23	67	0.46	65.4	121	122
3.00	5.27	60	0.49	59.4	108	108
3.00	5.35	61	0.48	60.3	109	110
3.00	5.43	62	0.47	61.3	111	112
3.00	5.50	63	0.47	62.2	113	114
3.00	5.58	64	0.46	63.1	115	116
3.00	5.65	65	0.45	64.0	117	118
3.00	5.73	66	0.44	64.9	119	120
3.00	5.81	67	0.44	65.8	121	122

Table 5.12: Results for the dehumidification simulation model with varying LiBr flowrate (decreasing F_r).

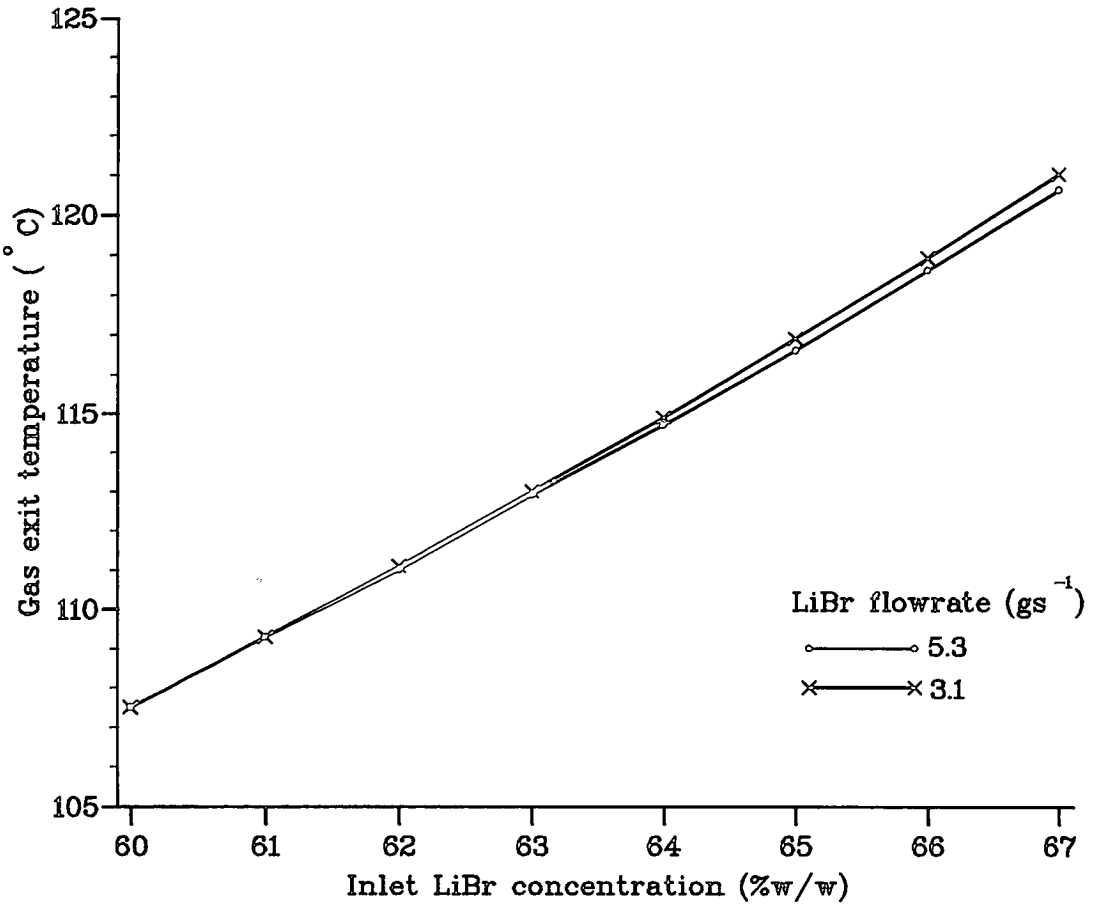

Figure 5.31: Effect on the gas exit temperature within the dehumidification column for varying LiBr flowrate.

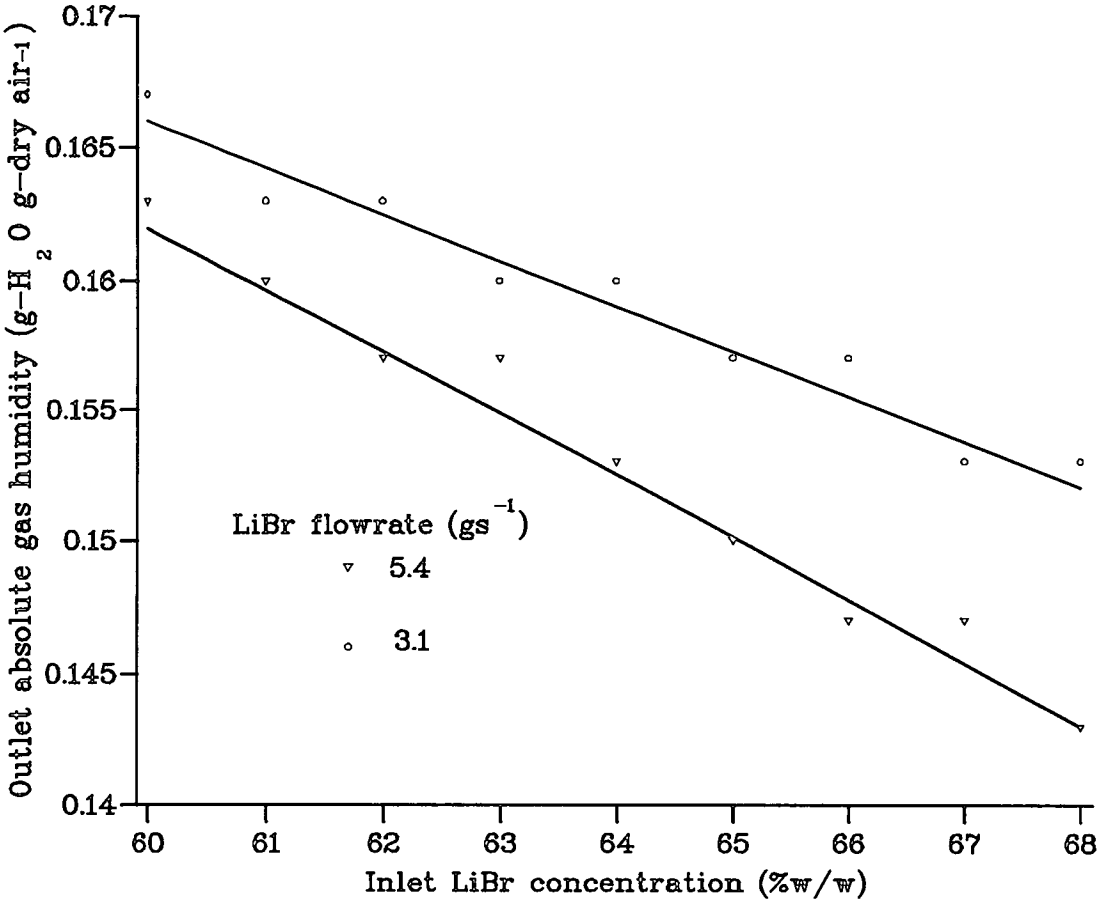

Figure 5.32: Variation of the exit gas humidity for varying LiBr flowrate.

The exit humidity of the gas stream did decrease with the higher flowrate. Indeed, the dehumidification capabilities of the absorber improved as the lithium bromide concentration increased. At the higher flowrate, the exit concentration of the liquid stream was higher therefore the exit vapour pressure was lower (despite the increase in the stream temperatures) and hence there was an improvement in the dehumidification of the absorber. However, the amount of water vapour absorbed into the lithium bromide stream remained low, indicating a low level of dehumidification. It was felt that the best way to proceed would be to remove the excess heat generated in the absorber and control the temperature of the gas and absorbent streams.

5.8 Results for the Countercurrent Dehumidification Model.

The second dehumidification program was written to investigate the enhancement in the absorption of water vapour from humid gas streams for the countercurrent flow of the gas and absorbent streams. It was felt that as the gas would be contacting the most concentrated lithium bromide solution prior to exit at the top of the absorber, that there would be an decrease in the exit gas humidity.

5.8.1 Simulation Results.

The simulation model was run firstly with experimental conditions and the results obtained compared to the experimental points. It can be seen from Figure 5.33 that the experimental temperature profile was in reasonable agreement to the profile obtained for the absorbent stream, flowing down through the column. The liquid temperature was measured, instead of the gas temperature, because liquid droplets enveloped the thermowells causing the readings to be higher than expected (see Chapter 4 'Experimental Studies'). The predicted exit gas temperature, at the top of the absorption column, was in close agreement with the experimental result. However, the bottom gas temperature (as measured) was about 15 degC lower than expected. As discussed in Section 5.4, this model used a calculation method which started at the top of the column and then worked to the bottom. Therefore, it was necessary to predict the top gas temperature and then proceed with calculations, checking the bottom temperature against the initial gas conditions input. Several iterations were required for this procedure. However, as shown in Figure 5.33 the bottom gas temperature had not converged to the initial input temperature within the maximum cycles (10).

Dehumidification column;-	
Lithium bromide conditions:	Flow = 5.31 gs^{-1}.
	Inlet temperature = 101 °C.
	Inlet concentration = 65 %w/w.
Gas conditions:	Gas flow = 2.00 gs^{-1}.
	Inlet Water vapour flow = 0.23 gs^{-1}.
	Inlet temperature = 86 °C.
Experimental Result:-	Outlet water vapour flow = 0.20 gs^{-1}
	Exit gas temperature = 102 °C

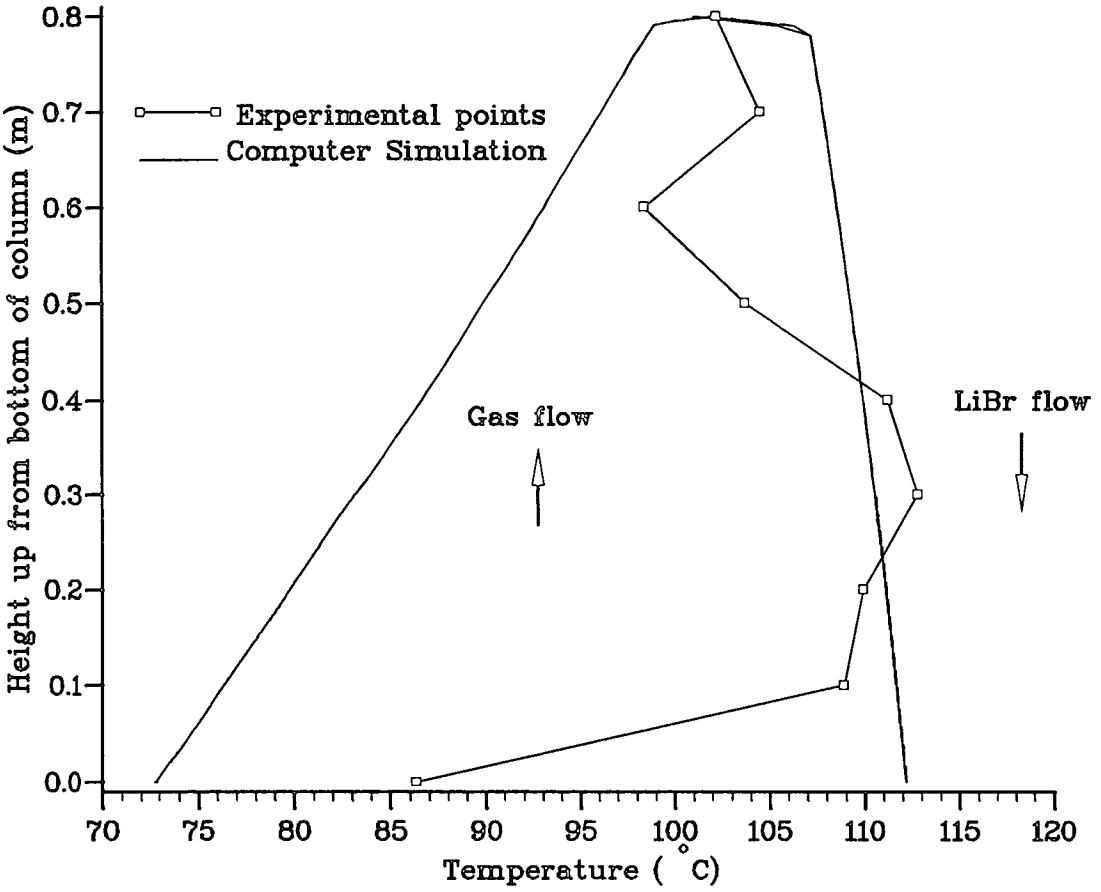

Figure 5.33: Temperature profile in absorber for countercurrent dehumidification.

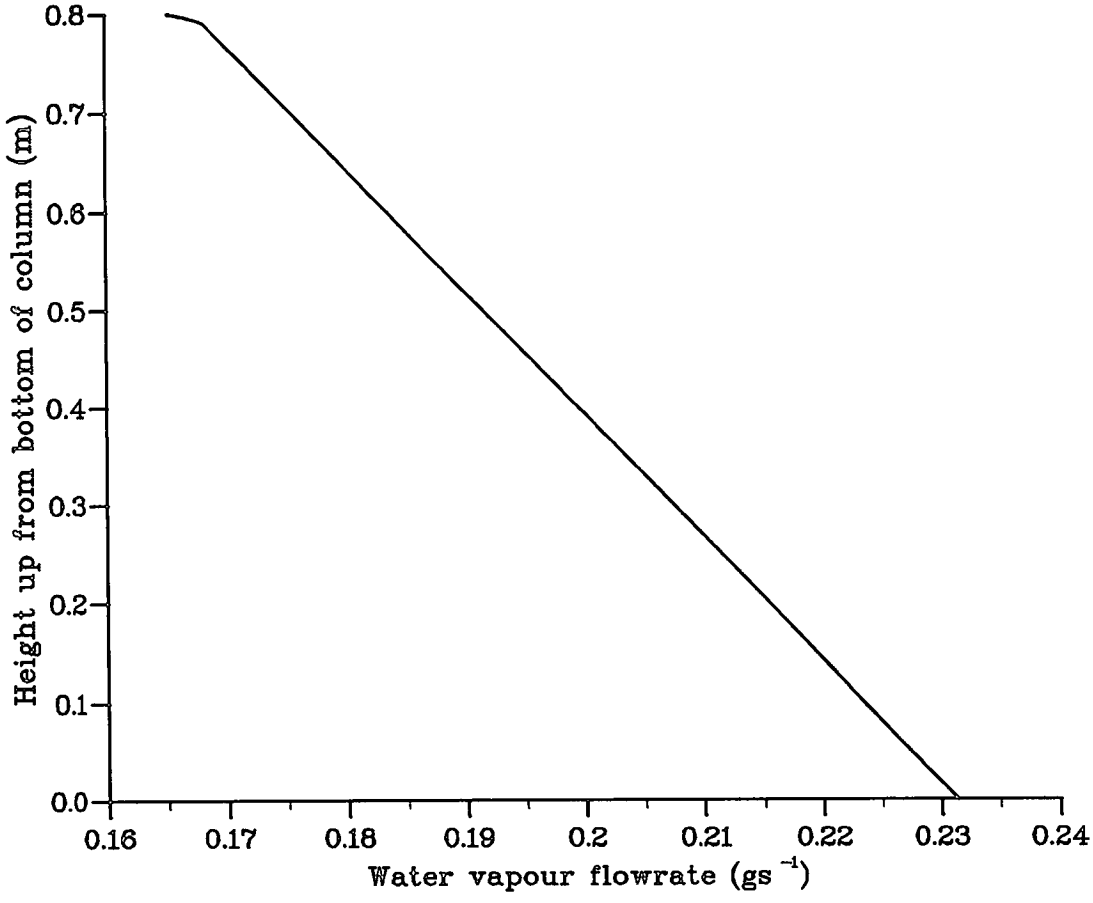

Figure 5.34: Water vapour flowrate in absorber for countercurrent dehumidification.

The profile of the water vapour flowrate through the absorber is shown in Figure 5.34. It can be seen that there was a steady rate of absorption of water vapour into the lithium bromide stream through most of the column. However, at the top the rate of absorption increased dramatically. The improvement in absorption also coincided with sharp increases in the temperatures of the gas and lithium bromide streams (Figure 5.33). The overall amount of water vapour absorbed was $0.06 gs^{-1}$, this corresponded to a change in the gas humidity from 0.11 $g\text{-}_{H_2O}$ $(g\text{-}_{dry\ air})^{-1}$ to 0.08 $g\text{-}_{H_2O}$ $(g\text{-}_{dry\ air})^{-1}$.

It was concluded that the sudden variation in the temperature of the two process streams was due to the thermal and mass imbalance at the top of the column as the concentrated absorbent solution entered the top of the absorber. Hence, there was a sharp increase in the water vapour absorbed, which resulted in a subsequent release of heat. As the simulation progressed down through the column, there was a more gradual increase in the gas stream as heat was being transferred from the liquid phase. The interfacial and bulk absorbent stream temperatures, which were essentially identical, remained approximately the same through the column after an equilibrium state had been reached.

In addition to testing the model with experimental conditions, another test simulation was carried out at a gas flowrate of 3 gs^{-1} (inlet humidity 0.12 $g\text{-}_{H_2O}$ $(g\text{-}_{dry\ air})^{-1}$). The previous studies indicated that maintaining a high absorbent concentration in the absorber was important for achieving a high absorption temperature. Similarly, for dehumidification, lower vapour pressures were exerted above highly concentrated absorbent solutions for a given temperature. Therefore, the inlet lithium bromide concentration input was 65 %w/w, which was felt to be the maximum absorbent concentration which could have been actually used in the experimental apparatus because of the risk of crystallisation. The liquid stream flowrate chosen was 7.8 gs^{-1}, which would not vary much in concentration as it flowed through the column. It should be noted

that in a full scale absorption heat transformer, there is a price to be paid for operating the cycle with a large inlet absorbent flowrate as this increases the total liquid circulating round the cycle and consequently raises the pumping costs of the system.

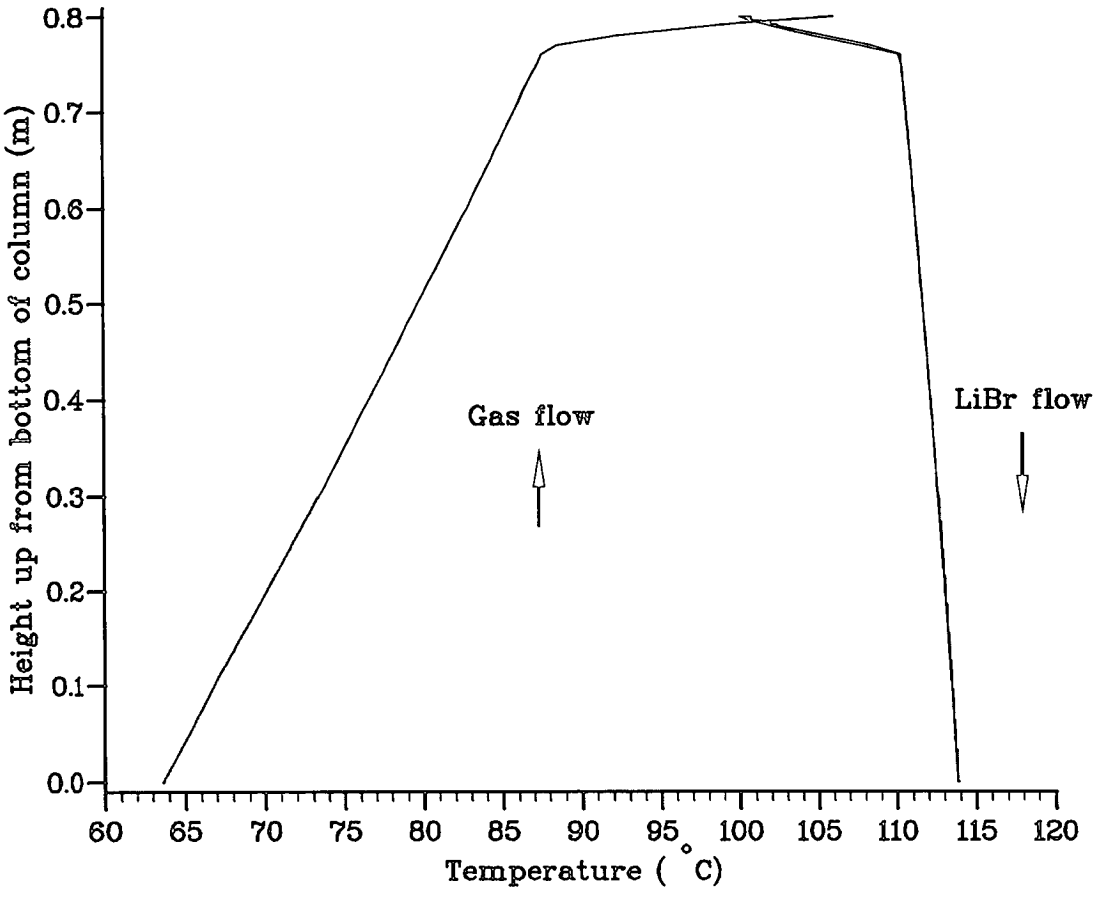

Figure 5.35: Variation in temperature profiles for countercurrent dehumidification at a high gas flowrate.

Similar temperature profiles were obtained for this test as in the previous simulation run, Figure 5.35. However, convergence problems were experienced in trying to obtain the bottom, inlet gas temperature.

The amount of water absorbed was 0.11 gs^{-1}, which resulted in an exit gas humidity of 0.08 $g\text{-}_{H_2O}$ $(g\text{-}_{dry\ air})^{-1}$), which would be too high if the stream was to be recycled back to the drying chamber. Again, a sharp decrease in the water vapour flowrate was shown over the top 0.05 cm of the absorption column.

Observations.

The results obtained for the countercurrent dehumidification model were not very good. Realistic exit gas stream temperatures and water vapour flowrates were obtained for the simulation runs carried out. However, there were problems in converging the bottom gas temperature to the initial value input at the start of the run. Part of the reason was because of the low gas heat load, which resulted in large temperature variations as water was absorbed, releasing heat. Therefore, although the overall profiles obtained for the model were realistic with respect to the absorption process, the actual temperatures output from the model were not. The main conclusions from running this model were:

- Rapid absorption of water vapour at the lithium bromide inlet, as the two streams reach equilibrium. The resultant release of heat caused the temperature of the streams to change rapidly.
- Absorbent temperature rapidly increased at the top of the column, before progressing through the column at a near constant value, indicating that the stream was in near equilibrium with the gas stream.
- The bulk absorbent and interfacial temperatures were identical over the length of the column. This was a result of the very large heat and mass transfer coefficients in the liquid phase.

- Gradual increase in the gas temperature, as heat was transferred from the hotter absorbent stream because the heat transfer coefficient between the interface and the gas stream was low.
- After the initial rapid absorption, the absorption process continued at a much slower rate. As heat was being transferred to the cooler gas stream, and because of heat losses, there was a constant shift in mass equilibrium between the two streams, therefore the absorption process was sustained.

The simulations carried out with the countercurrent dehumidification model were similar, but more difficult to model to those of the cocurrent case. It was again shown that the dehumidification of humid gas streams was small, principally because the heat of absorption was not being removed from the absorber. Therefore, the temperature of the gas and liquid streams increased until an equilibrium state was reached where very little further absorption occurred. The amount of vapour absorbed was slightly higher for the countercurrent model, this was simply because the exit gas stream was contacted with the inlet lithium bromide solution.

5.9 Conclusions.

The results obtained from each of the simulation models compared favourably with the experimental data collected (Chapter 4 'Experimental Studies'). The program written for simple absorption with heat removal to an external gas stream was tested extensively with a range of inlet conditions to find the optimum operating conditions necessary to achieving a high gas exit temperature.

The dehumidification models were not examined in as much detail as the reheat process. The reason for this was because the results obtained for the various simulation runs carried out did not show a high level of dehumidification. The exit gas humidities were higher than those required in order to make the gas stream suitable for recycle to the drying process. This highlighted the importance of removing the heat of absorption in order to achieve a low vapour pressure above the absorbent solution and therefore a low water vapour partial pressure.

In each of the models, the most important variable was the inlet absorbent concentration. A high absorbent concentration was required for the reheat studies in order to obtain as high an exit gas temperature as possible; in the dehumidification studies, lower partial pressures were obtained when the concentration in the absorption column was maintained at a high level. A summary of the effects of each of the primary variables and the main problems in achieving the objectives of the models are given in Tables 5.13 and 5.14.

Parameter	Operating conditions
LiBr concentration	High- to obtain maximum absorption temperature. Limited to 68%w/w due to crystallisation problems.
LiBr flowrate (&Circulation ratio)	High- maintain concentration through column
Gas flowrate	Best results for $3gs^{-1}$-
Mode of operation	Cocurrent absorption of steam into LiBr, generating high absorption temperature. Countercurrent heat removal to external gas
Problems	Inerts- reduced partial pressure of steam and reduced the maximum absorption temperature

Table 5.13: Optimal operating parameters for the simulation model with cocurrent absorption and heat removal to an external gas stream.

Parameter	Operating conditions
LiBr concentration	High- to maintain lower partial pressure. Limited to 65%w/w
LiBr flowrate	High- maintain concentration through column
Mode of operation	Countercurrent flows of gas and LiBr, to maximise dehumidification of gas stream
Problems	Need to remove heat of absorption in order to achieve a low water vapour pressure.

Table 5.14: Optimal operating parameters for the dehumidification simulation model.

Reheat Simulations.

The objective of the absorption model with simultaneous heat removal to an external gas stream was to maximise exit gas temperature. In the experimental studies used, the influence of inerts upon the performance of the absorption reheat column was recognised as a potential problem. The results presented for the simulation models in Sections 5.6.1 and 5.5 confirmed these early assumptions. It was also be noted that although every care was taken to ensure that inerts were removed from the experimental absorber prior to the start of each experimental run, their influence could not be removed completely. Therefore, when the column was operated at a low steam flowrate the exit temperatures obtained were particularly poor due to the increased effect of the inerts lowering the effect steam partial pressure. Hence, although the simulations with the ideal model (with no inerts) indicated that the reheat absorption column could be operated with low steam flow, in order to achieve the highest exit gas temperatures, this was not possible or even practical.

Dehumidification Simulations.

The dehumidification model was written to study the performance of a direct contact absorption column for the purpose of removing water vapour from humid gas streams. The simulation results obtained were not very good. Ideally exit humidities of between 0.03- 0.05 $g\text{-}_{H_2O}$ $(g\text{-}_{dry\ air})^{-1}$ were sought, for the purpose of making the humid gas streams suitable for recycling. However, as shown in these studies the temperature of the streams increased as the water vapour was absorbed into the absorbent stream. Therefore, a modification to the dehumidification model would be to include a heat removal routine into the program. The aim of the routine would be to remove the heat of absorption from the column and therefore operate the column isothermally. As a result the vapour pressure of the absorbent stream would be lowered thereby increasing the rate of absorption into the liquid and reduce the water vapour partial pressure.

5.9.1 Future Developments.

The models developed in this project have concentrated solely upon the absorption process, either for dehumidification or reheating. Ultimately the program would be extended to the whole absorption cycle, allowing detailed simulation studies to be carried out quickly without the need to construct a pilot plant. In addition, the model could readily simulate different operating conditions or even be adapted to for different configurations.

The potential development of these programs should not be restricted to the investigation of heat recovery and recycling of humid gas streams for spray drying. The heat transformer models could readily be used to study many other chemical engineering unit operations (e.g distillation). The power of computing systems is continually growing, making it progressively easier and quicker to model complex systems. Therefore, the development of this model is seen as being an important design tool for process engineers interested in incorporating a heat recovery system to a process.

A further development of the model would be to extend its use to include other working fluid combinations, provided that physical data were available. The benefit is that different absorption fluids could be tested for different operating conditions, allowing the performance of each system to be compared with other fluid pairs without the need for an extensive experimental programme.

Chapter 6

Industrial Case Study.

6.1 Overview.

An extensive study of a spray drying operation was undertaken at ICI (FCMO) (now Zeneca plc), at their Grangemouth works, where there are several spray drying units. These dryers are the final unit operation in the manufacture of a range of products. The investigation was split into two main parts:

1. An experimental study and assessment of the existing gas cleaning equipment, with the aim of gaining a detailed insight of this part of the drying operation.

2. The applicability and benefits of an absorption heat transformer as a heat recovery system for the drying operation. [1]

First of all, a brief overview of spray drying will be outlined, providing the necessary background for the remaining sections of this chapter and illustrate areas where improvements to the normal drying operation could be made. An in depth study of drying is giving in Masters' book 'Spray Drying' ([170]) and also in the book by Nonhebel and Moss 'Drying of solids' ([180]), on which some of the following points are based.

6.2 Background to Spray Drying.

6.2.1 Dryer Design.

The four main stages of a spray drying operation were laid out by Masters [170].

- Atomization of feed.
- Spray to gas contact- distribution and mixing.
- Moisture removal- rate of removal and the final moisture content.
- Product recovery.

[1] Further details of the studies undertaken at ICI (FCMO) are described in the reports- 'Absorption heat recovery from humid airstreams' ([32]) and 'Spray drying- Gas cleaning study' ([33]).

As well as the above design considerations to ensure that the material is dried to the correct specifications, it is becoming increasingly important to operate the dryer efficiently. Industrial spray dryers require a vast amount of primary energy in order to remove moisture from an extensive range of products (see Chapter 1 'Introduction', Table 1.2 'Range of products dried industrially'). In most cases direct fired burners, Figure 6.1, are used to generate the high temperatures required for drying. Dryers usually involve a single pass operation with little or no heat recovery; therefore areas of potential savings include:

- Heat recovery from the exhaust gas leaving the dryer.
- Regular maintenance of the dryer to prevent leaks and the resultant loss of energy. (The dryers are operated under a slight positive pressure; therefore any leaks would result in hot gas escaping to the surroundings.)

Finally, another important issue is the risk of environmental pollution, which is becoming increasingly important. There are two main pollution problems associated with dryer exhaust streams:

- Fine particles in the exhaust gas stream being released into the atmosphere, which could contaminate the surrounding area.
- Visible exhaust plumes due to oversaturation of the gas stream as it cools down upon leaving the dryer stack, causing a visible nuisance.

Operating Conditions.

The conditions of operation are critical to the preservation of the properties of the final dried product and its overall quality. These conditions include the

product residence time, the gas throughput, stream inlet temperature and water vapour partial pressure. Typical particle residence times in dryers range from a few seconds to a few minutes (Masters' provides an equation capable of determining the residence time based upon the size of the dryer [170], pp62- 64).

In many cases the product is sensitive to the temperature of operation. If the temperature were too high, the product could easily be degraded and if flammable might even ignite. It is not uncommon to find that if a dryer were operated at too high a temperature, the rate of evaporation from the wet material would be so rapid that particles could disintegrate, resulting in a greater percentage of small, shattered particles in the exhaust stream. These particles would need to be removed from the gas stream prior to discharge to the atmosphere.

As well as controlling the inlet temperature to the dryer, it is also important that the gas flow does not lead to 'dead- zone' areas in the drying chamber. 'Dead zones' occur in areas where there is insufficient gas circulation, causing semi- dried product to be deposited on the chamber walls where it builds up. The consequences of 'dead zones' are:

- The efficiency of the dryer would be reduced. Indeed if 'dead zones' should occur it can be concluded that the dryer was not designed satisfactorily.
- Subsequent build up could lead to over- drying, degradation and possibly ignition of the product.
- Product deposits which require chamber cleaning, usually using water, thus increasing the water consumption of the plant. The build up of deposits would also result in a drop in the production rate of the final dried material.

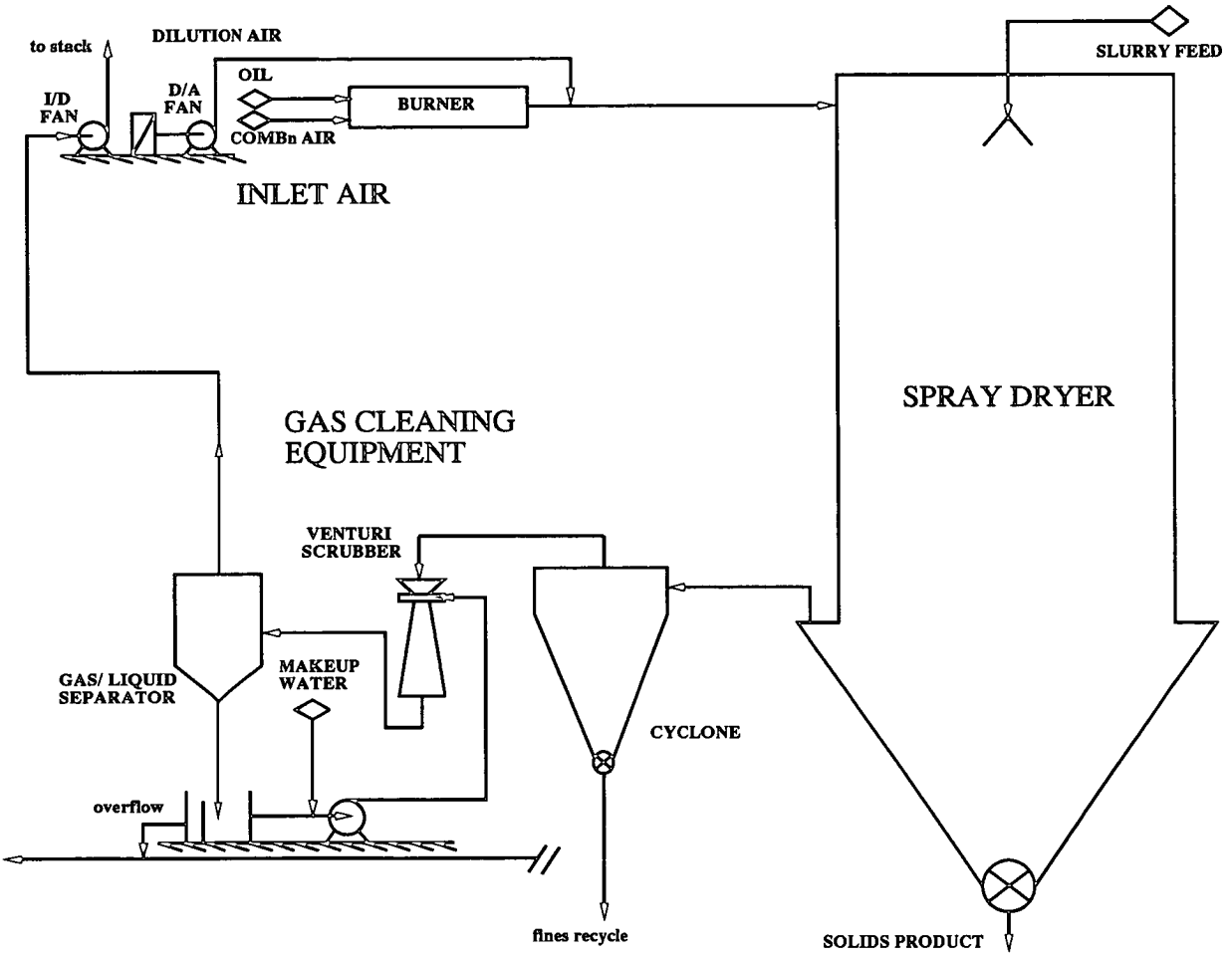

Figure 6.1: Schematic of drying operation, including gas cleaning equipment.

Atomization.

The drying of the product is also affected by the method of delivery of the material to the drying chamber. Solid particles are commonly delivered in a slurry containing less than 50%w/w solids, the remainder consisting of a solvent, which must be removed. In most cases the solvent is water. The slurry, upon entry to the drying chamber, is atomized to increase the rate of mass transfer of the water to the hot, drying medium, which is typically air.

The dispersion of the wet product at the top of the drying chamber is a very important design feature as it is necessary to ensure that there is an even distribution of slurry throughout the chamber. If the slurry were unevenly dispersed this could lead to an over concentration of the slurry in one area of the dryer, resulting in the slurry taking longer to dry, which could result in wet product being discharged from the chamber.

Various methods are used to inject slurry into the dryer including spinning discs or pressure nozzles (Figure 6.2). There are usually several injectors evenly spaced around the top of the dryer to ensure an even distribution of feed. Problems can be experienced with these injectors as a result of blockages in the associated pipework. This is a common problem associated with transporting a feed stream containing solid particles.

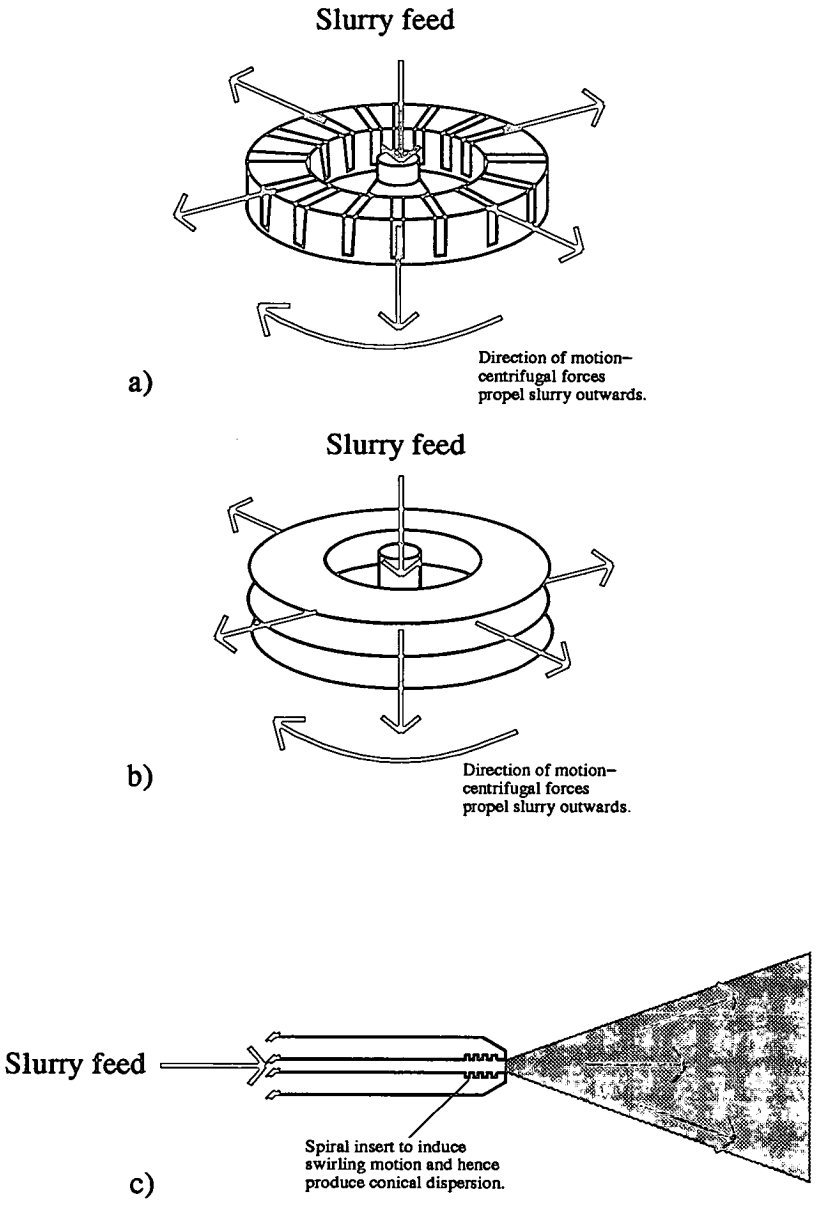

Figure 6.2: Slurry injection methods- a) Spinning curved vane b) Spinning disc c) Pressure nozzle.

6.2.2 Gas Cleaning Equipment.

After the product has been dried it is necessary to separate the solid particles from the humid gas produced. Figure 6.1 shows a product discharge point in the bottom of the dryer chamber, where the majority of the dried material is collected. However, the smaller particles are carried over in the exhaust gas stream and these must be separated from this stream, prior to its discharge to atmosphere. There are different types of gas cleaning equipment, the most common are listed below and also shown in Figure 6.3:

- Cyclones.
- Bag filters.
- Wet scrubbers, mostly commonly used are venturi scrubbers.
- Gravity settlers.
- Electrostatic precipitators.

Cyclones are capable of collecting particles down to a 'cut size' of 5.5 μm. The cut size represents the particle size which has a collection efficiency of 50 %, half of the particles are collected while the remainder pass through. As the particle size continues to decrease, the collection efficiency drops further, as shown in Figure 6.4.

Cyclones are can be operated over a wide range of operating conditions, between 25- 125 % of the design gas flowrate, without any adverse effects. The pressure drop across cyclones is usually 400- 2000 Nm^{-2}.

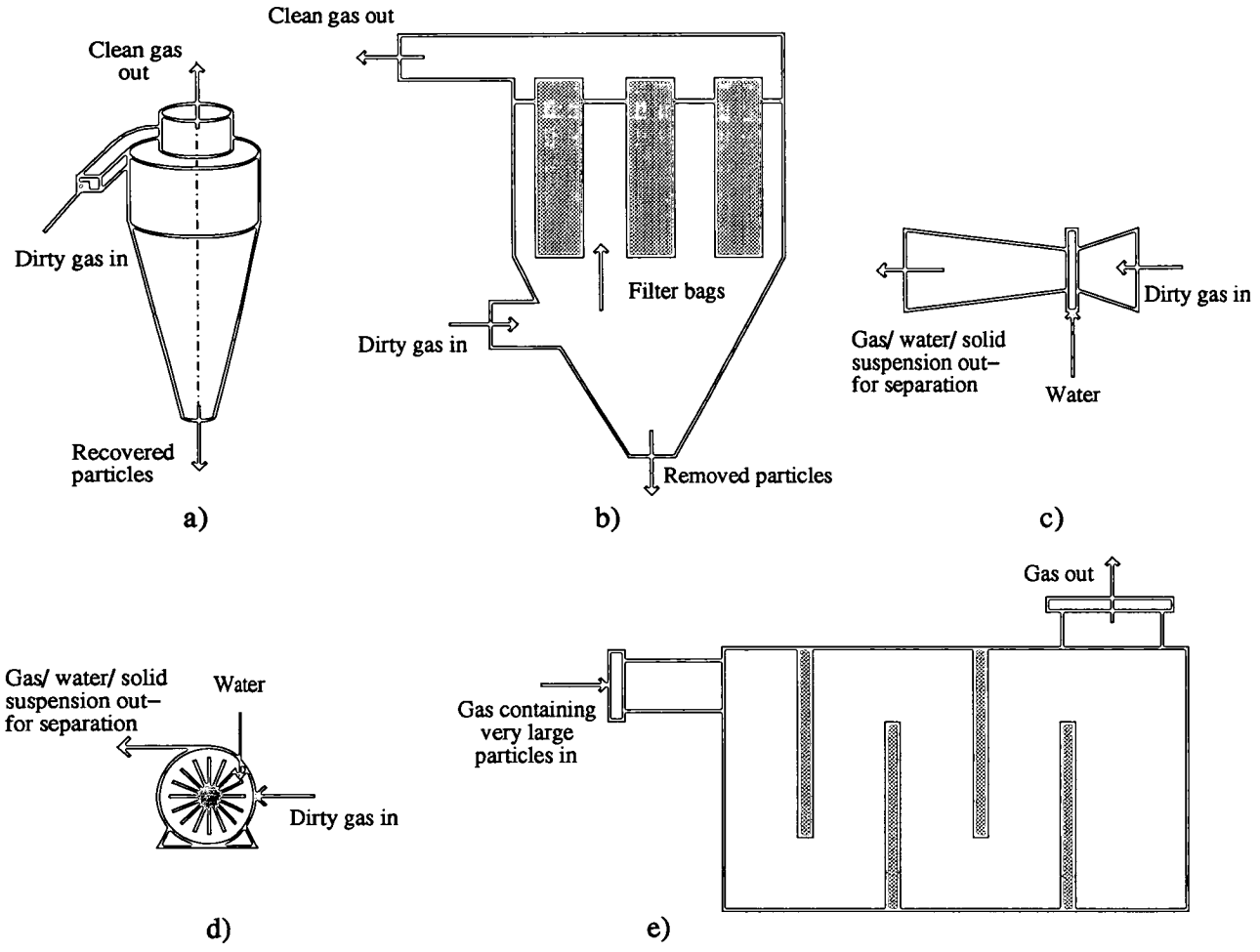

Figure 6.3: Examples of gas cleaning equipment a) Cyclone b) Bag filters c) Venturi scrubber d) Mop scrubber e) Gravity settler.

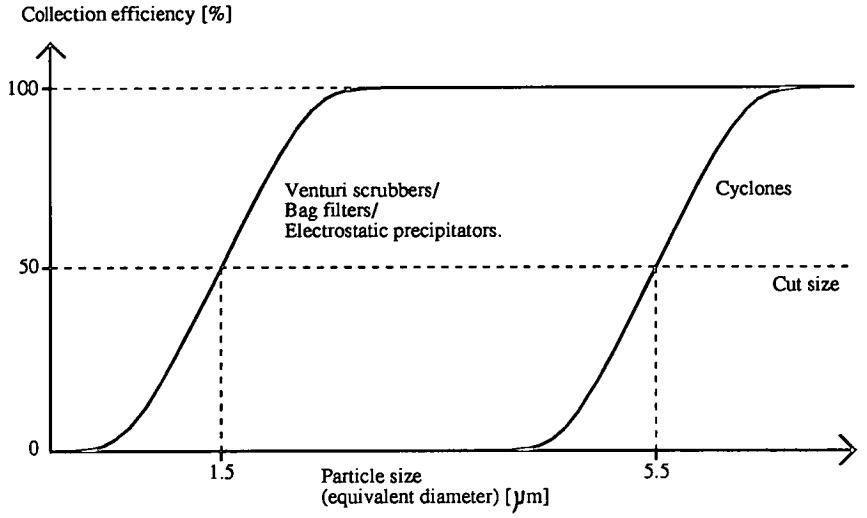

Figure 6.4: Collection efficiency curves showing typical cutoff sizes for venturi scrubbers and cyclones.

Bag filters. It can also be seen from Figure 6.4 that bag filters have a 'cut size' of 1.5 μm. Wet scrubbers and electrostatic precipitators are also capable of removing particles down to a size of 1-2 μm. As with cyclones, the normal operating pressure drop is approximately 400- 2000 Nm^{-2}. Bag filters have a very high product recovery rate. However, they are expensive due to high capital and maintenance costs. If the dried product has a high market value, and a high recovery rate is particularly important, then this may justify the use of bag filters to recover the product.

During normal operation, it is important that the filter cloth does not become worn, as this could result in the cloth tearing. The collection efficiency of the equipment would be reduced dramatically. As such there would normally be at least two filter arrangements, each of which would contain a few filter cloths, which would be operated in rotation. Hence one unit would be online while the other was under going maintenance/ cleaning.

An important condition of recovering waste heat from the exhaust gas is that the gas is clean, otherwise this could lead to fouling of the heat exchanger. Therefore, bag filters are extremely useful in aiding the recovery of heat from the exhaust gas stream, as they operate at a constant temperature. The fabrics which are used for filters can withstand temperatures up to 130 °C, corresponding to typical gas exit temperatures from drying chambers.

Gravity settlers are only good for removing large particles above 200 μm and as such are not normally used as primary gas cleaning devices.

Electrostatic precipitators have a very good collection rate, even down to small particles of the order 1-2 μm, and negligible pressure drop. However, they are not normally used for gas cleaning because of their high capital and operating costs. There is also a high risk of explosion due to the high operating voltages needed to generate the strong electrical field necessary for recovering the small dust particles.

Wet scrubbers. Finally, venturi and mop scrubbers have a very good collection efficiency down to very small 'cut sizes', typically 1.5 μm. However, to achieve this it is necessary to operate the scrubber at high pressure drops, typically 3000- 75000 Nm^{-2}. The collection efficiency in a scrubber can improved by increasing the pressure drop (see section 6.2.3 and [33]).

Cyclones, bag filters and electrostatic precipitators allow recovery of the dried product for further processing, whereas wet scrubbers rely upon the solid particles being transferred from the gas phase into the liquid phase, where they form a dilute suspension in the liquid. As the solid concentration in the liquid is

low it is not economical to reprocess the liquid stream and recover the solid particles. Therefore, scrubbers are not used for initial gas cleaning and are usually used in conjunction with other cleaning devices so as to minimise the risk of solids escaping.

In this particular study, a cyclone was used as the first stage of gas cleaning, with recovered particles being collected for further processing. The second stage of cleaning used a venturi scrubber to ensure that the majority of the fine particles were removed from the gas, which was then vented to atmosphere.

6.2.3 Venturi Scrubbers.

The most common method of gas cleaning involves the 'wetting- out' of the solid particles from the gas stream, either using a venturi scrubber or, as shown in Figure 6.3, a mop scrubber.

While investigating the performance of the gas cleaning equipment at ICI, it was felt that the bottleneck in the process was the venturi operation. As such this was the area where the study was concentrated. There was considerable scope for increasing the dryer throughput by reducing the pressure drop to the scrubber. However, it was also important to ensure that the venturi continued to operate efficiently, removing virtually all the solid particles from the gas stream and minimising the risk of emissions from the dryers.

Venturi Operation:

The venturi, Figure 6.6, operates by injecting water into the flow of dirty gas and captures the solid particles, Figure 6.5a). A list of the mechanisms employed in the scrubbers are itemised below:

Primary collection method:

1) Direct inertial impaction of the particles into the liquid droplet.

Secondary collection methods:

2) Brownian random motion of small particles.

3) Action of turbulent eddies capturing particles in droplet wake.

4) Diffusion of particle in flow stream.

5) Collection of particles by condensation of water vapour in the gas stream, as it is cooled.

The collection efficiency is directly proportional to the pressure drop across the device, which leads to an interesting optimisation problem. The particle capture rate could be improved at the expense of increasing the system pressure drop, thereby reducing the dryer throughput due to the extra load on the system fans. Although the collection efficiency can be improved by increasing the pressure drop, the benefits diminish with further increases. Alternatively, the scrubber could be operated at a lower pressure drop, which could lower the

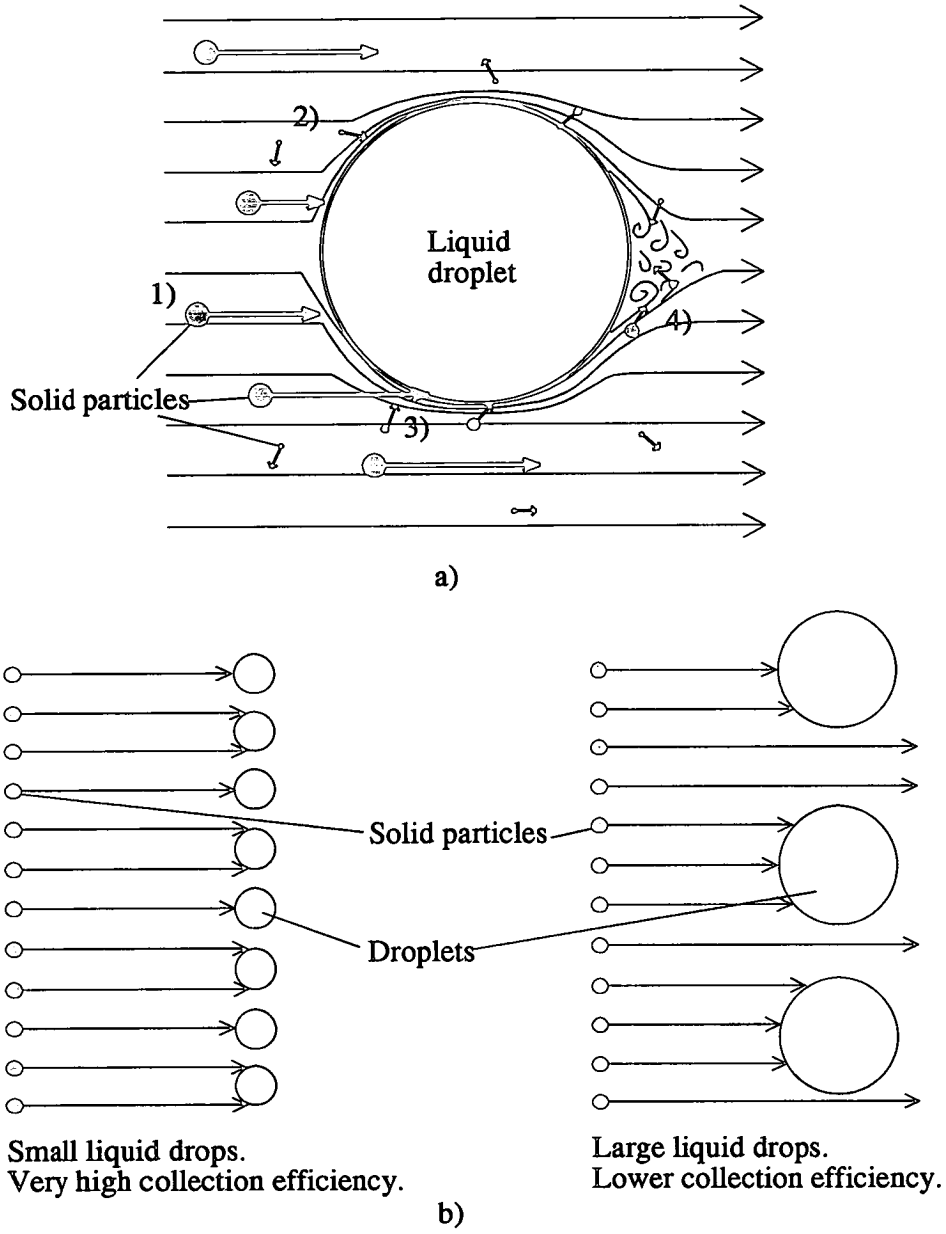

Figure 6.5: Venturi operation a) Illustration of different methods of particle capture b) Effect of droplet size on particle collection.

collection efficiency of the scrubber and thus increase the risk of particle emissions. There would, however, be a corresponding increase in the available head allowing an increase in the gas throughput.

Efficient gas cleaning using venturi scrubbers is dependent on many factors- gas/ liquid contact, liquid droplet size, stream flowrates, an explanation of each is provided below.

- Good liquid distribution over the cross- sectional area of the pipe. The collection efficiency of a venturi can drop dramatically due to liquid maldistribution and gas bypassing.
- The ideal liquid droplet size is around 70μm, Figure 6.5b)- the larger the droplets the less efficient the collection as the particles pass through the gaps between the droplets and are not captured. Smaller liquid droplets ensure that the particles impinge upon a liquid droplet. However, if the droplets are too small they accelerate too fast and the particle collection rate drops more rapidly due to a decrease in the relative velocities of the two streams.
- It is also important to have an adequate and reliable supply of water. The water consumption of the scrubber can be reduced by recirculating a proportion of the used water; however, this could affect the performance of the venturi. In the operation studied, the solid particles were liquid soluble, therefore it was important to ensure that the particle concentration in the water was as dilute as possible. The risk of liquid entrainment is reduced by passing the gas/ coloured liquid mixture through a separator.

Sections of a Venturi Scrubber:

There are three main sections in a venturi scrubber- a sharply converging section, a narrow throat and lastly a gradual diverging section, Figure 6.6.

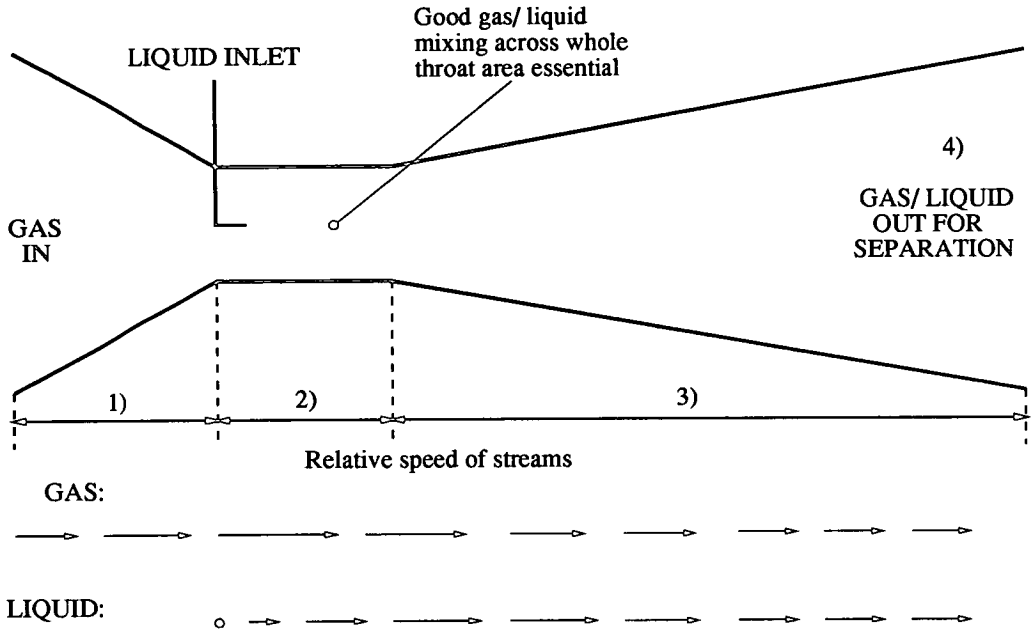

Figure 6.6: Cross section of a venturi scrubber showing relative speeds of gas and liquid.

1) Acceleration of the dirty gas stream into throat of the venturi, causes a large increase in the stream velocity and a subsequent reduction in pressure (potential energy is converted to kinetic energy). The liquid stream is injected as a fine mist of small droplets, evenly dispersed across the cross sectional area of the venturi throat.

2) Acceleration of liquid drops, resulting in the collection of the majority of the solid particles as a result of inertial impaction, due to the difference in the speeds of the gas and liquid streams. There is a reduction in the particle collection as the difference in the stream speeds decreases towards the end of the throat section.

3) As the pipe diameter widens the gas stream decelerates quicker than the liquid droplets, causing a second collection phase. Towards the end of the scrubber, the liquid speed also falls and particle collection drops off to zero. In this section, there is a increase in pressure as the kinetic energy of the streams is converted back to potential energy. Despite this pressure recovery section, there is still a significant pressure drop due to frictional losses.

4) Immediately following the venturi, the gas/ liquid stream is separated before the clean gas is vented to atmosphere.

6.2.4 Heat Recovery Objectives.

It is desirable and indeed economical to try to recover the waste heat associated with the exhaust gas from the drying operation and to utilise the energy again. As a result the overall energy consumption of the drying operation would be reduced. It was proposed to recycle the exhaust gas to the dryer inlet. However, to make this operation economically attractive, it was necessary to reheat the stream to as high a temperature as possible. In addition, the humid exhaust gas stream must also dehumidified, before it would be suitable for recycling to the drying chamber, otherwise there would be an increase in water partial pressure at the top of the dryer which would reduce the drying rate.

Ideally, the heat associated with the humid gas stream leaving the drying chamber could be recovered as the stream is at temperatures between 100- 130 °C. However, it is not possible to recover this heat as the gas contains a large proportion of solid particles, which would foul any heat recovery device used. Hence, any heat recovery device must be positioned after the gas cleaning equipment.

The gas leaving the venturi scrubbing unit is typically at a temperature of between 60- 80 °C, with a humidity of 0.16- 0.56 g-$_{H_2O}$ (g-$_{dry\ air}$)$^{-1}$ (assuming that the gas is saturated). As the solid particles from the gas stream get 'wetted- out', the gas stream becomes saturated with water, which causes a drop in the stream temperature. This removes the possibility of heat recovery by conventional methods because the temperature is too low.

Therefore any recovery system needs to be capable of reducing the gas humidity as much as possible, as well as reheating the gas to a suitable temperature for recycling. Objectives of this study were to dehumidify the gas to a humidity of about 0.03 g- $_{H_2O}$ (g-$_{dry\ air}$)$^{-1}$ and to heat the stream to between 150- 200 °C. As majority of the heat content of the stream is associated with the latent heat of the water vapour, this could be recovered using an absorption system.

6.3 Gas Cleaning Study.

The purpose of the gas cleaning study was investigate the operability of the gas cleaning equipment and to highlight potential modifications to the current setup which would improve dust removal from the exhaust dryer gas stream. Two identical dryers were studied.

6.3.1 Experimental Trials.

An experimental programme was set up to monitor the operation of the spray dryers at ICI's Grangemouth works and in particular the performance of the gas cleaning equipment. The readings which were taken, over a one week period, covered the following areas:

- Gas flowrate and inlet temperature in the drying chamber.
- Product identification- this was taken to see if there was any difference in the dryer performance as a result of drying different products.
- Solids throughput- initial slurry flowrate to the dryer, the solids loading and the specific gravity of the slurry feed stream.
- Solids loading on the cyclone.
- The solids content of the water leaving the venturi. (Using the above results on solids content it should have been possible to get an estimate of the particle loading in the gas stream leaving the venturi. However, the result which was obtained was very small and, because it was evaluated from the difference of two large numbers, it was not very accurate).
- Water flowrate to the venturi scrubber (measured using an ultrasonic meter).
- Pressure drops across the cyclone and venturi scrubber.

Four full sets of data were obtained, two for each of the drying units on the chemical plant. Several more sets of data, which did not contain details of the gas cleaning equipment, were also obtained. All of the data were used to calculate heat and mass balances for the whole drying operation and as a result

identify potential areas for energy reductions and heat recovery. In addition, the exhaust gas stream temperature and humidity readings were used as the basis for setting the inlet conditions used in the experimental heat transformer rig, Chapter 4 'Experimental Studies'.

6.3.2 Limitations of the Gas Cleaning Equipment.

The research highlighted that the gas cleaning equipment was the problem area for both drying operations. This was due to the exceptionally large pressure drops measured across the venturi scrubbers. The reason for this arose from the need to increase the dryer production, which in turn resulted in an increase in the gas flowrate through the whole drying operation. In order to ensure that the exhaust gas stream was clean, the water flow to the scrubber was also increased, which consequently had led to an increase in the pressure drop.

The current cleaning arrangement is now operating far beyond its design specifications and changes are now necessary, in order to optimise the system. This is particularly relevant to the venturi scrubber. The present gas cyclone may also be undersized for the current duty. However, it can operate above its design capacity without affecting its collection efficiency to a great extent. There may also be problems with liquid re-entrainment in the gas stream downstream of the scrubber, which has resulted in some emission problems. All of these factors were investigated before proposing areas for improvement to the cleaning equipment.

Potential Areas for Improvements to the Existing System.

As the scrubbing operation was the last operation prior to the venting of the exhaust gas stream it was important that the gas was completely free of particles (the design specification is for a final solids loading of 0.0032%w/w with respect to the original solids flow). Therefore, a further cleaning stage was proposed which would operate in series with the existing gas cleaning equipment (full details in the report 'Spray drying- Gas cleaning study' ([33]). The purpose of the extra stage was to ensure that the gas was cleaned to the deign specifications and thus minimise the risk of future particle emissions.

However, an extra cleaning stage would increase the pressure drop across the system and may in fact cause the gas throughput to decrease. This could occur if the fans were unable to cope with the extra pressure drop across the system. Therefore, instead of removing the process bottleneck, the problem would be magnified. This problem would be minimised by reducing the liquid throughput to the venturi scrubber, thereby reducing the pressure drop and perhaps even reducing the risk of liquid re-entrainment in the exhaust gas stream. However, it is not known how this change would affect the collection efficiency of the venturi scrubber and could only be assessed by implementation.

In addition, the new cleaning device could be a mop scrubber, which would supply its own shaft power and thus overcome the increase in pressure drop. The new scrubbing operation would operate countercurrently, Figure 6.7, which would mean that the cleanest water was contacted with the cleanest gas. The cascading of the water also reduces the water consumption of the scrubbers, which was quite high. A full study of the proposed system would need to carried out to assess the implications to the drying operation.

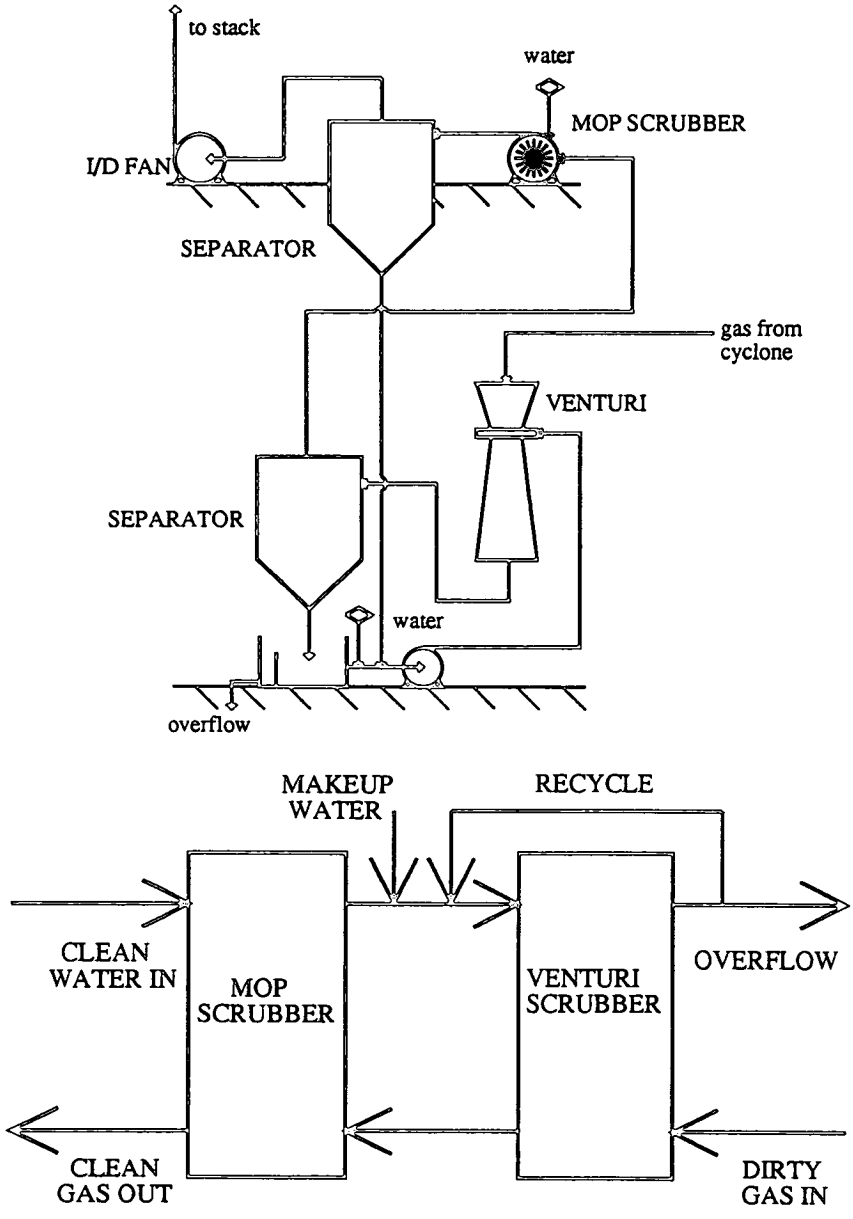

Figure 6.7: Two stage countercurrent gas scrubbing using a venturi and a mop scrubber.

6.4 Industrial Heat Transformer.

The second part of the industrial case study concentrated upon the need to recover the waste heat associated with the exhaust gas stream from the dryer, which was being vented to atmosphere. The investigation led to a preliminary design of an industrial heat transformer. Two important considerations of the study were the location and size of the heat recovery equipment.

The transformer would need to be retrofitted into the existing drying setup. It was therefore, necessary to design a system which was both compact and which could be incorporated into the drying cycle without too much disruption to operations.

A computer model was also written to investigate the potential benefits of a heat transformer to the drying operation. The results of this model highlighted three main benefits, which could be achieved, these are listed below:

- Lower energy consumption.
- Greater dryer throughputs.
- Cleaner exhaust gases

6.4.1 Design Basis.

The first stage of heat recovery involved the dehumidification of the humid gas stream by direct contact with an absorbent solution. In this case an aqueous solution of concentrated lithium bromide was proposed as the absorption working fluid.

After the gas stream has been dehumidified, it was then reheated in a novel design of compact heat exchanger, which used an absorbent/ steam mixture as the heating medium. A concentrated solution of aqueous lithium bromide was again used as the absorbent fluid.

As well as designing the heat transformer to dehumidify and reheat the exhaust gas stream it was also necessary to ensure that absorption system would not affect the normal operation of the drying cycle. Further important design considerations were:

- The gas stream must be clean as any particles in the stream would lead to contamination of the absorbent solution. Therefore, the proposed improvements to the gas cleaning process would need to be carried out before implementation of this heat recovery device.
- Any particles which remain in the gas stream after cleaning could be carried back to the dryer. As the particles are dry, they would degrade upon contact with hot air, resulting in a carbon build up on the dryer chamber walls and maybe inside the reheat column.

- There would also be a risk of absorbent carry over, in the gas stream, into the dryer. An analysis of the effects of absorbent contamination of the product would need to be evaluated, although every precaution would be taken to minimise this risk.

6.4.2 Proposed Design.

The material of construction for the heat transformer was stainless steel (type 316) as the absorbent solution proposed, in this case aqueous lithium bromide, was corrosive. The design of the heat transformer was based upon the facility constructed and tested at Edinburgh University, see Chapter 3 'Design and construction'. The reheat column would need to consist of many absorption tubes as opposed to the single double pipe exchanger, which was used on the small scale heat transformer. Each of the tubes would be fed with separate streams of lithium bromide and low pressure steam (LPS), which is readily available on site. The absorbent mixture would flow down the tubes while the gas would flow countercurrent to this, through the annular spaces been the tubes.

Due to the high risk of lithium bromide crystallisation at low temperatures, it may be necessary for the dehumidification column to be operated at a lower absorbent concentration than the reheat column because of its lower operating temperature. On the pilot plant, crystallisation of the solution was a problem which was easily remedied. The pipework was dismantled and then washed through with hot water, which dissolved the crystallised solution. However, on an industrial process such an occurrence would severely disrupt operations and cause severe problems for cleaning.

It would therefore be wise to operate the dehumidification column with an absorbent solution at a lower concentration than that used in the reheat column. Typical operations conditions for each column are listed in Table 6.1.

		Absorbent	Gas stream
Dehumidification	IN	65 %w/w, 85 °C	60-80 °C, 0.16- 0.56 g- $_{H_2O}$ $(g\text{-}_{dry\ air})^{-1}$
column:	OUT	~62 %w/w, 80 °C	80 °C, 0.03 g- $_{H_2O}$ $(g\text{-}_{dry\ air})^{-1}$
Reheat column:	IN	67 %w/w, 100 °C and LPS @100 °C	80 °C, 0.03 g- $_{H_2O}$ $(g\text{-}_{dry\ air})^{-1}$
	OUT	~65 %w/w, 180 °C	170 °C, 0.03 g- $_{H_2O}$ $(g\text{-}_{dry\ air})^{-1}$

Table 6.1: Operating conditions for the absorption heat transformer. In addition a separate steam supply would be required to regenerate the absorbent under vacuum in the generator.

Figure 6.8 illustrates different possible configurations which could be adopted to ensure that the correct absorbent concentrations were achieved in each column. The evaporators would be designed to hold the entire absorbent inventory in a dilute state, where there would be no risk of the solution crystallising. Such a precaution was necessary to enable the process to be shut down for maintenance. In addition, as the drying process was campaign oriented, the heat transformer would not be in continuous operation and as such the absorbent solution would require frequent dilution to a suitable storage concentration, around 60%w/w. This also means that the solution would then need to be reconcentrated up to the working concentration of around 67%w/w. A further precaution to prevent absorbent crystallisation. was the steam tracing of all lithium bromide pipework.

The generators would be operated under a vacuum of around 0.05- 0.1 bar and operate at a temperature of around 90 °C, therefore LP steam, which is readily available on site, could be used as the heat source.

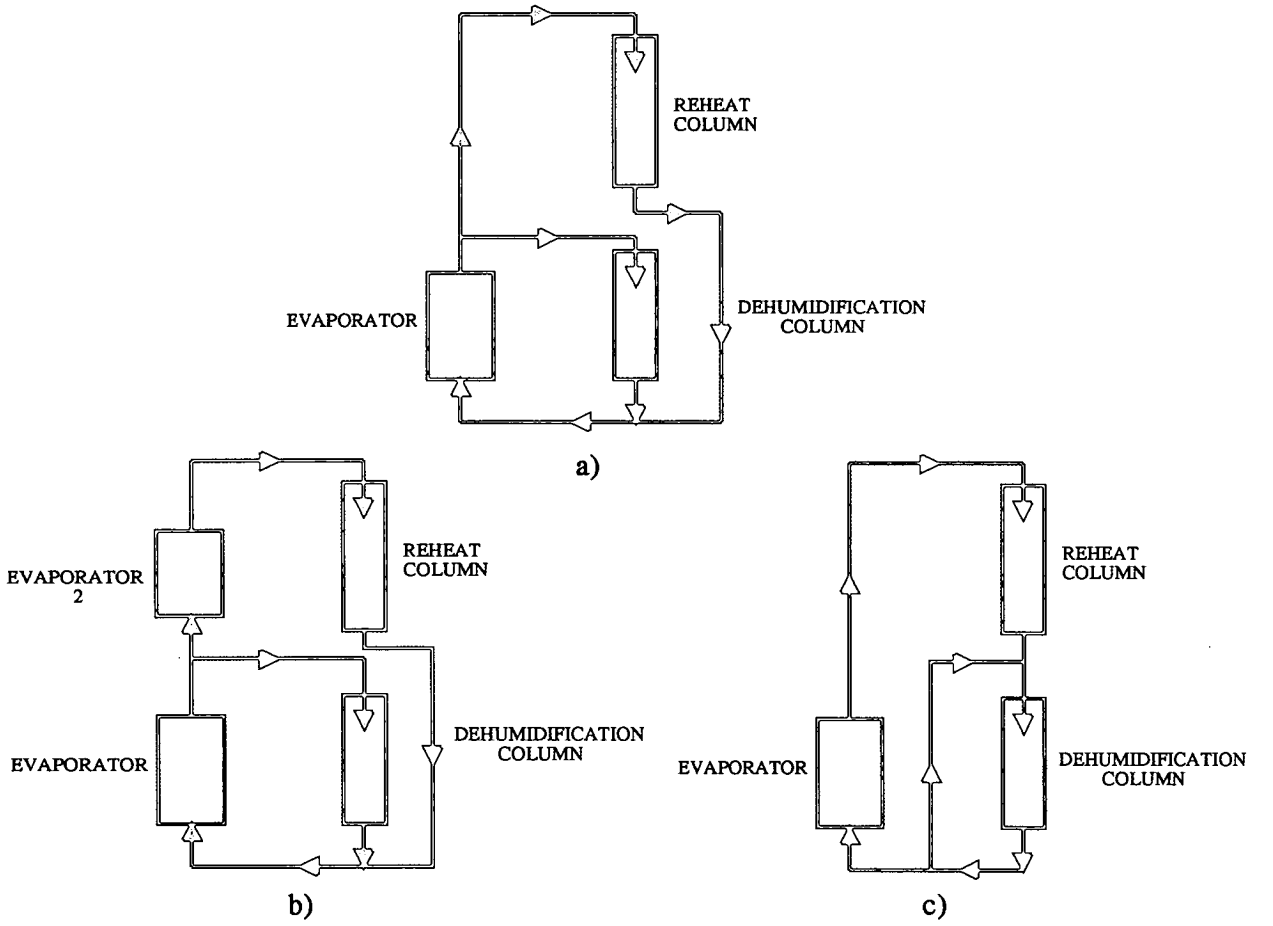

Figure 6.8: Different design configurations to give the optimum use of lithium bromide. a) Single evaporator, separate feeds to each column b) Separate evaporators and feeds for each column c) Single evaporator, columns in series, with recycle.

It should be noted that an exchanger would need to installed on the absorbent pipework leading to the dehumidification column, in order to control the inlet absorbent temperature. Otherwise, the solution would be too hot, resulting in a high water partial pressure and consequentially a higher gas exit humidity.

6.4.3 Retrofit Installation of the Heat Transformer.

The need for the equipment to be compact was an important design feature of the transformer. This applied particularly to this study where the available space for installing the rig was limited, see Figure 6.9. The reheat column was of novel design and utilised the latest technology in order to maximise the heat transfer to the gas stream. The dehumidification column design was based upon the column used in the experimental studies, with a packed section to increase the area available for mass transfer. The temperature of reheated gas stream leaving the heat transformer was set to 170 °C, corresponding to the maximum estimated temperature possible with the experimental pilot plant (see Chapter 4 'Experimental Studies'). Hence, this temperature was used as the basis for this particular study. The reheated gas was then suitable for recycling to the inlet of the drying chamber, where it replaced the existing dilution air, currently used in the dryer to lower the combustion gas temperature to the desired inlet level. It is estimated that 90 % of the exhaust gas stream would be recycled, with the remainder being vented to atmosphere (Section 6.5 discusses the benefits of recycling the gas and uses a computer model to quantify possible heat savings).

Instead of using a direct contact dehumidification column, which could cause problems due to absorbent entrainment in the gas stream, a possible alternative method for dehumidifying the gas stream would be to cool the gas. However, the gas would need to be cooled to a temperature of 41 °C, in order to meet the

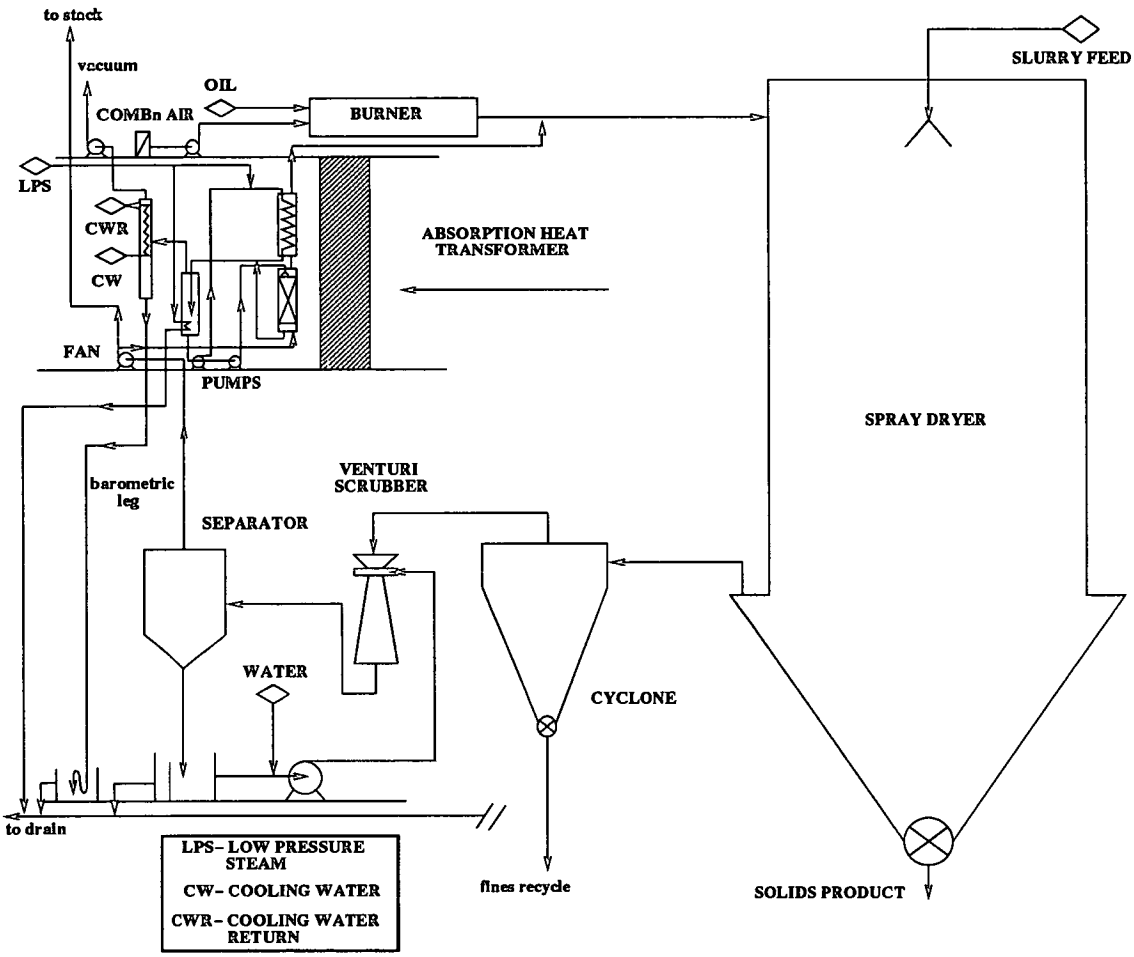

Figure 6.9: Proposed position of an absorption heat transformer (single evaporator, separate absorbent feed streams) in relation to the dryer and ancillary equipment.

desired outlet humidity specification of 0.03 g- $_{H_2O}$ (g-$_{dry\ air}$)$^{-1}$. The consequence of this is that the gas would require further heating before it would be suitable for recycling (see sample calculation for heating requirement in Appendix C 'Sample Calculations', Section C.3.1).

A more complex double heat pump arrangement could also be developed. The heat given up by the gas stream when it is being dehumidified at the low temperature, could be used as the heat source for a compression heat pump. The heat would then returned to the gas stream at a higher temperature, in the condensation stage of the heat pump. Compression heat pumps have been already used for such duties, for example in air conditioning units. It would, however, make the whole process rather more complex and also larger in size, which would make it more difficult to be installed.

Finally, another change for an industrial transformer, would be to replace the lithium bromide as the absorbent working fluid with sodium hydroxide (caustic soda). The advantage of this fluid is that it is used on chemical plants and therefore operators would be more used to handling it. However, there are two main disadvantages- poorer heat transfer properties and also the risk of crystallisation when operating with highly concentrated solutions. Chapter 2, 'Absorption Working Fluids', discussed the merits of aqueous lithium bromide as a working fluid in comparison to other fluid combinations.

6.5 Computer Model Heat Recovery Studies.

Computer programs were written to investigate the possible benefits that a heat transformer would bring to the drying operation. The areas investigated by the computer programs were concerned with:

- Reducing the oil flow to the direct fired burners, while maintaining the desired inlet gas flowrate and temperature to the dryer.
- Increasing the production rate by increasing the gas throughput in the drying chamber, assuming a constant oil flowrate and gas inlet temperature.

Both models were only concerned with maintaining the initial operating conditions of the dryer and did not investigate possible changes to the dried product incurred by varying the operating parameters. The current drying operation achieves the desired inlet drying temperature by mixing the hot combustion gases from the oil burner with clean ambient air. The incorporation of a heat transformer into the drying cycle would remove the need for this ambient air. Another consequence of removing the ambient air would be the removal of oxygen from the drying atmosphere, resulting in an inert drying atmosphere comprising mainly of nitrogen and carbon dioxide. Reheated, clean and dehumidified exhaust gas leaving the transformer would replace the dilution air. A schematic diagram of the new drying process, incorporating a two stage heat transformer, is shown in Figure 6.10.

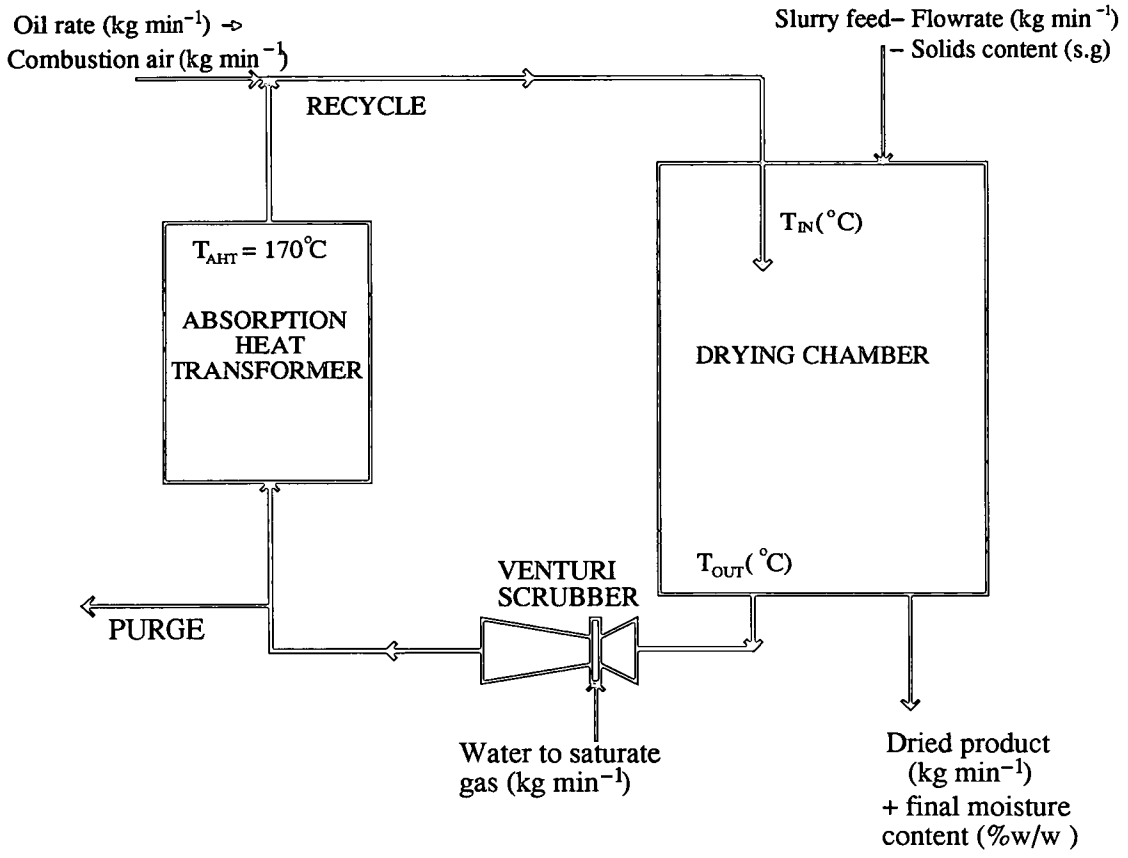

Figure 6.10: Basic simulation model to investigate the improvement in the performance of the spray dryer due to the inclusion of an A.H.T into the drying cycle.

6.5.1 Model for Reducing Oil Consumption.

This particular program was written for the purpose of estimating the possible fuel oil savings, a primary energy source, which could be achieved by recovering the heat in the exhaust gas stream. The inlet conditions (Table 6.2), were the oil flowrate to the burner and the dryer inlet temperature. Using these values, the inlet gas flowrate could be determined and also the recycle flow required to maintain this desired inlet conditions to the dryer. As the temperature of the recycled gas stream was set to 170 °C, less fuel oil was required to achieve the set dryer inlet temperature.

Independent	Oil flowrate (kg min^{-1})
	Inlet dryer temperature (°C)
	(Input at the start of the program.)
Dependent	Combustion gas flow (kg min^{-1})
	Total gas flow into dryer (kg min^{-1})
	Gas composition- N_2, CO_2, H_2O, O_2 and SO_2 (kg min^{-1})

Table 6.2: Operating parameters used in the computer model for reducing the oil consumption in the spray dryer.

Several assumptions were made concerning the performance of the dryer as a result of recycling exhaust gas:

- The effect of recycling water vapour to the drying process was neglected: the drying rate was assumed to remain constant.
- The inlet water partial pressure to the heat transformer was set to 0.199 bar, assuming that the gas leaves the venturi scrubber saturated with water vapour at a temperature of 60 °C.
- Exit water partial pressure from the heat transformer set to 0.064 bar, corresponding to the water vapour pressure above a solution of lithium bromide with a concentration of 65 %w/w and at a temperature of 80 °C.

It was not necessary to incorporate the slurry feed conditions or the product rate into the model, as these were assumed to be unaffected by the changes to the drying atmosphere. In addition, it was assumed that the amount of water in the gas stream entering the heat transformer would remain constant. This was a valid approximation as the heat transformer was downstream from the gas cleaning equipment. Therefore, the gas stream conditions, temperature and humidity, leaving the venturi scrubber were assumed to remain constant. Again, this was valid as the gas stream was saturated with water at a temperature of 60 °C. Finally, the gas stream leaving the absorption heat transformer and returning to the dryer had a water partial pressure of 0.064 bar.

Program Procedure to Determine Oil Savings:

The program, which was written to determine the maximum possible fuel savings to the drying process, involved a simple iteration. The initial gas flowrate was maintained by balancing the recycle and combustion gas flowrates, while maintaining the set dryer inlet temperature. A range of typical operating temperatures was input at the beginning of the program and progression to the next temperature occurred when the inlet gas flowrate converged to the initial total gas flowrate. The operating procedure is described below:

Algorithm for estimating oil saving in a spray dryer.

Step 1: *Input data: oil flowrate, range of inlet temperatures and the temperature step size.*

Step 2: *Calculate the combustion air flow from the oil flowrate, also the heat content and temperature of this stream.*

Step 3: *Evaluate the dilution air flowrate to give the desired inlet temperature.*

Step 4: *Recycle Y/ N?*

- *N) No recycle- Put results in file. Finish run.*
- *Y) Begin iteration loop on recycle flowrate...*

Step 5: *Find water in gas stream after venturi scrubber (assume saturated at 60 °C, giving a partial pressure of 0.199 bar).*

Step 6: *Find water content after heat transformer (assume the water partial presure in the exit gas is 0.064 bar).*

Step 7: *Difference between water in/ out is the amount of water transferred to the absorbent stream in the heat transformer.*

Step 8: *Set the gas exit temperature leaving the heat transformer to 170 °C.*

Step 9: *Recycle gas flow = Total gas flowrate - Combustion gases.*

Step 10: *Determine the composition of the recycle gas.*

Step 11: *Determine the new oil flowrate and combustion gas flow necessary to maintain the set dryer inlet temperature.*

Step 12: *New inlet gas flowrate to dryer = Combustion gas + Recycle gas.*

Step 13: *Repeat iteration to find recycle flow which will maintain desired inlet flowrate.*

6.5.2 Results Obtained for Reducing Oil Flowrates.

Table 6.3 illustrates the change in the composition of the drying atmosphere which was achieved by recycling exhaust air. Of principal interest was the change to the water and oxygen content of the gas stream. The water content was increased by approximately 350 %, which could potentially affect the drying rate of the slurry. The gas entering the drying chamber was at a very high temperature, 500+ ^{0}C, hence the mass transfer driving force at the top of the chamber would not be greatly affected by the increase in water content. Similarly, the outlet driving force, although reduced slightly would not be greatly altered as the exit gas humidity would only be increased from 0.15 to 0.19 g-$_{H_2O}$ (g-$_{dry\ air}$)$^{-1}$ (see Appendix C 'Sample Calculations', Section C.3.2). Hence, it was assumed that the effect of the extra water in the gas stream would be negligible. This conclusion could only be confirmed by carrying out experimental tests, studying the variation in the final product quality with changes in the drying conditions.

The complete removal of oxygen from the drying atmosphere means that the dryer could be operated with an inert atmosphere, which is particularly useful when drying flammable products. However, precautions must be taken to remove the risk of asphyxiation to operators, when carrying out maintenance on the drying chamber. Although the percentage of carbon dioxide would be increased fourfold, it is not expected that this would affect the drying process.

Gas composition-partial pressures	N_2	CO_2	H_2O	SO_2	O_2
No recycle	0.805	0.028	0.021	0.0002	0.146
Recycle	0.803	0.124	0.071	0.0009	-

Table 6.3: Composition of gas stream entering the dryer.

It should be noted that as the gas inlet temperature increases from 500 to 550 °C, Table 6.4, the total gas flowrate entering the dryer drops from 222 to 199 kg min^{-1} because a high gas inlet temperature requires less dilution air to lower the combustion gas temperature to the desired operating temperature. The combustion gas flow was estimated on the assumption that the fuel oil was burned using sufficient air to completely oxidise the oil, producing carbon dioxide only and no carbon monoxide. The calorific value of the oil was 40.3 MJ kg^{-1} and the initial oil flow used in determining the stream flowrates in Table 6.4 was 3 kg min^{-1}.

Inlet dryer temperature (°C)	Recycle gas flow (kg min^{-1})	Total gas flow in (kg min^{-1})	% gas recycled	Oil savings (*) (kg min^{-1})	Energy savings (kW)	COP
500	181	222	82	0.66	436	0.24
510	176	217	82	0.63	423	0.23
520	171	212	81	0.61	410	0.22
530	166	208	81	0.59	397	0.22
540	161	204	80	0.57	383	0.21
550	157	199	79	0.55	369	0.20

Table 6.4: Possible fuel savings which could be achieved by reheating and recycling the exhaust gas stream.

(*- Based upon an initial oil flowrate of 3 kg min^{-1})

The oil savings, which could be achieved by installing an absorption heat transformer, are approximately 20 %. However, energy is required to operate the heat transformer. Although the overall energy consumption of the drying operation has increased, the energy is not from a primary source. The evaporator requires 689 kW of heat to remove the absorbed water from the absorbent solution, while 1157 kW of heat must be removed in the condenser. These figures correspond to a lithium bromide solution of 67 %w/w operating with a flowrate of 454 kg min^{-1} in the reheat column and 65 %w/w and 1252 kg min^{-1} in the dehumidification column. These values are representative of the conditions required for this industrial operation.

The heat used by the heat transformer was assumed to be constant for all dryer operating temperatures, for ease of calculations. As such the COP (coefficient of performance of the A.H.T) is approximately 0.22. In the evaporator the energy supplied comes from low pressure steam, which is normally readily available on site. Indeed any waste heat energy source available at a temperature of between 90- 110 °C could be used in the generator. It may even be the case that the waste heat stream has a negative value, representing the cost involved in disposing of the steam. On many sites, the steam supplied to the chemical plants is part of a combined heat and power operation. Therefore, an increase in the consumption of low pressure steam could in fact be beneficial with respect to generating more power in the steam turbines. Further more, the heat removed in the condenser could be used to preheat other process streams. As such the heat transformer should not be considered as a 'stand alone' piece of equipment but as part of an integrated heat recovery system.

It can also been seen from Table 6.4 that the recycle gas stream constitutes between 79- 82% of the total gas inlet flow, the remainder being purged to atmosphere. This has the benefit of reducing the risk of solids escaping to atmosphere.

6.5.3 Model for Increasing Dryer Throughput.

A second computer program, which was similar to the 'Fuel saving' model (Section 6.5.1), was written to investigate the maximum possible increase in the production rate of the dryers which could be achieved by recovering the exhaust waste heat from the dryer exhaust.

In addition to the data input for the 'Fuel saving' model (oil flow and dryer inlet temperature, Table 6.2) it was necessary to include details about the slurry being dried and also the dryer outlet temperature. These extra details were required in order to determine the production increases which could be obtained by reheating and recycling a proportion of the exhaust gas stream. A full list of the variables used are listed below in Table 6.5. In addition to the assumptions made for the previous model, it was also assumed that all pieces of equipment (drying chamber, gas cleaning equipment, fans, pumps etc.) would be able to cope with the increase in gas flowrate.

Independent	Slurry feed conditions- flowrate (l min^{-1}), specific gravity (-), solids content (%w/w) and the desired final moisture content (%w/w)
	Outlet dryer temperature (°C)
Dependent	Total heat load to dryer (MJ min^{-1})
	Evaporative load (MJ min^{-1})
	Water removed from slurry (kg min^{-1})

Table 6.5: Additional variables required in the computer model for increasing the dryer throughput.

Program Procedure for Increasing Dryer Throughput:

As with the previous program, this model involved a simple iteration process, which determined the maximum increase in the dryer throughput for a particular oil flowrate and operating temperature. The computational procedure is described on the next page:

Algorithm for estimating increase in dryer throughput.

Step 1: *Input data as before, except adding: dryer outlet temperature and slurry properties- flowrate, specific gravity, solids content and the desired final moisture content of the dried product.*

Step 2: *Calculate the combustion air flowrate from the oil flowrate, also the heat content and temperature of this stream.*

Step 3: *Evaluate the dilution air flowrate to give the desired inlet temperature.*

Step 4: *Recycle Y/ N?*

- *N) No recycle- Put results in file. Finish run.*
- *Y) Begin iteration loop on recycle flowrate...*

Step 5: *Find water in gas stream after venturi scrubber (assume saturated at 60 °C, giving a partial pressure of 0.199 bar).*

Step 6: *Find water content after heat transformer (assume the water partial presure in the exit gas is 0.064 bar).*

Step 7: *Difference between water in/ out is the amount of water transferred to the absorbent stream in the heat transformer.*

Step 8: *Set the gas exit temperature leaving the heat transformer to 170 °C.*

Step 9: *Estimate the recycle gas flowrate, so as to maintain the set dryer inlet temperature.*

Step 10: *Determine the composition of the recycle gas.*

Step 11: *New inlet gas flowrate to dryer = Combustion gas + Recycle gas.*

Step 12: *Find new heat load entering dryer, determine the evaporation load of the gas stream (the percentage heat used for evaporation set by initial conditions)*

Step 13: *Find new slurry flowrate, which corresponds to the increase in evaporated water.*

Step 14: *Repeat iteration to find recycle flow which will maintain desired inlet temperature.*

6.5.4 Results for Increasing Dryer Throughput.

The results obtained for this computer model were based upon typical operating parameters for the dryer and were input at the start of the program. The computational method used in this particular computer program dealt solely with maintaining the dryer inlet temperature and increasing the recycle flowrate accordingly. It can be seen from Table 6.6 that the results obtained for the increase in gas flowrate in the dryer are wholly unrealistic. The potential increase in throughput indicated by the results would require major redesigning of the whole drying operation. A more realistic increase in the production rate of the dryers would be around 10%.

Inlet dryer temperature (°C)	Initial gas flow (kg min^{-1})	Recycle gas flow (kg min^{-1})	Total gas flow (kg min^{-1})	% gas strm. recycled	% gas flow increase
500	222	275	327	84.1	47.3
510	217	265	317	83.6	46.1
520	212	255	307	83.0	44.8
530	208	246	298	82.5	43.3
540	204	238	290	82.0	42.2
550	199	230	282	81.5	41.7

Table 6.6: Flowrates into the spray dryer for different inlet temperatures.

However, the effects of increased flowrates through the individual pieces of equipment would need to be studied in more detail. In particular a thorough investigation of the characteristic curve of the fan and also the system curve for the whole operation would be required. Any increase in gas flowrate would result in a larger pressure drop across the venturi scrubber, which would need to be countered by a corresponding increase in the fan throughput. Possible changes to the fans to meet this demand could be achieved by increasing the fan speed, by increasing the power input or, as may be necessary, replacing the existing fans with more powerful ones.

Another area which would need to be investigated to see if an increase in production could be achieved is the slurry feed equipment. It may be necessary to add an extra feed atomizer to be able to cope with the increase in throughput. Although the installation of an atomizer may be straight forward, the extra pressure nozzle (or rotating disc, depending on the method used) may affect the flow distribution within the chamber. If the flow patterns within the dryer are changed significantly this could affect final product quality.

As with the previous study, the new drying atmosphere would become free of oxygen, providing an inert drying atmosphere. In conjunction with this there is a corresponding increase in the percentage of water in the gas stream (see Table 6.3).

6.5.5 Future Work and Developments.

Both of the above models used a 'black box' approach with respect to the individual pieces of equipment. It was assumed that any changes to the drying operation could be achieved without difficulty and without affecting the final product quality. In reality, this would not be the case and a more detailed study would need to be carried out which integrated all the pieces of equipment together and attempted to simulate the whole drying process. Figure 6.11 highlights the main areas where changes to the existing programs would need to be developed. Additions to the program would include:

- Determination of the pressure drop through the whole drying operation, especially the venturi scrubber and the absorption heat transformer.
- Collection efficiency of the gas cleaning equipment, at varying gas throughputs.
- Estimation of the performance characteristics of the fan.
- Detailed study of the drying chamber with particular attention to the changes to the drying rate of the product. Any simulation of the drying process would be very approximate as it is not fully understood how an increase in gas flowrate would affect the flow patterns within the chamber.

An increase in the water content of the inlet gas stream may also affect the final product quality obtained from the dryer.

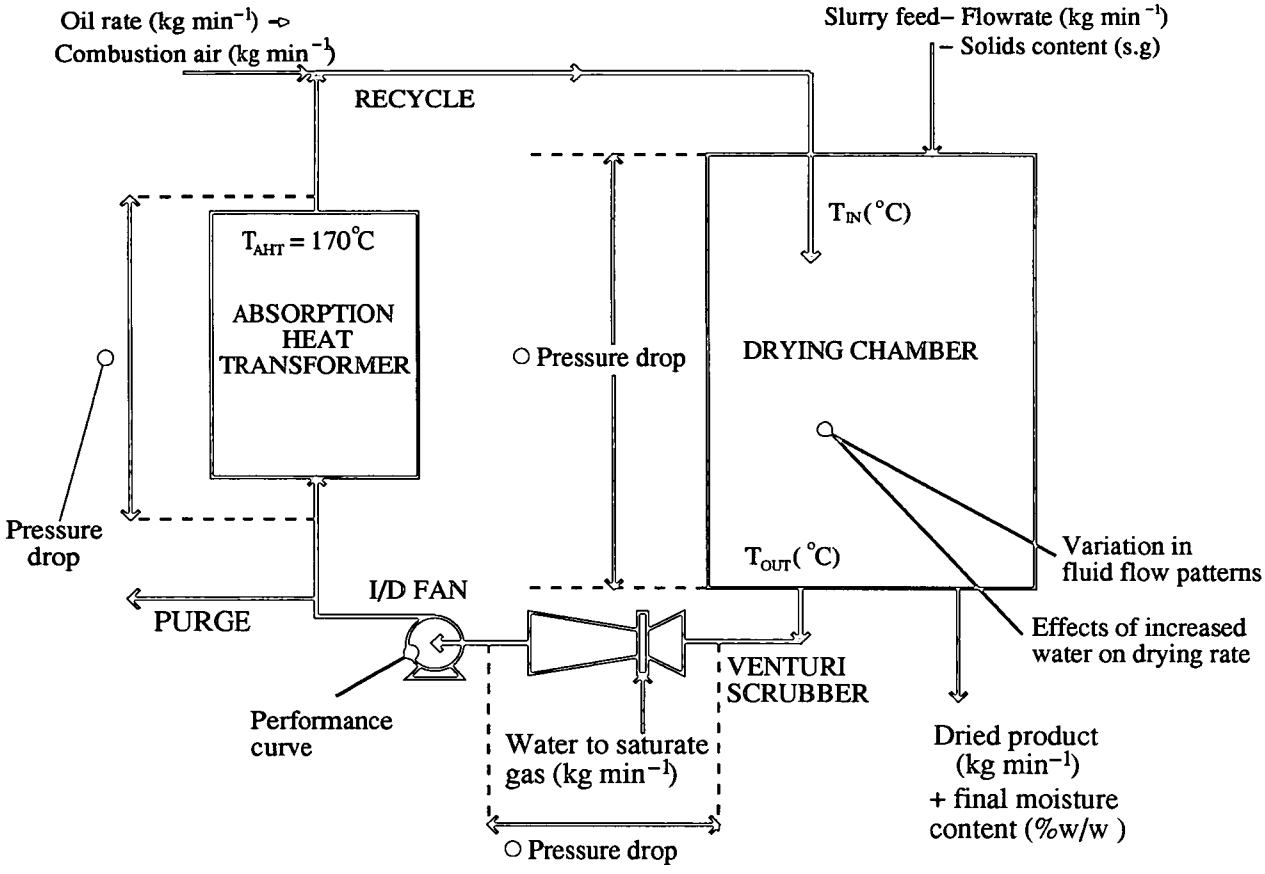

Figure 6.11: Proposed detailed simulation model for investigating increased performance of a dryer using an A.H.T, including pressure drops and fan characteristics.

6.6 General Energy Recovery.

Heat recovery schemes and complete heat integrated systems are becoming an important feature of chemical plants. There are many funding programs available which encourage users to adopt new and novel ways of recovering heat. These schemes include ETSU ('Energy Technology Support Unit') in Britain and there are also various European schemes, such as the JOULE experimental and THERMIE demonstration programmes.

6.6.1 Industrial Heat Pump Systems.

Heat pumps, both compression and absorption systems, are seen as efficient ways of utilising energy resources. There are many examples of successful industrial applications, particularly of compression heat pumps. However, the widespread adoption of absorption heat recovery schemes is limited due to the overall lack of experience and knowledge that companies have with this technology. The following examples illustrate the potential uses of absorption heat pumps systems in industry, see also Chapter 2 'Absorption Working Fluids'. Each of the examples has operated satisfactorily and generated large energy savings quickly, which has in turn led to rapid pay back periods.

Heat pump. Dyeing plant, Osaka, Japan. An absorption heat pump recovers heat from a waste water stream on a dyeing plant. The heat pump had a coefficient of performance of 1.41. The pay back period was estimated to be 3 years based upon fuel savings, which would normally be used to heat the water stream. [151]

Heat pump. District heating, Trollhättan, Sweden. Another absorption heat pump system recovers waste heat available from another chemical process as the heat source in this particular example. The output from the heat pump is fed to the district heating system. Operating experience indicated that a COP of 1.3- 1.8 was possible. The cycle had been 100 % reliable and worked well even under part load. [93]

Heat transformer. Ethylene amine plant, Delfzijl, Netherlands. A heat transformer, using aqueous lithium bromide as the absorbent solution, with a maximum capacity of 6.7 MW, was commissioned in Delfzijl in October 1985. The unit was capable of producing 11 tonnes $hour^{-1}$ of steam at 145 °C and 4.6 bar. The primary energy consumption, required for the pumps, was only 53 kW. [149]

Heat transformer. Evaporation plant, Lund, Sweden. Another heat transformer using aqueous sodium hydroxide as the working fluid was recently commissioned in a pulp and paper mill in Lund, Sweden. The system, which was incorporated into an evaporation plant, aims to reduce the steam consumption of the plant. It was estimated that the pay back period for the heat transformer would about four and a half years. [58]

6.6.2 Potential Uses for Heat Pumps in Drying Processes.

In addition to the examples highlighted above, the potential use of heat pumps systems is widespread. However, as can be seen from these examples, each particular application is unique. Therefore, the heat recovery system must be tailor made for each case study.

The heat transformer developed in this study, section 6.4, was designed using standard chemical engineering equipment- a packed column for dehumidification; an evaporator using steam as the heat source; a condenser to remove heat at the low temperature side of the process; and a heat exchanger for reheating the exhaust gas stream. The exchanger design was of novel construction because of its highly extended surface area. This was required to enhance the transfer of heat to the gas phase. Therefore, the use of this type of heat recovery device can readily be reproduced without too much specialist knowledge.

As energy concerns become an increasingly important issue, it is worth extending the potential use of absorption heat transformers from spray drying to other drying methods. There are many different kinds of drying operations, some of which utilise hot air as the drying medium- for example fluidised bed, tray, band, rotary drum and pneumatic dryers. Other methods such as agitated vessel and drum dryers dry the wet product by indirect contact with a heating medium. Obviously, direct comparisons can be drawn between spray drying and the other 'hot air' dryers, where an absorption heat transformer could easily be retrofitted into the drying operation.

In timber drying, dehumidifiers are particularly useful for maintaining a dry atmosphere during the drying cycle. Figure 6.12 shows how a conventional compression heat pump is used to condense the water from the airstream, before it then reheats and recycles into the main drying chamber. The temperatures involved in timber drying are quite low, only about 80 °C, so as to prevent the warping of the wood. There is no reason why a low temperature absorption heat transformer could not be designed to carry out this operation. The transformer would have the added benefit of not requiring a primary energy source to drive any part of the equipment. In fact, it would be entirely possible to use solar energy as the energy source, required in the evaporator of the absorption cycle.

A potential problem resulting from the use of direct contact between the absorbent and humid gas streams, is the risk of absorbent contamination of the product. The risk of contamination would be minimised by positioning a demister pad after the dehumidification stage. However, the use of a direct contact dehumidifier could limit the use of this particular design of open cycle heat transformer in the food processing and pharmaceutical industries, where product purity is of prime concern.

The reheating of the exhaust air using the indirect contact absorption column does not pose contamination problems. In some cases the absorption reheater could be used as the main heat source for the drying process. The maximum temperature achieved from the test rig used in these studies indicated that temperatures around of 150- 160 °C could be obtained. This temperature range corresponds to the drying temperature used to dry a wide variety of dried products. As well as providing reheating air for recycling, the heat generated in the heat transformer cycle could be used directly to dry wet solids in agitated vessels.

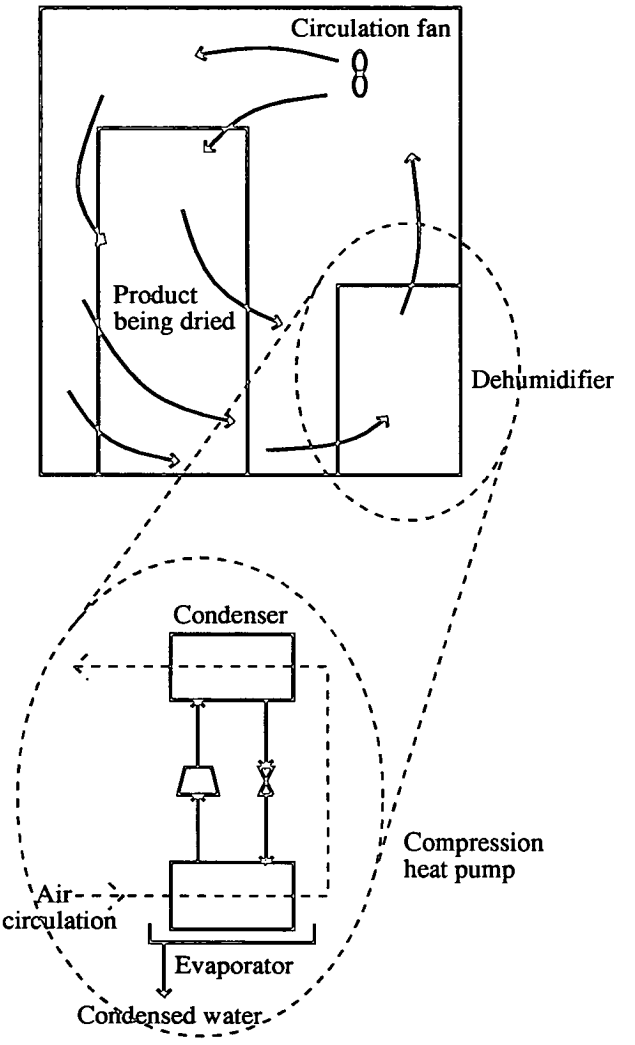

Figure 6.12: Example of a dehumidifier used in timber drying.

6.7 Conclusions.

It has been shown that an absorption heat transformer can be used to recover and upgrade waste heat from an exhaust gas stream, using low pressure steam as a heat source. In addition to heat recovery, other possible benefits which can be achieved by including a heat transformer cycle into a spray drying operation include:

- Reduction of the exhaust gas plume leaving the stack.
- Possible increase in the production rate of the dryer.
- Utilisation of low pressure steam, which may be readily available as a 'waste' heat source.

It was felt that the operating conditions used in spray drying were most demanding and, as such, would be the most severe and limiting operating temperatures that a heat transformer would be required to operate under. Therefore, the technique could be more easily fitted to operations which operate at lower temperatures.

Although the heat transformer apparatus was designed for the purpose of testing the applicability of retrofitting the cycle to a drying operation, the system could readily be adapted for a wide range of uses throughout the chemical industry.

Chapter 7

Electronic Composition Meter.

7.1 Introduction.

7.1.1 History.

An electronic composition meter was developed which displayed the composition of a refrigerant mixture, inferred from measurements of pressure and temperature at points in a refrigeration cycle where there was vapour-liquid equilibrium.

The first prototype of the meter was tested on the absorption heat transformer (A. H. T) pilot plant described in Chapter 3 'Design and Construction', where it was used to determine the composition of an aqueous lithium bromide solution. The meter was further developed for use with a binary refrigerant mixture and then later extended for use with a ternary component mixture. It is also possible to adapt the meter for use with 4- component mixtures whose equilibrium relationships are well characterised.

7.1.2 Application.

The primary application of this meter was felt to lie in the refrigeration and air conditioning industry. The majority of this equipment currently employs CFCs as refrigerants, but under the terms of the Montreal Protocol these must be phased out by 1996 (see also Chapter 1 'Introduction'). In many applications replacement refrigerants are likely to involve mixtures rather than pure substances.

The switch to refrigerant mixtures is particularly important for the largest single users of CFCs: automobile air-conditioning. Constant vibration gives rise to leaks and 'topping- up' of the refrigerant fluid is customary every six months or so. If a refrigerant mixture is used instead to a single pure component in the air- conditioning cycle, there will be preferential leakage of the most volatile component (MVC) from the cycle which may lead to changes in the mixture properties. Therefore, the 'topping- up' operation must be able to restore the refrigerant mixture to its original composition. The electronic composition meter provides an instantaneous reading of the refrigerant composition in the equipment- allowing the mixture to be restored to its original composition quickly and accurately.

At present, commonly used methods for measuring the composition of a mixture- densitometry and chromatography- tend to take some time and involve expensive equipment. The ECO- (Electronic COmposition) METER gives an instantaneous reading from its program.

7.1.3 Development.

The stages of development for the device can be split into three main parts, each of which is discussed in turn.

- Prototype composition meter using an EPROM chip to store data.
  - The first meter was used to determine the concentration of an aqueous lithium bromide solution in the A.H.T experimental rig. This was followed by the adaptation of the meter for use with a binary mixture of the new HFC refrigerants, R32 and R134a.
- Development of the binary refrigerant meter for use with the mixture R32- R134a. A HP48 programmable calculator was used to determine the composition of the mixture directly using known VLE equations.
- Extension of the binary meter to determine the composition of a ternary refrigerant mixture using a leakage path model developed by Teresa Matias in the Department of Chemical Engineering [171]. The calculator was programmed with a reduced form of the equations used in this model. The ternary refrigerant mixtures investigated were three different blends of the refrigerants- R32, R134a and R125.

The programming required for the generation of the LiBr- H_2O and also the R32- R134a data, used in the EPROM meters, was carried out by the author using known VLE equations for each mixture. In addition, the software written for the binary and ternary mixtures on the HP48 calculator was also undertaken by the author. The binary mixture software was written using known VLE equations, while the software for the ternary mixture was developed from the work of Teresa Matias.

7.2 Lithium Bromide/ Water Composition Prediction.

The first ECO- meter was built using standard electronic components with an EPROM (Erasable Programmable Read Only Memory) chip to store the composition data in a large 2-D array. The lithium bromide concentration was inferred from measurements of temperature and pressure in the generator of the experimental apparatus, where there was vapour- liquid equilibrium. These readings were used to reference a particular composition from the large data matrix, Figure 7.1.

The data was generated from a series of established empirical equations [24], describing the properties of aqueous lithium bromide, see Appendix B 'Lithium Bromide Physical Property Charts' for VLE equations. The equations were programmed into a computer and the compositions determined for a specified range of temperatures and pressures. The resulting data array of compositions was then transferred to the EPROM chip.

In this prototype the temperature and pressure were each converted from a voltage by an 8- bit A/D converter to give a hexadecimal number, ranging from 0 to 256. For example, the pressure range used in the lithium bromide meter was 0.05 - 0.301 bar corresponding to the hexadecimal range of 00 - FF (256bits). This gave a ± 0.001 bar discrimination on the pressure reading. The temperature range adopted was 85 - 110.6 °C, giving an accuracy of ± 0.1 degC. In total, the number of compositions stored on the memory chip was 65536, with each composition being accessed from the two- dimensional matrix of pressures and temperatures. Figure 7.1 illustrates that for a pressure- temperature pair of (0.09 bar, 100 °C) the composition was 65 %/w, corresponding to the entry in the matrix at coordinates (40, 150). Each combination of temperature and pressure provides a unique composition reading.

The composition was displayed as a weight percentage of the less volatile component in the mixture, in this case lithium bromide. The solution concentration was only displayed to ± 1 %w/w and therefore only required a two digit LED display. The reason only two digits were displayed was for simplicity, there was no reason why more accurate data could not be generated and stored on the EPROM chip, it would only increase the complexity of the display electronics [1]

[1] All electronic circuitry was developed and produced by Matthew Rea of the Department of Chemical Engineering.

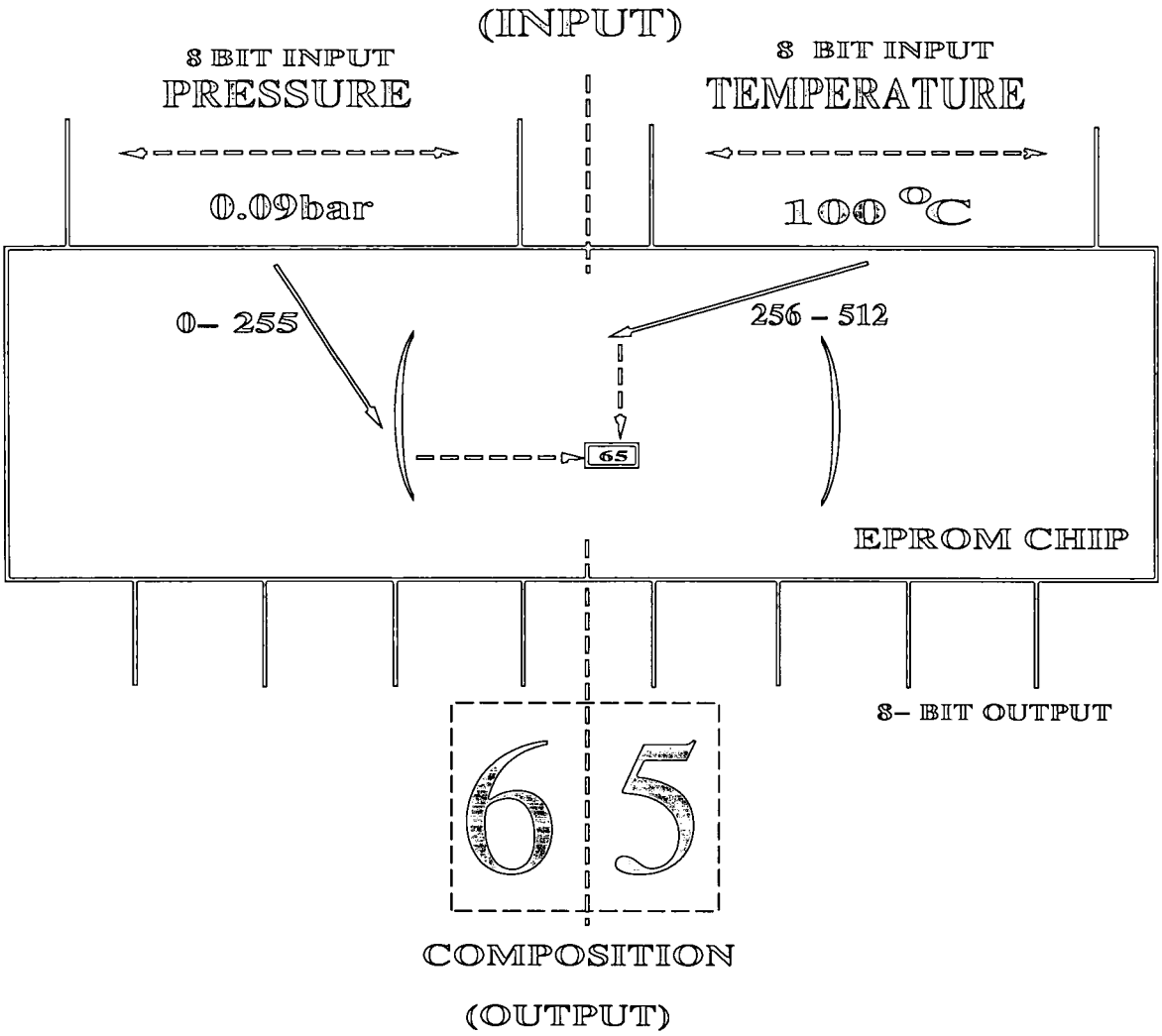

Figure 7.1: Graphical representation of how the absorbent composition is determined using pressure and temperature readings.

7.3 Binary refrigerant mixture of R32- R134a.

7.3.1 EPROM chip.

The second meter to be constructed again used an EPROM chip to store the refrigerant data. However, instead of being tested on lithium bromide, the components used were R32 and R134a, new 'ozone- friendly' refrigerants which could be a potential mixture replacement for pure R12 in refrigeration equipment. The data was displayed as the weight percent of R32, the more volatile component.

As with the previous EPROM chip, the data was generated from well characterised equilibrium equations for the binary mixture, Section 7.3.2. The data was generated and displayed to greater accuracy than the lithium bromide meter, in this case ± 0.1 %w/w. The temperature and pressure ranges used in this meter were set to 0- 35 °C and 4- 16 bar, which were representative of typical operating conditions for refrigeration equipment. The precision of the readings was therefore 0.14 °C and 0.05 bar respectively. Refrigerant compositions were easily reproduced within this operating range and did not suffer from any unexpected instrumental drift. In addition to providing a fast and accurate measurement of a refrigerant mixture, the readings would also be reliable over period of time.

7.3.2 Determination of the Composition for R32-R134a.

The composition of the binary refrigerant mixture of R32- R134a was determined using simple vapour- liquid equilibrium equations, which were dependent upon the temperature and pressure of the system. In an ideal system, the total pressure exerted by a binary mixture can be expressed by Equation 7.1, where the component vapour pressures are determined using Antione's equation, Equation 7.2. However, although it was assumed that the vapour phase of this mixture was ideal, the effects of liquid non- idealities had to be incorporated into the equations for predicting the composition of the mixture.

$$P_T = (x_1.P_1^*) + (x_2.P_2^*); \quad x_2 = (1 - x_1) \tag{7.1}$$

$$ln\ P^* = A - \frac{B}{T + C}\ ; \quad where\ T\ in\ [K] \tag{7.2}$$

The non- ideality of each component in the liquid phase was expressed as an activity coefficient, which was determined using the Wilson energies calculated for the mixture, Equations 7.3 and 7.4. Component 1 refers to R32, the most volatile component. Similar Equations exist for the computation of the activity coefficient of R134a, except the subscripts used in Equations 7.3 and 7.4 are reversed.

$$ln\ \gamma_1 = -ln(x_1 + (\Lambda_{12}.x_2)) + x_2.[\frac{\Lambda_{12}}{x_1 + (\Lambda_{12}.x_2)} - \frac{\Lambda_{21}}{(\Lambda_{21}.x_1) + x_2}] \tag{7.3}$$

$$\Lambda_{12} = -\frac{V_2}{V_1}\ .\ exp(-\frac{E'_{12} + (E''_{12}.T)}{R.T}\ );\quad where\ T\ in\ [K] \tag{7.4}$$

As the activity coefficient was dependent upon the component mole fractions, it was necessary to use an iterative method for accurately predicting the mixture composition. After an initial estimate of the mixture composition was made using Equation 7.5, which assumed that the system was ideal (i.e. $\gamma = 1$), the

component activities could be determined using Equation 7.3. By substituting the results obtained for the component activities into Equation 7.5, a better estimate of the mixture composition was obtained. The process was repeated until the mixture composition was accurate to 0.05 mole fraction. Finally, the result was converted to a weight fraction of the most volatile component, in this case R32.

$$x_1 = \frac{P_T - \gamma_2 . P_2^*}{\gamma_1 . P_1^* - \gamma_2 . P_2^*} \tag{7.5}$$

7.3.3 HP48 programmable calculator.

Later developments with the binary composition prediction involved the real time computation of the refrigerant composition from the temperature and pressure readings using the above equations. This was in preference to using the EPROM chip, which was essentially just a large 'lookup' table.

A programmable calculator, in this case a Hewlett Packard 'HP48', was used to store the necessary vapour pressure equations used to compute the refrigerant composition (Section 7.3.2). There were two modes of operation for the calculator, which were both simple to use.

Manual- Readings of temperature and pressure were input by the user. The result was then displayed as a weight percentage of R32. Also displayed were the input readings of temperature and pressure.

Automatic- The HP48 has an infra red sensor, which was linked to a processor board containing the necessary electrical components to convert temperature and pressure measurements to digital readings. The sampling end of the probe, containing a type- K thermocouple and a pressure

transducer, simply attached to any suitable sample point on the refrigeration equipment, using a standard stainless steel $^1/_4$" Swagelok fitting. This provided a direct reading of the refrigerant mixture conditions in the refrigeration cycle. Final results were in the same format as the manual operation- composition, temperature and pressure again being displayed.

7.3.4 Further modifications.

After the successful testing of the meter using the HP48 calculator, the electronic circuit board was further developed by Tim Campbell of Neat Systems Ltd. The new circuit, which could easily be reproduced for mass production, fitted into the upper section of specially developed sampling device, Figure 7.2. The calculator was easily inserted and removed from the sampling section of the meter, making it entirely portable, which would be particularly useful if there were several sampling points on a refrigeration system.

7.4 Ternary refrigerant mixture of R32- R134a- R125.

The principle of vapour-liquid equilibrium measurements may be extended in a number of ways to determine the composition of a mixture of three or more refrigerants, or even take into account the presence of lube oil within the refrigerant mixture. Two methods of determining the composition of a ternary

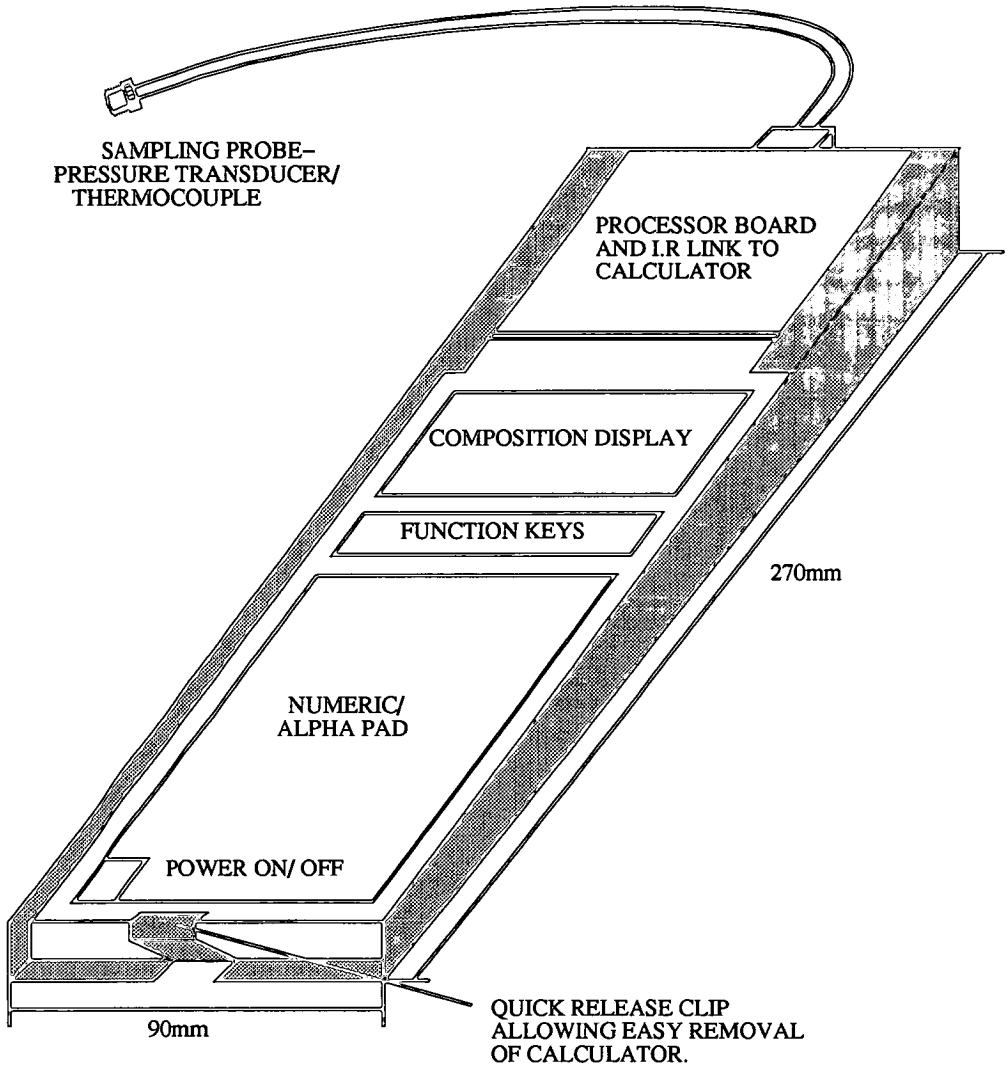

Figure 7.2: Diagram of HP48 calculator and measuring equipment.

refrigerant mixture are summarised below. They are the leakage path method and the multiple measurement method, although all of the work to date has been concerned solely with the former for a ternary mixture of R32, R134a, and R125.

7.4.1 Leakage path method.

This particular method examined the change of composition of a mixture as the more volatile components leaked preferentially from the high- pressure side of the refrigeration equipment. It has been shown that the path taken by the mixture was insensitive to temperature; and that the locus of compositions crossed mixture isobars at a steep angle, providing a unique determination of the composition of a 'leaked' mixture of known initial composition, thus removing the problem of composition determination for mixtures containing an azeotrope.

Figure 7.3 [2] illustrates the unique leakage path for each of three favoured mixtures of R32/R125/R134a [Blends (a), (b) and (c)]. The procedure for finding the mixture composition first of all used the readings of temperature and pressure to find the mass fraction of R134a in the mixture, Figure 7.4. Next the mass fraction of R32 was determined using the known leakage paths of the different blends, Figure 7.3. The fraction of R125 was then inferred by difference.

[2] Data reproduced from a report by Teresa R. Senos Matias 'Differential Leakage in a Closed System' [171]

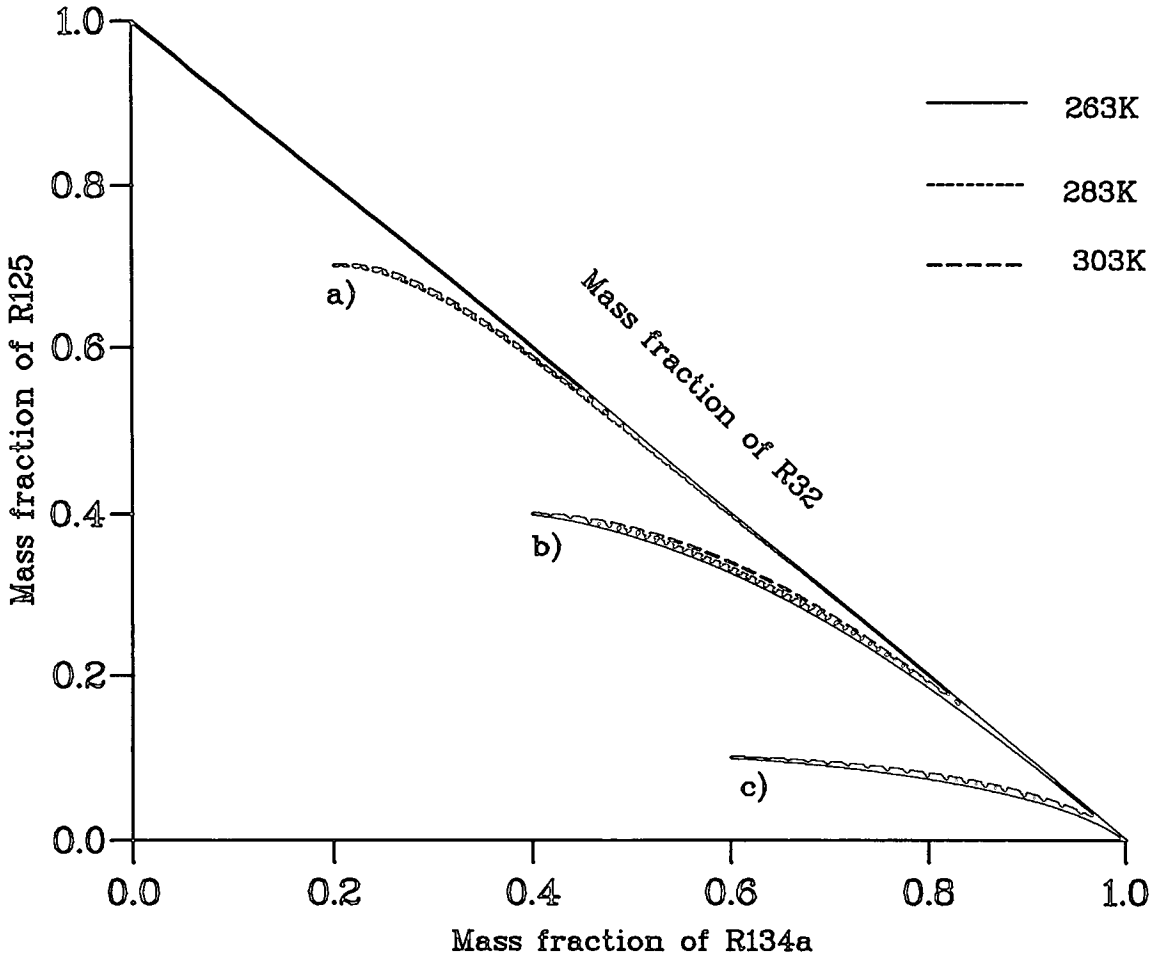

Figure 7.3: Leakage paths for R32/R125/R134a, showing temperature sensitivity.

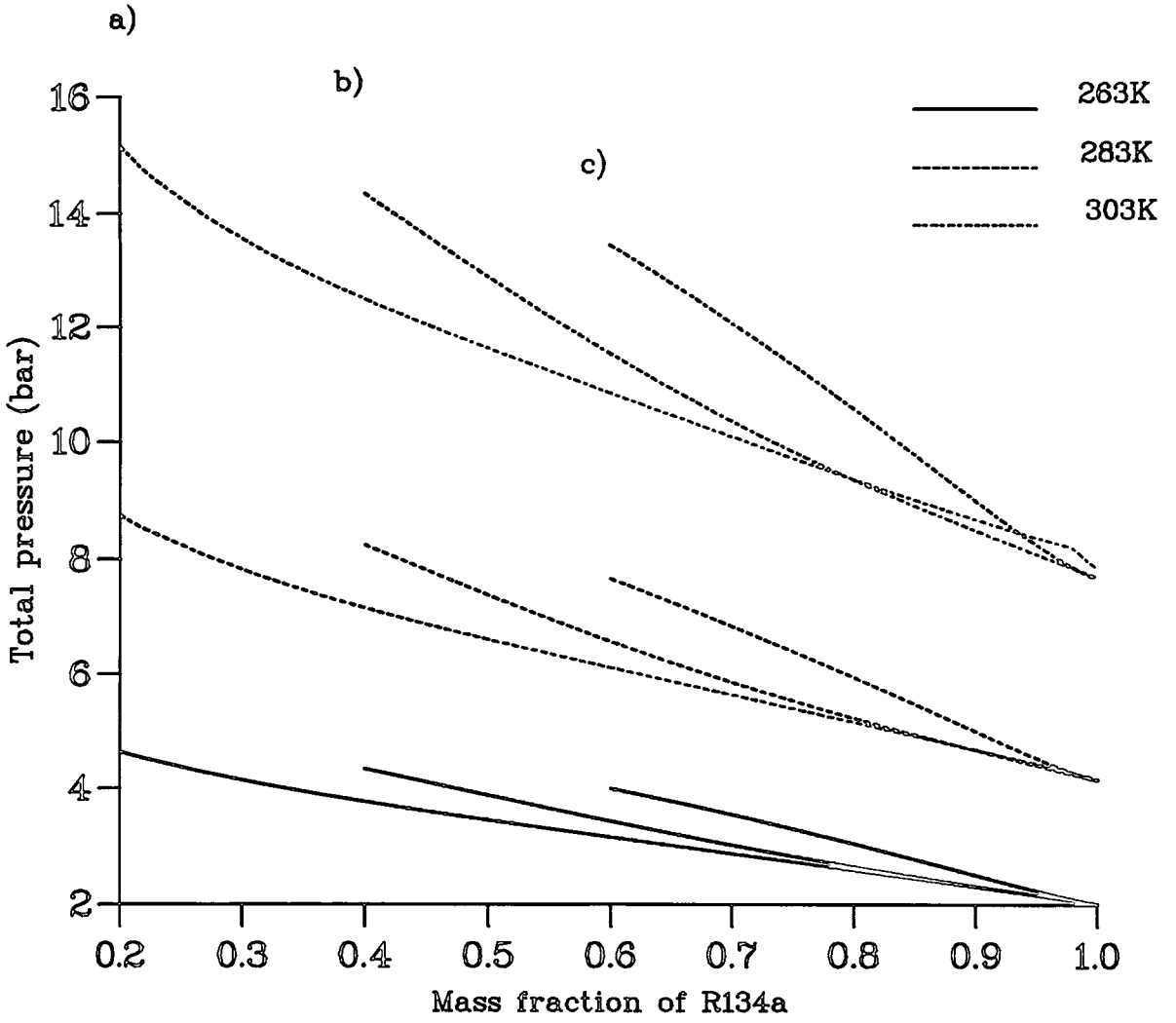

Figure 7.4: Variation of the total system pressure as a result of refrigerant leakage, from a known initial mixture of R32/R125/R134a.

The model developed by Teresa Matias accurately predicted the composition of the different refrigerant blends over a full range of possible values (i.e. starting from the initial blend composition and finishing when only the LVC remained in the system). However, the portable composition meter was increasingly inaccurate in predicting the mixture composition as the MVC leaked from the system because of the assumptions made in simplifying the model. The modifications to the model were necessary in order to reduce the size of the composition prediction program and also to speed up it up. This was not felt to be a major problem as the meter would only be used to restore the composition to its original composition, which it could do quite accurately. Accurate monitoring of mixtures which were widely different from the original blend (i.e containing very little of the MVC) was felt to be unnecessary. Such depleted mixtures would be of less use in refrigeration equipment as the performance of the cycle operating under these conditions would be greatly reduced.

7.4.2 Multiple Measurement Method.

This model involves inferences from two (or more) points within the refrigeration circuit where vapour and liquid are in equilibrium. Therefore, the composition of a ternary mixture may be determined uniquely, without reference to leakage. This would be the preferred method for large- scale equipment on which several sensors would be permanently mounted, providing the meter with the necessary data points to determine the mixture composition. It would also permit accurate restoration of a desired initial composition in multicomponent mixtures whose leakage history was unknown.

7.5 Results and Conclusions.

LiBr/ H_2O composition prediction. During the experimental studies with the two stage absorption heat transformer, the composition meter was invaluable as it allowed the absorbent concentration to be measured quickly and rapidly. As well as providing an estimate of the concentration of the lithium bromide solution in the generator, the temperature and pressure of the system were also given. The results were accurate over the period of study.

Composition prediction of new refrigerant mixtures. The binary refrigerant meter using the EPROM meter was felt to be limited in its use, as the temperature and pressure ranges were preprogrammed into the chip. The use of the programmable calculator, although requiring the computation of the refrigerant composition each time readings were taken, had the benefit of being more versatile. Indeed, the time taken to calculate the refrigerant mixture was only a few seconds and so was felt to be a minor drawback of the system.

Experimental field trials carried out using the binary and ternary meters were very promising. The tests were carried out by an independent group, who found each meter to provide accurate and reliable results for different refrigerant mixtures of pre-determined composition. The meter have also generated a lot of interest in the commercial sector, where the potential of such a meter is great.

7.5.1 Future developments.

Instrumentation. The sensing probe attached to the meter can be easily reproduced using readily available equipment. Although the electrical instrumentation was developed especially for this project, it is only an electronic printed circuit board which could easily be mass produced. As the same readings would be used for all combinations of refrigerant mixtures, the circuit would remain the same and could easily be used for different applications.

Alternative mixtures. The development of this particular device has progressed significantly from the initial EPROM meter used to measure the composition of an aqueous solution of lithium bromide. The latest meter uses simplified VLE equations to estimate the composition of a ternary refrigerant mixture, using the leakage path method and provides an accurate measure of a ternary refrigerant mixture.

The next stage of development would be to test the meter with new refrigerant mixtures, which are well characterised. The influence of lubricating oil and even 4 component mixtures could also be investigated. Computational methods have been developed in the Department of Chemical Engineering to deal with this. Eventually, there would be different computer disks of information for each group of mixtures, while the probe would remain the same. Ultimately, a large data base of refrigerants could be held on disk. This raises the possibility of using the meter to identify an unknown refrigerant mixture simply from readings of temperature and pressure.

Chapter 8

Conclusions.

The main objectives of this project have been met- an open loop absorption heat transformer cycle was successfully tested for the purpose of recovering waste heat from spray dryer exhausts. However, the initial single stage cycle which was first used was surpassed by a two stage absorption process which dehumidified and reheat humid gas streams in successive stages. The first absorption stage used a direct contact absorption column to dehumidify the humid gas stream from an inlet humidity of around 0.20 g-$_{H_2O}$ (g-$_{dry\ air}$)$^{-1}$ to 0.03- 0.05 g-$_{H_2O}$ (g-$_{dry\ air}$)$^{-1}$ This stage was followed by an indirect contact reheat absorber, which reheated the gas to approximately 150- 160 °C.

8.1 Experimental Studies.

As discussed in Chapter 4 'Experimental Studies' it was not possible to both dehumidify and reheat the humid gas stream in one stage. Therefore, the two operations were separated into absorption columns. Each of the absorption processes was extensively tested over a range of operating conditions, using aqueous lithium bromide as the working fluid.

In the dehumidification column, the humid gas and concentrated lithium bromide solution flowed countercurrent to each other so as to maximise the absorption of water vapour into the liquid phase. Three different absorbers were tested to see which one gave the best dehumidification results. The first column, was a simple falling film absorber, which gave poor results because of poor liquid- gas contact. The column was then packed with small glass helices, which improved the amount of water vapour absorbed, although the results were still outside the limits set out at the start of the project. Finally a heat exchanger was used as the dehumidification column. Cooling water was used as the heat transfer medium to remove the heat of absorption from the top of the column. This had the effect of lowering the partial pressure above the absorbent solution and therefore increased rate of transfer to the liquid phase. In addition, the large surface area of the cooling coil also provided good liquid- gas contact. There was a significant improvement in the dehumidification of humid gas streams with this column.

The best results were obtained using an inlet absorbent concentration of 64 %w/w and a flowrate of 8.5 gs^{-1} was used, in conjunction with a high water flowrate in the cooling coil (approximately 9 gs^{-1}). This helped to maintain a low vapour pressure above the absorbent solution and therefore improve the absorption of water vapour.

The reheat experiments involved the heating of the dried gas stream using a concentrated lithium bromide and steam as the heating medium. The steam, which flowed cocurrent to the concentrated lithium bromide solution, was absorbed into the liquid very rapidly. This generated very high temperatures at the top of the inner absorption tube. The gas stream flowed countercurrent to the absorption mixture, resulting in high exit temperatures at the top of the column. The best results were obtained when a lithium bromide solution of 68 %w/w and low flowrate (around 2 gs^{-1}) was used, while the steam flowrate was 0.16 gs^{-1} ($F_r \sim$ 12- 14). The highest exit gas temperatures were achieved at gas flowrates of 3 gs^{-1}.

8.1.1 Absorption Working fluids.

The most common absorption working fluids currently being used are ammonia-water and water- lithium bromide. In this particular project, the latter pair was used because higher operating temperatures were possible, without the need for high pressure equipment. In addition, there was no need for a rectification section because lithium bromide has a negligible vapour pressure. However, the system was limited by the maximum operating concentration possible due to crystallisation problems at very high concentrations. The lowest temperature point of the cycle was the generator, which was operated under vacuum at a temperature of approximately 100 °C. The maximum concentration which could be used in the apparatus without the risk of crystallisation was 68- 69 %w/w. This problem has led researchers to look for ways to improve the solubility of the fluid pair by adding a third component. In addition, research has also been carried out into the development of new working fluids.

The development of high temperature absorption systems has involved the search for suitable fluid mixtures which are stable at temperatures around 200 °C. The separate studies by the Universities of Graz and Essen have resulted in several organic fluid pairs being proposed for use in absorption cycles. Extensive experimental studies are needed to measure the performance of the working pairs. One of the refrigerants suggested by both groups was TFE (trifluoroethanol). However, the component is toxic and so its use would not be recommended except perhaps for use in industrial units. The best combinations of refrigerant- absorbent mixtures use amines or alcohols as the refrigerant and aromatic or cyclic compounds, which have a high stability, as the absorbent. Glycerol and 1,4 butanediol were also suggested as absorbents because of their high stability.

8.2 Simulation Studies.

The computer models were written to investigate the absorption process in detail, with particular reference to the temperature and mass flow profiles within the absorber. The models enabled each of the different aspects of the heat transformer to be studied: dehumidification of humid gas streams, simple absorption of steam into lithium bromide and also heat removal to an external gas stream. The results obtained complemented the experimental studies well and again showed the importance of the absorbent concentration in achieving a high exit gas temperature.

8.3 Industrial Heat Recovery.

A comprehensive study of the industrial spray drying operation and associated gas cleaning equipment was undertaken in order to gain an insight into the heat recovery and gas recycling requirements of the industrial process. It was necessary to design an absorption heat transformer which could easily be retrofitted into the existing process. The main benefits of incorporating a heat transformer into the drying operation are reduced fuel consumption, a reduction in the visible plume caused by venting humid gas to atmosphere and also the potential for increasing the dryer throughput.

The temperature of heat source required for the industrial heat transformer would need to be around 100 °C. It was therefore proposed to use LP steam, which could be used in both the generator and also directly as the steam supply for the absorption tube in reheat column. Indeed any waste heat stream available at a temperature around 100 °C could be utilised in the cycle.

8.4 Future Work and Recommendations.

The experimental studies showed the best operating conditions required to achieve the objectives of dehumidifying and reheating humid gas streams. However, further work needs to examine the actual temperature profiles within the column. In the model for the reheat column, results obtained could then be compared to the results predicted by the computer model. The temperature profiles obtained from the absorption simulation models indicated a rapid rise in the temperature of the streams at the top of the column, as the steam was

absorbed into the liquid phase. The resultant weak lithium bromide mixture then flowed down the column at approximately a constant temperature. The temperature of the external gas stream increased more gradually because of the lower heat transfer coefficient between the absorption tube and the gas stream in the outer annulus of the reheat absorber.

The direct contact dehumidification column was operated successfully when a heat exchanger was used, which allowed the temperature and hence exit water vapour pressure at the top of the column to be controlled. However, before such a system could be used on an industrial basis, further work needs to be carried out to investigate the risk of absorbent carry over into the drying operation. In addition, the computer model needs refinement to include the removal of heat to a cooling coil, which was used to control the temperature at the top of the column.

As highlighted previously, although water- lithium bromide is a popular working fluid pair, new working fluids should be tested to see if they can achieve better results for both the dehumidification and reheat processes. Such studies should involve computer simulations to first of all identify the best working fluid mixtures. Thereafter, the best fluids could be tested in a new pilot plant.

Appendix A

Operating Instructions.

A.1 Preparation of the Working Fluid Mixture.

The absorbent used in these studies was lithium bromide (99% purity) which was purchased from Aldrich Chemicals Ltd. Lithium nitrate was used as a corrosion inhibitor and was added to the solution in a ratio of 99:1 (LiBr: $LiNO_3$). Care was taken when handling these chemicals, as they were both oxidants and would cause minor irritation if exposed to skin. It was necessary to follow the COSHH regulations concerning the use of these chemicals and extreme care was exercised when making up a concentrated absorbent solution.

Preparation Procedure.

Step 1: Ensure that all safety procedures are followed- wear goggles, gloves and face mask.

Step 2: Weigh out desired weights of lithium bromide and lithium nitrate, in a ratio of 99:1.

Step 3: Measure out enough distilled water into a large beaker so that the final solution concentration was between 40- 50%.

Step 4: Add some powder mixture to the distilled water.

Step 5: Mix solution with a glass rod to ensure that all the powder is dissolved.

Step 6: Once the solution was made, it was used to charged the apparatus, using a vacuum to pull mixture into the lithium bromide generator/ reservoir.

A.2 Startup Procedure.

Step 1: Switch on computer and start monitoring program

Step 2: Heat up the system by circulating hot air throughout the absorption columns and the associated pipework. Once the apparatus had been heated up and all the streams circulated, it quickly came to a steady state and continued to operate with only minor adjustments required.

Step 3: Heat up the lithium bromide solution in the generator and switch on the vacuum. Do not allow the solution to become too concentrated otherwise this could lead to problems of crystallisation. Maintain at a concentration between 50- 55%.

Step 4: Open bleed valve on reheat column and switch on reheat steam generator to remove all inert gases.

Step 5: Circulate lithium bromide to heat up the pipework and switch on the lithium bromide reheaters.

Step 6: Switch on the steam generator to full power. Once steam is generated, reduce the power to give desired inlet gas humidity.

Step 7: Start to concentrate lithium bromide solution to desired working concentration.

Step 8: Input flowrates of streams and start data logging files on the PC.

Step 9: Periodically take readings of the inlet and outlet gas humidities and input readings.

Step 10: Vary power input to steam boilers and lithium bromide generator, so as to maintain desired flows and concentration.

A.3 Shutdown Procedure.

Step 1: Stop the computer program by pressing ⟨F1⟩.

Step 2: Switch off steam boilers, for both columns.

Step 3: Switch off power to lithium bromide generator and reduce vacuum on system to about 0.1- 0.2bar, which will still allow liquid to be flashed from the high pressure side.

Step 4: Continue to circulate lithium bromide. Place a beaker of hot water at the charging point and close the valve beneath generator, while also opening the charging valve. As a result the lithium bromide flow is stopped and water is now circulating round the system. This was to flush out the lithium bromide pipework and prevent the risk of crystallisation, in both the pipework and also the generator when it cools down.

Step 5: Switch off the metering pump and also the lithium bromide reheaters.

Step 6: Switch off the vacuum pumps.

Step 7: Switch of the air heaters and finally the air flow.

Appendix B

Lithium Bromide Physical Property Charts.

The physical property data used for both the experimental and computer simulation studies were mostly taken from the papers of M^{c}Neely [172] and Brunk [24], as well as the work of Liu [165]. Graphs of the main physical properties are provide below.

B.1 Vapour Pressure Equilibrium.

The solution vapour pressure, Equation B.3, was dependent upon the temperature of the lithium bromide and also it concentration. The coefficients

α and β were derived from the absorbent concentration using 3^{rd} order polynomials, Equations B.1 and B.2. The constants used in the expressions depended on the solution concentration. (Full details in [24]).

$$\alpha = \Sigma a_i . w^i \tag{B.1}$$

$$\beta = \Sigma b_i . w^i \tag{B.2}$$

$$log_{10}(14.5038.p) = k_0 + \frac{k_1}{1.8.T' + 491.67} + \frac{k_2}{(1.8.T' + 491.67)^2} \tag{B.3}$$

$$T' = \frac{T - \beta}{\alpha} \tag{B.4}$$

p [bar]. T / T' [°C]. w [%w/w].

Only a limited range of lithium bromide concentrations and solution temperatures were used to generate Figure B.1. The ranges were applicable to the conditions encountered during this project.

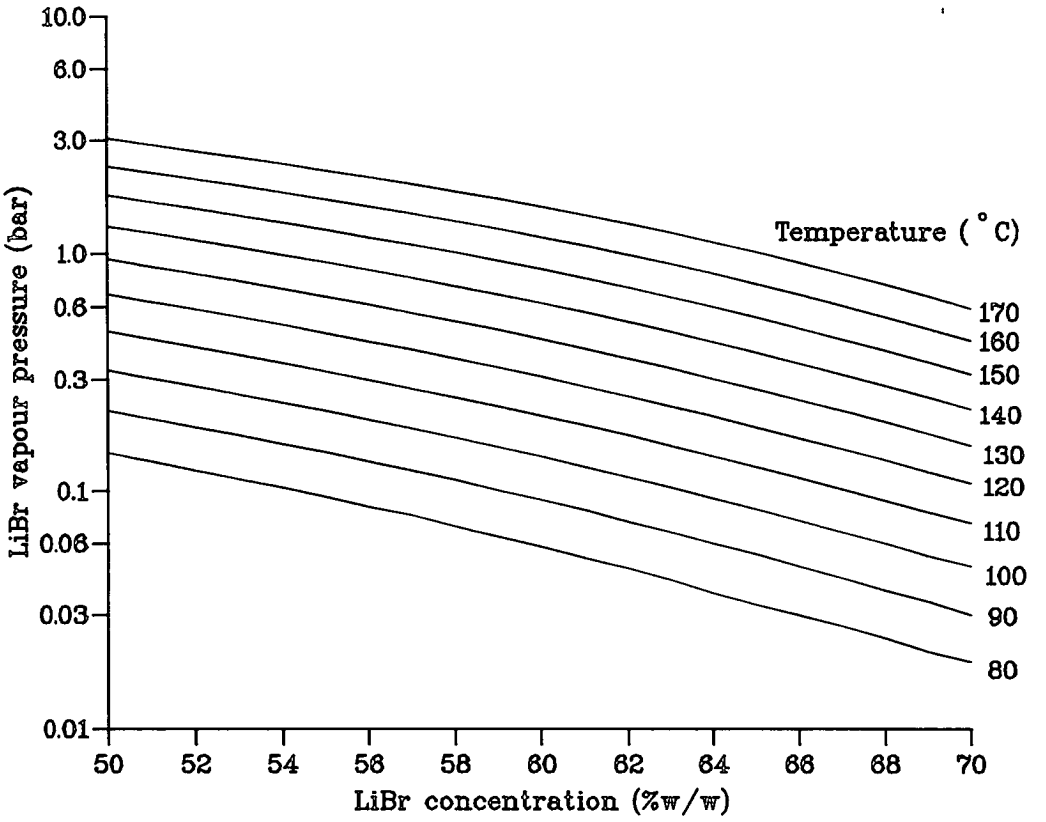

Figure B.1: Vapour pressure equilibrium chart for aqueous lithium bromide solution.

B.2 Enthalpy.

A similar equation to the vapour pressure was used to determine the liquid enthalpy, Equation B.5, where A, B and C were determined from the solution concentration. The terms A, B and C were determined from a standard polynomial equation ($\Sigma_{n=0}^{4}$ A_n. w^n), with the constant values provided in the papers by M^{c}Neely [172] and Brunk [24]. Also shown on Figure B.2 is the crystallisation line. The line represents temperature at which a particular concentration of lithium bromide solution crystallise.

$$h = 2.326.\,[A + B\,(1.8T + 32) + C\,(1.8T + 32)^2\,] \qquad \text{(B.5)}$$

h [kJ kg^{-1}]. T [°C]. w [%w/w]. Base enthalpy (0 kJ kg^{-1}) is 0 °C for a 50 %w/w mixture of water and lithium bromide.

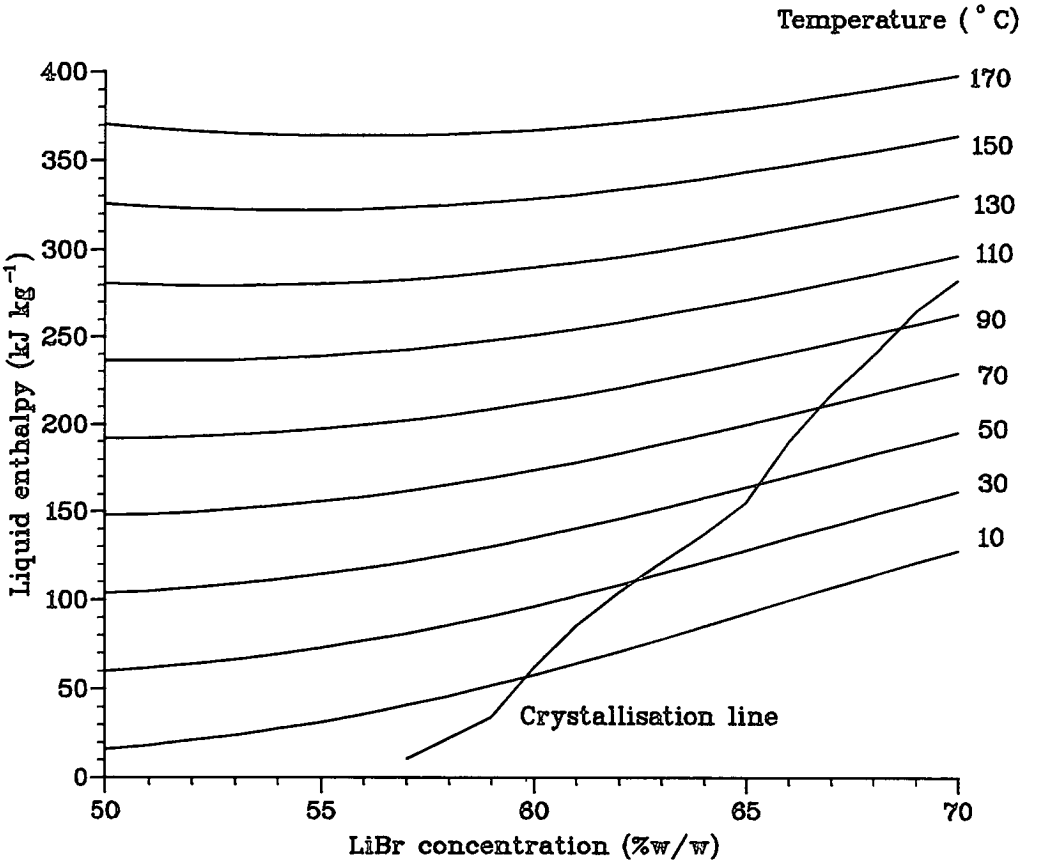

Figure B.2: Enthalpy chart for aqueous lithium bromide solution.

B.3 Density.

The equation expressing the liquid density was reproduced from the PhD thesis of Liu [165], see Equation B.6. Again, it was expressed as a function of the absorbent concentration and temperature.

$$\rho = [(11.015 - (20.98.w) + (18.8.w^2).w^{1/2}.(273 + T)^{-0.15}].1000 \quad \text{(B.6)}$$

ρ [kg m^{-3}]. T [°C]. w [%w/w].

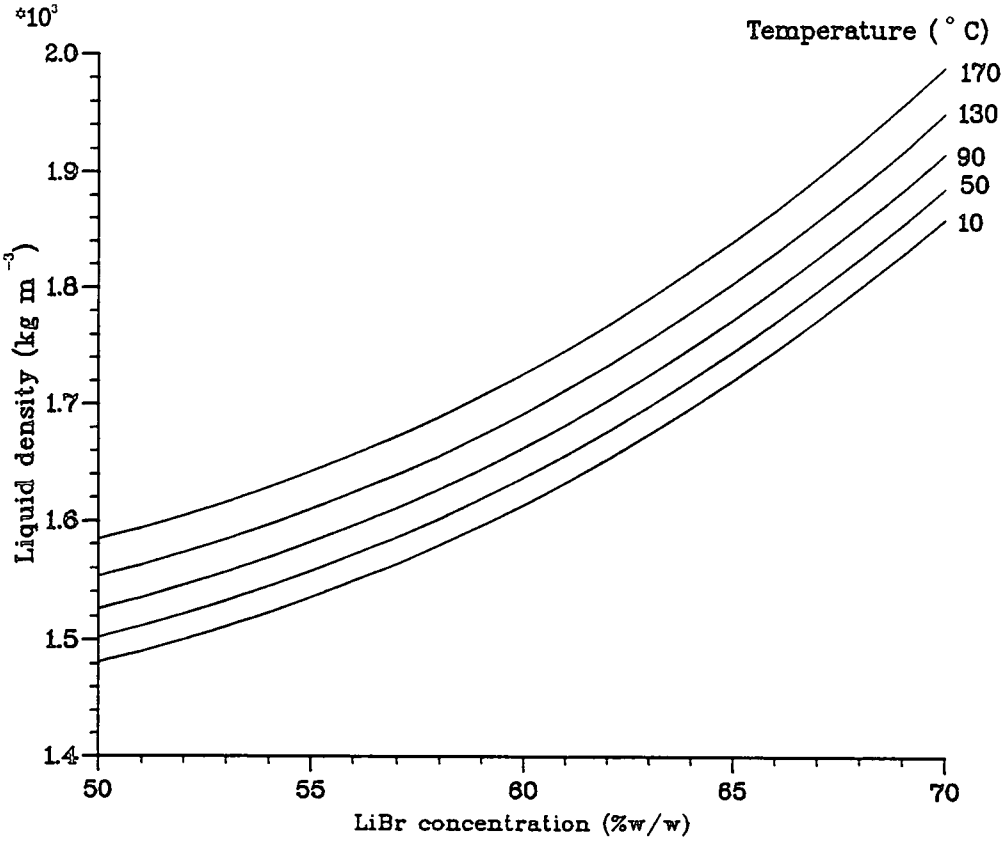

Figure B.3: Density chart for aqueous lithium bromide solution.

B.4 Heat Capacity.

The lithium bromide heat capacity was determined from Equation B.7, given by Brunk [24]. However, it was only valid for temperatures up to 100°C. Above this temperature, the correlation behaves oddly. Therefore, it was necessary to assume a constant value for the stream heat capacity above this temperature.

$$c_P = [\,\Sigma_{i=0}^{2}\,\Sigma_{j=0}^{4}\, a_{i,j}.\, w^i.\, T^j].\, 4.168 \qquad \text{(B.7)}$$

c_p [kJ kg^{-1} K^{-1}] T [°C]. w[%w/w]

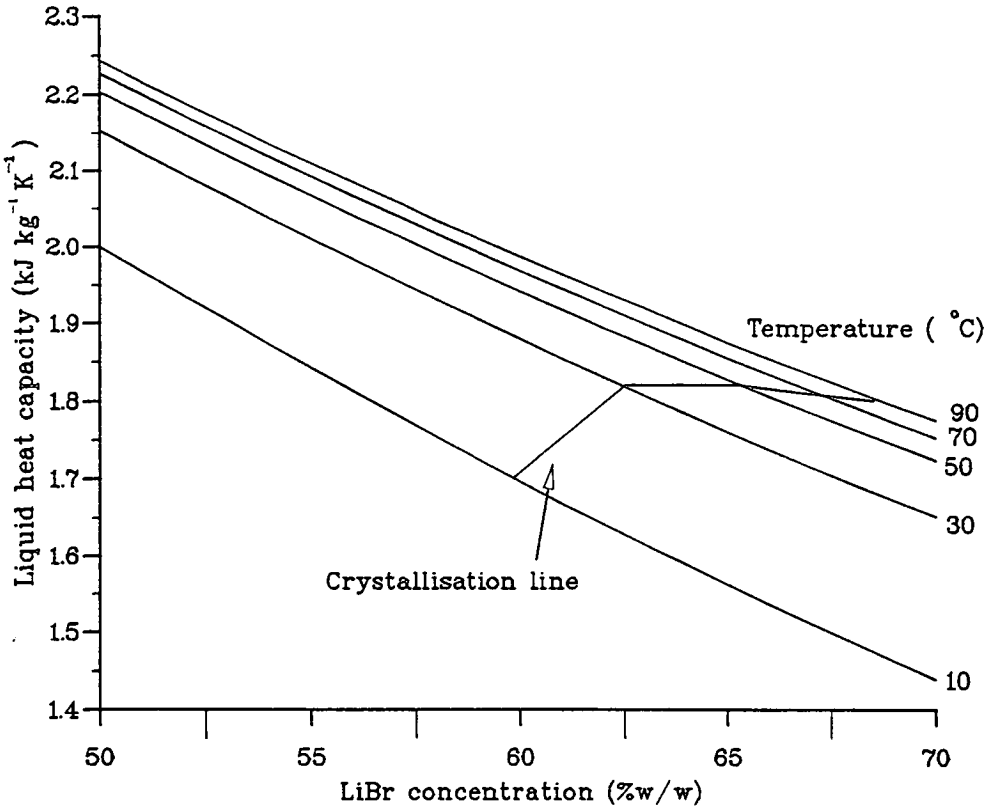

Figure B.4: Heat capacity chart for aqueous lithium bromide solution.

Appendix C

Sample Calculations.

The sample calculations summarised in this Appendix cover a wide range of topics. The design calculations, equipment sizing and preliminary heat and mass balances for the heat transformer cycle all relate to the work covered in Chapter 3 'Design and Construction'. The derivation of experimental and theoretical heat transfer coefficients relate to Chapter 4 'Experimental Studies'. The last section provides some background calculations for Chapter 6 'Industrial Case Study'.

C.1 Design Calculations.

Within this section, basic design calculations for the sizing of the equipment for the single stage pilot plant are outlined (supplementary to Chapter 3, 'Design and Construction'). In addition, mass and heat balances for the two stage heat transformer cycle are presented.

C.1.1 Single Stage Pilot Plant.

The first absorption heat transformer cycle to be constructed was initially designed to provide a maximum gas superficial velocity through an absorption column of $2ms^{-1}$. Therefore based upon the flowrate provided by the air blower it was possible to find the appropriate size for the column. The remainder of the cycle was designed to be of a comparable size to the absorber.

Using the air blower, the maximum gas flowrates possible were around 250 l min^{-1} $_{20°C}$ (5 gs^{-1}). Therefore to achieve a superficial velocity through the absorber of 2 ms^{-1}, the column diameter had to be 2" (0.054 m) (see below).

Gas flowrate (Q_G) $= 250$ l min^{-1} (as measured on the air rotameter)
Maximum velocity (u_G) $= 2$ ms^{-1}

Column cross-sectional area, A
$= Q_G / u_G$
$= (250 \times 10^{-3}) / (60 \times 2)$
$= 2.08 \times 10^{-3}$ m^2

Internal diameter (d)
$= \sqrt{(4.\ A)/\pi}$
$= 0.05$ m ($\sim$ 2")

The heaters used for generating the water vapour necessary to humidify the dry gas stream had a maximum capacity of 3kW. Assuming heat losses of 300W, the maximum steam flowrate was around $1.2 gs^{-1}$. This corresponded to an inlet humidity of 0.24 g- $_{H_2O}$ $(g\text{-}_{dry\ air})^{-1}$, which was typical for spray dryer exhausts.

$$\begin{aligned} \text{Heater power} &= 3\text{kW} \\ \text{Losses} &= 300\text{W (10\%)} \\ \text{Maximum steam flowrate} &= 1.2\ gs^{-1} \\ \\ \text{Gas humidity} &= (1.2 / 5) = 0.24\ \text{g-}_{H_2O}\ (\text{g-}_{dry\ air})^{-1} \end{aligned}$$

C.1.2 Cycle Heat and Mass Balances.

As a design basis, the inlet gas flowrate to the two stage absorption cycle was $2gs^{-1}$, with an initial humidity of 0.12g- $_{H_2O}$ $(g\text{-}_{dry\ air})^{-1}$. In addition, the gas stream was assumed to have an inlet temperature of 100°C. By making several assumptions about the performance of each of the pieces of experimental apparatus- i.e dehumidification column, reheat column, generator and condenser- it was possible to determine full heat and mass balances for the open loop absorption cycle. The following sections outline the procedure used to determine the overall heat and mass balances for the cycle for each of the main components, as well as listing the assumptions made.

Dehumidification Column.

The dehumidification column was designed to reduce the humidity of a simulated dryer exhaust gas stream to a level suitable for recycling. The column operated with LiBr and gas streams flowing countercurrent to each other. The

assumptions used in order to determine a preliminary mass balance round the absorber are detailed below:

Assumptions: 1) Inlet LiBr concentration = 67 %w/w
2) Inlet LiBr temperature = 100 °C
3) Concentration change = 1 %w/w
4) Exit water vapour partial pressure equal to vapour pressure above inlet LiBr solution

Gas flowrate = 2 gs^{-1}

Water vapour flowrate = 0.24 gs^{-1} (H_{in} = 0.12 g- $_{H_2O}$ $(g\text{-}_{dry\ air})^{-1}$)

Vapour pressure above 67 %w/w LiBr @ 100°C = 0.07 bar

= Exit water vapour pressure

Exit water vapour flowrate = 0.09 gs^{-1}

Amount of water absorbed = (0.24 - 0.09) = 0.16 gs^{-1}

Inlet LiBr conc = (Mass LiBr) / (Mass LiBr + Mass H_2O)

Outlet LiBr conc = (Mass LiBr) / (Mass LiBr + Mass H_2O + Absorbed H_2O)

Rearrange in terms of LiBr and solve for H_2O:

Total water content in absorbent stream = 3.18 gs^{-1}

LiBr mass flow = 6.46 gs^{-1}

Inlet absorbent flowrate = 9.64 gs^{-1}

Outlet absorbent flowrate = 9.78 gs^{-1}

Reheat Column.

In the reheat column, it was important to raise the gas stream temperature to as high a level as possible. The temperature lift in the single stage absorber was assumed to be 70 degC. Therefore, the heat duty in the column was around 180 W (see below). The inlet LiBr concentration was assumed to be 67 %w/w, the same as the dehumidification column. The steam used in the reheat column was sufficient to cause a change in the LiBr concentration of 1 %w/w. Using the same assumptions as were used in the previous section it was possible to find the steam flow required in the reheat column and also the LiBr flowrate.

Heat to gas (Q)	$= m.\ c_P.\ \Delta T_G$
	$= (2.09.\ 1.\ 70) = 150$ W
Losses	$= 20$ W
Total heat required	$= 170$ W
	= Heat released in absorption tube
	$= (m.\ h)_{LiBr_{in}} + (m.\lambda)_{RS} - (m.\ h))_{LiBr_{out}}$ [1]
	[1] where, $m_{LiBr_{out}} = m_{LiBr_{in}} + m_{RS}$]
Hence,	Heat in = Heat out
$(m.\ h)_{LiBr_{in}} + (m.\lambda)_{RS}$	$= Q + (m.\ h))_{LiBr_{out}}$
Rearrange in terms of m_{RS}:	
Steam flowrate	$= 0.1$ gs^{-1}
LiBr inlet flowrate	$= 6.47$ gs^{-1}
LiBr outlet flowrate	$= 6.57$ gs^{-1}

Generator.

The inlet flowrate to the generator was simply the sum of the exit LiBr streams from the dehumidification and reheat columns. While the outlet streams from the generator were the flows of concentrated LiBr pumped back to the top each absorber, in addition to the flow of evaporated water to the condenser. Therefore, it was only necessary to determine the heat balance around this piece of equipment. The operating conditions in the generator were assumed to be 100 °C and 0.07 bar.

Inlet LiBr flowrate
(@ 66 %w/w, 110 °C $= (9.78 + 6.57)\ gs^{-1}$
Inlet enthalpy $= 280\ Jg^{-1}$

Outlet LiBr flowrate
(@ 67 %w/w, 100 °C $= (9.64 + 6.47)\ gs^{-1}$
Outlet enthalpy $= 262\ Jg^{-1}$

Evaporated water $= 0.24\ gs^{-1}$
Heat of vaporisation $= 2529\ Jg^{-1}$ [2]

Heat in = Heat out

$(m.\ h)_{LiBr_{in}} + Q = (m.\ h))_{LiBr_{out}} + (m.\lambda)_{H_2O_{absorbed}}$

Rearrange and solve for Q:

$Q = (16.11 \times 262) + (0.24 \times 2529) - (16.35 \times 280)$
$= 250\ W$

Condenser.

The condenser was operated at the same pressure as the generator, 0.07 bar, while the temperature was 20 °C. Cooling water was used as the heat transfer medium. It was assumed that the cooling water flowed countercurrent to the vapour flow and that it entered the condenser at 15 °C. A temperature change of 15 degC was also assumed for the water stream. Therefore, the flowrate of the cooling medium was 9.8 gs^{-1} (590 cc min^{-1}).

Heat required to condense
water vapour, from generator (Q) $= (m.\lambda)_{H_2O_{absorbed}}$
$= (0.24 \times 2556) = 616\ W$

C.2 Derivation of Experimental Results.

A selection of the more complex experimental calculations are provided in the following sections. The main equations used in each of the computational steps are also included.

C.2.1 Reheat Column Heat Transfer Characteristics.

Calculation of the overall heat transfer coefficient for the reheat column, based upon the external, plain tube area, including a simple error analysis is detailed below.

$$Q_G = U_O . A_O . \Delta T_{G_{LM}} \tag{C.1}$$

$$Q_G = m_G . c_{P_G} . \Delta T_G \tag{C.2}$$

$$U_O = \frac{m_G . c_{P_G} . \Delta T_G}{A_O . \Delta T_{LM}} \tag{C.3}$$

$$\frac{1}{U_O} = \frac{1}{h_G} + \frac{1}{h_{LiBr}} . \frac{r_O}{r_I} + \frac{x}{k} . \frac{r_O}{r_{LM}} \tag{C.4}$$

$$Nu = \frac{h_G . d_H}{k_G} \tag{C.5}$$

$$A_{ann} = \frac{\pi}{4} . [d_O^2 - d_I^2] \tag{C.6}$$

$$Re = \frac{m_G . d_H}{A_{ann} . \mu_G} \tag{C.7}$$

T_G	ρ_G[1]	μ_G x 10^2	k_G x 10^2
(°C)	(kg m^{-3})	($gm^{-1}s^{-1}$)	($Wm^{-1}K^{-1}$)
40	1.13	1.85	2.72
60	1.06	1.9	2.87
80	1.00	2.0	3.02
100	0.95	2.1	3.18
120	0.90	2.2	3.33
140	0.85	2.25	3.47
160	0.82	2.35	3.61

Table C.1: Variation of the gas density, viscosity and thermal conductivity with temperature.

[1] ρ_G derived from the ideal gas law:

$$\frac{P_1 . V_1}{T_1} = \frac{P_2 . V_2}{T_2} \tag{C.8}$$

Calculation of overall outside heat transfer coefficient

$$
\begin{aligned}
A_O &= 0.055\ m^2 \\
m_G &= 4\ gs^{-1} \\
c_{P_G} &= 1.0\ Jg^{-1}k^{-1} \\
\Delta T_G &= 101 - 25 = 76\ degC \\
\Delta T_{top} &= 104 - 101 = 3\ degC \\
\Delta T_{bot} &= 103 - 25 = 78\ degC \\
\Delta T_{LM} &= 23\ degC \\
Q_G &= (4 \times 1.0 \times 76) = 304\ W\ [C.2] \\
U_O &= 304 / (0.055 \times 23) \\
&= \underline{240}\ \pm 350\ Wm^{-2}K^{-1}\ [C.3]
\end{aligned}
$$

Calculation of outside gas heat transfer coefficient

$$
\begin{aligned}
d_O &= 22.2 \times 10^{-3}\ m \\
d_I &= 20.2 \times 10^{-3}\ m \\
d_{LM} &= 21.2 \times 10^{-3}\ m \\
x\ (\text{Wall thickness}) &= 1mm = 1 \times 10^{-3}\ m \\
k\ (\text{Wall thermal conductivity}) &= 16\ Wm^{-1}K^{-1} \\
h_I\ (\text{HTC for inner tube}) &= 3000\ Wm^{-2}K^{-1} \\
h_G &= 1/(\ 1/240 - [1/3000 \times (22.2/\ 20.2)] \\
&\quad - [(0.001/16) \times (22.2/21.2)]\ ) \\
&= \underline{270\ Wm^{-2}K^{-1}}\ [C.4]
\end{aligned}
$$

Determination of the gas Nusselt number

$$
\begin{aligned}
d_H &= 50 - 22.2mm = 27.8mm = 2.8 \times 10^{-2}\ m \\
k_G &= 2.8 \times 10^{-2}\ Wm^{-1}K^{-1} \\
Nu_G &= (270 \times 2.8 \times 10^{-2}) / 2.8 \times 10^{-2} \\
&= \underline{270}\ [C.5]
\end{aligned}
$$

Determination of the gas Reynolds number

$$
\begin{aligned}
d_H &= 2.8 \times 10^{-2}\ m \\
A_{ann} &= \pi/4.\ [\ (\ 5 \times 10^{-2})^2 - (\ 2.2 \times 10^{-2})^2]\ [C.6] \\
&= 1.58 \times 10^{-3}\ m^2 \\
\mu_G &= 2 \times 10^{-2}\ gm^{-1}s^{-1} \\
Re &= (4 \times 2.8 \times 10^{-2}) / (\ 1.58 \times 10^{-3} \times 2 \times 10^{-2}) \\
&= \underline{3500}\ [C.7]
\end{aligned}
$$

Error analysis for above calculation:

Absolute error in temperatures $= \pm$ 1degC

$\delta(\Delta T_G) = (2/\ 50).\ 100\% = \pm\ 4\ \%$

$\delta(\Delta T_{top}) = (2/\ 2).\ 100\% = \pm\ 100\ \%$

$\delta(\Delta T_{bot}) = (2/\ 38).\ 100\% = \pm\ 5.3\ \%$

$\delta(\Delta T_{LM}) = (0.74/\ 2.94).\ 100\% = \pm\ 25.3\ \%$

Total error in U_O:

Relative error $= \pm\ 135.9\ \%$

Absolute error $= \pm\ 370\ Wm^{-2}K^{-1}$

C.2.2 Derivation of the Gas Heat Transfer Coefficient.

This section outlines the calculation steps for the determination of the gas H.T.C, using two different methods. Firstly, the heat transfer coefficient based upon the experimental correlation developed for the reheat column used in these studies. The second correlation is standard equation proposed by Sieder-Tate for turbulent flow in tubes.

Calculation of gas heat transfer coefficient using Equation 4.3

$m_G = 3\ gs^{-1}$

$d_H = 2.8 \times 10^{-2}$ m

$k_G = 3.3 \times 10^{-2}\ Wm^{-1}K^{-1}$

$Re = (3 \times 2.8 \times 10^{-2}) / (1.58 \times 10^{-3} \times 2.2 \times 10^{-2})$

$= 2400$

$Nu = 0.41.\ (2400)^{0.78}$

$= 178$

$h_G = (178 \times 3.3 \times 10^{-2}) / (2.8 \times 10^{-2})$

$= \underline{209\ Wm^{-2}K^{-1}}$

Calculation of gas heat transfer coefficient using Sieder- Tate Eqn.

$Nu = 0.027.\ (2400)^{0.8}.\ 0.9$

$= 12.3$

$h_G = (12.3 \times 3.3 \times 10^{-2}) / (2.8 \times 10^{-2})$

$= \underline{14.5\ Wm^{-2}K^{-1}}$

C.2.3 Prediction of the Gas Exit Temperature.

A sample calculation predicting the gas exit temperature from known inlet conditions, using the method detailed in Chapter 4 (based upon the effectiveness of the heat exchanger) is detailed below.

Inlet Conditions:

Inner Tube

$m_{LiBr_{top}} = 2.82\ gs^{-1}$

$m_{RS} = 0.14\ gs^{-1}$

$m_{LiBr_{bot}} = 2.96\ gs^{-1}$

$w_{LiBr_{top}} = 59$ %w/w

$w_{LiBr_{av}} = 58$ %w/w

$c_{P_L} = 1.8\ J\ g^{-1}K^{-1}$

$T_{absn} = 147$ °C (based on $w_{LiBr_{av}}$ and 1 bar v.p)

Outer tube (gas):

$m_G = 3.00\ gs^{-1}$

$d_H = 2.8 \times 10^{-2}$ m

$T_{G_{bot}} = 92°C$

$c_{P_G} = 1.0\ J\ g^{-1}K^{-1}$

Derived values:

$Re = (3.00 \times 2.8 \times 10^{-2}) / (1.58 \times 10^{-3} \times 2.1 \times 10^{-2})$

$= 2530$

$B = 1/(h_I.\ A_I) + x/(k.\ A_R)$

$= 1/(3000.\ 0.051) + 0.001 / (16.0.053)$

$= 0.0077\ KW^{-1}$

$(U.A)_O^{-1} = [3695 \times (2530)^{-1.3}] + 0.0077$

$= 0.15\ KW^{-1}$

$(U.A)_O = 6.7\ WK^{-1}$

$C_G = 3.00 \times 1 = 3\ WK^{-1}$ (C_{min}) (Equation 4.10)

$C_L = 2.96 \times 1.8 = 5.2\ WK^{-1}$ (C_{max}) (Equation 4.10)

$NTU = (U.A)_O / (C_{min})$

$= 6.7 / 3 = 2.2$ (Equation 4.13)

$\varepsilon = \underline{0.78}$ (Equation 4.14)

$= [C_L.\ (T_{absn} - T_{L_{out}})] / [\ C_{min}.\ (T_{absn} - T_{G_{in}})\ ]$ [Equation 4.12]

Calculation of exit temperatures:

$T_{LiBr_{bot}}$ = 122°C (from a rearrangement of Equation 4.12)

Q = 130 W

No heat losses:

$T_{G_{top}} = [(C_L \cdot (T_{absn} - T_{LiBr_{bot}}) / C_G] + T_{G_{bot}}$

43 + 92

= <u>135 °C</u>

Heat losses: ($Q_{losses} \sim$ 29 W (assuming T_{amb} = 20 °C)

$T_{G_{top}}$ = <u>126 °C</u>

Experimental result:

$T_{G_{top}}$ = <u>131 °C</u>

C.3 Industrial Transformer.

The following calculations refer to the industrial case study, which investigated the viability of using an open cycle heat transformer cycle as a heat recovery device for the recovery of waste heat from an industrial spray dryer.

C.3.1 Dehumidification by Cooling- Extra Heat Duty.

In the industrial case study it was proposed to removed the majority of the water vapour present in the dryer exhaust stream by cooling the stream. The heat of condensation would then be used as the heat source of a compression heat pump, which had a COP of 2. The temperature lift in the heat pump cycle was set at 35 degC.

The following calculation illustrates the heat released by a humid gas stream with an inlet humidity of 0.16 g- $_{H_2O}$ g- $_{dry\ air}^{-1}$ (Gas flowrate = 157 kg min^{-1}) and at a temperature of 60 °C, the temperature of the gas leaving the gas

cleaning equipment. The gas would be cooled to 41 °C, where the saturation humidity was only 0.03 g- $_{H_2O}$ g- $_{dry\ air}^{-1}$.

Inlet water content	= 24.34 kg min^{-1}
Outlet water content	= 4.71 kg min^{-1}
Amount condensed	= (24.34 - 4.71) = 19.63 kg min^{-1}
Heat to be removed per kg	= (Latent heat of condensation) + (Removal of sensible heat) = 2257 + 2(20) = 2297 kJ kg^{-1}
Total heat to be removed	= (2297 x 19.63) = 45090 kJ min^{-1} = 752 kW
Use a compression heat gas stream:	pump to return energy to dried
COP	= 2
Heat output	(2 x 752) = 1504 kW
$\Delta T_{lift_{HP}}$	= 35 degC
Outlet T_G	= 40 + 35 = 75 °C
Heat required	= [(157 / 60). 1.1. 35] = 100 kW

It can be seen from the calculation that there was a considerable amount of low grade heat released by the condensation of the water stream. As only a small proportion of the heat was returned to the gas stream, to heat it up to 75 °C. The remained could be used elsewhere on site.

C.3.2 Increase in Water Content in Drying Chamber.

It would be impossible to remove all of the water vapour from the humid dryer exhaust gas stream, prior to recycling it back to the drying chamber. Therefore, the effects of the increased water content of the gas stream are discussed below.

At the top of the dryer, the mass transfer driving force evaporating the water from the slurry would not be affected by the increased water in the hot gas. However, at the outlet from the dryer, where the temperature was only around 100°C, the effects of the increased water are more pronounced.

Present setup:	
Total inlet gas flowrate	= 199 kg min^{-1}
Inlet water content	= 2.66 kg min^{-1}
Inlet humidity	= 0.01 g- $_{H_2O}$ g- $_{dry\ air}^{-1}$
Water evaporated from slurry stream	= 27.0 kg min^{-1}
Outlet water content	= 29.66 kg min^{-1}
Total outlet gas flowrate	= 226 kg min^{-1}
Exit humidity	= 0.15 g- $_{H_2O}$ g- $_{dry\ air}^{-1}$
Exit partial pressure	= 0.20 bar
Saturation vapour pressure (@ 100 °C)	= 1 bar
Proposed setup (with AHT):	
Inlet water content	= 9.49 kg min^{-1}
Inlet humidity	= 0.05 g- $_{H_2O}$ g- $_{dry\ air}^{-1}$
Outlet water content	= 36.49 kg min^{-1}
Total outlet gas flowrate	= 226 kg min^{-1}
Exit humidity	= 0.19 g- $_{H_2O}$ g- $_{dry\ air}^{-1}$
Exit partial pressure	= 0.24 bar

It can be seen from the above calculation that the exit partial pressure increased only slightly from 0.20 bar to 0.24 bar because of the increased initial water in the gas stream. Hence, the recycling of the dehumidified and reheated exhaust gas was not thought to significantly decrease the performance of the dryer. As the exit gas stream temperature was 100 °C, the saturation water vapour pressure at the bottom of the drying chamber was 1 bar. Consequently, the pressure driving force at dryer outlet would only be reduced from 0.8 bar to 0.76 bar (5 % reduction).

Appendix D

Full Set of Results for the Single Stage Absorption Column.

$\dot{m}_G$ (gs^{-1})	H (g_{H_2O} $(g_{dry\ air})^{-1}$)	$p_{H_2O_{in}}$ (bar)	$p_{H_2O_{out}}$ (bar)	$T_{G_{in}}$ (°C)	$T_{G_{out}}$ (°C)	$\dot{m}_{LiBr}$ (gs^{-1})	w_{LiBr} (%)	$T_{LiBr_{in}}$ (°C)
0.20	3.45	0.85	0.74	100	144	6.8	66	100
0.20	3.45	0.85	0.82	100	147	3.4	67	100
0.20	3.45	0.85	0.79	100	147.5	5.1	67	101
0.40	1.25	0.67	0.61	101	130	3.4	65	100
0.40	1.90	0.75	0.71	100.5	138	3.4	65	101
0.50	0.60	0.49	0.44	103	122	2.6	62	103
0.50	1.00	0.62	0.58	103	122	3.4	56	102
0.50	1.00	0.62	0.59	100	119	3.4	56	100
0.50	1.00	0.62	0.55	100	128	5.1	58	103
0.50	1.00	0.62	0.56	100	130	3.4	63	100.5
0.50	1.00	0.62	0.58	104.5	136	3.4	63	138
0.50	1.20	0.66	0.56	100	131	5.1	65	100
0.50	1.20	0.66	0.52	100	137.5	6.8	65	100
0.50	1.20	0.66	0.60	100	137.5	3.4	65.5	100
0.50	1.40	0.69	0.67	107	127	3.4	56	113.5
0.50	1.40	0.69	0.66	100	126	3.4	57	102
0.50	1.40	0.69	0.62	100	139	5.1	66	100
0.50	1.40	0.69	0.59	100	140	6.8	66	100.5
0.50	1.54	0.71	0.68	102	128	3.4	58	101
0.58	0.35	0.36	0.06	99	116	3.4	65	105
0.60	0.50	0.44	0.43	102	94	3.4	58	100
0.60	0.92	0.59	0.54	101	128	3.4	66	101
0.60	0.93	0.60	0.53	103	146	3.4	70	100
0.60	0.93	0.60	0.55	99.5	133	3.4	65	100
0.80	0.63	0.50	0.47	102	122.5	3.4	58	101
0.98	0.18	0.23	0.20	102	107	1.5	64	100.5
0.98	0.26	0.29	0.27	104	107	1.7	65	98
1.00	0.19	0.23	0.14	102	116	3.4	70	104.5
1.00	0.20	0.24	0.21	100	110	3.4	64	101
1.00	0.30	0.32	0.26	100.5	116	3.4	70	101
1.00	0.63	0.50	0.44	100	130	3.4	65	100.5
1.00	1.07	0.63	0.60	105	142	3.4	70	100
1.00	1.08	0.63	0.60	103	142	3.4	70	101
1.20	0.15	0.19	0.15	96	92	3.4	58	96
1.22	0.41	0.40	0.37	103	115	3.4	58	100.5
1.50	0.13	0.18	0.14	100	106	3.4	65	97
1.52	0.13	0.17	0.15	101	108	3.4	65	102
1.96	0.10	0.14	0.13	102	103.5	5.1	65.5	99
2.00	0.20	0.24	0.20	110	112	6.8	65	100
2.00	0.24	0.28	0.24	100	120	5.1	69.5	100
2.04	0.11	0.15	0.14	100	103	3.4	66	101.5

Table D.1: Full set of experimental results for the single stage absorber operating in cocurrent mode.

Appendix E

Publications.

J. S. Currie and C. L. Pritchard. Open cycle absorption heat transformer for the recovery of waste heat from dryers. In A. Valero and G. Tsataronis, editors, *ECOS '92 : The International Symposium on Efficiency, Costs, Optimisation and Simulation of Energy Systems,* pages 599- 606, 15^{th}- 18^{th} June 1992. Conference held in Zaragoza, Spain.

C. L. Pritchard and J. S. Currie. Absorption- dehumidification: a 'unit-operation' for heat recovery from dryers. In P. A. Pilavachi, editor, *Energy Efficiency in Process Technology,* pages 190 -200, 19^{th}- 22^{nd} October 1992. Conference held in Vouliagmeni (Athens), Greece.

J. S. Currie and C. L. Pritchard. Absorption heat recovery and plume reduction from humid dryer exhaust streams. In *IChemE Research Event* , pages 257-259, 6^{th}- 7^{th} January 1993. Conference held in Birmingham, UK.

J. S. Currie and C. L. Pritchard. Energy recovery and plume reduction from an industrial spray drying unit using an absorption heat transformer. *Heat recovery systems and CHP* , Vol. 14 (No. 3), pages 239- 248 1994.
Special edition containing papers from the 4^{th} International Workshop on Heat Pump Research and Applications, part of the CHISA '93 Conference, held in Praha, Czech Republic August 29^{th}- September 3^{rd} 1993.

Bibliography

[1] K. Abrahamsson and Å. Jernqvist. Modelling and simulation of absorption heat cycles. 19- 21 January 1994. Prepublished copy of paper for IAHP '94 conference in Louisiana.

[2] Alefeld and Radermacher. Working substances for absorption heat pumps, 1980.
German Patent. GER. OFFEN 2852 312.

[3] Anon. Fluid pairs for high temperature and industrial applications. In W. Raldow, editor, *New working pairs for absorption processes*, pages 185–188, 14^{th} - 16^{th} April 1982. Proceedings of a workshop in Berlin. Sponsored by : Swedish Council for Building Research.

[4] Anon. Fluid pairs for multi-stage and novel systems. In W. Raldow, editor, *New working pairs for absorption processes*, pages 189–191, 14^{th} - 16^{th} April 1982. Proceedings of a workshop in Berlin
Sponsored by : Swedish Council for Building Research.

[5] Anon. Working group on 'dryers'. In P. A. Pilavachi, editor, *Improved energy efficiency in the process industries*, pages 279– 280, 24^{rd}- 24^{th} October 1990. Brussells, Belgium.

[6] Anon. Working group on 'Energy and the Environment'. In P. A. Pilavachi, editor, *Improved energy efficiency in the process industries*, pages 285– 286, 24^{rd}- 24^{th} October 1990. Brussells, Belgium.

[7] Anon. All steamed up- airless drying. *The Chemical Engineer*, (539):16, 25 March 1993.

[8] S. Arh and B. Gašperšič. Development and comparison of different advanced absorption cycles. *Rev. Int. Froid.*, 13:41–49, January 1990.

[9] Aspen Technology Inc. *ASPEN plus Users Guide*, August 1988. pp 5.1 - 5.9.

[10] B. L. Backstrom. Process intergration: Absorption heat pumps and flue gas cleaning. In T. Saito, editor, *Heat Pumps: 'Solving Energy and Environmental Challenges'. Proceedings of the 3rd International Agency Heat Pump Conference*, pages 139– 144, 12th- 15th March 1990. Tokyo, Japan.

[11] H. D. Baehr. New refrigerants- research into their thermodynamic property data. In T. Saito, editor, *Heat Pumps: 'Solving Energy and Environmental Challenges'. Proceedings of the 3rd International Agency Heat Pump Conference*, pages 243– 251, 12th- 15th March 1990. Tokyo, JAPAN.

[12] R. Berlocchio. Chlorofluoroinated hydrocarbon- organic solvent couples. In *Absorption Heat Pumps Congress*, pages 45– 53, 20th- 22nd March 1985. Paris.

[13] R Best. A methanol- lithium bromide, zinc bromide mixture applied to solar absorption heat pumps. In *Proceeding of the International Conference on Solar Building Technology*, volume 2, pages 437– 443, 1977.

[14] G. Bisio. The exergy efficiency of the devices for upgrading thermal energy with thermal sources and sinks of finite capacity. In A. Valero and G. Tsataronis, editors, *ECOS '92: The International Symposium on Efficiency, Costs, Optimization and Simulation of Energy Systems*, pages 73– 80, 15th- 18th June 1992. Zaragoza, Spain.

[15] H Bjurström and W Raldow. The absorption process for heating, cooling and energy storage- an historical survey. *Energy Research*, 5:43– 59, 1981.

[16] H. Bokelmann and G. Alefeld. Advances in Heat Transformers. In T. Saito, editor, *Heat Pumps: 'Solving Energy and Environmental Challenges'. Proceedings of the 3rd International Agency Heat Pump Conference*, pages 107– 116, 12th- 15th March 1990. Tokyo, Japan.

[17] H. Bokelmann and H-J. Ehmke. Determination of enthalpy- concentration diagrams for absorption heat pump working fluids. *Ki Klima Kälte Heizung*, 13(6):241–244, June 1985.

[18] H. Bokelmann and M. Renz. Thermophysikalische eigenschaften von trifluoroethanol- stoffsystemen für absorptionswärmepumpen. *Ki Klima Kälte Heizung*, 11(10):403– 406, 1983.

[19] H. Bokelmann and F. Steimle. Development of advanced heat transformers utilising new working fluids. *Rev. Int. Froid*, 9:51–59, January 1986.

[20] I. Borde. New working fluids for absorption units utilising low grade heat. In W. Raldow, editor, *New working pairs for absorption processes*, pages

105–106, 14^{th} - 16^{th} April 1982. Proceedings of a workshop in Berlin. Sponsored by : Swedish Council for Building Research.

[21] I. Borde. Absorption heat recovery systems. In F Moser, editor, *Proceedings of the 2^{nd} International workshop on Research Activities on Advanced Heat Pumps*, pages 539– 549, September 1988. Graz, Austria.

[22] I. Borde and M. Jelinek. Absorption heat pumps with organic refrigerant-absorbent fluid pairs. In F Moser, editor, *Proceedings of the 2^{nd} International workshop on Research Activities on Advanced Heat Pumps*, pages 89– 101, September 1988. Graz, Austria.

[23] J. W. J. Bouma. Experience with a heat transformer in the chemical industry. *IEA Heat Pump Centre newsletter*, 8(4):12–15, December 1990.

[24] M. F. Brunk. Thermodynamische und physikalische Eigenschaften der Lösung Lithiumbromid/ Wasser als Grundlage für die Prozeβsimulation von Absorptions- Kälteanlagen. *Ki Klima Kälte Heizung*, (10):365–372, 1982.

[25] CEC. *Absorption Heat Pumps Congress*, 20^{th}- 22^{nd} March 1985. Held in Paris. Report EUR 10007 EN.

[26] CEC. Thermie- Promotion of energy technology for Europe, 1992. Promotional Literature.

[27] P. Ciambelli and V. Tufano. The upgrading of waste heat by means of water- sulphuric acid absorption heat transformers. *Heat Recovery Systems and CHP*, 7(6):517– 524, 1987.

[28] E. C Clark. Chemical heat pumps drive to upgrade waste heat. *Chemical Engineering*, pages 50–51, 20 February 1984.

[29] Executive Committee. Montreal protocol: 1991 assessment. report of the refrigeration, air- conditioning and heat pumps technical options committee. Technical report, December 1991.

[30] Coulson and Richardson. *Unit Operations. Volume 2.* Pergamon Press, 3rd edition, 1980.

[31] J. S. Currie. Absorption heat recovery from dryer exhausts. Internal literature review, January 1990.

[32] J. S. Currie. Absorption heat recovery from humid airstreams. Technical report, 4^{th} November 1991. Internal Zeneca report following work during Summer 1991 at Grangemouth works.

[33] J. S. Currie. Spray drying- Gas cleaning study. Technical report, 1^{st} October 1991. Internal Zeneca report following work during Summer 1991 at Grangemouth works.

[34] R. Dagani. Chemical heat pump cools as well as heats. *C and EN*, pages 36 – 37, 20th October 1980.

[35] P. V. Danckwerts. Significance of liquid film coefficients in gas absorption. *Ind and Eng Chem*, 43(6):1460–1467, June 1951.

[36] P. V. Danckwerts and A. J. Gillham. Methods for predicting the rates of absorption with chemical reaction in packed columns, and tests with 1.5in raschig rings. *Trans. Instn. Chem Engrs.*, 44:T42–T54, 1966.

[37] F. DeMaria and R. R. White. Transient response study of gas flowing through irrigated packing. *AIChE Journal*, 6(3):473–481, September 1960.

[38] E. Van den Bulck. Performance characteristics of open cycle solid desiccant heat transformers. In F Moser, editor, *Proceedings of the 2nd International workshop on Research Activities on Advanced Heat Pumps*, pages 69–77, September 1988. Graz, Austria.

[39] DeVault. Advanced absorption technology development in the United States. In T. Saito, editor, *Heat Pumps: 'Solving Energy and Environmental Challenges'. Proceedings of the 3rd International Agency Heat Pump Conference*, pages 69–80, 12^{th}- 15^{th} March 1990. Tokyo, Japan.

[40] S. Devotta and V. R. Pendyala. Modified Joback Group Contribution Method for Normal Boiling Point of Aliphatic Halogenated Compounds. Details on the B.Pt of various HFCs, CFCs, HCFCs and BCFCs.

[41] E. Dietrich, P. Le goff, and M. Barkaoui. Valeur maximale du coefficient de performance d'une pompe a chalcur a absorption. *Entropie*, (118):8–23, 1984.

[42] *Å*. Jernqvist et al. On the efficiencies of absorption heat pumps. *Heat recovery systems and CHP*, 12(6):469 – 480, 1992.

[43] *Å*. Jernqvist et al. On the efficiencies of absorption heat transformers. *Heat recovery systems and CHP*, 12(4):323–334, 1992.

[44] S. I. Pereira Duarte and R. Bugarel. Optimal working conditions for an absorption heat transformer- analysis of the water- lithium bromide theoretical cycle. *Heat Recovery Systems and CHP*, 9(6):521– 532, 1989.

[45] K. Eriksson and *Å*. Jernqvist. Heat transformer with self circulation: Design and preliminary operational data. *Rev. Int. Froid*, 12:15–20, January 1989.

[46] M. Erkert and B. Stemmler. Working medium pair for sorption heat pumps, 1981.
German Patent. GER. OFFEN 30 03 471.

[47] A. B. Brahim et al. Properties and performances of the system calcium chloride- lithium chloride- water. In F Moser, editor, *Proceedings of the International workshop on Research Activities on Advanced Heat Pumps*, pages 269–277, October 1986. Graz, Austria.

[48] A. Bothe et al. New working fluid systems for absorption heat pumps. In P Zegers and J Miriam, editors, *Proceeding of workshop on 'Absorption heat pumps'*, pages 13– 22. CEC, 12^{th}- 14^{th} April 1988. Held in London. Report EUR 11888 EN.

[49] A. P. Burdukov et al. Experimental study of the absorption of water vapour by thin films of aqueous lithium bromide. *Heat Transfer- Soviet Research*, 12(3):118–123, May- June 1980.

[50] A. Rojey et al. Heat Transformers: Present state of a new technology. *Proceedings of the Institution of Mechanical Engineers*, 197A:71– 77, January 1983.

[51] B. E. Siddig-Mohammed et al. Study of the operating characteristics of a reversed absorption heat pump system (heat transformer). *Chem. Eng. Res. Des.*, 61:283–289, September 1983.

[52] C. Chiappetta et al. Thermophysical properties of hexafluoroisopropanol (HFIP). *Ki Klima Kälte Heizung*, International Edition:15–18, 1989.

[53] C. Z. Zhuo et al. Steady state dynamic simulation of an absorption heat transformer. In F Moser, editor, *Proceedings of the 3^{rd} International workshop on Research Activities on Advanced Heat Pumps*, pages 335–345, September 24^{th} - 26^{th} 1990. Graz, Austria.

[54] D. M. Manole et al. Interplay of heat and mass transfer processes within a vertical film absorber. In E. Carnevale et al., editor, *Flowers '94. Enery for the 21^{st} Century: Conversion, Utilisation and Environmental Quality*, pages 791– 798, 6^{th}- 86^{th} July 1994. Proceedings of Florence World Energy Research Symposium. Held in Florence, Italy.

[55] D. S. Ward et al. Integration of evacuated tubular solar collectors with LiBr absorption cooling systems. *Solar Energy*, 22:335–341, 1979.

[56] D. W. Townsend et al. The future of heat engines and heat pumps in the process industries. In *NW Branch papers No. 3. Institution of Chemical Engineers*, page 14.1, 1981.

[57] E. Dietrich et al. Relations between coefficient of performance energy storage capacity and temperature lift for thirty working pairs used in absorption and adsorption heat pumps. In F Moser, editor, *Proceedings of the International workshop on Research Activities on Advanced Heat Pumps*, pages 215–233, October 1986. Graz, Austria.

[58] G. Aly et al. Integration of absorption heat transformers in the process industry- applications in the olechemical, pulp and paper industries. In *International Conference on Energy Efficiency in Process Technology*, 19^{th}- 22^{nd} October 1992. Athens.

[59] G. Cacciola et al. Theoretical performance of an absorption heat pump using ammonia- water- potassium hydroxide solution. *Heat Recovery Systems and CHP*, 10(3):177– 185, 1990.

[60] G. Otter et al. Search for new sorption heat pump working pairs with predictive methods in chemical thermodynamics. In F Moser, editor, *Proceedings of the 2^{nd} International workshop on Research Activities on Advanced Heat Pumps*, pages 129–141, September 1988. Graz, Austria.

[61] G. S. Grover et al. Thermodynamic design data for absorption heat pump systems operating on water- lithium chloride- Part II Heating. *Heat Recovery Systems and CHP*, 8(5):419–423, 1988.

[62] G. S. Grover et al. Thermodynamic design data for absorption heat transformer systems- Part III Operating on water- lithium chloride. *Heat Recovery Systems and CHP*, 8(5):425–431, 1988.

[63] H. C. Meacham et al. Status of the double effect absorption heat pump (DEAHP). In T. Saito, editor, *Heat Pumps: 'Solving Energy and Environmental Challenges'. Proceedings of the 3^{rd} International Agency Heat Pump Conference*, pages 537– 543, 12^{th}- 15^{th} March 1990. Tokyo, Japan.

[64] H. J. Laue et al. Overview of industrial heat pump activities in Europe. In T. Saito, editor, *Heat Pumps: 'Solving Energy and Environmental Challenges'. Proceedings of the 3^{rd} International Agency Heat Pump Conference*, pages 905– 918, 12^{th}- 15^{th} March 1990. Tokyo, Japan.

[65] H. Jaster et al. Vapour compression for waste heat recovery. In *NW Branch papers No. 3. Institution of Chemical Engineers*, page 15.1, 1981.

[66] H. L. Shulman et al. Performance of packed columns. Parts I-III. *AIChE Journal*, 1(2):247–264, June 1955.

[67] I. Borde et al. Development of advanced absorption systems driven by low temperature heat sources. In P. A. Pilavachi, editor, *Energy Efficiency in Process Technology*, pages 521– 530, October 19^{th}- 22^{nd} 1992. Athens, Greece.

[68] J. M. Landauro-Paredes et al. Experimental study of the operating characteristics of a H2O/LiBr absorption cooler. *Chem. Eng. Res. Des.*, 61:362–370, November 1983.

[69] J. P. Rignac et al. Heat and mass transfers in heap pump absorbers: Study of film tubular absorbers with tangential feed and turbulence promoters. In *Absorption Heat pumps*, pages 362–372, 1988.

[70] K. Abrahamsson et al. Heat transformer systems for evaporation applications in the pulp and paper industry. *Nordic Pulp and Paper Research Journal*, 7(1-1992):9–16, 1992.

[71] K. M. Berntsson et al. *Learning from experiences with Heat Transformers in Industrial Processes.* CADDET. CASU, December 1989. Analyses Series No. 2.

[72] K. Onda et al. Gas absorption with chemical reaction in packed columns. *Journal of Chemical Engineering in Japan*, 1(1):62–66, 1968.

[73] K. Onda et al. Mass transfer coefficients between gas and liquid phases in packed columns. *Journal of Chemical Engineering in Japan*, 1(1):56–62, 1968.

[74] K. P. Tyagi et al. Working fluids for heat transformers. *Heat Recovery Systems and CHP*, 9(2):175– 181, 1989.

[75] K. R. Patil et al. Thermodynamic properties of aqueous electrolyte solutions. 1. vapour pressures of aqueous solutions of LiCl, LiBr and LiI. *Journal of Chemical Engineering Data*, 35:166 – 168, 1990.

[76] K. R. Patil et al. Thermodynamic design data for absorption heat pump systems operating on water- lithium iodide- Part I Cooling. *Heat Recovery Systems and CHP*, 11(5):341– 350, 1991.

[77] K. R. Patil et al. Thermodynamic design data for absorption heat pump systems operating on water- Lithium Bromide- Part II Heating. *Heat Recovery Systems and CHP*, 11(5):351– 360, 1991.

[78] K. R. Patil et al. Thermodynamic design data for absorption heat transformers- Cpart III Operating on water- Lithium Iodide. *Heat Recovery Systems and CHP*, 11(5):361– 369, 1991.

[79] K. R. Patil et al. Thermodynamic properties of aqueous electrolyte solutions. 2. vapour pressure of aq. solutions of NaBr, NaI, KCl, KBr KI, RbCl, CsCl, CsBr, CsI, $MgCl_2$, $CaCl_2$, $CaBr_2$, CaI_2, $SrCl_2$, $SrBr_2$, SrI_2, $BaCl_2$, $BaBr_2$. *Journal of Chemical Engineering Data*, 36:225– 230, 1991.

[80] K. R. Patil et al. Thermodynamic properties of aqueous electrolyte solutions. 3. vapour pressure of aq. solutions of $LiNO_3$, LiCl + $LiNO_3$ and LiBr + $LiNO_3$. *Journal of Chemical Engineering Data*, 37:136– 138, 1992.

[81] L. Vamling et al. CFC alternatives for high temperature heat pump applications. In *Heat Pumps- Proceedings of the 4th International Conference*, pages 71–81, 1991.

[82] M. A. R. Eisa et al. Classified references for absorption heat pump systems from 1975 to May 1985. *Journal of Heat Recovery Systems*, 6(1):47– 61, 1986.

[83] M. A. R. Eisa et al. Thermodynamic design data for absorption heat transformers- Part I. Operating on water- lithium bromide. *Journal of Heat Recovery Systems*, 6(5):421–432, 1986.

[84] M. A. R. Eisa et al. Thermodynamic design data for absorption heat transformers- Part II. Operating on water- calcium chloride. *Journal of Heat Recovery Systems*, 6(6):443–450, 1986.

[85] M. A. R. Eisa et al. A study of the operating characteristics of an experimental absorption cooler using water- lithium bromide- ethylene glycol as a ternary working system. *International Journal of Energy Research*, 12:459–472, 1988.

[86] M. Barkaoui et al. Modelisation du desorbeur a film ruisselant. Communication presented at the Intl Symp. 'Pompes a chaleur chimiques de hautes performances'. 14^{th}- 16^{th} September 1988.

[87] M. Narodoslawsky et al. The influence of excess properties on the performance of absorption heat pumps. In F Moser, editor, *Proceedings of the International workshop on Research Activities on Advanced Heat Pumps*, pages 199– 214, October 1986. Graz, Austria.

[88] M. Narodoslawsky et al. New working pairs for medium and high temperature industrial absorption heat pumps. *Heat Recovery Systems and CHP*, 8(5):459– 468, 1988.

[89] M. Narodoslawsky et al. Thermodynamic search for new AHP and AHT working fluids. In F Moser, editor, *Proceedings of the 2^{nd} International workshop on Research Activities on Advanced Heat Pumps*, pages 115–127, September 1988. Graz, Austria.

[90] M. Narodoslawsky et al. Ethyl chloride: A viable alternative for medium and high- temperature compression heat pump cycles. In *Heat Pumps- Proceedings of the 4th International Conference*, pages 101–114, 1991.

[91] M. R. Jeday et al. Evaluation criteria of refrigerant- sorbent pairs for absorption heat pumps. In F Moser, editor, *Proceedings of the 2^{nd} International workshop on Research Activities on Advanced Heat Pumps*, pages 103– 113, September 1988. Graz, Austria.

[92] M. S. Bhatt et al. Thermodynamic modelling of absorption- resorption heating cycles with some new working pairs. *Heat Recovery Systems and CHP*, 12(3):225– 233, 1992.

[93] M. Wimby et al. A large absorption heat pump. In *Large Scale Applications of Heat Pumps. 3rd International Symposium*, pages 21–24, 25^{th}- 27^{th} March 1987. Conference held in Oxford, England.

[94] N. Bennani et al. Absorption heat pump cycle: Performance analysis of water- glycerol mixture. *Heat Recovery Systems and CHP*, 9(3):257– 263, 1989.

[95] N. Issiki et al. Studies of the mechanism and enhancement of absorption heat and mass transfer. In *Absorption Heat pumps*, pages 399–408, 1988.

[96] N. Kolev et al. Systems containing contact economisers for flue gas heat utilisation. In P. A. Pilavachi, editor, *Energy Efficiency in Process Technology*, pages 683– 691, October 19^{th}- 22^{nd} 1992. Athens, Greece.

[97] P. Le Goff et al. Analyses exergetique et economique des pompes a chaleur a sorption.
Communication presented at the Intl Symp. 'Pompes a chaleur chimiques de hautes performances'. 14^{th}- 16^{th} September 1988.

[98] P. Le Goff et al. Co-current, counter-current or cross-current gas-liquid absorber with integrated or separated heat exchange.
Communication presented to the Intl W'shop on absorption heat pumps. London 12^{th}- 14^{th} April, 1988.

[99] P. Le Goff et al. A gas- liquid absorber with integrated heat exchange for reactions with high thermal effect, June 1988.
Communication to ACHEMA.

[100] P. Le Goff et al. Modelling of a 'reverse- rectification' absorption heat pump. In F Moser, editor, *Proceedings of the 2^{d} International workshop on Research Activities on Advanced Heat Pumps*, pages 187– 197, September 1988. Graz, Austria.

[101] P. Le Goff et al. Un nouveau concept: La rectification-inverse. son application aux pompes a chaleur a absorption, September 1988.
Communication presented at Intl Symp. 'Pompes a chaleur chimiques de hautes performances.

[102] P. Le Goff et al. Advances in chemical heat pumps and heat transformers. In T. Saito, editor, *Heat Pumps: 'Solving Energy and Environmental Challenges'. Proceedings of the 3^{d} International Agency Heat Pump Conference*, pages 117– 126, 12^{th}- 15^{th} March 1990. Tokyo, Japan.

[103] P. Le Goff et al. A high temperature heat transformer operating by 'reverse- rectification'. In F Moser, editor, *Proceedings of the 3rd International workshop on Research Activities on Advanced Heat Pumps*, pages 271– 278, September 1990. Graz, Austria.

[104] P. Riesch et al. Part-load behaviour of an absorption heat transformer. In *Large Scale Applications of Heat Pumps. 3rd International Symposium*, pages 155–160, 25th- 27th March 1987. Conference held in Oxford, England.

[105] P. V. Danckwerts et al. Kinetics of CO_2 absorption in alkaline solutions. *Chem. Eng. Sci.*, 18:63–72, 1963.

[106] R. Bañares-Alcántara et al. Development of an expert system for physical property predictions. *Computers and Chemical Engineering*, 9(2):127–142, 1985.

[107] R. Best et al. Thermodynamic design data for absorption heat transformers- Part III. Operating on ammonia- water. *Heat Recovery Systems and CHP*, 7(3):259–272, 1987.

[108] R. Best et al. Thermodynamic design data for absorption heat transformers- Part IV Operating on ammonia- lithium nitrate. *Heat Recovery Systems and CHP*, 10(5- 6):539– 548, 1990.

[109] R. Best et al. Thermodynamic design data for absorption heat pump systems operating on ammonia- lithium nitrate- Part II Heating. *Heat Recovery Systems and CHP*, 11(2- 3):103– 111, 1991.

[110] S. C. Bikos et al. Design and energy analysis of absorption- driven multiple effect evaporators. In P. A. Pilavachi, editor, *Energy Efficiency in Process Technology*, pages 970– 971, October 19th- 22nd 1992. Athens, Greece.

[111] S. K. Chaudhari et al. A comparative study of the operating characteristics of water- lithium chloride and water- calcium chloride absorption heat pumps. *Journal of Heat Recovery Systems*, 6(1):39–46, 1986.

[112] T. Furukaw et al. High emperature heat storage using hydrate. In T. Saito, editor, *Heat Pumps: 'Solving Energy and Environmental Challenges'. Proceedings of the 3rd International Agency Heat Pump Conference*, pages 833– 841, 12th- 15th March 1990. Tokyo, JAPAN.

[113] T. Sonoda et al. Wasted heat recovery and temperature upgrading by absorption heat pump and other systems. *CLIMA 2000- ventilating and air conditioning systems*, 6(Ch. 122):111–116, 1985.

[114] U. Nowaczyk et al. Selection and investigation of new working fluid systems for absorption heat pumps. In F Moser, editor, *Proceedings of the International workshop on Research Activities on Advanced Heat Pumps*, pages 185–198, October 1986. Graz, Austria.

[115] U. Plöcker et al. Absorption heat transformers for the chemical industry. *Chemie Ingenieur Technik*, 60(2):103–108, 1988.

[116] V. M. Kripalani et al. Performance analysis of a vapour absorption heat transformer with different working fluid combinations. *Journal of Heat Recovery Systems*, 4(3):129–140, 1984.

[117] Welty et al. *Fundamentals of Momentum, Heat and Mass Transfer.* John Wiley and Sons, Inc., 1^{st} edition, 1969.

[118] Y. Nagaoka et al. Research on an air- source gas absorption heat pump air conditioner. In T Saito, editor, *Heat Pumps: 'Solving Energy and Environmental Challenges'. Proceedings of the 3^{rd} International Agency Heat Pump Conference*, pages 81– 91, 12^{th}- 15^{th} March 1990. Tokyo, Japan.

[119] ETSU. Energy efficiency demonstration scheme report: An assessment of 'replication', June 1986. Harwell Laboratory, Didcot. Oxon.

[120] ETSU. Good practice guide: Guidance notes for the implementation of heat recovery from high temperature wast gas streams, 1990. Harwell Laboratory, Didcot. Oxon.

[121] ETSU. Energy efficiency publications list, February 1993. Harwell Laboratory, Didcot. Oxon.

[122] Health & Safety Executive. COSHH assessments. HMSO, 1988. Published booklet.

[123] P. D. Fairchild and W. Fulkerson. Energy technology R and D and the greenhouse effect. In T. Saito, editor, *Heat Pumps: 'Solving Energy and Environmental Challenges'. Proceedings of the 3^{rd} International Agency Heat Pump Conference*, pages 231– 241, 12^{th}- 15^{th} March 1990. Tokyo, Japan.

[124] M. B. Fehrm. Exhaust air heat pump potential in Europe. In T. Saito, editor, *Heat Pumps: 'Solving Energy and Environmental Challenges'. Proceedings of the 3^{rd} International Agency Heat Pump Conference*, pages 733– 745, 12^{th}- 15^{th} March 1990. Tokyo, Japan.

[125] C. A. I. Ferreira. Thermodynamic and physical property data equations for ammonia- lithium nitrate and ammonia- sodium thiocyanate solutions. *Solar Energy*, 32(2):231–236, 1984.

[126] A. Fredenslund and et al. Group- contribution estimation of activity coefficients in nonideal liquid mixtures. *AIChE Journal*, 21(6):1086– 1099, November 1975.

[127] T. Furukawa and T. Sonoda. Characteristics of H_2O/LiBr absorption heat pump for the temperature change of external fluids. In *International congress refrigeration, 17th, Vienna*, August 1987.

[128] A. Gidner and Å. Jernqvist. Energy conservation in the sugar industry. In *International Conference on Energy Efficiency in Process Technology*, 19^{th}- 22^{nd} October 1992. Athens.

[129] M Gierow. Falling film absorbers and generators for absorption heat cycles: Comparison of two working pairs using new mass diffusivity data and computer simulations. Master's thesis, Department of Chemical Engineering I, Lund Institute of Technology, Lund, Sweden., March 1993. LUTKDH/ (TKKA- 1001)/ 1- 56/ (1993).

[130] M. Gierow and Å. Jernqvist. Measurement of mass diffusivity with holographic interferometry for H_2O/ NaOH and H_2O/ LiBr working pairs. 19^{th}- 21^{th} January 1994. Prepublished copy of paper for IAHP '94 conference in Louisiana.

[131] M. Gierow and Å. Jernqvist. Selection of working pairs for sorption heat pumps- a computer simulation study. 19^{th}- 21^{th} January 1994. Prepublished copy of paper for IAHP '94 conference in Louisiana.

[132] J Gribbin. *Hothouse earth: The greenhouse effect and Gaia.* Black Swan, 1990.

[133] G Grossman. Adiabatic absorption and desorption for improvement of temperature- boosting absorption heat pumps. *ASHRAE Transactions*, 88(2):359– 367, 1982.

[134] G. Grossman. Combined heat and mass transfer in absorption processes. In W. Raldow, editor, *New working pairs for absorption processes*, pages 115–117, 14^{th} - 16^{th} April 1982. Proceedings of a workshop in Berlin Sponsored by : Swedish Council for Building Research.

[135] H. Halozan. Market niches in Europe. In T. Saito, editor, *Heat Pumps: 'Solving Energy and Environmental Challenges'. Proceedings of the 3^{rd} International Agency Heat Pump Conference*, pages 307– 316, 12^{th}- 15^{th} March 1990. Tokyo, Japan.

[136] W. T. Hanna and W. H. Wilkinson. Absorption heat pumps and working pair developments in the US since 1974. In W. Raldow, editor, *New working pairs for absorption processes*, pages 71–81, 14^{th} - 16^{th} April 1982. Proceedings of a workshop in Berlin. Sponsored by : Swedish Council for Building Research.

[137] G. G. Haselden. Alternative cycles for heat pumping. In *NW Branch papers No. 3. Institution of Chemical Engineers*, pages 3.1–3.7, 1981.

[138] H. T. Haukås. Future of refrigeration with CFC regulations. In T. Saito, editor, *Heat Pumps: 'Solving Energy and Environmental Challenges'. Proceedings of the 3rd International Agency Heat Pump Conference*, pages 201– 211, 12th- 15th March 1990. Tokyo, JAPAN.

[139] R. W Haywood. *Thermodynamic Tables in SI metric units.* Cambridge University Press, 2nd edition, 1984.

[140] W. Hölbling et al. The COP of two and three stage absorption heating systems. In F Moser, editor, *Proceedings of the International workshop on Research Activities on Advanced Heat Pumps*, pages 255– 267, October 1986. Graz, Austria.

[141] T. Heppenstall. Absorption cycle heat pumps. *Journal of Heat Recovery Systems*, 3(2):115–128, 1983.

[142] R. Higbie. The rate of absorption of a pure gas into a still liquid during short periods of exposure. *Trans Amer Inst Chem Engr*, 35:365–389, 1935.

[143] H. Hlawiczka. The funding of heat pumps within the German energy R and D programme in the sector of end- use technologies- results, experiences, evaluation, future prospects. In T. Saito, editor, *Heat Pumps: 'Solving Energy and Environmental Challenges'. Proceedings of the 3rd International Agency Heat Pump Conference*, pages 369– 383, 12th- 15th March 1990. Tokyo, Japan.

[144] D. L. Hodgett. Efficient drying using heat pumps. *The Chemical Engineer*, pages 510–512, July/ August 1976.

[145] D. L. Hodgett. Absorption heat pumps and working pair developments in Europe since 1974. In W. Raldow, editor, *New working pairs for absorption processes*, pages 57–69, 14th - 16th April 1982. Proceedings of a workshop in Berlin. Sponsored by : Swedish Council for Building Research.

[146] S Iyoki and T Uemura. Studies on corrosion inhibitor in water- lithium bromide absorption refrigerating machines. *Refrigeration*, 53(614):3– 7, Dec 1978. Japanese.

[147] S. Iyoki and T. Uemura. Studies on the water- lithium bromide- ethylene glycol absorption refrigerating machine. *Reito (Japan)*, 56:279 – 288, April 1981.

[148] S. Iyoki and T. Uemura. Physical and thermal properties of the water-lithium bromide- zinc chloride- calcium bromide system. *Int J. Refrigeration*, 12:272 – 277, September 1989.

[149] P. F. Jansen and J. W. Wormgoor. Performance of and operational experience with a large scale heat transformer. In *3rd International Symposium on the Large Scale Application of Heat Pumps*, pages 45– 49, 25^{th}- 27^{th} March 1987. Conference held in Oxford, England.

[150] H. F Gibbard (Jr) and G. Scatchard. Liquid- vapour equilibrium of aqueous lithium chloride, fron 25°C to 100°C and from 1.0 to 18.5 molal, and related properties. *Journal of Chemical and Engineering Data*, 18(3):293–298, 1973.

[151] S. Kannoh. Heat recovery from warm waste water at dyeing process by absorption heat pump. *Journal of Heat Recovery Systems*, 2(5/6):443–451, 1982.

[152] T. Kashiwagi. Advances in working fluids and cycles for absorption systems. In T. Saito, editor, *Heat Pumps: 'Solving Energy and Environmental Challenges'. Proceedings of the 3^{rd} International Agency Heat Pump Conference*, pages 93– 105, 12^{th}- 15^{th} March 1990. Tokyo, JAPAN.

[153] J. U. Keller. R and D work on heat transformations by absorption processes. In W. Raldow, editor, *New working pairs for absorption processes*, pages 121–122, 14^{th} - 16^{th} April 1982. Proceedings of a workshop in Berlin. Sponsored by : Swedish Council for Building Research.

[154] W Kern. Economic criteria for application of single stage or double stage absorption heat transformers. In *3rd International Symposium on the Large Scale Application of Heat Pumps*, pages 149– 154, 25^{th}- 27^{th} March 1987. Conference held in Oxford, England.

[155] C. J. King. The additivity of individual phase resistances in mass transfer operations. *AIChE Journal*, 10(5):671–677, September 1964.

[156] K. F. Knoche and W. Raatschen. New working pairs for the application in absorption heat pumps. *VDI- Berichte*, (539):181–191, 1984.

[157] P. Kolbusz. Industrial applications of heat pumps, September 1975. Booklet from the ECRC at Capenhurst ECRC/N845. Lit. Survey.

[158] S. Kurosawa. Technological innovation in gas fired absorption water chiller heater. *Refrigeration*, 62(711):12–23, January 1987. Japanese Association of refrigeration.

[159] S. Kurosawa. Current and future perspectives of absorption heat pumps in commercial applications in Japan. In *Recent developments in Heat Pump Technology*, March 1988. Jar International Symposium. Held in Tokyo.

[160] S. Kurosawa. Current states of gas air- conditioning system in japan. In *Advanced Absorption Workshop*, October 1988.

[161] J. Lawton. Closed and open cycle heat pumping for drying. In *NW Branch papers No. 3. Institution of Chemical Engineers*, pages 9.1–9.7, 1981.

[162] R. M. Lazzarin. Solar- assisted absorption heat pumps feasibility. *Solar Energy*, 26:223–230, 1981.

[163] B. Linhoff and K. J. Carpenter. Energy conservation by exergy analysis: The quick and simple way. In *World Congress of Chemical Engineering*, pages 248– 255, 1981.

[164] B. Liu. Draft of report submitted following work in Chem. Eng. Dept., University of Edinburgh. Internal report, 1990.

[165] B Liu. *Pompes à chaleur à Absorption pour hautes et tres hautes temperatures.* PhD thesis, Laboratoire des Sciences du Genie Chimique, INP, Lorraine, France, December 1990. PhD Thesis.

[166] R. Low. Absorption heat pumping- an overview. Internal communication.

[167] Hydronyl Ltd. Tower packings. ICI Engineering Research brochure, 1951.

[168] R. A. Macriss and T. S. Zamacki. Absorption fluids data survey- European and Japanese data. In F Moser, editor, *Proceedings of the International workshop on Research Activities on Advanced Heat Pumps*, pages 175–183, October 1986. Graz, Austria.

[169] W. Malewski. Absorption heat pumps for high temperature and industrial application. In W. Raldow, editor, *New working pairs for absorption processes*, pages 127–129, 14^{th} - 16^{th} April 1982. Proceedings of a workshop in Berlin. Sponsored by : Swedish Council for Building Research.

[170] K. Masters. *Spray drying: An introduction to principles, operational practice and applications.* Chemical and Process Engineering Series. Leonard Hill Books, London, 1972.

[171] Teresa R. Senos Matias. Differential leakage in a closed system. Internal report, University of Edinburgh, 1993.

[172] L. A. McNeely. Thermodynamic properties of aqueous solutions of LiBr. *ASHRAE Trans.*, pages 413–434, 1979.

[173] M. Mentiply. Thermodynamic properties of working fluids. Internal literature review, 1990., January 1990.

[174] A. C. Mercer. Improving the energy efficiency of industrial spray dryers. *Journal of Heat Recovery Systems*, 6(1):3–10, 1986.

[175] G. Minds and J. Nyvad. New drying methods for aqueous solutions at low temperatures. In P. A. Pilavachi, editor, *Energy Efficiency in Process Technology*, pages 179– 189, October 19^{th}- 22^{nd} 1992. Athens, Greece.

[176] G. Moss. Working fluids for heat pumps, 1982.
European Patent EP65 858.

[177] S. S. Murthy and A. M. K. Poduval. Performance of a R114 high temperature compression heat pump for drying. In F Moser, editor, *Proceedings of the 3^{rd} International workshop on Research Activities on Advanced Heat Pumps*, pages –, September 1990. Graz, Austria.

[178] D. Nalto. Alternatives to CFC refrigerants. In T. Saito, editor, *Heat Pumps: 'Solving Energy and Environmental Challenges'. Proceedings of the 3^{rd} International Agency Heat Pump Conference*, pages 713– 720, 12^{th}- 15^{th} March 1990. Tokyo, JAPAN.

[179] A. E. Nasser and T. R. Osman. Simple LiBr/H2O absorption cycle limitations. *Applied Energy*, 17:251–262, 1984.

[180] G. Nonhebel and A. A. H. Moss. *Drying of solids in the chemical industry.* Butterworths, 1971.

[181] Norman. *Absorption, distillation and cooling towers*, pages 206–213.

[182] B. Norton and F. N. de Silva. High temperature, pressurized wood drying: Experimental and simulation results. In P. A. Pilavachi, editor, *Energy Efficiency in Process Technology*, pages 210– 219, October 19^{th}- 22^{nd} 1992. Athens, Greece.

[183] D. Oakley. Sprays reveal their secrets. *The Chemical Engineer*, (539):18–21, 25 March 1993.

[184] Department of the Envionment-Global Atmosphere Division. CFCs in the UK refrigeration and air conditioning industries. Usage and the Scope for Substitution. HMSO, 1992.

[185] M. A. Osei-Bonsu and R. J. Treece. The development of absorption cycle heat pumps applied to industrial process heat recovery. In *3rd International Symposium on the Large Scale Application of Heat Pumps*, pages 197 – 204, 25^{th}- 27^{th} March 1987. Conference held in Oxford, England.

[186] R Perry and D Green, editors. *Perry's Chemical Engineers' Handbook.* M^{c}Graw- Hill, 6^{th} edition, 1985. International Student Edition.

[187] M. Pflugl and F. Moser. Behaviour of absorbers with falling films of salt solutions in heat pump applications. In *Large Scale Applications of Heat Pumps. 3rd International Symposium*, pages 141–148, 25^{th}- 27^{th} March 1987. Symposium held in Oxford, England.

[188] H. R. C. Pratt. The performance of packed absorption and distillation columns with particular reference to wetting. *Trans. Instn. Chemical Engineers*, pages 195–214, 1951.

[189] C. L. Pritchard. An open cycle heat transformer for waste heat recovery from dryers. In F Moser, editor, *Proceedings of the 3^{rd} International workshop on Research Activities on Advanced Heat Pumps*, pages 379–390, September 1990.

[190] Demonstration project at BIP Chemicals Ltd. Heat recovery form a boiler exhaust to pre-heat air to a spray dryer. *Journal of Heat Recovery Systems*, 6(1):11–23, 1986.

[191] C. Ramshaw. New heat pump. *The ICI Engineer.*

[192] D. Reay. Energy conservation in industrial drying. *The Chemical Engineer*, pages 507–509, July/ August 1976.

[193] D. A. Reay. The energy conservation demonstration projects scheme-support for heat recovery. *Journal of Heat Recovery Systems*, 4(1):43–50, 1984.

[194] M. Renz and F. Steimle. Comparison of the thermodynamic properties of working fluids for absorption systems. In *I.I.R Meeting Commun. E1- E2 Jerusalem*, 1982.

[195] R. Rivero and P. Le Goff. On the performance criteria of sorption heat pumps and heat transformers. In A. Valero and G. Tsataronis, editors, *ECOS '92: The International Symposium on Efficiency, Costs, Optimization and Simulation of Energy Systems*, pages 575– 586, 15^{th}- 18^{th} June 1992. Zaragoza, Spain.

[196] P. A. Rowles. Future prospects for industrial heat pumps in North America. In T. Saito, editor, *Heat Pumps: 'Solving Energy and Environmental Challenges'. Proceedings of the 3^{rd} International Agency Heat Pump Conference*, pages 919– 932, 12^{th}- 15^{th} March 1990. Tokyo, Japan.

[197] V. E. Sater and O. Levenspiel. Two-phase flow in packed beds. *I&EC Fundamentals*, 5(1):86–92, February 1966.

[198] N. I. Sax. *Dangerous properties of industrial materials.* Van Nostrand Reinhold company Limited, 6^{th} edition, 1984.

[199] G. Scalabrin. Liquid sorption drying process utilising mechanical energy and desorption by air. In A. S. Mujumdar, editor, *Drying of solids*, pages 268–275, 1990.

[200] G. Scalabrin. Liquid sorption air dehumidification with TVF solution reconcentration. *Technology Today*, (6):326–332, December 1991.

[201] G. Scalabrin and G. Scaltriti. Liquid sorption drying process utilising heat at moderate thermal level. In A. S. Mujumdar, editor, *Drying '87*, pages 270–277, 1987.

[202] Jürgen Scharfe. New working fluids offer higher performance and new applications. In *Absorption Heat pumps*, pages 342–344, 1988.

[203] T. K. Sherwood and R. L. Pigford. *Absorption and extraction.* McGraw-Hill, 2nd edition, 1952.

[204] H. L. Shulman and J. J. De Gouff (Jr). Mass transfer coefficients and interfacial areas for raschig rings. *Industrial and Engineering Chemistry*, 44(8):1915 – 1922, August 1952.

[205] I. Shwarts and A. Shitzer. Solar absorption system for space cooling and heating. *ASHRAE Journal*, 19:51– 54, 1977.

[206] I. E Smith and C. O. B Carey. Thermal transformers for upgrading industrial waste heat. In *International Symposium on the Industrial application of heat pumps*, pages 251– 260. BHRA Fluid Engineering, 24^{th}- 26^{th} March 1982. Paper H1.

[207] W. K. Snelson and J. B. Codrington. An absorption cycle heat pump for drying applications in Canadian Industry. In *Large Scale Applications of Heat Pumps. 3rd International Symposium*, pages 69–76, 25^{th}- 27^{th} March 1987. Conference held in Oxford, England.

[208] S. S Stecco and M. J. Moran, editors. 28^{th} May- 1^{st} June 1990. Proceedings of Florence World Energy Research Symposium. Held in Florence, Italy.

[209] K. Stephan. Absorption heat pumps and working pair developments in the Europe until 1974. In W. Raldow, editor, *New working pairs for absorption processes*, pages 19–35, 14^{th} - 16^{th} April 1982. Proceedings of a workshop in Berlin. Sponsored by : Swedish Council for Building Research.

[210] K. Stephan. Absorption heat transformer cycles. *NATO ASI Series E, Applied Sciences*, (53):352– 373, 1983.

[211] J. T. Strack. A review of R&D activities on industrial heat pumps by a Canadian electric utility. In *3rd International Symposium on the Large Scale Application of Heat Pumps*, pages 177– 183, 25^{th}- 27^{th} March 1987. Conference held in Oxford, England.

[212] I. Strϕmmen. Incorporation of heat pumps in drying processes. In T. Saito, editor, *Heat Pumps: 'Solving Energy and Environmental Challenges'. Proceedings of the 3^{rd} International Agency Heat Pump Conference*, pages 155– 162, 12^{th}- 15^{th} March 1990. Tokyo, Japan.

[213] S. Suda. Experimental evaluation of the heat pump performance in connection with metal hydride properties. *Journal of the Less- Common Metals*, (104):211– 222, 1984.

[214] R. E Treybal. *Mass transfer operations.*

[215] R. E Treybal. Adiabatic gas absorption and stripping in packed towers. *Industrial and Engineering Chemistry*, 61(7):36–41, July 1969.

[216] K. P. Tyagi. Pressure- temperature- concentration equations for vapour absorption binary mixtures. *Journal of Heat Recovery Systems*, 4(3):181–185, 1984.

[217] W. van Gool et al. Heat pumps and exergy analysis. In T. Saito, editor, *Heat Pumps: 'Solving Energy and Environmental Challenges'. Proceedings of the 3^{rd} International Agency Heat Pump Conference*, pages 639– 646, 12^{th}- 15^{th} March 1990. Tokyo, Japan.

[218] Various. Review: the quarterly magazine of renewable energy. Published by the Department of Energy, Winter 1990/ 91.

[219] Various. Review: the quarterly magazine of renewable energy. Published by the Department of Energy, Autumn 1991.

[220] P. V.Danckwerts. *Gas- Liquid reactions.* McGraw-Hill, 1st edition, 1970.

[221] S. M. Walas. *Reaction kinetics for chemical engineers*, pages 136–145.

[222] K. Watanabe. Current status of thermophysical properties research on CFC alternatives. In T. Saito, editor, *Heat Pumps: 'Solving Energy and Environmental Challenges'. Proceedings of the 3^{rd} International Agency Heat Pump Conference*, pages 263– 282, 12^{th}- 15^{th} March 1990. Tokyo, JAPAN.

[223] The Watt Committee on Energy Working Group on Renewable Energy Sources. Renewable Energy Sources. Technical Report 22, The Watt Committee on Energy, 1990. Published by Elsevier Applied Science.

[224] J. J. W. Westra. An absorption heat transformer test plant with TFE-pyrrolidinone as working pair. In F Moser, editor, *Proceedings of the 2nd International workshop on Research Activities on Advanced Heat Pumps*, pages 45– 55, September 1988. Graz, Austria.

[225] E. P. Whitlow. Trends of efficiences in absorption refrigeration machines. *ASHRAE Journal*, pages 44–48, December 1966.

[226] G. L. Williams. The exhaust air heat recovery heat pump for residential applications in Canada. *Journal of Heat Recovery Systems*, 4(3):165–180, 1984.

[227] J. S Williamson, B. H Khoshaim, R Mallory, and A Meiners, editors. *SOLERAS: Solar Buildings. Proceedings of the 5th Soleras workshop*, May 1984. Held at Riyadh, Saudi Arabia.

[228] D. Woolnough. It's more than hot air. *The Chemical Engineer*, (539):35, 1993.

[229] S. Yanniotis and P. Le Goff. Absorption- driven multiple effect evaporators a study of the absorber- regenerator couple. In P. A. Pilavachi, editor, *Energy Efficiency in Process Technology*, pages 437–447, October 19th- 22nd 1992. Athens, Greece.

[230] F. Yoshida and T. Tanaka. Air-water contact operations in a packed column. *Ind and Eng Chem*, 43(6):1467–1473, June 1951.

[231] W. C. Yu and G. Astarita. Design of packed towers for selective chemical absorption. *Chemical Engineering Science*, 42(3):425–433, 1987.

[232] C. Z. Zhuo and C. H. M. Machielson. Thermodynamic assessment of an absorption heat transformer with tfe- pyr as the working pair. *Heat Recovery Systems and CHP*, 14(3):265– 272, May 1994. Special edition containing papers from the 4th International Workshop on Heat Pump Research and Applications, part of the CHISA '93 Conference, held in Praha, Czech Republic August 29th- September 3rd 1993.

[233] K. H. Zimmerman, editor. *Heat Pumps: Prospects in heat pump technology and marketing.* Lewis Publishers, Inc., 28th- 30th April 1987. Proceedings of the 1987 Internation Energy Agency Heat Pumps Conference. Held in Orlando, Florida.

I finally got it altogether... but I forgot where I put it.